

**BIOELECTROCHEMICAL CONVERSION OF CARBON DIOXIDE
TO METHANE FOR BIOGAS UPGRADING**

A Dissertation
Presented to
The Academic Faculty

by

Christine M. Dykstra

In Partial Fulfillment
of the Requirements for the Degree
Doctor of Philosophy in the
School of Civil and Environmental Engineering

Georgia Institute of Technology
December 2017

COPYRIGHT © 2017 BY CHRISTINE M. DYKSTRA

BIOELECTROCHEMICAL CONVERSION OF CARBON DIOXIDE TO METHANE FOR BIOGAS UPGRADING

Approved by:

Dr. Spyros G. Pavlostathis, Advisor
School of Civil and Environmental
Engineering
Georgia Institute of Technology

Dr. Jim Spain
School of Civil and Environmental
Engineering
Georgia Institute of Technology

Dr. Lawrence Bottomley
School of Chemistry and Biochemistry
Georgia Institute of Technology

Dr. Xing Xie
School of Civil and Environmental
Engineering
Georgia Institute of Technology

Dr. Ching-Hua Huang
School of Civil and Environmental
Engineering
Georgia Institute of Technology

Dr. Sotira Yiacoumi
School of Civil and Environmental
Engineering
Georgia Institute of Technology

Date Approved: [August 17, 2017]

ACKNOWLEDGEMENTS

First and foremost, I would like to thank my advisor, Dr. Spyros G. Pavlostathis, for his immense support and guidance as I journeyed through my graduate studies. Along the way, he generously shared his wisdom and knowledge, challenged me to think and grow as a researcher, and patiently corrected many pages of manuscripts with tireless attention to detail. He once shared with me a poem by C.P. Cavafy, with the lines: “Keep Ithaka always in your mind. Arriving there is what you are destined for. But do not hurry the journey at all. Better if it lasts for years, so you are old by the time you reach the island, wealthy with all you have gained on the way, not expecting Ithaka to make you rich.” While my journey has not yet ended, I want to thank Dr. Pavlostathis for giving me the opportunity to gain a wealth of knowledge and experience during my journey at Georgia Tech.

In addition to my advisor, I would like to thank the members of my thesis committee: Dr. Jim Spain, Dr. Ching-Hua Huang, Dr. Sotira Yiacoumi, Dr. Xing Xie and Dr. Lawrence Bottomley. I would also like to thank Dr. Guangxuan Zhu for his incredible support in the laboratory, without which this research would not have been possible.

I thank Xiaoferi (Sophie) Zeng for all of the thoughtful discussions and her companionship inside the lab and out. I thank Bianca Costa for her hard work and dedication while working as an undergraduate research assistant. I also thank Zeou Dou, my other labmates and my friends for all of their support.

Last but not least, I would like to thank my family for helping me become the person I am today and for giving me the determination to never give up. Finally, to Matthew Jones, who has been by my side for this journey, supporting me through many rough seas. Thank you.

TABLE OF CONTENTS

ACKNOWLEDGEMENTS	iii
LIST OF TABLES	viii
LIST OF FIGURES	xi
LIST OF SYMBOLS AND ABBREVIATIONS	xix
SUMMARY	xx
INTRODUCTION	1
1.1 Preface	1
1.2 Research Objectives	3
1.3 Approach	4
1.3.1 Assessment of Methanogenic BES Processes under Well-Defined Conditions	4
1.3.2 Develop and Test a Zero-Valent Iron Amended Biocathode	4
1.3.3 Microbial Community Assessment	5
1.3.4 Assessment of BES Performance under Applied, Non-Ideal Conditions	5
1.4 Broader Impacts	6
CHAPTER 2. BACKGROUND	7
2.1 Biogas Upgrading	7
2.1.1 Anaerobic Digestion	7
2.1.2 Methanogens and Methanogenesis	9
2.1.3 Biogas Composition	11
2.1.4 Current Methods of Biogas Upgrading	13
2.2 Bioelectrochemical Systems (BESs)	14
2.2.1 Types of BESs	14
2.2.2 Electromethanogenesis	18
2.2.3 Bioelectrochemical Systems for Biogas Upgrading	20
CHAPTER 3. MATERIALS AND METHODS	22
3.1 General Analytical Methods	22
3.1.1 pH	22
3.1.2 Chemical Oxygen Demand (COD)	22
3.1.3 Ammonia	23
3.1.4 Sulfate	23
3.1.5 Total and Volatile Suspended Solids (TSS and VSS)	23
3.1.6 Total Gas Production	24
3.1.7 Gas Composition	24
3.1.8 Volatile Fatty Acids (VFAs)	25
3.1.9 Total Dissolved Carbon Dioxide Species (C _T)	25
3.1.10 Protein	26
3.1.11 Iron (II)	26

3.2	Electrochemical Analysis	28
3.2.1	Current and Current Density	28
3.2.2	Coulombic Efficiency (CE), Cathode Capture Efficiency (CCE) and Energy Efficiency	28
3.2.3	Cyclic Voltammetry	30
CHAPTER 4. GAS AND CARBON TRANSPORT IN A METHANOGENIC BES		
	31	
4.1	Introduction	31
4.2	Materials and Methods	33
4.2.1	BES Configurations	33
4.2.2	Biocathode Inoculum (EHM suspended growth culture)	37
4.2.3	Gas and Carbon Transport	38
4.2.4	Normalization of Gas Rates to Membrane Surface Area and Mean Net Driving Pressure (NDP)	39
4.2.5	Theoretical Estimation of Biomass Growth and Cell Lysis Products	40
4.2.6	Analytical Methods	42
4.3	Results and Discussion	43
4.3.1	BES Performance -- Comparison of Different Configurations	43
4.3.2	Bioanode Effects on Biocathode and Overall System Performance	51
4.3.3	Evaluation of BES Gas Transport	52
4.3.4	Evaluation of BES Carbon Transport	59
4.3.5	Demonstration of Biocathode Acetogenesis	64
4.4	Summary	65
CHAPTER 5. METHANOGENIC BIOCATHODE MICROBIAL COMMUNITY DEVELOPMENT AND THE ROLE OF BACTERIA		
	67	
5.1	Introduction	67
5.2	Materials and Methods	70
5.2.1	BES Setup.	70
5.2.2	Inocula.	71
5.2.3	Microbial Community Analysis.	72
5.2.4	Analytical Methods.	74
5.3	Results and Discussion	75
5.3.1	Performance of BES with MM- and EHM-inoculated Biocathodes.	75
5.3.2	Change in Microbial Community Structure.	84
5.3.3	Phylogeny of Suspended Growth Cultures and Cathode Biofilms.	90
5.3.4	Proteobacteria in Suspended Growth and Cathode Biofilm Cultures.	107
5.4	Summary	112
CHAPTER 6. ZERO VALENT IRON-AMENDED BIOCATHODE		
	114	
6.1	Introduction	114
6.2	Materials and Methods	116
6.2.1	BES Setup.	116
6.2.2	Zero-Valent Iron Biocathode.	118
6.2.3	Precipitate Analysis.	118
6.2.4	Microbial Community Analysis.	119

6.2.5	Analytical Methods.	120
6.3	Results and Discussion	120
6.3.1	ZVI-Free Biocathode.	120
6.3.2	ZVI-Amended Biocathode.	126
6.3.3	ZVI-Amended Biocathode at Various Potentials.	135
6.3.4	BES Performance with Mid-Cycle ZVI Addition and Short-Term Open Circuit Conditions.	138
6.3.5	Phylogeny and Microbial Community Diversity of ZVI Biocathode.	142
6.3.6	Precipitate Formation and Characterization.	145
6.4	Summary	154
CHAPTER 7.	THE EFFECT OF HYDROGEN SULFIDE ON BES PERFORMANCE	156
7.1	Introduction	156
7.2	Materials and Methods	160
7.2.1	Serum Bottle Tests.	160
7.2.2	Measurement of Sulfide Transport.	162
7.2.3	BES Performance with Cathode H ₂ S.	165
7.2.4	Carbon Balance.	168
7.3	Results and Discussion	170
7.3.1	Serum Bottle Tests.	170
7.3.2	Sulfide Transport within a BES.	174
7.3.3	Effect of H ₂ S on BES Performance.	179
7.3.1	Biocathode Methane Production at Various Initial Hydrogen Sulfide Concentrations	181
7.3.2	Carbon Balance	183
7.3.3	Phylogeny and Microbial Community Assessment	187
7.4	Summary	197
CHAPTER 8.	EFFECT OF HYDROGEN SULFIDE AND ZERO VALENT IRON ON BES PERFORMANCE AND MICROBIAL COMMUNITIES	199
8.1	Introduction	199
8.2	Materials and Methods	201
8.2.1	Effect of H ₂ S on BES Performance with a ZVI-Amended Biocathode	201
8.2.1	Electron Transfer Mechanisms	202
8.2.2	Microbial Community Analysis	203
8.3	Results and Discussion	204
8.3.1	Effect of H ₂ S on BES Performance with a ZVI-Amended Biocathode	204
8.3.2	Electron Transfer Mechanisms	208
8.3.3	Microbial Community Analysis	215
8.4	Summary	232
CHAPTER 9.	BIOELECTROCHEMICAL BIOGAS UPGRADING	234
9.1	Introduction	234
9.2	Materials and Methods	236
9.2.1	Catholyte Recycle System	236
9.2.2	BES Biogas Upgrading with Anaerobic Digester Biogas	238

9.3	Results and Discussion	239
9.3.1	Catholyte Recycle System	239
9.3.2	BES Biogas Upgrading with Anaerobic Digester Biogas	243
9.4	Summary	250
CHAPTER 10. CONCLUSIONS AND RECOMMENDATIONS		252
10.1	Conclusions	252
10.2	Recommendations	254
10.2.1	Research Recommendations	254
10.2.2	Development Recommendations	256
REFERENCES		260

LIST OF TABLES

Table 2.1	- Stages of Anaerobic Digestion	8
Table 2.2	- Anaerobic Digestion Biogas Composition for Various Carbon Sources	13
Table 2.3	- Summary of Common Figure 2.2 Parameters for BES Configurations	16
Table 2.4	- Reaction Equations and Standard Redox Potentials (EH° or ΔE°) ^a	18
Table 4.1	- Description of BES configurations used in this study.	37
Table 4.2	- Henry's Law Constants Corrected for Temperature and Ionic Strength	43
Table 4.3	- Initial Rate and Total Methane Production by Various BES Configurations.	45
Table 4.4	- Coulombic Efficiency (CE) and Cathode Capture Efficiency (CCE) of Various BES Configurations Tested in this Study.	51
Table 4.5	- Mean Rate of Increase (+) or Decrease (-) in Headspace Gas Over the Course of a 1 d Incubation, Normalized to PEM Surface Area and Mean Net Driving Pressure (NDP).	55
Table 5.1	- Bacterial and Archaeal Shannon Diversity Indices for Suspended Growth Cultures and Biocathode Biofilms	86
Table 5.2	- Relative Abundance (%) of Archaeal Community Members in Suspended Growth Cultures and Biocathode Biofilms	95
Table 5.3	- Relative Abundance, Closest GenBank Relatives and Roles of Related Bacterial Species for OTUs in Suspended Growth Cultures and Biocathode Biofilms.	101
Table 5.4	- Closest GenBank Match and Relative Abundance of Identified Bacterial OTUs in the MM and EHM Suspended Growth and Biofilm Cultures	102
Table 5.5	- Composition of δ -Proteobacteria in the MM and EHM Suspended Growth Cultures	109
Table 6.1	- BES Performance under Different Cathode Conditions	122

Table 6.2 - BES Performance at Various Applied Potentials	136
Table 6.3 - BES Performance with Mid-Cycle ZVI Addition and Voltage Application	138
Table 6.4 - Elemental Composition of the Biocathode Precipitate (SEM-EDS)	149
Table 7.1 - BES2 Feeding Schedule	168
Table 7.2 - Comparison of BES1 and BES2 prior to H ₂ S Addition	179
Table 7.3 - BES1 and BES2 OTU Counts	188
Table 7.4 - Archaeal Community Analysis	189
Table 7.5 - Bacterial and Archaeal Shannon Diversity Indices	192
Table 7.6 - Bacterial OTUs with a Relative Abundance $\geq 1\%$	196
Table 8.1 - BES Setups	202
Table 8.2 - Mean Biocathode H ₂ and CH ₄ Production Rates	210
Table 8.3 - Cathode Capture Efficiency (CCE) During H ₂ and CH ₄ Production	214
Table 8.4 - OTU Counts in Anode and Cathode Biofilm and Suspended Biomass Samples from BES1 – BES4	216
Table 8.5 - Closest GenBank Relatives and Archaeal Relative Abundance for Defined OTUs in Cathode Biofilm and Suspended Biomass	222
Table 8.6 - Closest GenBank Relatives and Archaeal Relative Abundance for Defined OTUs in Anode Biofilm and Suspended Biomass	222
Table 8.7 - Closest GenBank Relatives and Bacterial Relative Abundance for Defined OTUs in Cathode Biofilm and Suspended Biomass	223
Table 8.8 - Closest GenBank Relatives and Bacterial Relative Abundance for Defined OTUs in Anode Biofilm and Suspended Biomass	225
Table 8.9 - Bacterial and Archaeal Shannon Diversity Indices	226
Table 9.1 - BES Setups	238
Table 9.2 - Maximum Current Density and Cathode Capture Efficiency under Various Configurations	247

Table 9.3 - Mean Biocathode 3-Day CH₄ Production Rates and Final Gas Composition 248

LIST OF FIGURES

Figure 2.1	- Carbon Flow During Anaerobic Digestion	9
Figure 2.2	- Schematic of a bioelectrochemical system	15
Figure 3.1	- Iron (II) calibration curve.	27
Figure 4.1	- Schematic of BES showing three gas transport processes, as described in Section 4.3.3. (CE, counter electrode; RE, reference electrode; WE, working electrode).	35
Figure 4.2	- BAn-BCa cyclic voltammetry scan for the determination of the applied potential (V vs. Ag/AgCl) at which oxygen evolution occurs (1.4 V). The scan was conducted at a scan rate of 50 mV/s under unfed conditions.	35
Figure 4.3	- Activity profiles of the MFC (A, B) and BES configurations BAn-ACa (C, D, E), AAn-BCa (F, G, H), and BAn-BCa (I, J, K) during a typical 7-day feeding cycle.	46
Figure 4.4	- Pitting corrosion of the anode stainless steel rod in the AA-BC BES configuration.	48
Figure 4.5	- Mean rates of gas appearance/disappearance in the anode (An) and cathode (Ca) headspace of the AAn-ACa #1, AAn-ACa #2, BAn-ACa and AAn-BCa BES configurations over the course of 1 d, normalized to the PEM surface area and the mean net driving pressure.	53
Figure 4.6	- Time course of carbon species (suspended and biofilm growth, cell lysis products, acetate (aq), total inorganic carbon (aq), CH ₄ (aq), CO ₂ (g), and CH ₄ (g)) during a feeding cycle in the BAn-BCa anode (A), cathode (B) and whole system (C).	62
Figure 4.7	- Time course of current density during carbon flow analysis of the BA-BC BES configuration.	63
Figure 5.1	- Headspace gas pressure (A) and gas composition (B) of the EHM suspended growth culture over three, representative feeding cycles. Dashed vertical lines indicate the wasting of a portion of the culture and replacement with fresh medium, accompanied by the complete flushing of the headspace with H ₂ /CO ₂ (80:20 v:v). The increase in total headspace pressure on days other than those at the end of a 7-d feeding cycle (i.e., days not indicated by dashed	76

vertical lines), was due to the addition of H₂/CO₂ without any gas release.

- Figure 5.2 - Time course of anode acetate concentration (A), BES current density normalized to the PEM surface area (B), and cathode headspace methane (C) during three representative feeding cycles following 56 d of cathode biofilm establishment; MM-B, MM-inoculated biocathode; EHM-B, EHM-inoculated biocathode. Error bars represent mean values \pm one standard deviation, $n = 3$. 79
- Figure 5.3 - Time course of BES current density (A) and headspace methane (B) over the course of the first three feeding cycles for the MM-inoculated biocathode BES (MM-BES) and the EHM-inoculated biocathode BES (EHM-BES). 80
- Figure 5.4 - Cyclic voltammetry scan of inactive BES after the EHM-biocathode was maintained unfed in fresh catholyte and a N₂-filled headspace for 24 h. Scan conducted at a rate of 50 mV/s. Vertical broken line denotes an applied potential of -1.1 V which H₂ evolution was noted. 83
- Figure 5.5 - Cyclic voltammograms of the MM-BES and EHM-BES. Scans were conducted at the end of a feeding cycle at a scan rate of 100 mV/s. 83
- Figure 5.6 - Cyclic voltammograms of an abiotic (i.e., uninoculated) BES with anolyte and catholyte at various ionic strengths (1.21, 1.26, 1.31, 1.36 and 1.41 M), starting at open circuit potential. Scans conducted at a scan rate of 50 mV/s. The vertical arrow shows how the CV curve shifts due to double layer compression, while the horizontal arrow shows how the open circuit potential shifts due to decreasing ohmic resistance. 84
- Figure 5.7 - Rarefaction curves for the EHM culture, EHM biocathode, MM culture and MM biocathode. Lower and upper limits of rarefaction depths were 10 and 100, respectively, and the number of steps (i.e., rarefied OTU table sizes) was 100. 86
- Figure 5.8 - 2-D Principal Coordinate Analysis (PCA) plots for bacterial communities (A) and archaeal communities (B) of the MM suspended growth, MM biocathode, EHM suspended growth and EHM biocathode cultures. 87
- Figure 5.9 - 3-D Principal Coordinate Analysis (PCA) plots for bacterial communities (A) and archaeal communities (B) of the MM suspended growth, MM biocathode, EHM suspended growth and 88

EHM biocathode cultures. Axes are scaled to the percent variation explained by the principal coordinates.

- Figure 5.10 - Redundancy analysis (A) and canonical correspondence analysis (B) plots to determine changes in OTU abundance attributed to biofilm development and higher buffer strength (MM Biocathode and EHM Biocathode), or higher temperature (35 vs. 22oC) with a more complex (dextrin and peptone) substrate (MM culture). EHM was maintained with a lower buffer strength (100 vs. 300 mM) and a simple (CO₂/H₂) substrate. 89
- Figure 5.11 - Phylogenetic Tree showing the relationship of suspended growth cultures and BES biocathodes Bacteria OTUs ($\geq 1\%$ relative abundance) to their closest matched species in GenBank. 92
- Figure 5.12 - Phylogenetic tree showing the relationship of suspended growth cultures and BES biocathodes Archaea OTUs ($\geq 1\%$ relative abundance) to their closest matched species in GenBank. 93
- Figure 5.13 - Phylogenetic tree showing the relationship of EHM-biocathode (EHM-B; blue diamond) Bacteria OTUs ($\geq 1\%$ relative abundance) to their closest matched species in GenBank. 94
- Figure 5.14 - Bacterial community structure in suspended growth culture and biofilm samples. MM, mixed methanogenic suspended growth culture; MM-B, MM-inoculated biocathode; EHM, enriched methanogenic suspended growth culture; EHM-B, EHM-inoculated biocathode. 97
- Figure 5.15 - Relative abundance of classes within the phylum Proteobacteria for MM suspended growth culture (A), MM-inoculated biocathode BES (B), EHM suspended growth culture (C) and EHM-inoculated biocathode BES (D). 100
- Figure 5.16 - Relative abundance heatmap of OTUs most closely related to species classified as a carbohydrate fermenter (CF); amino acid fermenter (AAF); hydrogen producer (HP); hydrogen scavenger (HS); acetogen (Ac); exoelectrogen (EE); hydrocarbon degrader (HD); mediator producer (MP); implicated in biofilm formation (BF); found in anode biofilm (AB); found in cathode biofilm (CB); and unknown function (Unk). Mixed methanogenic suspended growth culture (MM); MM-inoculated biocathode (MM-B); Enriched hydrogenotrophic methanogenic suspended growth culture (EHM); EHM-inoculated biocathode (EHM-B). Note that most identified OTUs were related to species that belong 107

to more than one class and, therefore, the row total for each culture exceeded 100%.

Figure 6.1	- Analyte at the end of a feeding cycle prior to the addition of ZVI to the cathode (A) and at the end of a feeding cycle after ZVI addition to the cathode (B).	121
Figure 6.2	- Time course of headspace hydrogen in the anode (A) and cathode (B) for various BES configurations (ZVI-free abiotic cathode, AC0; abiotic cathode with 1 g/L ZVI, AC1; ZVI-free biocathode, BC0; biocathode with 1 g/L ZVI, BC1; biocathode with 2 g/L ZVI, BC2), and in the anode (C) and cathode (D) of the BC1 system at various applied potentials (-0.65 to -0.80 V vs. SHE).	123
Figure 6.3	- Time course of headspace methane in the anode (A) and cathode (B) for various BES configurations (ZVI-free abiotic cathode, AC0; abiotic cathode with 1 g/L ZVI, AC1; ZVI-free biocathode, BC0; biocathode with 1 g/L ZVI, BC1; biocathode with 2 g/L ZVI, BC2), and in the anode (C) and cathode (D) of the BC1 system at various applied potentials (-0.65 to -0.80 V vs. SHE).	124
Figure 6.4	- Time course of headspace carbon dioxide in the anode (A) and cathode (B) for various BES configurations (ZVI-free abiotic cathode, AC0; abiotic cathode with 1 g/L ZVI, AC1; ZVI-free biocathode, BC0; biocathode with 1 g/L ZVI, BC1; biocathode with 2 g/L ZVI, BC2), and in the anode (C) and cathode (D) of the BC1 system at various applied potentials (-0.65 to -0.80 V vs. SHE).	125
Figure 6.5	- Time course of Fe ²⁺ concentration in the catholyte of the abiotic cathode (AC1) and biocathode (BC1) when initially amended with 1 g/L ZVI.	128
Figure 6.6	- Time course of hydrogen in the headspace of the anode (A) and cathode (B) over the course of four feeding cycles in which 0 g/L (BC0), 1 g/L (BC1) or 2 g/L (BC2) ZVI was added at the start of the first cycle.	130
Figure 6.7	- Diagram showing the anaerobic corrosion of ZVI, which produces Fe ²⁺ and H ₂ . Methanogens use the H ₂ resulting from ZVI corrosion to reduce CO ₂ to CH ₄ , in addition to utilizing electron equivalents directly from the biocathode.	131
Figure 6.8	- Time course of cathode headspace CH ₄ over the course of four feeding cycles during which 0, 1 or 2 g/L ZVI was added only at the start of the first feeding cycle. Error bars represent mean values ± one standard deviation, n = 3.	131

Figure 6.9	- Charge transferred during a 7-d feeding cycle in various BES configurations (AC0, ZVI-free abiotic cathode; AC1, abiotic cathode with 1 g/L ZVI; BC0, ZVI-free biocathode; BC1, biocathode with 1 g/L ZVI; BC2, biocathode with 2 g/L ZVI).	133
Figure 6.10	- Time course of cathode headspace CH ₄ over the course of four feeding cycles with 1 g/L initial ZVI and cathode potential at -0.65, -0.70, -0.75 or -0.80 V vs. SHE, respectively. Error bars represent mean values ± one standard deviation, <i>n</i> = 3.	137
Figure 6.11	- Time course of CO ₂ (A), H ₂ (B) and CH ₄ (C) in the cathode headspace during the first feeding cycle of BC1 and two later tests using the same biocathode: a ZVI addition test in which 1 g/L ZVI was added on the third day of a feeding cycle (red dash-dot line), and a voltage test in which 1 g/L ZVI was added on the first day of a feeding cycle under open circuit conditions and -0.80 V was applied on the second day of the feeding cycle (black dashed line).	141
Figure 6.12	- Phylogenetic tree showing the relationship of the biocathode (BC; blue circle) and ZVI biocathode (ZVI-BC; red square) Bacteria OTUs (≥1% relative abundance) to their closest matched species in GenBank.	144
Figure 6.13	- Relative abundance of bacterial phyla in the ZVI-free biocathode (BC) and ZVI-exposed biocathode (ZVI-BC).	145
Figure 6.14	- Precipitate formed in the cathode after the addition of ZVI was white under reducing conditions (A), spontaneously turned blue when exposed to air (oxygen) (B), and turned orange-yellow when electrochemically oxidized (abiotically) with a platinum electrode poised at +1.2 V vs. Ag/AgCl, with 50 mM NaCl as anolyte (C).	148
Figure 6.15	- SEM-EDS analysis of a blue powder precipitate sample collected from the biocathode following ZVI addition and exposure to air.	149
Figure 6.16	- Cyclic voltammogram of biocathode precipitate (A) magnified from -0.025 to +0.025 V (B) to highlight two oxidation peaks (I at 0.85 V and II at -0.16 V vs. Ag/AgCl) and two reduction peaks (I' at 0.09 V and II' at -0.55 V vs. Ag/AgCl). The scan rate was varied from 50 to 200 mV/s to determine reaction reversibility and identify redox pairs.	150
Figure 6.17	- Cyclic voltammogram of biocathode precipitate (A) magnified from -0.10 to +0.10 V (B). The red line indicates a redox peak at -0.61 V versus Ag/AgCl (-0.41 V versus SHE) that became more pronounced as the precipitate was progressively reduced. Scans were conducted on the oxidized precipitate and then at intervals	151

of 5, 15, and 30 min at a cathode potential of -0.8 V versus SHE (Scan rate 100 mV/s).

Figure 6.18	- Cyclic voltammogram of the precipitate following pre-reduction for 30 min at -1 V (vs. Ag/AgCl). After 5 min without an applied voltage, the peak current of the redox peak at -0.61 V (vs. Ag/AgCl) was lower, indicating a lower concentration of the reduced species. After applying a voltage of -1 V (vs. Ag/AgCl) for 1 additional min, the peak current increased, indicating a higher concentration of the reduced species (Scan rate 100 mV/s).	152
Figure 6.19	- Abiotic electrochemical reduction of blue precipitate (A) to white precipitate (B) by applying -1 V (vs. Ag/AgCl) cathode potential, followed by precipitate sorption to the carbon felt electrode, yielding a clear catholyte (C).	153
Figure 6.20	- White precipitate in close association with the carbon felt electrode and biofilm in the ZVI-amended biocathode.	154
Figure 7.1	- Molar Fraction of Sulfide Species versus pH	159
Figure 7.2	- Cyclic voltammograms of an abiotic anode with total sulfide ion concentrations of 0.00, 0.05, 0.10 and 0.15 mM	164
Figure 7.3	- Cyclic voltammetry maximum current versus total sulfide ion concentration	165
Figure 7.4	- Linear biocathode CH ₄ production during the first 3 days of two feeding cycle	167
Figure 7.5	- Time course of MM serum bottle CH ₄ production with 0% H ₂ S (MM control) and 1% initial H ₂ S in the headspace (MM + H ₂ S)	171
Figure 7.6	- Time course of EHM serum bottle CH ₄ production with 0% H ₂ S (EHM Control) and 1% initial H ₂ S in the headspace (EHM + H ₂ S)	172
Figure 7.7	- Time course of CH ₄ production by the MM culture under hydrogenotrophic conditions with 0% (Control), 0.38%, 0.75%, 1.50% and 3.00% H ₂ S in the headspace	173
Figure 7.8	- Cyclic voltammetry conducted on the cathode over time following the addition of 3% H ₂ S (v/v) to the cathode headspace	176
Figure 7.9	- Time course of maximum current during CV from -1.2 V to 0.2 V (vs. Ag/AgCl) and system current at the applied cathode voltage of 0.2 V (vs. Ag/AgCl).	177

Figure 7.10	- Anode cyclic voltammetry conducted over time following the addition of 3% H ₂ S (v/v) to the cathode headspace	178
Figure 7.11	- Time sequence of anolyte total sulfide ion concentration following the addition of 3% H ₂ S (v/v) to the headspace of the cathode.	178
Figure 7.12	- Time course of current density in BES1 (control) and BES2, during which H ₂ S was added to 1% H ₂ S (v/v) in the cathode headspace on days 1, 7 and 15.	180
Figure 7.13	- Comparison of the initial 3-day methane production rate at initial cathode headspace hydrogen sulfide concentrations of 0-6% (v/v); <i>n</i> is the number of feeding cycles represented.	183
Figure 7.14	- Carbon balance of BES1 (control), A; and BES2 with 3% initial H ₂ S (v/v) in the cathode headspace, B.	185
Figure 7.15	- Biomass distribution between suspended and biofilm biomass in the anode and cathode of BES1 and BES2 after 3-d incubation.	186
Figure 7.16	- Biofilm growth on the BES1 cathode (A) was visibly thinner than the biofilm growth on the BES2 cathode (B).	186
Figure 7.17	- Bacterial community of BES1 and BES2 anode (A) and cathode (B) biofilm and suspended	191
Figure 8.1	- Time course of biocathode headspace H ₂ (A) and CH ₄ (B) in BES4 during a 3-day feeding cycle before and after 3% v/v H ₂ S addition	205
Figure 8.3	- Time course of biocathode headspace CO ₂ (A) and CH ₄ (B) in BES1-BES4 during a 3-day feeding cycle	208
Figure 8.4	- Time course of BES1, BES2, BES3 and BES4 biocathode H ₂ production (A) and CH ₄ production (B)	212
Figure 8.5	- Comparison of Biocathode CH ₄ Production Rate with H ₂ Production Rate as Electron Equivalents of CH ₄ for BES1-BES4.	214
Figure 8.9	- 2D Principal coordinate analysis plots for the anode biofilm and suspended biomass in BES1, BES2, BES3 and BES4.	230
Figure 8.10	- 3D Principal coordinate analysis plots for the anode biofilm and suspended biomass in BES1, BES2, BES3 and BES4; Front view (A), Overhead view (B).	230

Figure 8.11	- Canonical correspondence analysis plot (A) and redundancy analysis plot (B) for the anode biofilm and suspended growth in BES1, BES2, BES3 and BES4.	231
Figure 9.1	- Schematic of catholyte recycle system	237
Figure 9.2	- Time course of CO ₂ and CH ₄ in the cathode headspace in the feeding cycle prior to implementing catholyte-recycle. Error bars represent mean ± standard deviation; <i>n</i> = 3.	240
Figure 9.3	- Time course of headspace CO ₂ and CH ₄ in the catholyte recycle bottle	242
Figure 9.4	- Time course of current density (A), cathode headspace CO ₂ (B) and cathode headspace CH ₄ (C) when fed with 100% CO ₂ (days 1-3) and anaerobic digester biogas (days 3-6).	246
Figure 10.1	- Diagram of Membrane-Based Catholyte Recycle System	257
Figure 10.2	- Suggested Process Diagram (A) and Architecture (B) for a Continuous-Flow Methanogenic BES	258

LIST OF SYMBOLS AND ABBREVIATIONS

AD	Anaerobic digestion
BES	Bioelectrochemical system
CH ₄	Methane
CO ₂	Carbon dioxide
EHM	Enriched hydrogenotrophic methanogenic
H ₂	Hydrogen
H ₂ S	Hydrogen sulfide
MEC	Microbial electrolysis cell
MES	Microbial electrosynthesis
MFC	Microbial fuel cell
MM	Mixed methanogenic
N ₂	Nitrogen
OTU	Operational taxonomic unit
SRB	Sulfate-reducing Bacteria
VFA	Volatile fatty acid
WRRF	Water resource recovery facility
ZVI	Zero valent iron

SUMMARY

Biogas produced by anaerobic digestion contains a mixture of carbon dioxide (CO_2), methane (CH_4) and other trace gases. To increase the energy content (i.e., CH_4) of biogas, current methods separate or sequester CO_2 . Instead, bioelectrochemical systems (BESs) may be utilized to directly convert biogas CO_2 to CH_4 , but BES biogas upgrading systems are relatively undeveloped. Therefore, the overall objective of this research was to develop and test a bioelectrochemical system (BES) designed to convert carbon dioxide into methane for the purpose of upgrading the energy content of anaerobic digester biogas, with the specific objectives to: i) analyze and describe the processes taking place in an electromethanogenic BES under well-defined conditions; ii) investigate the microbial communities in an electromethanogenic BES under varied conditions; iii) test BES performance under applied, non-ideal conditions (e.g., hydrogen sulfide in the biogas feed, actual digester biogas feed); and iv) develop and test a zero-valent iron (ZVI) amended biocathode to improve CH_4 production.

This research demonstrated that the transport of carbon and gases through the proton exchange membrane of a methanogenic BES can influence the extent of biocathode CH_4 production. A carbon balance of a batch-fed BES demonstrated transient microbial carbon storage and a net transport of carbon from anode to cathode, which allowed for a higher molar production of CH_4 than the initial molar input of CO_2 in the cathode.

Next, the bacterial community of a biocathode was explored by comparing a biocathode inoculated with a mixed methanogenic (MM) culture and a biocathode inoculated with an enriched hydrogenotrophic methanogenic (EHM) culture, developed

from the MM culture following pre-enrichment with H₂ and CO₂ as the only externally supplied electron donor and carbon source, respectively. This study showed that H₂/CO₂ pre-enriched inoculum enhanced biocathode CH₄ production, although the archaeal communities in both biocathodes converged primarily (86-100%) on a phylotype closely related to *Methanobrevibacter arboriphilus*. The bacterial community of the MM-biocathode was similar to that of the MM inoculum but was enriched in *Spirochaetes* and other non-exoelectrogenic, fermentative Bacteria. In contrast, the EHM-biocathode bacterial community was enriched in *Proteobacteria*, exoelectrogens and putative producers of electron shuttle mediators. Similar biomass levels were detected in the MM- and EHM-biocathodes. Thus, although the archaeal communities were similar in the two biocathodes, the difference in bacterial community composition was likely responsible for the 3.8-fold higher CH₄ production rate observed in the EHM-biocathode.

Zero-valent iron (ZVI), which has previously been used to improve CH₄ production in anaerobic digesters, has not been previously explored in methanogenic biocathodes. This study found that the total CH₄ produced during a 7-day feeding cycle with 1 and 2 g/L initial ZVI was 277% and 285% higher, respectively, than the mean CH₄ production in the four prior cycles without ZVI addition. Furthermore, CH₄ production by the ZVI-amended biocathodes remained elevated throughout three subsequent feeding cycles, despite catholyte replacement and no new ZVI addition. The higher CH₄ production could not be fully explained by complete anaerobic oxidation of the ZVI and utilization of produced H₂ by hydrogenotrophic methanogens. Microbial community analysis showed that the same phylotype, most closely related to *Methanobrevibacter arboriphilus*, dominated the archaeal community in the ZVI-free and ZVI-amended biocathodes. However, the bacterial

community experienced substantial changes following ZVI exposure, with more *Proteobacteria* and fewer *Bacteroidetes* in the ZVI-amended biocathode. Furthermore, a redox-active precipitate formed in the ZVI-amended biocathode, which sorbed to the electrode and/or biofilm and likely acted as a redox mediator to increase electron transfer and CH₄ production.

The effect of H₂S, a common biogas contaminant, on BES performance was also examined. Although inhibitory to methanogenesis in anaerobic digestion, the addition of up to 3% H₂S initial concentration (v/v) to the CO₂ added to the cathode headspace resulted in improved CH₄ production and system current. Using an abiotic setup, the transport of H₂S across the proton exchange membrane into the anode compartment and its subsequent oxidation was demonstrated. Thus, H₂S added to the cathode headspace travels to the anode, where it donates electrons and increases system current. However, the 3-d rate of CH₄ production declined above 3% H₂S, indicating an inhibitory effect at relatively large concentrations.

The performance of the ZVI-amended biocathode was also assessed when 3% (v/v) H₂S was added to the cathode headspace. Following amendment with H₂S, the ZVI-amended biocathode removed more headspace CO₂ (100% vs. 89% previously) over the course of a 3-d incubation and produced CH₄ at a 61% faster rate of production. The electron transfer mechanisms in the biocathodes of four BESs (control, ZVI-amended, H₂S-amended and ZVI/H₂S-amended) were assessed by measuring the amount of H₂-mediated CH₄ production in the biocathode. Although the majority of the CH₄ produced by the control BES and BES with H₂S-amended biocathode could be explained by H₂-mediated CH₄ production, 74% and 32% of the CH₄ produced in the BES4 and BES3 biocathodes,

respectively, could be attributed to H₂-mediated CH₄ production. This suggests that in the presence of ZVI, the modes of electron transfer shift away from H₂-mediated transfer and possibly towards more direct electron transfer. An analysis across the anode and cathode biofilm and suspended biomass communities indicated exoelectrogens were enriched in the anode and cathode of better performing systems. Of the three factors (biofilm development, biocathode ZVI amendment and biocathode H₂S amendment) analyzed with principal coordinate analysis, canonical correspondence analysis and redundancy analysis, ZVI had the greatest effect on the cathode bacterial community, while biofilm growth had the greatest effect on the anode bacterial community.

To advance BES biogas upgrading technology, the effect of a catholyte recycling system was tested and the performance of three developed BESs (control, ZVI-amended and H₂S-amended) were compared between a CO₂-fed cycle and a cycle fed with real anaerobic digester biogas. The recycling of catholyte increased the mean biocathode CH₄ production rate by 45%, indicating that recycling relieved mass transfer limitations at the interface of the cathode surface and the catholyte. A nearly linear rate of CH₄ production was observed throughout the course of 3, 7-d feeding cycles (21 d), indicating that a continuous-flow biocathode system is capable of maintaining a stable rate of CH₄ production over time. When the biocathodes of three BESs (control, BES1; H₂S-amended, BES2; ZVI-amended, BES3) were fed with biogas from a stock anaerobic digester, the maximum current density in BES1 and BES2 increased by 13% and 35%, respectively. In contrast, the ZVI-amended biocathode in BES3 experienced an 18% decline in maximum current density between the CO₂-fed cycle and the biogas-fed cycle. In the biogas-fed cycle, each biocathode removed CO₂ from the headspace to a lower fraction (i.e., greater

CH₄ fraction) of total gas than in the CO₂-fed cycles. However, the cathode capture efficiency, a measure of how efficiently electron equivalents at the cathode were used for the reduction of CO₂ to CH₄, was lower in the biogas-fed cycles than the CO₂-fed cycles. Further research is needed to determine what mechanism(s) are responsible for the observed changes in BES performance.

This research has advanced the understanding of BES biogas upgrading by developing insights into the physicochemical processes (e.g., carbon and gas transport), microbial communities and effect of ZVI and H₂S on the performance of a methanogenic BES. Improving understanding of these fundamental processes may guide the design of future BES biogas upgrading systems and move future wastewater resource recovery facilities (WRRFs) closer to net-zero energy status.

INTRODUCTION

1.1 Preface

The burning of fossil fuels supplies 85% of the world's energy and is a significant contributor to the estimated 49 gigatonnes of carbon dioxide (CO₂) released into the atmosphere each year from human activity (IPCC 2014). Evidence for accumulation of CO₂ in the atmosphere is clear and the average global CO₂ concentration continues to rise by 2.0 ± 0.1 ppm per year (IPCC 2014). CO₂ is a known greenhouse gas, capable of absorbing solar radiation and emitting infrared thermal radiation. The presence of greenhouse gases in the atmosphere creates the greenhouse effect, in which emitted thermal radiation traps heat in the lower atmosphere and increases the surface temperature on Earth. Rising CO₂ concentrations in the atmosphere are expected to increase the greenhouse effect and contribute to rising global temperature and climate change (IPCC 2014). Wastewater treatment utilizes biological processes that both produce and consume CO₂, making treatment systems a logical venue for the reduction and/or reuse of CO₂.

The traditional goals of wastewater treatment focus on producing an effluent of sufficient quality (i.e., low COD, low nutrients) so as to reduce the negative effects of its release into the environment. However, as the world faces new environmental challenges, the paradigm has shifted to view wastewater as a resource with great potential for energy and resource recovery. It is estimated that typical domestic wastewater contains an internal chemical energy of 17.7-28.7 kJ/g COD (Heidrich et al. 2011), making wastewater a largely untapped resource for energy recovery.

Anaerobic digestion is used to stabilize high-strength waste streams such as municipal primary and secondary sludge, as well as agricultural waste. Through a complex set of biological conversions, municipal anaerobic digestion produces an ammonia-rich digestate, and biogas that contains primarily a mixture of CO₂ and methane (CH₄), along with other trace gases (e.g., H₂S, H₂). Although anaerobic digestion is a relatively mature technology from the perspective of traditional treatment goals, under the new paradigm for wastewater treatment, the opportunity for improved energy recovery is great. Current research has focused on upgrading biogas produced from anaerobic digestion to obtain a higher CH₄ content, which may then be used as a carbon-neutral fuel source for the production of energy. Although the combustion of CH₄ produces CO₂, the use of biogas CH₄ as an energy source utilizes fuel derived from waste organic carbon produced via photosynthetic CO₂ assimilation rather than liberating sequestered carbon from fossil fuels.

As new goals emerge in wastewater treatment, new treatment technologies are required. One promising area of research is bioelectrochemical systems (BESs), a relatively new technology in its application to wastewater treatment. BESs are devices that use microbes to catalyze oxidation and/or reduction reactions at solid electrodes and take advantage of the flow of electrons from an anode to a cathode. The most well-known type of BES is the microbial fuel cell (MFC), in which the electron transfer from the oxidation reaction(s) at the anode to the reduction reaction(s) at the cathode is used to produce electricity. A second type of BES is the microbial electrolysis cell (MEC), in which biological anode-respiring reactions and a supplemental voltage drive the electrolysis of water at the cathode. Although an external voltage must be applied, the energy required to drive electrolysis with a MEC is much lower than in systems with abiotic catalysts. A third

type of BES is the microbial electrosynthesis cell (MES), which is similar to a MEC, with the exception that an external voltage is applied to help drive biological cathodic reactions for the production of biofuels, bioplastics, chemicals and other valuable bioproducts (Rabaey and Rozendal 2010).

BESs may be applied to a wide range of biological processes and, as such, are an emerging technology with potential for biogas upgrading and nutrient removal/recovery applications. While promising, many questions remain before BESs will be adopted on a larger scale. Few studies have examined the use of continuous-flow BESs or have utilized actual wastewater. In particular, little is known about the application of BESs to anaerobic digestion for the treatment of digestate and biogas upgrading. Furthermore, additional research is needed to identify microbes capable of extracellular electron transfer, an area which promises to expand the knowledge of microbial metabolism and electron transport (He and Angenent 2006, Rabaey and Rozendal 2010).

1.2 Research Objectives

The overall objective of this research was to develop and test a bioelectrochemical system (BES) designed to convert CO₂ into CH₄ for the purpose of increasing the energy content of anaerobic digester biogas. The specific objectives of this research were to:

- i) Analyze and describe the processes taking place in an electromethanogenic BES under well-defined conditions;
- ii) Investigate the microbial communities in an electromethanogenic BES under varied conditions;

- iii) Test BES performance under applied, non-ideal conditions (e.g., hydrogen sulfide in the biogas feed, actual digester biogas feed); and
- iv) Develop and test a zero-valent iron (ZVI) amended biocathode to improve CH₄ production.

1.3 Approach

1.3.1 Assessment of Methanogenic BES Processes under Well-Defined Conditions

A stock methanogenic BES was developed under well-defined conditions with an acetate-fed bioanode and a CO₂-fed biocathode. Subsequent BESs were developed from the stock BES for use in experimentation. To better understand the processes in a methanogenic BES under well-defined conditions, the anode and cathode compartments were analysed when paired with an abiotic cathode and abiotic anode, respectively. By comparing BES performance under different configurations, the abiotic and biological processes were described. Furthermore, using an abiotic system, the transport of gas and carbon within the system was described.

1.3.2 Develop and Test a Zero-Valent Iron Amended Biocathode

Under reducing conditions, ZVI undergoes anaerobic corrosion, producing H₂ and Fe²⁺ ions. Because the H₂ may be used by hydrogenotrophic methanogens to reduce CO₂ to CH₄, a biocathode amended with ZVI may be capable of increased CH₄ output. Thus, a novel, ZVI-amended biocathode was developed and tested. The concentration of amended ZVI in the biocathode was varied to determine an optimal concentration for the system.

The system performance was also assessed at various applied potentials to determine if ZVI addition could maintain biocathode CH₄ output with less energy input required.

1.3.3 Microbial Community Assessment

The microbial communities in the anodes, cathodes and suspended biomass of the inocula, control BES, ZVI-amended BES, sulfide-exposed BES and the ZVI/sulfide-exposed BES were analyzed using 16S rRNA gene sequencing for Bacteria and Archaea. After quality checking, the most abundant OTUs ($\geq 1\%$ relative abundance) were identified and submitted to GenBank. The OTUs and their closest matches from GenBank were assembled into phylogenetic trees. Principle coordinate analysis, redundancy analysis and canonical correspondence analysis were conducted to assess how similar the communities were to each other and to determine factors that influenced community changes.

1.3.4 Assessment of BES Performance under Applied, Non-Ideal Conditions

Hydrogen sulfide (H₂S) is a common biogas contaminant that may be inhibitory to methanogenesis (Chen et al. 2008). Therefore, to test how H₂S affects the performance of a methanogenic BES, the performance of a control BES was compared with a BES in which H₂S had been added to the cathode headspace to 1% H₂S (v/v). Following monitoring of several feeding cycles with 1% H₂S addition to the cathode, the amount of H₂S added was increased incrementally over several feeding cycles up to 6% H₂S. The performance of the BES was compared at each step and a carbon balance was conducted on a 3-d feeding cycle with an initial 3% H₂S in the cathode. ZVI produces Fe²⁺ during anaerobic corrosion, which has a strong affinity to sulfide ions, producing a highly-insoluble precipitate, FeS.

Therefore, a new ZVI-amended biocathode was developed and tested with H₂S addition to determine if the ZVI-amended biocathode would be effective in sulfide removal.

To better approximate applied conditions, the biogas from a stock, mesophilic anaerobic digester fed with dextrin and peptone was used as biocathode feed. The performance of four BES configurations (control, sulfide-amended biocathode, ZVI-amended biocathode, ZVI/sulfide-amended biocathode) was monitored and compared.

1.4 Broader Impacts

While anaerobic digestion currently allows for energy recovery, H₂S removal and specialized combustion equipment is necessary and may not be economical for smaller digesters. BES technology that can simultaneously remove H₂S and upgrade biogas to natural gas-quality CH₄ (>95% v/v) would allow for energy recovery using current natural-gas infrastructure, without the need for specialized combustion systems. Furthermore, BESs operate using inexpensive materials and utilize microorganisms as self-renewed catalysts. Thus, the development of BES biogas upgrading technology has the potential to help move wastewater treatment closer to net-zero energy status, as well as expand energy recovery options to smaller digester systems.

CHAPTER 2. BACKGROUND

2.1 Biogas Upgrading

In the seventeenth century, Flemish chemist Jan Baptist van Helmont noted that decaying organic matter produced a gas that was flammable. However, it wasn't until the early nineteenth century that the gas he identified was discovered to be methane (CH_4). Sixty years later, in 1868, Bechamp reported that “an organism” was responsible for the observed CH_4 production during organic decomposition. Although Bechamp was incorrect that a single microorganism was responsible for decomposition and CH_4 production, he was correct that the flammable gas was indeed a “biogas” (Abbasi et al. 2012, Deepanraj et al. 2014). In today's energy-intensive world, biogas has gained new focus as a method of recovering energy from wastewater treatment. Although biogas contains CH_4 , it also contains other gases that are not flammable or are otherwise undesirable (e.g., CO_2 , H_2S , N_2 , etc.), and reduce the energy content of the biogas. Increasing the energy content (i.e., CH_4 content) of the biogas is a process termed “biogas upgrading”.

2.1.1 Anaerobic Digestion

As scientists eventually discovered, anaerobic digestion and biogas production was not a single-step process, nor was it completed by a single microorganism, as Bechamp had proposed. In fact, anaerobic digestion is a multi-stage process that requires the cooperation of many different types of bacteria and archaea (Table 2.1). The flow of carbon from complex organic substrate to CO_2 and CH_4 is accomplished through four main stages (Figure 2.1). Hydrolysis, the first stage, converts complex compounds (carbohydrates,

proteins and fats) into simple organic compounds (sugars, amino acids, fatty acids). Acidogenic bacteria then convert these simple compounds into organic acids (e.g., propionate, butyrate, etc.) and alcohols (Deepanraj et al. 2014). A separate group of autotrophic bacteria called acetogens, convert the products of acidogenesis into acetate, CO₂ and H₂ (Küsel and Drake 2011). In the final stage, methanogens use the products of acetogenesis, along with CO₂ and H₂ generated from fermentation during acidogenesis, to produce CH₄ and CO₂. Methanogens and methanogenesis are further discussed in Section 2.1.2.

Table 2.1 - Stages of Anaerobic Digestion

Stage	Reactions	Microorganisms involved
Stage I - Hydrolysis	$(C_6H_{10}O_5)_n + nH_2O = n(C_6H_{12}O_6)$	<i>Clostridium, Proteus, Vibrio, Bacillus, Peptococcus, Bacteriodes, Staphylococcus Lactobacillus, Escherichia, Bacillus, Staphylococcus, Pseudomonas, Sarcina,</i>
Stage II - Acidogenesis	$C_6H_{12}O_6 + 2H_2O \rightarrow 2CH_3COOH + 4H_2 + CO_2$ $C_6H_{12}O_6 + 2H_2 \rightarrow 2CH_3CH_2COOH + 2H_2O$ $C_6H_{12}O_6 \rightarrow CH_3CH_2CH_2COOH + 2H_2 + 2CO_2$ $C_6H_{12}O_6 \rightarrow 2CH_3CH_2OH + 2CO_2$ $C_6H_{12}O_6 \rightarrow 2CH_3CHOHCOOH$	<i>Desulfovibrio, Selenomonas, Streptococcus, Veillonella, Desulfobacter, Desulfomonas, Clostridium, Eubacterium</i>
Stage III - Acetogenesis	$CH_3CH_2OH + H_2O \rightarrow CH_3COOH + 2H_2$ $2CH_3CH_2OH + 2CO_2 \rightarrow CH_4 + 2CH_3COOH$ $CH_3CH_2COOH + 2H_2O \rightarrow CH_3COOH + 3H_2 + CO_2$ $CH_3CH_2CH_2COOH + 2H_2O \rightarrow 2CH_3COOH + 2H_2$ $CH_3CHOHCOOH + H_2O \rightarrow CH_3COOH + CO_2 + 2H_2$	<i>Clostridium, Syntrophomonas</i>
Stage IV - Methanogenesis	$CH_3COOH \rightarrow CH_4 + CO_2$ $CO_2 + 4H_2 \rightarrow CH_4 + 2H_2O$	<i>Methanobacterium, Methanobrevibacterium, Methanoplanus, Methanospirillum</i>

Table adapted from Deepanraj et al. (2014).

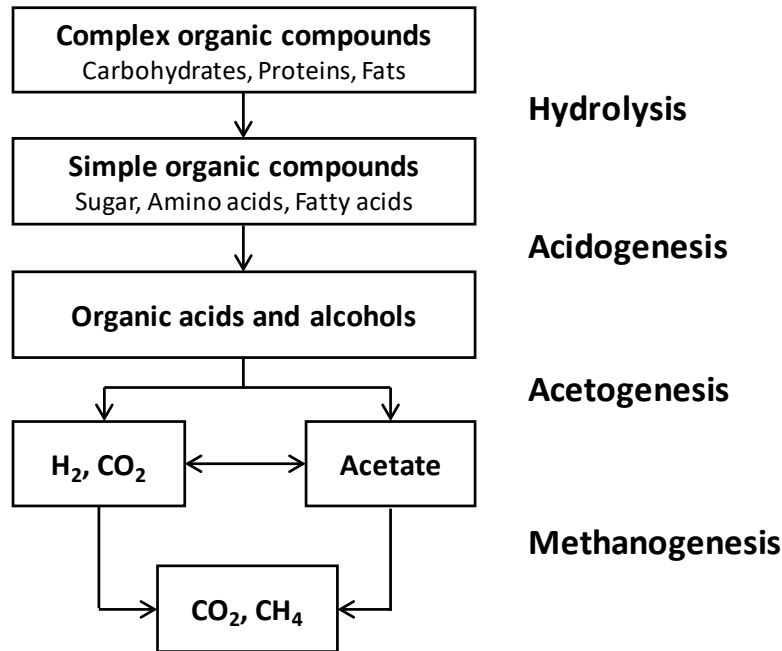


Figure 2.1 - Carbon Flow During Anaerobic Digestion

2.1.2 Methanogens and Methanogenesis

Methanogens belong to the domain Archaea, the kingdom of Euryarchaeota, and are typically divided into 5 orders: *Methanobacteriales*, *Methanococcales*, *Methanomicrobiales*, *Methanosarcinales*, and the unique hyperthermophile, *Methanopyrales* (Boone and Garrity 2001, Ferry 1993). Methanogens utilize three methanogenic pathways: hydrogenotrophic, methylotrophic and acetoclastic. Hydrogenotrophic methanogenesis involves the reduction of CO_2 using H_2 . Methylotrophic methanogenesis produces methane from methylated compounds, such as methanol or methylated amines. The conversion of methanol to CH_4 and CO_2 involves the simultaneous reduction and oxidation of separate methanol molecules to the reduced and

oxidized end products. Aceticlastic methanogenesis is the conversion of acetate into CO₂ and CH₄ (Ferry 1993).

Archaea produce at least 16 proteins specific to their domain that do not have homologues produced by Bacteria or Eukaryotes. Of these proteins, 6 have been found in every sequenced archaeal genome and can serve as molecular markers of the domain. Within archaeal species, methanogens may be molecularly identified by 31 unique proteins, of which 20 are found in all sequenced methanogens and the remaining 11 are present in all methanogens with the exception of one specialized human intestinal microbe (*Thermoplasmata* sp.) thought to have selectively lost the genes. To assist in further molecular classification, a number of proteins have been identified that are specific to particular methanogenic orders (Gao and Gupta 2007).

Several important enzymes have been identified in the methanogenesis process. One enzyme specific to methanogens is methyl-Coenzyme M methyl reductase (MCR), which catalyzes the final reaction of methanogenesis, producing CH₄. Another key enzyme, Coenzyme B-Coenzyme M heterodisulfide reductase (Hdr) is involved in the regeneration of Coenzyme M. Hdr may be found as a cytoplasmic enzyme (HdrABC) or as a membrane-bound enzyme (HdrED). The cytoplasmic HdrABC is common in methanogens and may be related to methylotrophic methanogenesis, while the membrane-bound HdrED enzyme is exclusively found in *Methanosarcinales* (Buan and Metcalf 2010). Hydrogenotrophic methanogens require hydrogenases to activate H₂ for use as a reductant with CO₂. Four different [Ni-Fe]-hydrogenases and one [Fe]-hydrogenase are known to be expressed in methanogens. The four [Ni-Fe]-hydrogenases are more common under nickel-sufficient conditions; the [Fe]-hydrogenase tends to be produced under

nickel-limited conditions. Identifying genes have been described for all five types of hydrogenase (Thauer et al. 2010). On the other hand, under H₂ limitation, the expression of genes encoding F₄₂₀-reducing hydrogenase (Frh), formate dehydrogenase (Fdh) and formyl-MFR dehydrogenase (Fwd) is upregulated. Additionally, the expression of two enzymes that catalyze the conversion of methenyl-tetrahydromethanopterin (methenyl-H₄MPT) to methylene-H₄MPT can provide insight into H₂ availability. The conversion may be catalyzed by either F₄₂₀-dependent methylene-H₄MPT dehydrogenase (Mtd) or H₂-dependent methylene-H₄MPT dehydrogenase (Hmd). Under H₂-limited conditions, expression of Mtd genes are upregulated and expression of Hmd genes are downregulated (Browne and Cadillo-Quiroz 2013).

2.1.3 Biogas Composition

The biogas produced by anaerobic digestion contains a mixture of energy-rich CH₄ and fully-oxidized CO₂, along with other trace gases (e.g., H₂S, N₂, H₂). The biogas CH₄ content may be estimated based on the mean oxidation state of the carbon in the anaerobic digestion feedstock. Fats, proteins and carbohydrates yield different amounts of CH₄ and CO₂ during anaerobic digestion as shown in Table 2.2 (Gujer and Zehnder 1983). Therefore, when the anaerobic digester feedstock is fixed, there are inherent limits to upstream biogas upgrading. Some efforts have been made to increase biogas CH₄ content within the digester by recycling the produced gas to improve CO₂ mass transfer (Müller et al. 2017). However, this method will only increase biogas CH₄ content up to the theoretical limit, as determined by the mean oxidation state of the feedstock carbon. Another method of upgrading biogas within the digester is to introduce electrodes to provide additional reducing power for CO₂ conversion to CH₄ (Zhao et al. 2015). However, this method may

affect fermentation in the digester and corrosion of the electrodes may occur. Thus, a significant portion of research on biogas upgrading has focused on downstream gas purification, as discussed further in Section 2.1.4.

Biogas also carries contaminants such as hydrogen sulfide (H_2S), which is formed during anaerobic digestion when sulfate reducing bacteria (SRB) reduce sulfate to H_2S and/or from the release of HS^- during the degradation of HS^- -carrying amino acids (e.g., cysteine). H_2S is a toxic, corrosive, and malodorous gas that must be removed from the biogas prior to combustion or further biogas handling to prevent corrosive damage to equipment. The concentration of H_2S in biogas depends on the sulfur content of the anaerobic digestion feedstock but typically ranges from 0.6% to 1.9% (v/v) for the digestion of municipal sludge (Peu et al. 2012). Anaerobic digestion of alternative feedstocks (e.g., agricultural residue, algae, seaweed, etc.) is gaining interest because of the potential for energy recovery combined with solids destruction (Ge et al. 2016). However, alternative feedstocks often contain a higher sulfur content than typical municipal sludge and, therefore, the biogas H_2S concentration is higher. Using a typical carbon to sulfur ratio for pig bristles and harvested green seaweed, these feedstocks are estimated to result in a biogas with 2.0-4.9% and 5.5-17.7% H_2S , respectively (Peu et al. 2012).

Table 2.2 - Anaerobic Digestion Biogas Composition for Various Carbon Sources

Carbon source	Carbon mean oxidation state	Biogas CH ₄ (%)	Biogas CO ₂ (%)
Methanol, methylamine	-2	75	25
Fats	-1.4 to -1.9	68 - 74	26 - 32
Algae, Bacteria	-0.6 to -1.2	58 - 65	35 - 42
Proteins	0 to -0.6	50 - 58	42 - 50
Carbohydrates, Acetic acid	0	50	50
Citric acid	+1	38	62
Formic acid, Carbon monoxide	+2	25	75
Oxalic acid	+3	13	87
Urea	+4	0	100

Source: Gujer and Zehnder (1983).

2.1.4 Current Methods of Biogas Upgrading

Current biogas upgrading methods typically use physical/chemical treatment methods to remove CO₂ from biogas. The primary method of CO₂ removal is through liquid absorption, which includes water scrubbing, organic solvent scrubbing and chemical scrubbing (Muñoz et al. 2015). Solid adsorption processes may also be used in a packed bed configuration with adsorbents (e.g., zeolites, activated carbon, silica-gel, activated alumina and polymeric sorbents), in a process called pressure swing adsorption (Cavenati et al. 2008, Muñoz et al. 2015, Sun et al. 2015). Although effective, adsorption systems require consumables or regeneration systems, and energy for gas compression, water compression and water cooling (Muñoz et al. 2015). Membrane technology has also been developed to separate CO₂ from CH₄. However, to be effective, membranes must be utilized in a multi-stage design and the biogas must be pre-compressed, requiring energy

input (Scholz et al. 2013). Moreover, the separated CO₂ is considered a waste product and is not converted into a useful fuel. Alternate methods of biogas upgrading have been proposed (e.g., cryogenics, algae biomass production) but are not currently practical for most anaerobic digesters (Sun et al. 2015).

2.2 Bioelectrochemical Systems (BESs)

2.2.1 Types of BESs

BESs consist of an anode, where an oxidation reaction occurs, and a cathode, where a reduction reaction occurs (Figure 2.2). The anode and cathode are connected by a circuit, which conducts electrons from the anode to the cathode, and contains either a resistor or external voltage. In the anode compartment, a substrate is oxidized, releasing electrons to the anode surface and protons into the anolyte. The protons migrate to the cathode through an optional proton exchange membrane, where they are used, in combination with the electrons from the circuit, to reduce a separate substrate in the cathode (Figure 2.2). BESs may be categorized based on their configuration, as described in Table 2.3. Microbial fuel cells (MFCs), which use a resistor in the circuit in order to harvest energy produced from a bioanode, are galvanic cells. Alternately, with the application of an external voltage, cathodic reactions can be controlled to produce chemical products. These types of BESs may be classified based on their final product and include microbial electrolysis cells (MECs), microbial electrosynthesis cells (MESs) and methanogenic biocathodes. MECs require an external voltage and produce hydrogen (H₂) in a cathode that is typically abiotic and uses a catalyst, such as platinum. MESs also require an external voltage but use a biocathode to produce multi-carbon compounds from CO₂. Similarly, a methanogenic

biocathode requires an external voltage and utilizes a biocathode. However, methanogenic biocathodes convert CO_2 to CH_4 , instead of multi-carbon compounds.

BES bioanodes and biocathodes typically consist of a biofilm attached to a solid, submerged electrode. The enzymes and metabolic activity of the microbes in the biofilm enhance the reaction rate and the transfer of electrons. Anodic biofilms have been shown to contain species that are termed “exoelectrogenic bacteria” because of their ability to directly use an electrode as an electron acceptor. Some of the species identified in anodic biofilms include several *Geobacter* and *Shewanella* species, *Citrobacter* spp., *Ochrobactrum anthropi*, *Desulfuromonas acetoxidans*, *Rhodopseudomonas palustris* and *Klebsiella pneumoniae* (Bond et al. 2002, Huang et al. 2015, Logan 2009, Xing et al. 2008, Xu and Liu 2011, Zhang et al. 2008, Zuo et al. 2008).

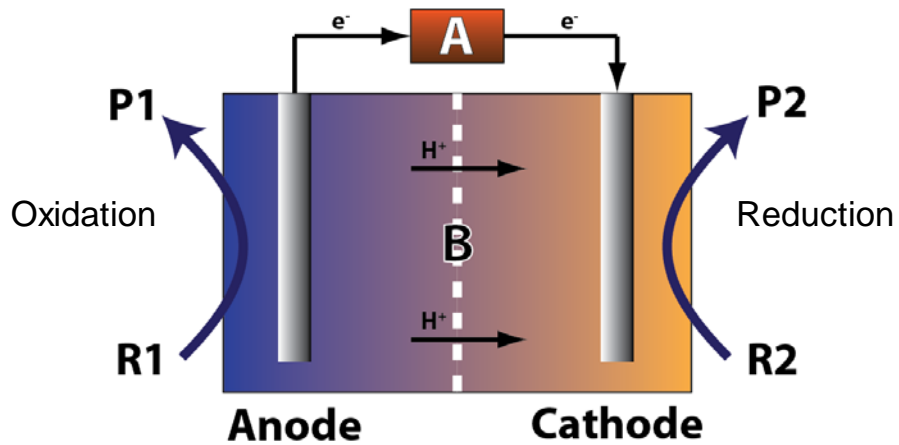


Figure 2.2 - Schematic of a bioelectrochemical system

Table 2.3 - Summary of Common Figure 2.2 Parameters for BES Configurations

	A	B	R1	P1	R2	P2
Microbial Fuel Cell (MFC)	Resistor; Power outlet	Optional membrane	Organics; acetate	CO ₂ , Oxidized products	O ₂ (abiotic); NO ₃ ⁻ (biocathode)	H ₂ O (abiotic); N ₂ (biocathode)
Microbial Electrolysis Cell (MEC)	External power supply	Optional membrane	Organics; acetate	CO ₂ , Oxidized products	H ₂ O (abiotic);	H ₂ , O ₂ (abiotic)
Microbial Electrosynthesis (MES)	External power supply	Optional membrane	Organics; acetate	CO ₂ , Oxidized products	Glucose; Acetate; Ethanol; Syngas (CO ₂ , CO, H ₂)	CH ₄ ; Glutamic acid; Butanol; Propionate; Caproate; Carboxylic acids; PHA ^a ; PHB ^b
Methanogenic Biocathode	External power supply	Optional membrane	Organics; acetate	CO ₂ , Oxidized products	O ₂ (abiotic); NO ₃ ⁻ (biocathode)	H ₂ O (abiotic); N ₂ (biocathode)

^a PHA: polyhydroxyalkanoates

^b PHB: polyhydroxybutyrate

In BESs that utilize an abiotic cathode, a precious metal catalyst is usually required. Because precious metals are cost-prohibitive for large-scale systems, researchers have looked at ways to improve efficiencies of less costly cathode materials, such as bismuth. However, these methods rely on special electrolytes or engineered promoters that must be added to the system (Medina-Ramos et al. 2014). More recently, biocathodes have been examined for their ability to eliminate the need for precious metals by microbially catalyzing the cathodic reaction (Huang et al. 2011, Rismani-Yazdi et al. 2008). In addition to using less expensive materials, biocathodes may also outperform abiotic precious metal catalysts. One study reported a nitrifying biocathode increased the maximum power density

by 18% over an abiotic cathode and reduced both activation and concentration losses (Tran et al. 2009).

Unlike anodic biofilms, much less is known about the microorganisms in biocathodes. *Methanobacterium* and, in some cases, *Methanobrevibacter*, dominate biofilms of methanogenic biocathodes (Cheng et al. 2009, Siegert et al. 2014, Siegert et al. 2015, Zhen et al. 2015). Bacteria are also present in methanogenic biocathodes and may assist in biofilm development at the cathode (Johnsen and Karlson 2004, Shi et al. 2008, Wick et al. 2004, Wick et al. 2007). Fermentative Bacteria that produce H₂ and CO₂ could potentially recycle cell lysis products into substrate for methanogens. Furthermore, some Bacteria may produce mediators that can act as electron shuttles (Logan 2009, Pham et al. 2008, Rabaey et al. 2005), potentially improving CH₄ production by biocathode methanogens. Bacteria may also be exoelectrogens capable of cathode biocatalytic H₂ formation (Geelhoed and Stams 2010).

To improve electron transfer between microorganisms and electrodes, mediators or other soluble electron carriers may be used in BESs. A number of extracellular electron shuttles have been identified such as manganese, iron, humate, phenazine and quinones (Kang et al., 2014; Rabaey and Rozendal, 2010). These molecules allow microbes to transfer electrons to the electrode without requiring direct contact. Although mediators may increase electron transfer, some mediators have limited stability, may produce toxic effects or may be lost in the flow through the system (Rabaey and Rozendal, 2010). Zero valent iron (ZVI) is a non-toxic, inexpensive, solid metal that is capable of producing Fe²⁺, a potential electron shuttle, through the process of anaerobic corrosion (Equations 2.1 and 2.2, Table 2.4). Moreover, ZVI is capable of stimulating methanogenesis by generating H₂

during corrosion (Equation 2.2, Table 2.4), which is in turn used by hydrogenotrophic methanogens (Equations 2.4-2.6, Table 2.4), as well as by acting as an electron donor itself (Equation 2.3, Table 2.4). In one study, the addition of ZVI to an anaerobic digester resulted in a 43.5% increase in methane production (Feng et al., 2014), which suggests that the use of ZVI may be beneficial for biogas upgrading with a methanogenic biocathode.

Table 2.4 - Reaction Equations and Standard Redox Potentials ($E_{H^{0'}}$ or $\Delta E^{0'}$)^a

Equation Number	Reaction Equation	$E_{H^{0'}}$ or $\Delta E^{0'}$ (V)
2.1	$Fe(s) \rightarrow Fe^{2+} + 2e^{-}$	0.440
2.2	$Fe(s) + 2H_2O \rightarrow Fe^{2+} + 2H_2 + 2OH^{-}$	-0.389
2.3	$CO_2 + 4Fe(s) + 8H^{+} \rightarrow CH_4 + 4Fe^{2+} + 2H_2O$	0.197
2.4	$CO_2 + 4H_2 \rightarrow CH_4 + 2H_2O$	0.170
2.5	$2H^{+} + 2e^{-} \rightarrow H_2$	-0.414
2.6	$CO_2 + 8H^{+} + 8e^{-} \rightarrow CH_4 + 2H_2O$	-0.244

^a Redox potentials are under standard environmental conditions (i.e., 25°C and 1 atm) at pH 7.

2.2.2 Electromethanogenesis

Electrochemical production of CH₄ from CO₂ is challenging, due in part to the stability of the CO₂ molecule. In most cases, transformation of CO₂ requires a nucleophilic attack on the carbon atom, which must bend the stable O-C-O bond (Jitaru 2007). Therefore, electrochemical CH₄ production usually requires precious metal catalysts and/or a large applied voltage. Moreover, current catalysts tend to poison quickly. However, methanogens are capable of catalyzing the conversion of CO₂ to CH₄ in anaerobic environments, a trait that highlights them as potentially useful for bioelectrochemical production of CH₄. Indeed, a study by Cheng et al. (2009) described a two-chamber electromethanogenesis cell that reduced CO₂ to CH₄ using a methanogenic biocathode at an applied voltage of -0.7 to -1.0 V, coupled to an abiotic anode. The authors also reported

that when a single-chamber BES was fed acetate, the methanogenic biocathode was capable of producing methane with 80% energy efficiency (Cheng et al. 2009). Villano et al. (2010) reported greater than 80% electron capture efficiency in a batch assay utilizing a methanogenic BES with the cathode poised at potentials more negative than -0.7 V. Later, Villano et al. (2011) reported a methanogenic biocathode coupled to a *Geobacter sulfurreducens* colonized bioanode, which was operated with the anode as the working electrode poised at 0.5 V and acetate as an electron donor. The authors reported that the rate of methane production was controlled by the acetate oxidation kinetics in the anode and that temperature was a significant factor in the oxidation kinetics (Villano et al. 2011).

The use of electrons from a cathode to drive the biological reduction of CO₂ to CH₄ through the actions of methanogens is termed “electromethanogenesis” (Cheng et al. 2009). Three mechanisms of CH₄ production have been proposed. Electromethanogenesis may proceed through the in situ production of H₂ at the cathode, which is then utilized by hydrogenotrophic methanogens to reduce CO₂, as given in Equation 2.4 (Table 2.4). In this case, the actual cathodic reaction is represented by Equation 2.5 (Table 2.4). CH₄ production may also result from the transfer of electrons from endogenous or exogenous redox mediators in place of H₂. More recently, it has been suggested that electromethanogenesis may also proceed through direct electron transfer from the cathode to the methanogens, resulting in the cathodic reaction given as Equation 2.6 (Table 2.4) (Cheng et al. 2009, Costa et al. 2013, Lohner et al. 2014). Biocathode CH₄ production has been shown to occur at potentials unable to produce CH₄ abiotically. However, it is unclear whether H₂ is an intermediary in the electron transfer from the cathode to the microorganism or whether direct electron transfer occurs (Villano et al. 2010). In a recent

study, a mutant archaeon, *Methanococcus maripaludis*, which lacked a hydrogenase gene, was reported to be capable of producing CH₄, suggesting it was capable of utilizing electrons directly from a cathode for CO₂ reduction (Lohner et al. 2014). While suggestive of direct electron transfer, it does not rule out the possibility of alternate redox mediators that may be produced endogenously and take the place of H₂ as the reducing agent. Moreover, it is not clear if direct electron transfer takes place in mixed culture biocathodes, where other microorganisms may catalyze the production of H₂ at the cathode, making the hydrogenase pathway more favorable.

2.2.3 Bioelectrochemical Systems for Biogas Upgrading

Thus far, studies of electromethanogenesis have been conducted in well-defined systems that utilize a defined medium as an anolyte and catholyte and feed cathodic chambers commercial gas mixtures of N₂ and CO₂ (Bajracharya et al. 2015, Cheng et al. 2009, Lohner et al. 2014, Villano et al. 2010, Zhen et al. 2015). Actual biogas from anaerobic digestion contains other gases, such as H₂S and CH₄, which have not been examined for their effect on BES performance. Under anaerobic conditions, sulfate is converted to H₂S by sulfate-reducing bacteria, which compete with methanogens for substrates, reducing methane production. Furthermore, the H₂S produced may be inhibitory to the anaerobic digestion process (Chen et al. 2008, Hilton and Oleszkiewicz 1988). H₂S can diffuse through a microbial cell membrane and enter the cytoplasm, where it may denature proteins or interfere with coenzyme production (Chen et al. 2008). Although several studies have investigated the effect of H₂S on traditional anaerobic digestion, the effect of H₂S on electromethanogenesis is unknown.

Additionally, the behavior of gases such as CO₂, CH₄, H₂ and N₂ in a BES is not well-understood. Concentration gradients within the liquid phases in a BES may drive transport of gases across a membrane. Moreover, CO₂ is a gaseous substrate, so it is important to understand the mass transfer of CO₂ from the gaseous phase to the liquid phase and its speciation as part of the carbonate system. As CO₂ enters a liquid phase, it first dissolves and then equilibrium is established between the dissolved CO₂ and carbonic acid, H₂CO₃. Because H₂CO₃ is a weak acid, it partly dissociates to bicarbonate, HCO₃⁻, which in turn partly dissociates to carbonate, CO₃²⁻. The speciation of CO₂ is important to understand because the dissolved form of CO₂ is the reactant in the formation of N-carboxymethanofuran, the first step in methanogenesis. When dissolved CO₂ is limited, the enzyme carbonic anhydrase is used to convert between CO₂ + H₂O and H₂CO₃ (Bartoschek et al. 2000). Furthermore, other gases such as N₂, H₂ and H₂S may be transported across the membrane (Chae et al. 2008, Jiang and Chu 2002, Ma et al. 2005, Sethuraman et al. 2009, Yamaguchi et al. 1996), and possibly affect BES operation. However, current studies have ignored the transport of gases and carbon within a BES.

CHAPTER 3. MATERIALS AND METHODS

3.1 General Analytical Methods

3.1.1 pH

All pH measurements were performed using the potentiometric method with a ATI Orion Model 370 digital pH meter (Orion Research Inc., Boston, MA) and a gel-filled combination pH electrode (VWR International, West Chester, PA). The meter was calibrated weekly with pH 4.0, 7.0, and 10.0 standard buffer solutions (Fisher Scientific, Pittsburg, PA).

3.1.2 Chemical Oxygen Demand (COD)

COD was measured using the closed reflux, colorimetric method as described in *Standard Methods* (Rice et al., 2012). An aliquot of 3 mL digestion solution composed of 4.9 g $K_2Cr_2O_7$, 6 g $HgSO_4$, 6 g Ag_2SO_4 and 500 mL H_2SO_4 was transferred to HACH COD digestion vials (HACH Company, Loveland, CO) and then 2 mL of sample was added to the vial. After tumbling the vial for 4-8 times, the content in the vials was digested at 150°C for 2 hours and then cooled down to room temperature. The absorbance was measured at 620 nm with a Hewlett-Packard Model 8453 UV/Visible spectrophotometer (Hewlett-Packard Co., Palo Alto, CA) equipped with a diode array detector, deuterium and tungsten lamps and a 1 cm path length. Samples were centrifuged and filtered through a 0.45 μm polypropylene membrane filter if the soluble COD was measured, otherwise well-mixed samples were used after appropriate dilution for total COD measurements. All samples

were prepared in triplicates and a calibration curve was prepared using 1 g/L standard solution of potassium hydrogen phthalate (KHP).

3.1.3 Ammonia

Ammonia concentration was measured using the distillation method described in *Standard Methods* (Rice et al., 2012). The samples were centrifuged at 12,000 rpm for 15 minutes and filtered through a 0.2 μm nitrocellulose membrane filter (Fisher Scientific, Pittsburgh, PA). The ammonia distillation was performed using a Labconco distillation apparatus (Labconco Corp., Kansas City, MO) and the distillate was received in a mixed indicator solution of 20 g $\text{H}_3\text{BO}_3/\text{L}$, methyl red 13.3 mg/L and methylene blue 6.67 mg/L. The distillate then was titrated with 0.2 N H_2SO_4 and the ammonia was quantified.

3.1.4 Sulfate

Sulfate (SO_4^{2-}) anion concentrations were determined using a Dionex ICS-3000 ion chromatography unit (Dionex Corporation, Sunnyvale, CA) equipped with a suppressed conductivity detector, a Dionex IonPac AG14A (4x50mm) precolumn, and a Dionex IonPac AS14A (4x250 mm) analytical column. The unit was operated in autosuppression mode with 1 mM $\text{NaHCO}_3/8$ mM Na_2CO_3 eluent and a flow rate of 1 mL/min. All samples were filtered through 0.2 μm membrane filters prior to injection. The minimum detection limit for sulfate was 0.05 mM.

3.1.5 Total and Volatile Suspended Solids (TSS and VSS)

TSS and VSS were determined according to procedures described in *Standard Methods* (Eaton et al., 2005). Whatman GF/C glass fiber filters (47 mm diameter and 1.2

μm nominal pore size; Whatman, Florham Park, NJ) were washed with deionized (DI) water and ignited at 550°C for 20 minutes in a Fisher Isotemp Model 550-126 muffle furnace before use. The filters were then cooled in a desiccator and weighed. Samples of known volume were filtered through the glass fiber filters. The filters were then rinsed with 10 mL DI water to remove dissolved organics and inorganic salts. The filters containing the samples were dried at 105°C for 90 minutes. After cooling in a desiccator, the dry weight was recorded and the filters containing the dry samples were ignited at 550°C for 20 minutes. After ignition, the samples were cooled down in a desiccator and the weight was measured. TSS and VSS concentrations were then calculated. TSS was calculated as the difference between the weight of the filter after the sample was dried at 105°C and the tare weight of the filter divided by the sample volume. VSS was calculated as the difference between the weight of the filter after the sample was dried at 105°C and the weight of the filter after the sample was burned at 550°C divided by the sample volume.

3.1.6 Total Gas Production

Total gas production in closed assay bottles and large volume reactors was measured by either the acid brine displacement method or with a Sper Scientific (Scottsdale, AZ) pressure transducer (resolution –1 atm to 1.974 atm with an accuracy of 0.002 atm).

3.1.7 Gas Composition

The gas composition was determined by a gas chromatography (GC) unit (Agilent Technologies, Model 6890N; Agilent Technologies, Inc., Palo Alto, CA) equipped with two columns and two thermal conductivity detectors. Methane (CH_4) and dinitrogen (N_2) were separated with a 15 m HP-Molesieve fused silica, 0.53 mm i.d. column (Agilent

Technologies, Inc.). Carbon dioxide (CO₂) and hydrogen sulfide (H₂S) were separated with a 25 m Chrompac PoraPLOT Q fused silica, 0.53 mm i.d. column (Varian, Inc., Palo Alto, CA). Helium was used as the carrier gas at a constant flow rate of 6 mL/min. The 10:1 split injector was maintained at 150°C, the oven was set at 40°C and the detector temperature was set at 150°C. All gas analyses were performed by injecting a 100 µL gas sample. The minimum detection limits for CH₄, CO₂, H₂S, and N₂ were 500, 800, 100 and 50 ppmv, respectively.

3.1.8 Volatile Fatty Acids (VFAs)

VFAs (C₂ to C₇; i.e., acetic, propionic, iso-butyric, n-butyric, iso-valeric, n-valeric, iso-caproic, n-caproic and heptanoic acids) were measured after acidification of filtered samples with a 5% (w/w) H₃PO₄ solution (sample:acid, 2:1 volume ratio) using an Agilent 6890 Series GC unit equipped with a flame ionization detector and a 30-m Nukol Polar, 0.32-mm I.D. column (Supelco, Bellefonte, PA). Injections were performed with a 1:1 split ratio. Samples used for the measurement of VFAs were prepared by centrifugation at 10,000 rpm for 30 minutes and filtration through 0.22-µm PVDF membrane filters before acidification. The minimum detection limit for each acid mentioned above was 0.25, 0.10, 0.03, 0.02, 0.10, 0.08, 0.02, 0.02, 0.05 mM, respectively.

3.1.9 Total Dissolved Carbon Dioxide Species (C_T)

Dissolved CO₂ was measured by drawing a 5 mL sample of medium using a locking gas-tight syringe and injecting it into an inverted 24 mL sealed serum bottle containing 10 mL 6 N sulfuric acid, resulting in a final pH ≤ 2.0. The serum bottle was hand-shaken and then allowed to equilibrate for 1 h at 22±2°C. CO₂ evolved to the bottle's headspace was

quantified using pressure and gas composition measurements. Using a calibration curve based on a 100 mM NaHCO₃ standard solution, the calculated moles of CO₂ released into the headspace of the serum bottle were converted into the total molar concentration of carbonate species (C_T, i.e., H₂CO₃^{*}, HCO₃⁻ and CO₃²⁻).

3.1.10 Protein

Biofilm protein was extracted from three, 1.3x1.3x0.6 cm pieces of the electrode felt by vortexing with 1 N NaOH and glass beads for 20 min, or bead beating with an Omni Bead Ruptor 4 (Omni International, Kennesaw, GA) at high speed for 5 min. Suspended growth biomass protein was extracted by centrifuging a liquid sample at 13,000 g for 10 min to concentrate cells, followed by the addition of 1 N NaOH to the biomass pellet and then vortexing for 20 min, or bead beating with an Omni Bead Ruptor 4 (Omni International, Kennesaw, GA) at high speed for 5 min. Samples were heated at 100°C for 10 min, followed by two centrifugation steps (13,000 g for 5 min) to obtain a purified supernatant. Protein was measured using PierceTM BCA Protein Assay Kit (Thermo Scientific, Rockford, IL) and a BioTek Synergy HT 96-well microplate spectrophotometer (BioTek, Winooski, VT).

3.1.11 Iron (II)

Iron (II) ions (Fe²⁺) were quantified using a method described by Kazumi et al. (1995), modified for smaller volume samples and relatively high Fe²⁺ concentrations. All glassware was pre-rinsed with HCl and DI prior to use. Aliquots of 0.25 mL well-mixed anolyte or catholyte were added to 5 mL 1 N HCl in glass vials. During the sampling, care was taken not to expose the samples to oxygen and cause oxidation of Fe²⁺ to Fe³⁺. Each

sample was taken in triplicate. For each replicate, a clean, HCl-rinsed tube was prepared with 5 mL of 50 mM HEPES buffer (N-2-hydroxyethylpiperazine-N'-2-ethanesulfonic acid; pH=7) and 50 μ L of FerroZine[®] Iron Reagent solution (HACH, Loveland, CO). Prior to use, each tube was inspected for a color change and discarded if any color was noted. A 100 μ L aliquot of the acidified sample was added to a prepared tube containing the HEPES buffer and FerroZine[®] solution, and then vortexed for 10 s to completely mix. The tubes were then incubated at 22 \pm 2 $^{\circ}$ C for 5 min and then the absorbance was measured at 562 nm using a HACH DR 3900 spectrophotometer (HACH Company, Loveland, CO). A calibration curve ($R^2=0.999$) was prepared using a ferrous solution by dissolving reagent-grade iron (II) sulfate heptahydrate ($\text{FeSO}_4 \cdot 7\text{H}_2\text{O}$; Sigma Aldrich, St. Louis, MO) in DI (Figure 3.1).

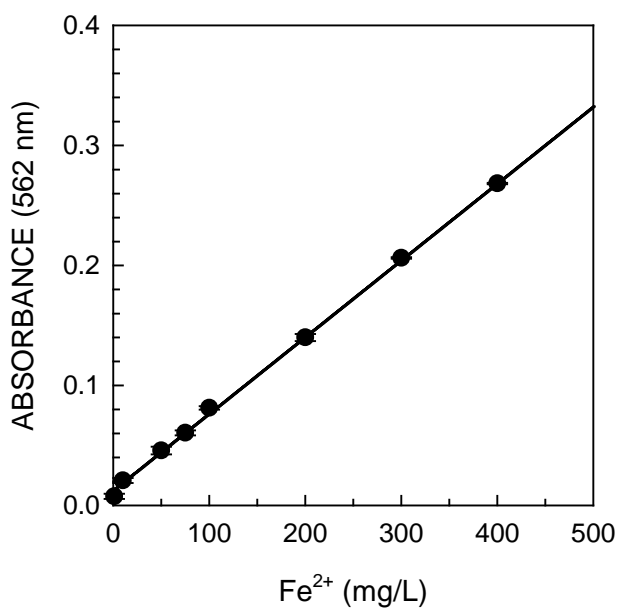


Figure 3.1 - Iron (II) calibration curve.

3.2 Electrochemical Analysis

3.2.1 Current and Current Density

Current was measured using a Gamry Interface 1000 potentiostat (Warminster, PA) with Gamry PHE200 software. Each current measurement was assessed following a 180 s equilibration period. Because of the large and unknown surface area of the porous carbon felt used in the BES electrodes, the limiting area was assumed to be the area of the proton exchange membrane (6.16 cm²). Thus, current measurements were converted to current density by normalizing the current to the size of the proton exchange membrane.

3.2.2 Coulombic Efficiency (CE), Cathode Capture Efficiency (CCE) and Energy Efficiency

The Coulombic efficiency (CE) refers to the percentage of the cumulative equivalents produced from the oxidation of acetate (meq_{Ac}) that are transferred as cumulative electric charge (meq_i). Equations for meq_{Ac}, meq_i and CE are given as Equations 3.1-3.3, where I represents current, t represents the length of the batch cycle and F represents Faraday's constant (96,485 C/eq). C₀ and C were initial and final concentrations of acetate (mmol), as measured using the method described in Section 3.1.8.

$$meq_{Ac} = (C_0 - C) * 8 \frac{meq}{mmol} \quad (\text{meeq}) \quad (3.1)$$

$$meq_i = \frac{(\int_0^t I * dt)}{F} \quad (\text{meeq}) \quad (3.2)$$

$$CE = \left(\frac{meq_i}{meq_{Ac}} \right) * 100\% \quad (\%) \quad (3.3)$$

The cathode capture efficiency (CCE) indicates the percentage of the cumulative equivalents transferred as electric charge (meq_i) that are recovered as cumulative equivalents of methane (meq_{CH_4}). The methane equivalents recovered and CCE may be calculated using Equations 3.4 and 3.5, where n_{CH_4} is the amount of methane produced (mmol) during the batch cycle.

$$meq_{CH_4} = n_{CH_4} * 8 \frac{meq}{mmol} \quad (meeq) \quad (3.4)$$

$$CCE = \left(\frac{meq_{CH_4}}{meq_i} \right) * 100\% \quad (\%) \quad (3.5)$$

The energy efficiency, η_E , is calculated as the ratio of the energy recovered as methane (W_{CH_4}) to the energy added to the system as external electrical energy (W_{input}) (Equation 3.6). The energy recovered may be calculated using Equations 3.7, where the Gibbs free energy change due to the complete oxidation of methane is ΔG_{CH_4} (-817.97 kJ/mol). The cumulative electrical charge, C , and the applied voltage, E_{app} , may be calculated with Equations 3.8 and 3.9, respectively. The potential of the anode and cathode are denoted by V_{anode} and $V_{cathode}$, respectively. While $V_{cathode}$ was maintained at a constant value using the potentiostat, V_{anode} was allowed to fluctuate, which resulted in the fluctuation of E_{app} over time. Using C and E_{app} , the input energy may be calculated as given by Equation 3.10.

$$\eta_E = \frac{W_{CH_4}}{W_{input}} * 100\% \quad (\%) \quad (3.6)$$

$$W_{CH_4} = n_{CH_4} * \Delta G_{CH_4} \quad (\text{kJ}) \quad (3.7)$$

$$C = \int_0^t I * dt \quad (\text{C}) \quad (3.8)$$

$$E_{app} = V_{cathode} - V_{anode} \quad (\text{V}) \quad (3.9)$$

$$W_{input} = C * E_{app} \quad (\text{kJ}) \quad (3.10)$$

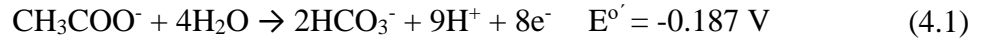
3.2.3 Cyclic Voltammetry

Cyclic voltammetry (CV) was conducted using a Gamry Interface 1000 potentiostat (Warminster, PA) with Gamry PHE200 software. The applied potential was swept from a starting voltage, typically the voltage under open circuit conditions following a delay, to a more oxidizing potential. Then, the applied potential was swept to a more reducing potential, followed by a return to the starting voltage. The CV scan rate ranged from 10 mV/s to 200 mV/s, depending on the application.

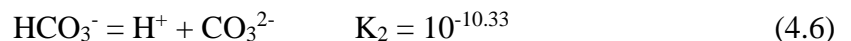
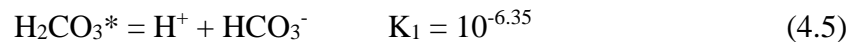
CHAPTER 4. GAS AND CARBON TRANSPORT IN A METHANOGENIC BES

4.1 Introduction

Anaerobic digestion produces a gaseous mixture of carbon dioxide (CO₂), methane (CH₄) and other trace gases. Many biogas upgrading methods, such as absorption/adsorption, membrane technology or cryogenics separate or sequester CO₂, resulting in a waste product. Some biogas upgrading methods also require expensive consumables or are energy intensive (Bauer et al. 2013, Muñoz et al. 2015). However, bioelectrochemical systems (BESs) may be utilized to directly convert CO₂ to CH₄ by pairing an oxidation reaction at the anode with the overall reduction of CO₂ to CH₄ at the cathode. A bioanode forms a biofilm enriched in exoelectrogenic Bacteria capable of oxidizing organic compounds, transferring released electrons to a solid electrode. If acetate is considered as the organic compound undergoing oxidation, the reaction at the anode is as shown in Equation 4.1 (Hamelers et al. 2010). Electrons are transferred to the anode electrode and then travel through an external circuit to the cathode with the assistance of a small applied potential (< 1 V). A methanogenic biocathode is enriched in methanogenic Archaea that are able to accept electrons from the cathode electrode, either directly or indirectly via electron shuttles, and catalyze the reduction of CO₂ to CH₄ in a process termed electromethanogenesis (Equation 4.2) (Cheng et al. 2009).



Methanogenic biocathodes require consideration of mass transport processes because they contain interfaces between solids, liquids, and gases. For BES biogas upgrading, gaseous CO_2 is introduced into a biocathode, while methanogenic Archaea reside in a submerged biofilm (Cheng et al. 2009, Fu et al. 2015, Lohner et al. 2014, Siegert et al. 2014, Villano et al. 2010, Zhen et al. 2015). When CO_2 is introduced as a gas, dissolution to the liquid phase (i.e., catholyte) occurs first (Equation 4.3). The dissolution of a gas into a liquid occurs towards an equilibrium condition at which Henry's Law describes the ratio of the gas partial and total pressure to its aqueous concentration (Equations 4.4-4.6). Once in the catholyte, CO_2 is involved in dynamic equilibria between carbonic acid/dissolved gaseous CO_2 (i.e., H_2CO_3^*), bicarbonate (HCO_3^-), and carbonate (CO_3^{2-}); at neutral pH (7.0), the predominant liquid-phase carbon species is HCO_3^- .



Dissolved gases may also diffuse through the proton exchange membrane (PEM) separating anode and cathode chambers, potentially affecting BES performance (Chae et

al. 2008, Jiang and Chu 2002, Ma et al. 2005, Sethuraman et al. 2009). Nafion 117 PEM is permeable to oxygen to some degree, which can affect the microbial fuel cell (MFC) efficiency by competing as an electron acceptor (Chae et al. 2008, Sethuraman et al. 2009) or enhancing the growth of exoelectrogenic bacteria such as *Shewanella* (Lu et al. 2016, Rosenbaum et al. 2010). Nafion 117 PEM is also permeable to CO₂ (Jiang and Chu 2002, Ma et al. 2005, Yamaguchi et al. 1996), which creates the potential for carbon transport between anode and cathode. However, gas transport in a BES has not been sufficiently quantified or assessed for its effect on the performance of a methanogenic biocathode. In addition to carbon transport between chambers, carbon also cycles among various forms (i.e., organic compounds, CO₂, CH₄, biomass) within each chamber. Understanding the carbon flow within a BES is important for performing a system-wide carbon balance, assessing overall BES efficiency and potentially developing alternative BES configurations as well as more accurate BES mathematical models. Therefore, the objective of this study was to systematically evaluate gas (N₂, CO₂, CH₄, and H₂) and carbon transport within a methanogenic BES.

4.2 Materials and Methods

4.2.1 BES Configurations

Four BES configurations were evaluated. Each BES was a dual chamber, H-type system with two 300-mL (250 mL liquid volume) glass chambers separated by a Nafion 117 PEM (Figure 4.1). Each chamber was continuously mixed magnetically and contained an electrode, consisting of four highly-porous, carbon felt strips (approximately 86 cm², 15 cm³; Alfa Aesar, Ward Hill, MA) attached to a stainless steel rod (Alfa Aesar, Ward Hill,

MA), serving as the working (cathode) or counter (anode) electrode. An Ag/AgCl electrode (+0.199 V vs. SHE; BASi; West Lafayette, IN) was placed immediately adjacent to the carbon felt electrode in each chamber to act as a reference electrode. The working, counter, and cathode reference electrodes were connected to a Gamry Interface 1000 potentiostat (Warminster, PA) and the cathode potential was poised at -0.8 V during biofilm development and throughout the present study. All reported voltage values are with reference to the standard hydrogen electrode, SHE. The selected cathode potential was based on a preliminary test, in which the biocathode CH₄ production decreased by 96% when the applied potential was changed from -0.8 to -0.7 V. In the present study, the anode potential was periodically measured against an adjacent Ag/AgCl reference electrode and was consistently below 1.4 V, the threshold value for the production of O₂ at the anode used in this study, determined through cyclic voltammetry (Figure 4.2). Each chamber was sealed with a butyl rubber stopper, flushed with N₂ (anode) or CO₂ (cathode) to create anoxic conditions. All BES configurations were operated in batch mode and maintained at room temperature (22±2°C).

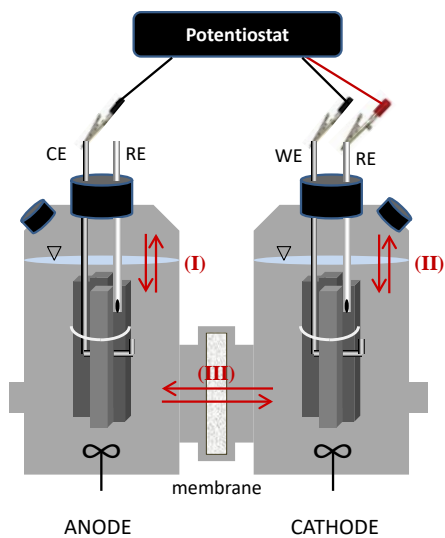


Figure 4.1 - Schematic of BES showing three gas transport processes, as described in Section 4.3.3. (CE, counter electrode; RE, reference electrode; WE, working electrode).

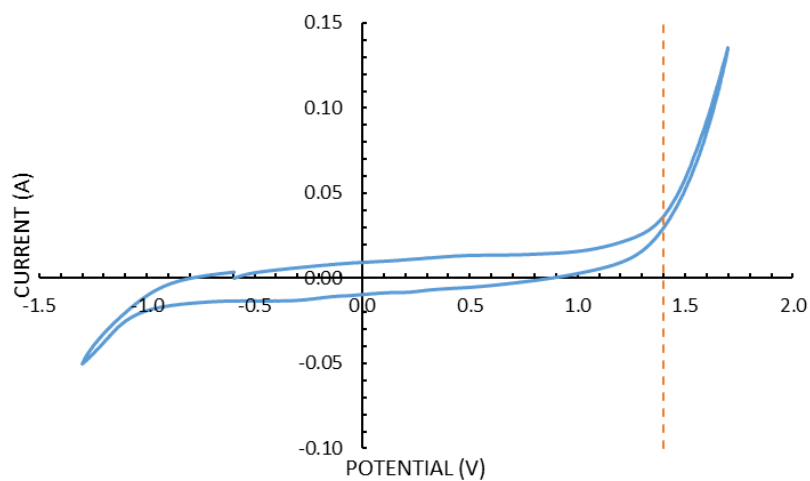


Figure 4.2 - BAn-BCa cyclic voltammetry scan for the determination of the applied potential (V vs. Ag/AgCl) at which oxygen evolution occurs (1.4 V). The scan was conducted at a scan rate of 50 mV/s under unfed conditions.

To serve as bioanode inoculum, a stock MFC was developed, consisting of a carbon felt anode, connected through an external 150 Ω resistor to a Pt-coated carbon cathode exposed to air (Table 4.1). Other BES configurations were set up as described in Table 4.1.

Anolyte and catholyte were prepared with a phosphate buffer ($\text{NaH}_2\text{PO}_4 \cdot \text{H}_2\text{O}$, 13.8 g/L; Na_2HPO_4 , 14.2 g/L), NH_4Cl , 0.31 g/L; KCl , 0.13 g/L; mineral stock 12.5 mL/L and 2.5 mL/L of either anolyte vitamin stock (Liu and Logan, 2004) or catholyte vitamin stock (Cheng et al., 2009), followed by bubbling with N_2 for 1 h. The MFC and bioanodes were batch-fed with sodium acetate at an initial concentration of 1,200 mg COD/L. The MFC and BESs were wasted/fed once per week, resulting in a hydraulic retention time (HRT) of 8.75 and 7.00 d, respectively.

A stepwise approach to BES evaluation was adopted for each component individually. First, an abiotic anode was paired with an abiotic cathode (AAn-ACa) to investigate gas transport under abiotic conditions. Next, an MFC was developed, which provided biofilm inoculum for a bioanode paired with an abiotic carbon cathode (BAn-ACa). With cathode inoculum from a suspended growth enriched hydrogenotrophic methanogenic culture, described in Section 4.2.2, a biocathode with an abiotic carbon felt anode (AAn-BCa) was developed and evaluated. Finally, a developed bioanode was paired with a developed biocathode to form the BAn-BCa configuration and the carbon flow within and between the anode and cathode over the course of a 7-d feeding cycle was assessed.

Table 4.1 - Description of BES configurations used in this study.

BES Configuration	Applied Voltage (V)	Anode Type	Cathode Type	Anode Inoculum	Cathode Inoculum
Stock MFC	None	Bioanode	Platinum air cathode	MFC ^a	NA
AAn-ACa #1, 2	None	Abiotic carbon felt	Abiotic carbon felt	NA ^b	NA
BAn-ACa	-0.80	Bioanode	Abiotic carbon felt	Stock MFC	NA
AAn-BCa	-0.80	Abiotic carbon felt	Biocathode	NA	EHM ^c
BAn-BCa	-0.80	Bioanode	Biocathode	BAn-ACa bioanode	AAn-BCa biocathode

^a MFC fed with synthetic wastewater composed of furfural, 5-hydroxymethyl-furfural, syringic acid, vanillic acid and 4-hydroxybenzoic acid (Zeng et al., 2015).

^b NA, not applicable.

^c EHM, an enriched hydrogenotrophic methanogenic, suspended growth culture, developed from a stock, mixed methanogenic culture by feeding only H₂ and CO₂ (80:20, v/v; see Section 4.2.2).

4.2.2 *Biocathode Inoculum (EHM suspended growth culture)*

The biocathode inoculum was an enriched hydrogenotrophic methanogenic (EHM) suspended growth culture. The inoculum for the EHM culture was obtained from a stock mixed methanogenic culture, previously developed with inoculum from a mesophilic, municipal anaerobic digester. The stock culture was incubated at 35°C, had a retention time of 35 d and was fed with a mixture of dextrin and peptone, along with anaerobic medium (Okutman Tas and Pavlostathis 2005) over a period of several years. To develop the EHM culture, which was then used as biocathode inoculum, 1.5 L sample of the stock methanogenic culture was combined with 0.5 L of catholyte medium (100 mM phosphate

buffer, pH 7.0; NH₄Cl, 0.31 g/L; KCl, 0.13 g/L, mineral stock 12.5 mL/L and catholyte vitamin stock 5 mL/L) (Cheng et al. 2009). The EHM culture was fed five times per week by adding a mixture of hydrogen (H₂) and CO₂ (80:20, v/v) to the headspace, up to a total pressure of 1.65 atm. The EHM culture was wasted once per week for a retention time of 7 d and the wasted volume was replaced with catholyte medium, pre-degassed by bubbling with N₂ for 1 h. Then, the headspace of the EHM culture was flushed with the H₂/CO₂ mixture and pressurized to 1.65 atm.

4.2.3 Gas and Carbon Transport

To better understand gas transport across the PEM, the rate of appearance or disappearance of common headspace gases (N₂, CO₂, H₂, and CH₄) was assessed for systems with abiotic components (AAn-ACa, BAn-ACa, AAn-BCa). N₂ is often used for flushing to create anoxic conditions. In the AAn-ACa #1 system, the anode headspace was flushed with 100% N₂ and the cathode headspace was flushed with 100% CO₂ to approximate initial conditions in a batch BES system. In the AAn-ACa #2 system, the anode headspace initially contained 100% N₂ and the cathode headspace contained a mixture of CO₂ (17%), CH₄ (40%), and H₂ (42%) to approximate a mixed-gas condition during a feeding cycle. To prevent O₂ from entering the system, each chamber was maintained under a low positive pressure (≥ 0.10 atm) relative to atmospheric pressure. Routine gas analysis did not detect O₂ in the headspace gas (effective detection limit 0.07% O₂). To obtain an estimate of the maximum rate of gas transport, triplicate measurements of headspace gas pressure and composition were taken after 1-d incubation, as the net driving pressure (NDP) was greatest at the start of incubation. Measured rates were normalized to the PEM surface area and the mean NDP, as discussed in Section 4.2.4. After

evaluating initial fluxes, the systems continued to be monitored over the course of a 7-d period.

A typical 7-d feeding cycle of the BAn-BCa system was monitored to evaluate system-wide carbon flow. Anode and cathode samples were taken initially and on days 1, 3, 5, and 7, and analyzed for acetate, CO₂ (aq), CO₂ (g), and CH₄ (g). Protein analysis of the suspended biomass in the anolyte and catholyte was conducted only at the end of a cycle due to the limited volume of anolyte and catholyte available. Protein analysis of the biofilm was only conducted at the end of the cycle to avoid any disruption caused by the removal of carbon felt from the electrode. To further quantify the suspended biomass, volatile suspended solids (VSS) measurements of the suspended biomass in the anolyte and catholyte were conducted at the end of the cycle. Protein and VSS were not present in the anolyte and catholyte initially, allowing for the estimation of net biofilm and suspended biomass growth during the feeding cycle.

4.2.4 Normalization of Gas Rates to Membrane Surface Area and Mean Net Driving Pressure (NDP)

The rate of appearance or disappearance of each gas in the anode and cathode headspaces was determined by taking gas pressure and composition measurements over time. In a BES system like the one shown in Figure 4.1, the transfer of a gas across a PEM is limited by its surface area. Thus, to take this into account, rates were normalized to the surface area of the PEM, resulting in a gas flux.

Furthermore, gas transfer between anode and cathode is driven by the concentration gradient of that gas in solution on each side of the PEM (i.e., anolyte and catholyte).

However, accurate dissolved gas concentrations may be difficult to obtain. If the anode and cathode are assumed to be well-mixed systems and gas/liquid mass transfer is assumed to be sufficiently rapid, then the concentration of the dissolved gas in the anolyte or catholyte may be related by Henry's Law to the partial pressure and total pressure of the gas in the headspace. Thus, the driving force of gas transport across the PEM may be approximated by the net driving pressure (NDP), which is the difference in partial pressures times the total pressure of a gas between the anode and cathode headspace. Over a short period of time, gas partial pressure and NDP change may each be assumed to vary linearly; thus, a mean NDP over a 1-d period was calculated and used to normalize gas fluxes to the mean NDP. It must be noted that in the case where a source or sink for a gas exists within the anolyte or catholyte (i.e., biofilm), the chemical or biological activity may keep the concentration of a dissolved gas at disequilibrium with the concentration in the headspace. In this case, the partial pressure and, in turn, the NDP, may not be a sensitive measure of the true driving force of gas transfer across the PEM.

4.2.5 Theoretical Estimation of Biomass Growth and Cell Lysis Products

Due to experimental limitations, the biofilm biomass growth and cell lysis products were not directly measured to be incorporated in the carbon balance. However, these parameters may be estimated using cell growth relationships and published biomass growth yield values.

First, the anode biomass growth was estimated. At the end of the 7-d incubation cycle, protein analysis indicated 85% of the total biomass in the anode was biofilm-associated and the remaining 15% was suspended. Using VSS measurements of the

suspended biomass and assuming a biomass composition of $C_5H_7O_2N$, 2.00 mmol carbon as suspended biomass was estimated to be present. Therefore, as biofilm represented 85% of the total biomass, 11.31 mmol carbon was estimated to be present in the biofilm at the end of incubation. Because fresh anolyte was used at the start of incubation (i.e., no suspended biomass), all of the final suspended biomass was considered to be suspended biomass growth. However, only a portion of the biomass in the biofilm at the end of the cycle was from net growth during the cycle. Therefore, to estimate the biomass growth, the net specific growth rate was calculated to be $1.44E-03\text{ d}^{-1}$ using literature values for the true yield, observed yield and decay rate for exoelectrogens (Wilson and Kim, 2016). Assuming the growth rate followed first-order kinetics, a total increase in biofilm biomass of 0.11 mmol carbon was estimated. Thus, a total of 2.11 mmol carbon was estimated to be in the form of net biomass (suspended and biofilm-associated) at the end of the feeding cycle.

Next, the cathode biomass growth was estimated. Based on protein analysis, the biofilm-associated and suspended biomass represented 89% and 11% of the total biomass in the cathode, respectively. Based on VSS measurements, 2.74 mmol carbon was calculated to be present as suspended biomass at the end of 7-d incubation. Therefore, the biofilm biomass was estimated to contain 22.15 mmol carbon at the end of incubation. However, not all of the biofilm biomass represented growth during the 7-d incubation. Therefore, an estimated yield coefficient for hydrogenotrophic methanogens was used (0.45 g VSS/g H_2) to first estimate the true yield of biomass (Rittmann and McCarty, 2001) based on the amount of H_2 required to produce the total yield of CH_4 . An estimated decay coefficient of 0.03 d^{-1} was used as a middle approximation for anaerobic microorganisms.

Assuming growth and decay followed first-order kinetics, the observed growth of the cathode biofilm biomass represented 0.61 mmol carbon over the 7-d cycle. Thus, a total of 3.35 mmol carbon was estimated to be related with net biomass growth (suspended and biofilm) at the end of the 7-d feeding cycle.

Cell lysis products were another form of carbon not directly measured. Cell lysis products may be utilized by other microorganisms and re-enter the carbon cycle. However, to estimate cell lysis products, it was assumed that they were formed from decayed biomass and were conserved in the system. Cell lysis/decay was assumed to occur following first-order kinetics with a decay coefficient of 0.013 d^{-1} for exoelectrogens at the anode biofilm and 0.05 d^{-1} for all other anaerobic microorganisms (suspended and cathode biofilm). Given the estimated anode biomass, cell lysis products were estimated to represent 0.36 mmol carbon. In the cathode, total cell lysis products were estimated to represent 0.78 mmol carbon.

4.2.6 Analytical Methods

Dissolved CO_2 was measured as described in Section 3.1.9. Henry's law constants (K_H) for N_2 , CO_2 , CH_4 and H_2 in the phosphate buffer medium used for the catholyte and anolyte were calculated by correcting mean reported K_H values for each gas in DI water for temperature and ionic composition of the medium. A mean and standard deviation was calculated for reported K_H values compiled by Sander (2015). K_H values were then corrected for a temperature of 22°C using the van't Hoff equation and reported constants (Sander 2015). The K_H values were then corrected for the medium inorganic (i.e., salt)

components following the method of Weisenberger and Schumpe (1996). The corrected K_H values used in this study are listed in Table 4.2.

Table 4.2 - Henry's Law Constants Corrected for Temperature and Ionic Strength

Gas	K_H (atm/M)	No. of reported values (n)
Nitrogen (N ₂)	18.0 ± 0.8 ^a	2
Carbon dioxide (CO ₂)	31.9 ± 3.2	22
Methane (CH ₄)	776.4 ± 162.9	28
Hydrogen (H ₂)	1424.6 ± 14.5	7

^a Mean ± standard deviation.

Dissolved N₂, H₂, and CH₄ were calculated using the Henry's law constants in Table 4.2 assuming equilibrium. Biofilm and suspended growth protein were measured as described in Section 3.1.10.

4.3 Results and Discussion

4.3.1 BES Performance -- Comparison of Different Configurations

A stock MFC was developed with a bioanode and an air cathode. Over a typical cycle, the bioanode pH decreased from 6.9 to 6.3 and the mean acetate removal was 71±17% per 7-d cycle over the course of the initial 14, weekly feeding cycles. MFC acetate concentration and current density during a typical cycle are shown in Figure 4.3A. Some acetate was mineralized to CO₂, as shown by the increasing CO₂ concentration in the MFC headspace (Figure 4.3B), although only 0.1% of the acetate carbon removed was recovered as headspace CO₂. CH₄ was not detected in the MFC headspace.

A bioanode paired with an abiotic cathode (BAn-ACa) was developed using a biofilm-bearing clipping from the stock MFC bioanode. During a typical feeding cycle, the pH of the BAn-ACa anolyte and catholyte remained between 6.7 and 6.8; the mean anode potential was 0.98 ± 0.23 V. During the 7-d incubation, the anode removed 82% of the initial acetate, with 69% removal in the first day, indicating an initial period of rapid acetate uptake. However, when acetate removal was slower, substantial current was still maintained (Figure 4.3C). For example, 85% of the acetate removed during the 7-d feeding cycle was removed during the first day; however, only 24.5% of the total electrons transferred as current during the cycle were transferred during the first day, implying carbon storage in the bioanode biofilm. Freguia et al. (2007) found that during high-substrate consumption periods in MFC bioanodes (i.e., immediately following a batch feeding), acetate may be converted into carbon storage polymers that are later oxidized when acetate concentrations are low. The results of the present study are consistent with the conversion of acetate to carbon storage polymers and the peak in current density on day 2 may represent a metabolic shift from microbial oxidation of acetate to oxidation of carbon storage polymers.

The gas composition in the headspace of the BAn-ACa anode is shown in Figure 4.3D. The anode headspace concentration of CO_2 and H_2 increased linearly due to gas transport from the cathode. The gas composition in the headspace of the BAn-ACa cathode is shown in Figure 4.3E. In the cathode, headspace CO_2 declined by 80% over the first day of incubation due to significant CO_2 dissolution into the catholyte and then declined at a rate similar to the rate of CO_2 appearance in the anode headspace, indicating that dissolution into the catholyte was relatively fast compared to transport through the PEM.

Over the course of the 7-day incubation, the cathode headspace CO₂ decreased by 91%. In contrast, H₂, which was produced abiotically at the cathode, increased linearly ($R^2 = 1.00$) in the cathode headspace at a mean rate of 1.18 ± 0.01 mmol/L-d (normalized to the cathode liquid volume). Stoichiometrically and ignoring microbial growth, four moles of H₂ are required for the production of one mole of CH₄ via hydrogenotrophic methanogenesis. Therefore, in the absence of biocatalysis, the abiotically-produced H₂ would account for 0.30 ± 0.001 mmol/L-d CH₄, as CH₄ equivalents (Table 4.3).

Table 4.3 - Initial Rate and Total Methane Production by Various BES Configurations.

BES Configuration	Rate^b (mmol CH₄/L-d)	Total^c (mmol CH₄/L)
BAn-Aca ^d	0.30	2.08
AAn-BCa	3.29	9.90
BAn-BCa	3.85	10.87

^a Mean values of 3 technical replicates (variation < 3%).

^b Rate of CH₄ production over the first day of incubation, normalized to the catholyte volume based on cathode headspace CH₄ data.

^c Total CH₄ produced over 7 d of incubation, normalized to the catholyte volume based on cathode headspace CH₄ data.

^d Equivalent CH₄ estimated based on H₂ abiotically produced at the cathode and the stoichiometric ratio of 4 mol H₂:1 mol CH₄.

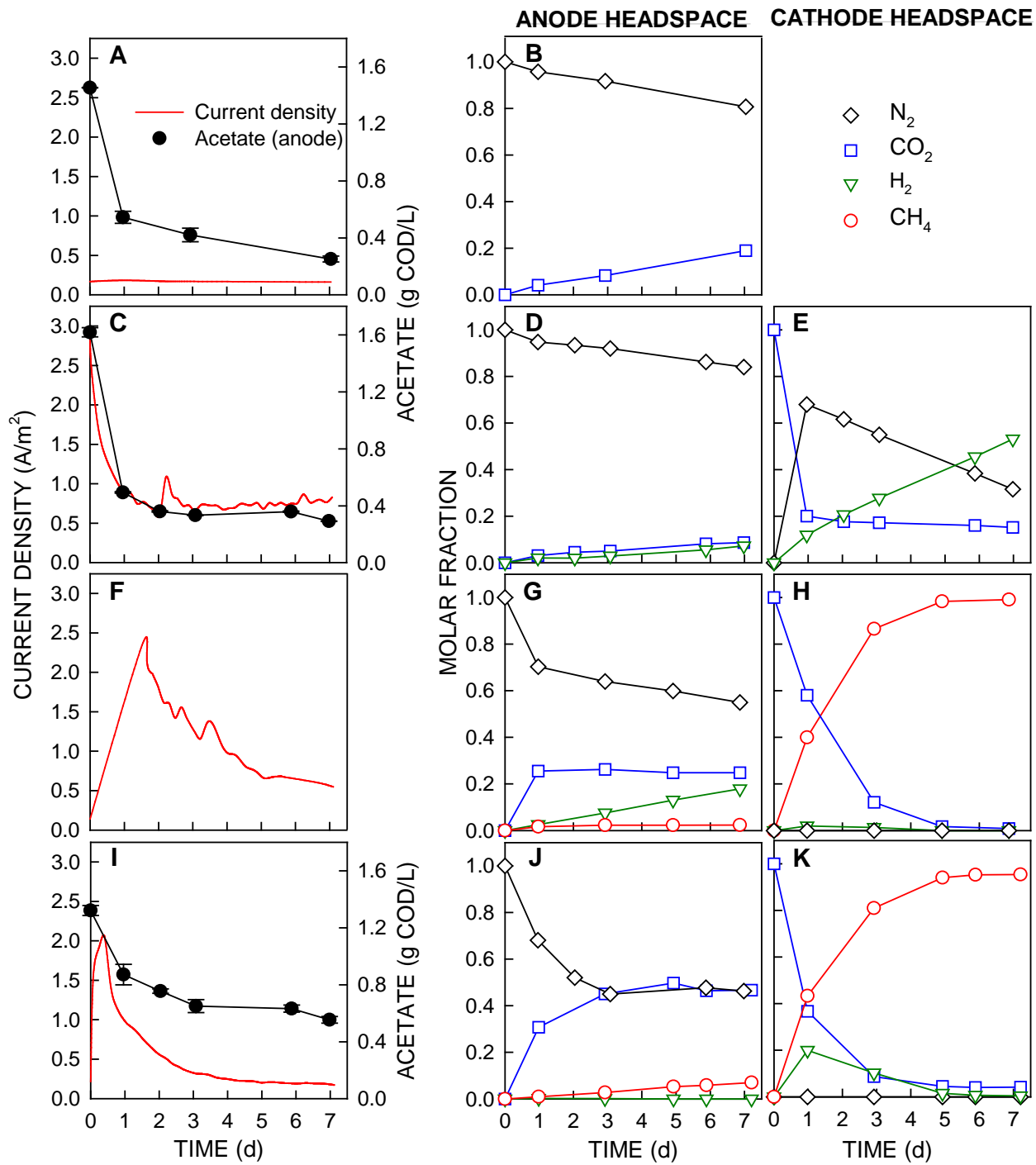


Figure 4.3 - Activity profiles of the MFC (A, B) and BES configurations BAn-ACa (C, D, E), AAn-BCa (F, G, H), and BAn-BCa (I, J, K) during a typical 7-day feeding cycle.

An abiotic anode with biocathode (AAn-BCa) BES was established by inoculating a carbon felt cathode with the EHM culture. The anode and cathode pH varied from 6.7 to 6.8 and from 6.7 to 7.1, respectively. The oxidizing conditions at the abiotic anode caused the anode stainless steel rod to undergo pitting corrosion (Figure 4.4). In this process, pits developed due to metal oxidation on the surface of the rod at sites of imperfections and the microenvironment inside the pit allowed the metal to act as an electron donor and propagate corrosion (Refaey et al. 2005). Thus, the stainless steel rod acted as a sacrificial anode during BES operation in the AAn-BCa configuration. The mean anode potential over a typical feeding cycle was 1.12 ± 0.16 V. The AAn-BCa current density profile was similar to that of the biocathode substrate, CO₂ (Figure 4.3F, H). Examination of the abiotic anode headspace indicated transport of CO₂, CH₄, N₂, and H₂ across the PEM (Figure 4.3G, H). The mean rate of AAn-BCa biocathode CH₄ production over the first day following feeding, as well as the total CH₄ produced over the 7-d feeding cycle are given in Table 4.3. Although the 1-d AAn-BCa mean CH₄ production rate was more than 10-fold greater than the CH₄ equivalents of abiotically produced H₂, as calculated for the BAn-ACa system, the total CH₄ produced was only about 5-fold greater (Table 4.3), likely due to substrate (i.e., CO₂) limitations. Regardless, the microbial activity on the biocathode substantially enhanced the rate of CH₄ production, in terms of electron equivalents, over that expected from abiotic H₂ production alone. This result could be due to direct electron transfer to Archaea, the production of electron shuttles or microbial catalysis of H₂ production at the cathode.

Finally, a BAn-BCa system was set up. The anode and cathode pH varied from 6.6 to 6.8 and from 6.7 to 7.0, respectively. Ammonia declined from an initial value of 72.8

mg N/L in both the anode and cathode chambers and remained between 70.0 and 67.2 mg N/L in the anode and cathode chambers, respectively, during a typical 7-day feeding cycle. Low ammonia utilization supports the relatively low biomass growth developed in the system, consistent with the growth of anaerobic and exoelectrogenic microorganisms (Wilson and Kim, 2016). The mean anode potential was 1.00 ± 0.10 V. The anode acetate concentration declined more slowly than in other bioanodes and the peak current density occurred 0.5 d into the incubation (Figure 4.3I). In contrast, the peak current density in the BAn-ACa configuration occurred immediately upon feeding, suggesting that the presence of a biocathode affected the current density profile. The peak current density in the AAn-BCa configuration occurred at 2 d, which may be due to the formation of pits on the stainless steel rod electrode. Spikes in current density after day 2 may represent additional pitting, which facilitated corrosion and electron transfer.



Figure 4.4 - Pitting corrosion of the anode stainless steel rod in the AA-BC BES configuration.

The BAn-BCa anode headspace gas composition (Figure 4.3J) displayed an initial rapid increase in CO_2 , followed by a decreasing rate of CO_2 increase, likely due to acetate/carbon oxidation, as evidenced by the decreasing acetate concentration, and/or transport of CO_2 across the PEM. As observed in the AAn-BCa biocathode, gas transport

through the PEM was also evident during BES operation; CH₄ and H₂ from the cathode entered the anode, while N₂ from the anode crossed into the cathode. H₂ appeared transiently in the BAn-BCa cathode headspace (Figure 4.3K), but was not detected on day 5. Detection of transient H₂ during the start-up period of electromethanogenic biocathodes has been previously reported (Rotaru et al., 2014; Villano et al., 2010; Villano et al., 2011). Initially, CO₂ declined in the BAn-BCa cathode headspace more rapidly than in the AAn-BCa biocathode, but the final BAn-BCa cathode CO₂ headspace concentration was greater than the final CO₂ headspace concentration in the AAn-BCa cathode. At the end of the BAn-BCa feeding cycle, the cathode CO₂ concentration became the limiting substrate, even as anode acetate concentrations remained above levels observed in the MFC and BAn-ACa anode. In the reverse situation, anode conditions may also affect biocathode operation, as further described in Section 4.3.2. Thus, biofilm activity at one electrode affects biofilm activity at a partner electrode resulting in an overall performance that reflects the integration of sub-processes in an interconnected bioelectrochemical system.

The 1-d mean CH₄ production rate in the BAn-BCa cathode was slightly greater than in the AAn-BCa cathode (Table 4.3). The maximum CH₄ production rates in the AAn-BCa and BAn-BCa biocathodes were 1,335.2±0.7 and 1,561.7±53.6 mmol/d-m², respectively. These rates are normalized to the PEM area to compare with literature reported CH₄ production rates. Cheng et al. (2009) first reported a biocathode CH₄ production rate of 200 mmol/d-m² when the cathode was poised at -0.8 V. At a greater poised potential of -0.9 V, Villano et al. (2010) reported a CH₄ production rate of 1,067 mmol/d-m². Fu et al. (2015) reported a thermophilic biocathode poised at -0.8 V with a CH₄ production rate of 1,103 mmol/d-m². Zhen et al. (2015) reported a methanogenic

biocathode poised at -0.9 V achieved a 5-h maximum CH₄ production rate of 1,519 mmol/d-m². Compared to the previously reported rates, the BAn-BCa biocathode in the present study achieved a similar rate of CH₄ production over the course of 1-d at an applied potential of -0.8 V.

The Coulombic efficiency (CE) and cathode capture efficiency (CCE) of each system over a typical 7-d feeding cycle are given in Table 4.4. CE represents the fraction of cumulative electron equivalents produced from the oxidation of acetate transferred as cumulative electric charge. CCE represents the fraction of cumulative electron equivalents transferred as electric charge recovered as cumulative CH₄ equivalents. The highest CE and CCE values were achieved by the BAn-BCa configuration, indicating a synergistic effect between bioanode and biocathode. In the MFC, the CE was relatively low, which may be due to O₂ entering through the air cathode membrane, although no O₂ was detected in the MFC headspace. In the BAn-ACa configuration, the CE was lower than in the MFC, indicating either a less efficient anode biofilm or a greater conversion of acetate to carbon storage polymers, which would mean acetate removal was greater than the total carbon oxidation in the anode, thus leading to an underestimation of the CE. Regardless, the applied potential in the BAn-ACa abiotic cathode was capable of producing H₂ at a high CCE (97.8%) from water electrolysis, indicating very low energy is lost in this reaction. Similarly, the BAn-BCa had a high CCE, indicating efficient methanogenesis. However, despite a similar total CH₄ production to that of the BAn-BCa biocathode, the AAn-BCa biocathode had a very low CCE (5.7%) because of relatively high current sustained in the system, likely due to accelerated corrosion of the anode rod.

Table 4.4 - Coulombic Efficiency (CE) and Cathode Capture Efficiency (CCE) of Various BES Configurations Tested in this SStudy.

BES Configuration	CE (%)	CCE (%)
MFC	25.1	NA ^a
BAn-ACa	8.8	97.8
AAAn-BCa	NA ^b	5.7
BAn-BCa	56.6	97.6

^a NA, not available; the MFC CCE could not be calculated because the reaction product (H₂O) could not be quantified in the air cathode.

^b NA, not available; the AAAn-BCa CE was not measured because the oxidation of the stainless steel anode rod could not be accurately quantified.

4.3.2 Bioanode Effects on Biocathode and Overall System Performance

To clarify the role of the bioanode in biocathode and overall system performance, a test was performed. The cathode potential was controlled by poisoning it at -0.8 V (vs. SHE) using an adjacent Ag/AgCl reference electrode, thus fixing the cathode potential. The anode voltage was not controlled and fluctuated depending on the anode conditions. Because the current was determined by the cell voltage, $E(\text{cell}): E(\text{cell}) = E(\text{cathode}) - E(\text{anode})$, the current may theoretically be affected by the anode potential, which in turn may be affected by the anode conditions. To test this hypothesis, the BAn-BCa system anode was fed acetate at three different concentrations (0.4, 1.0 and 1.6 g COD/L), while the cathode was consistently fed with CO₂ to an initial pressure of 1.85 atm. Anolyte and catholyte were exchanged for fresh media in between feedings to ensure consistent initial conditions with the exception of the anode acetate concentration. The system was incubated for 24 h to minimize the effect of biofilm changes. Current, voltage and methane production were monitored. At higher initial acetate concentrations, higher anode voltage and current density were observed. The mean current density for 0.4, 1.0 and 1.6 g COD/L

setups was 1.56, 1.92 and 2.04 A/m², respectively. Methane production was similarly affected, with production rates of 0.25, 0.32 and 0.37 mmol/L-d for setups fed with 0.4, 1.0 and 1.6 g COD/L, respectively. Therefore, the anode conditions affected the current and, indirectly, the biocathode performance.

4.3.3 Evaluation of BES Gas Transport

The mean rates of gas appearance/disappearance in the headspace of BES configurations with one or two abiotic chambers (i.e., AAn-ACa, BAn-Aca, and AAn-BCa) over the course of 1 d, normalized to the PEM surface area and the mean NDP, are shown in Figure 4.5 and listed in Table 4.5. The BAn-BCa configuration was excluded from the flux evaluation because gas/liquid equilibrium was not achieved due to gas-consuming and gas-producing processes in the liquid phases, and, thus, the true NDP could not be assessed using headspace gas measurements. In the first abiotic configuration (AAn-ACa #1), the anode and cathode headspace initially contained only N₂ and CO₂, respectively. The 1-d decline of N₂ in the anode headspace (0.56 mmol) was slightly less than the N₂ increase in the cathode headspace (0.60 mmol), due to N₂ release from the catholyte, which was pre-saturated with N₂ during medium preparation. CO₂ appearance in the anode headspace was 25% slower than the decline of CO₂ in the cathode headspace due to CO₂ dissolution and retention by the medium. The calculated Henry's law constant for CO₂ in the anolyte and catholyte was 31.9±3.2 atm/M (Table 4.2), indicating a significant capacity for CO₂ dissolution. Indeed, after 7 d incubation to evaluate a near-equilibrium condition, only 45% of the total amount of CO₂ removed from the cathode headspace evolved in the anode headspace, with 55% remaining in the liquid anolyte and catholyte.

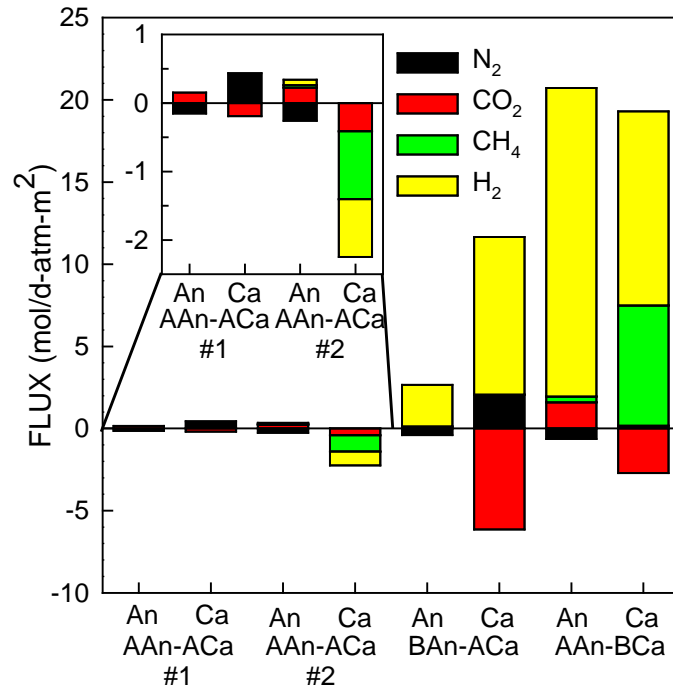


Figure 4.5 - Mean rates of gas appearance/disappearance in the anode (An) and cathode (Ca) headspace of the AAn-ACa #1, AAn-ACa #2, BAn-ACa and AAn-BCa BES configurations over the course of 1 d, normalized to the PEM surface area and the mean net driving pressure.

In the second abiotic configuration (AAn-ACa #2), the anode headspace was initially filled with 100% N₂ but the cathode headspace contained a mixture of CO₂, CH₄, and H₂ (18, 40, and 42%, respectively). Over 1 d incubation, N₂ declined in the anode headspace, but was not detected in the cathode headspace. Instead, gas was primarily transported from cathode to anode. There was a higher rate of CO₂ appearance in the anode headspace of AAn-ACa #2 than in AAn-ACa #1, suggesting that the transport of other gases through the PEM may increase CO₂ transport. Although H₂ is a smaller molecule, it appeared in the AAn-ACa #2 anode headspace at a lower rate normalized to NDP than CO₂, which may be due in part to the larger H₂ Henry's law constant (atm/M), meaning

that, at the same partial pressure, less H_2 will be dissolved than CO_2 , possibly leading to a slower transport through the PEM. Furthermore, CO_2 has been found to have greater reactivity with diamine carriers in the Nafion 117 PEM, which increases selectivity for CO_2 transport (Yamaguchi et al., 1996). CH_4 appeared in the AAn-ACa #2 anode headspace at the slowest rate, despite a similar mean NDP as H_2 , indicating PEM gas selectivity. In the cathode headspace of the AAn-ACa #2 configuration, there was a greater decline in CH_4 , H_2 , and CO_2 than was accounted for in the headspace of the anode because of dissolution and retention by the medium, which did not initially contain these dissolved gases.

Table 4.5 - Mean Rate of Increase (+) or Decrease (-) in Headspace Gas Over the Course of a 1 d Incubation, Normalized to PEM Surface Area and Mean Net Driving Pressure (NDP).

Gas	BES Configuration	Mean NDP (atm)	Mean Gas Rate (mmol/d-atm-m ²) ^{a,b}	
			Anode	Cathode
Nitrogen	AAn-ACa #1 ^c	0.920	-152.2	437.0
	AAn-ACa #2 ^c	1.077	-259.5	0.0
	BAn-ACa	0.740	-401.3	2,071.3
	AAn-BCa	0.898	-636.2	166.7
Carbon Dioxide	AAn-ACa #1 ^c	1.045	3.7	-191.1
	AAn-ACa #2 ^c	0.762	5.4	-413.7
	BAn-ACa	0.891 ^e	2.9 ^e	-6,144.4
	AAn-BCa	0.669 ^e	38.1	-2,711.3 ^e
Methane	AAn-ACa #1 ^c	NA ^d	NA	NA
	AAn-ACa #2 ^c	0.364	35.5	-990.3
	BAn-ACa	NA	NA	NA
	AAn-BCa	0.183 ^e	366.3	7,332.3 ^e
Hydrogen	AAn-ACa #1 ^c	NA	NA	NA
	AAn-ACa #2 ^c	0.386	80.5	-20.3
	BAn-ACa	0.028 ^e	2,544.2	230.6 ^e
	AAn-BCa	0.006 ^e	18,767.5	283.9 ^e

^a Gas rates normalized to the NDP and a PEM surface area of 6.16 cm².

^b Mean values of three technical replicates.

^c Configuration operated under open circuit conditions (i.e., no electrochemical reactions).

^d NA, not applicable (e.g., gas not present in the system).

^e Indicates presence of processes that either produce or consume gas and thus the NDP used for normalization may not be related to the concentration gradient actually driving gas transport.

In the BAn-ACa configuration, the bioanode and cathode headspaces were initially filled with N₂ and CO₂, respectively. H₂ was generated abiotically at the cathode and evolved to the headspace. The appearance of N₂ in the BAn-ACa cathode headspace was

greater than in the AAn-ACa #1 and #2 cathodes (Figure 4.5), which was likely due to a stripping effect, as the cathode-produced H₂ evolved in media pre-saturated with N₂. In the AAn-ACa #1 cathode, the theoretical dissolved N₂ concentration at equilibrium was 4.96 mM after 1 d incubation. Thus, the greater N₂ observed in the BAn-ACa cathode headspace after 1 d was equivalent to the removal of 2.88 mM, or 58% of the theoretically dissolved N₂. The appearance of H₂ in the anode headspace (0.18±0.02 mmol/L-d), due to transport across the PEM from the cathode, was faster than in the AAn-ACa #2 system (0.077±0.002 mmol/L-d), possibly due to the BAn-ACa cathode maintaining a high H₂ concentration in the catholyte, driving faster transport across the PEM. Unexpectedly, the appearance of CO₂ in the headspace of the BAn-ACa bioanode was slower than in the anode headspace of the abiotic configurations, despite the production of CO₂ in the bioanode and a greater mean NDP than in the AAn-ACa #2 configuration. CH₄ was not detected in the anode; thus, methanogenesis either did not take place or was negligible (effective detection limit 0.06% CH₄). Rather, the abundance of H₂ in the anode may have stimulated acetogenesis with the CO₂ generated in the bioanode and/or transported across the PEM from the cathode. Indeed, in a separate experiment, described in Section 4.3.5, acetogenesis was observed in the bioanode of the BAn-BCa system. The CO₂ demand from stimulated acetogenesis in the BAn-ACa bioanode would also explain the greater than expected rate of CO₂ decline in the cathode headspace, as a greater concentration gradient would form across the PEM, driving faster transport of CO₂.

In the AAn-BCa configuration, a biocathode was paired with an abiotic anode and voltage was applied, which caused the anode's stainless steel rod to act as a sacrificial anode and undergo pitting corrosion (Figure 4.4). The anode and cathode headspaces were

initially filled with N_2 and CO_2 , respectively. N_2 decline in the AAn-BCa anode headspace was faster than in the BAn-ACa anode headspace. The 1-d rate of N_2 appearance in the AAn-BCa cathode headspace was between the rates observed in the cathodes of AAn-ACa #2 and AAn-ACa #1. The 1-d rate of CO_2 removal from the headspace of the AAn-BCa cathode was 71% greater than the appearance of CO_2 in the anode headspace, indicating rapid CO_2 dissolution into the medium. Although CO_2 concentration in the cathode headspace was less than 15% following day 3, dissolved CO_2 would still be available for continued CH_4 production due to the relatively small Henry's law constant (atm/M) of CO_2 (Table 4.2). In the AAn-BCa biocathode, headspace H_2 concentration increased over 1 d incubation (Figure 4.5) and peaked at 2%. Afterwards, a decline in H_2 concentration was observed, indicating utilization of H_2 by methanogens. By day 4, H_2 was no longer detected in the biocathode headspace, yet the AAn-BCa abiotic anode headspace continued to experience a linear increase in H_2 , indicating continued H_2 transport across the PEM from the cathode. This observation indicates that dissolved H_2 was present in the catholyte but was not at equilibrium with the headspace because of the biocathode biological activity that consumed H_2 . The continued presence of dissolved H_2 in the catholyte, as evidenced by the continuous transport into the anode, suggests that H_2 is an important electron donor in biocathode CH_4 production, even when it is not detected in the cathode headspace. Over the course of 1 d incubation, the biocathode produced 0.80 mmol CH_4 and 0.04 mmol H_2 , representing 6.48 mmol electron equivalents. In contrast, the BAn-ACa abiotic cathode produced 0.16 mmol H_2 and no CH_4 over 1 d incubation, representing 0.32 mmol electron equivalents. Thus, the presence of biofilm on the AAn-BCa biocathode significantly increased the output of electron equivalents. At 7 d incubation, the total CH_4 production in

the BAn-BCa biocathode declined due to substrate (CO_2) limitations, though CH_4 production was still over 5-fold higher than the CH_4 equivalents of H_2 produced by the BAn-ACa cathode (Table 4.3).

In abiotic configurations, gas transport in a BES may be represented as shown in Figure 4.1. Two of the three processes that control gas transport (I and II; Figure 4.1) are driven by equilibria between liquid and gas phases. At these liquid-gas interfaces, transport occurs when the ratio of the gas partial pressure to dissolved gas concentration in the liquid phase is greater than or less than the Henry's law constant (i.e., disequilibrium). In contrast, the third process (III; Figure 4.1), can be approximated as a liquid-liquid interface, although the actual mechanism of gas diffusion through the PEM is much more complex. This third process may be represented as diffusion, which is controlled by a concentration gradient between the anolyte and catholyte. The concentration in the anolyte and catholyte, which sets up the concentration gradient, is in turn controlled by the gas partial pressure and total pressure in their respective headspaces. Thus, if a gas is equally soluble in the anolyte and catholyte, the consequence of a disparate gas composition in the headspace of the anode and cathode is that gas transport will occur until the partial pressure of the gas and total pressure are equal in the two headspaces. The rate of gas transport across the PEM is different for each gas and is also influenced by the gas solubility in the liquid phase as well as PEM selectivity. Thus, it is important that the mass transfer of gases be accounted in mass balances for systems under dynamic, i.e., non-equilibrium, conditions.

However, in the BAn-ACa and AAn-BCa configurations, biological or electrochemical processes either produced or consumed gases monitored in this study. For example, the bioanode of the BAn-ACa configuration oxidized acetate to CO₂, thus creating a source of CO₂ in the anolyte. In contrast, the biocathode of the AAn-BCa configuration reduced CO₂, producing CH₄. These dynamics mean that the NDP of a gas in the headspace may be an unreliable estimate of gas transport driving force because the concentration of dissolved gas in the liquid (e.g., anolyte or catholyte) may not be near equilibrium with its headspace partial pressure.

4.3.4 Evaluation of BES Carbon Transport

To better understand the carbon transport in a methanogenic BES, acetate, total dissolved CO₂, CO₂ (g), CH₄ (g), and CH₄ (aq) were assessed during a 7-d feeding cycle for the anode and cathode of a separate, established BAn-BCa system (Figure 4.6). Suspended growth biomass was only measured at the end of the cycle due to the large liquid volume required for such measurement; biofilm growth and cell lysis products were estimated as described in Section 4.2.5. The current density over the cycle (Figure 4.7) was greater than in other setups, more likely as a result of a larger quantity of CO₂ added to the cathode to reduce any possible substrate mass transfer limitations. In the anode chamber, the total assessed carbon declined significantly through day 3, due primarily to the disappearance of acetate, followed by a slow increase in assessed carbon. Over the course of 7 d, 99.2% acetate removal was achieved, with 92% removed during the first 24 h. The faster acetate removal in this BAn-BCa system than in the previously-described BAn-BCa system could be due to greater substrate availability in the cathode (e.g., higher current), biofilm differences in the anode and cathode and/or a larger degree of acetate conversion

to carbon storage polymers. Acetate was the largest fraction of the assessed carbon on the first day following feeding (Figure 4.6B). However, afterwards, aqueous inorganic carbon species were the predominant form of carbon measured, which remained relatively constant between day 3 and 7. The anode headspace CO_2 slowly increased over time as acetate and/or carbon storage polymers were oxidized and/or CO_2 transported from the cathode. Anode gaseous and dissolved CH_4 increased gradually, consistent with transport across the PEM from the cathode. Combined headspace and dissolved CH_4 represented only a small fraction (4%) of the total assessed carbon in the anode after 7 d incubation. Anode suspended biomass and net biofilm growth represented 38% and 2% of assessed anode carbon, respectively, at the end of 7 d incubation. However, biomass growth does not take into account carbon storage polymers or other intermediates, which may represent a substantial portion of the unaccounted carbon (Figure 4.6).

The types of carbon assessed in the cathode are shown in Figure 4.6B. Over the course of the first 24 h, the headspace CO_2 was removed primarily through dissolution into the catholyte, conversion to CH_4 , and possibly some transport across the PEM to the anode chamber (Figure 4.6B). During the first day of incubation, flux of CO_2 from cathode to anode is supported by the fact that the measured, dissolved CO_2 in the cathode was 36% greater than in the anode. Some cathode carbon may have also been converted to biomass, transient carbon storage polymers or an internal intermediate of methanogenesis (Freguia et al. 2007; Ni et al. 2015). However, following day 1, the total assessed cathode carbon increased throughout the remainder of the cycle, surpassing the initially assessed carbon by day 3. This result indicates additional input of carbon through the transport of dissolved CO_2 from the anode across the PEM to the cathode, or from cell lysis in the cathode

chamber. Flux of CO₂ into the cathode after day 1 is also supported by the fact that the actual dissolved CO₂ concentration in the anode was below the calculated equilibrium concentration based on the anode headspace measured CO₂ concentration. From day 1 to day 7, the cathode dissolved CO₂ concentration declined from 55% of that in the anode to 20%, supporting concentration-driven transport of CO₂ from anode to cathode. Moreover, after 7 d of incubation, the gaseous CH₄ in the biocathode headspace was 27% greater on a molar basis than the initial CO₂ added to the biocathode, indicating conversion of CO₂ produced by the anode and transported to the biocathode. When dissolved CH₄ in the catholyte was accounted for, the final CH₄ production in the cathode was 40% greater on a molar basis than the initially added carbon to the cathode.

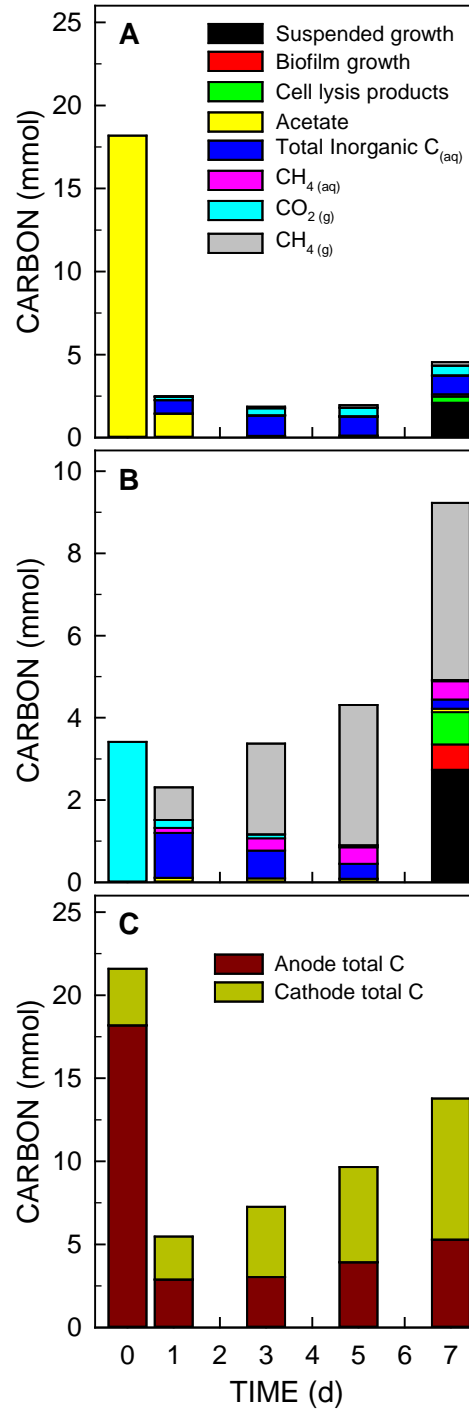


Figure 4.6 - Time course of carbon species (suspended and biofilm growth, cell lysis products, acetate (aq), total inorganic carbon (aq), CH₄ (aq), CO₂ (g), and CH₄ (g)) during a feeding cycle in the BAN-BCa anode (A), cathode (B) and whole system (C).

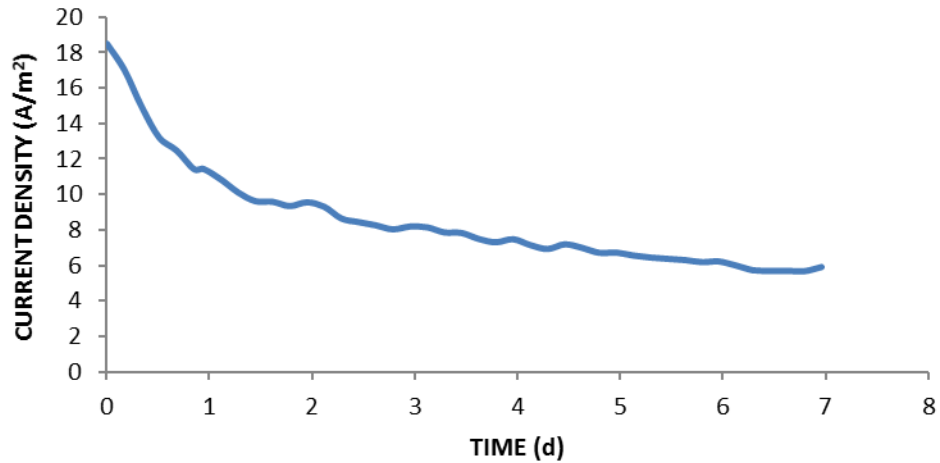


Figure 4.7 - Time course of current density during carbon flow analysis of the BA-BC BES configuration.

At the end of the 7-d incubation, suspended biomass and biofilm net growth represented 32% and 7% of the total assessed carbon, respectively. However, microbial carbon storage polymers and methanogenesis intermediates were not measured and thus not accounted for. Protein analysis of suspended and biofilm biomass in the cathode showed that 89% of total biomass was biofilm-associated, with only 11% as suspended biomass. Acetate, which could have originated from acetogenesis (see Section 4.3.5) or from the migration of acetate across the PEM from the anode chamber (Chae et al. 2008, Nevin et al. 2011), was detected at trace levels in the cathode (≤ 23.4 mg COD/L). The cathode headspace CH_4 concentration increased at a nearly linear rate of 2.6 ± 0.1 mmol/L-d ($R^2 = 0.979$) over the duration of the feeding cycle, indicating CO_2 was not limiting throughout the incubation period. Normalized to the PEM surface area, the cathode headspace CH_4 increased at $1,070 \pm 46$ mmol/d-m², which is similar to previously reported

CH₄ production rates in methanogenic cathodes (Fu et al., 2015; Villano et al., 2010; Zhen et al., 2015).

Figure 4.6C illustrates that a complete carbon balance was not achieved, which is more likely due to the formation of carbon storage polymers and intermediates. On the 7th day of incubation, the total assessed carbon represented only 55% of the initially supplied carbon to the system (i.e., both anode and cathode). While not directly measured, microbial carbon storage is implied by the initial decrease of total assessed carbon over the first day, followed by the gradual increase in total assessed carbon over the remainder of the feeding cycle. Additionally, the relatively modest decline in current density (Figure 4.7) and continued increase of the anode CO₂ concentration over the course of the cycle (Figure 4.6), indicate that a carbon source other than acetate continued to be oxidized in the anode throughout the cycle. The carbon balance showed an overall transport of carbon from anode to cathode (Figure 4.6A). Although 84% of the carbon initially added to the system was in the anode, at the end of the 7-day incubation, only 38% of system-wide total assessed carbon was in the anode, with the remaining 62% in the cathode.

4.3.5 *Demonstration of Biocathode Acetogenesis*

To better understand the origin of acetate observed in the biocathode at the end of a feeding cycle, an experiment was conducted with the un-fed (i.e., no acetate added) BAn-BCa bioanode, which was supplied with new media and flushed with CO₂ (70%) and H₂ (30%), simulating a condition in which H₂ and CO₂ are available in the anode, primarily due to H₂ transport across the PEM from the cathode. The cathode was flushed with 100% CO₂ and the system was incubated for 1 d under open circuit conditions to exclude

electrochemical reactions. The relatively short (1 d) incubation period was intended to minimize changes in the anode and cathode biofilm communities. During the course of incubation, the anode acetate concentration increased by 0.123 ± 0.009 mM, indicating acetogenesis occurred under conditions where H_2 and CO_2 were available. Acetate was not detected in the cathode after 1 d incubation; however, a small amount of CH_4 , corresponding to acetogenic methanogenesis from 0.041 mM acetate, was detected in the cathode. Although the CH_4 produced in the cathode could be due, in part, to hydrogenotrophic methanogenesis utilizing H_2 produced from the fermentation of dead biomass, it is likely that some of the produced CH_4 was due to acetoclastic methanogenesis of acetate that diffused from the anode to the cathode.

4.4 Summary

Bioelectrochemical systems (BESs) may be used to upgrade anaerobic digester biogas by directly converting CO_2 to CH_4 . The objective of this study was to evaluate gas (N_2 , CO_2 , CH_4 , and H_2) and carbon transport within a methanogenic BES. Four BES configurations were evaluated: abiotic anode with abiotic cathode (AAn-ACa), bioanode with abiotic cathode (BAn-ACa), abiotic anode with biocathode (AAn-BCa), and bioanode with biocathode (BAn-BCa). Transport of N_2 , a gas commonly used for flushing anoxic systems, out of the anode headspace ranged from 3.7 to 6.2 L/d-atm- m^2 , normalized to the proton exchange membrane (PEM) surface area and net driving pressure (NDP). CO_2 was transported from the cathode to the anode headspace at rates from 3.7 to 5.4 L/d-atm- m^2 . The flux of H_2 from cathode to anode headspace was 48% greater when the system had a biocathode (AAn-BCa) than when H_2 was produced at an abiotic cathode (BAn-ACa), even though the abiotic cathode headspace had 75% more H_2 than the AAn-BCa biocathode at

the end of 1 d. A 7-d carbon balance of a batch-fed BAn-BCa BES showed transient microbial carbon storage and a net transport of carbon from anode to cathode. After a 7-d batch incubation, the CH₄ production in the biocathode was 27% greater on a molar basis than the initial CO₂ supplied to the biocathode headspace, indicating conversion of CO₂ produced in the anode. This research expands the current understanding of methanogenic BES operation, which may be used in improving the assessment of BES performance and/or in the development of alternative BES designs and mathematical models. Gas transport across a BES PEM affects the overall transport of gases between the anode and cathode chambers. Biological activity at one electrode affects the biological activity at the partner electrode, and in turn affects the overall BES performance. Therefore, gas and carbon transport rates must be taken into account for accurate BES characterization, particularly when substrates and/or products are gases. The results of this study expand our current understanding of methanogenic BES operation, which may be used in improving the assessment of BES performance and/or in the development of alternative BES designs as well as mathematical models.

CHAPTER 5. METHANOGENIC BIOCATHODE MICROBIAL COMMUNITY DEVELOPMENT AND THE ROLE OF BACTERIA

5.1 Introduction

Biogas produced by anaerobic digestion contains a mixture of carbon dioxide (CO₂), methane (CH₄) and other trace gases. To increase the energy content (i.e., CH₄) of biogas, current methods separate or sequester CO₂, resulting in a waste product (Muñoz et al. 2015). Instead, bioelectrochemical systems (BESs) may be utilized to directly convert biogas CO₂ to CH₄ (Geppert et al. 2016). A methanogenic BES pairs an oxidation reaction in the bioanode with the overall reduction of CO₂ to CH₄ in the biocathode in a process termed electromethanogenesis (Cheng et al. 2009). Methanogenesis in the biocathode may proceed via several known mechanisms. Hydrogen (H₂), produced at the cathode from the reduction of protons: $2\text{H}^+ + 2\text{e}^- \rightleftharpoons \text{H}_2$ ($E_{\text{H}}^{\circ} = -0.421$ V vs. standard hydrogen electrode, SHE; pH 7), may be utilized by hydrogenotrophic methanogens to reduce CO₂: $\text{CO}_2 + 4\text{H}_2 \rightleftharpoons \text{CH}_4 + 2\text{H}_2\text{O}$ ($\Delta E_{\text{H}}^{\circ} = 0.170$ V). At an applied voltage sufficient to overcome thermodynamic limitations and losses, H₂ may be produced abiotically at a cathode. However, in biocathodes, H₂ production may also be catalyzed by extracellular enzymes, providing an electron donor for methanogenesis at a smaller applied potential (Deutzmann et al. 2015, Yates et al. 2014). Electrons may also be transferred from the cathode to other mediators that, in turn, act as electron donors for the microbial reduction of CO₂. Alternately, direct electron transfer from the cathode to methanogens may occur: $\text{CO}_2 + 8\text{H}^+ + 8\text{e}^- \rightleftharpoons \text{CH}_4 + 2\text{H}_2\text{O}$ ($E_{\text{H}}^{\circ} = -0.224$ V vs. SHE; pH 7) (Lohner et al. 2014).

Methanobacterium and, in some cases, *Methanobrevibacter*, dominate biofilms of methanogenic biocathodes (Cheng et al. 2009, Siegert et al. 2014, Siegert et al. 2015, Zhen et al. 2015). While Archaea are undoubtedly important in a methanogenic biocathode, Bacteria may also play a significant role. Some Bacteria may function as anchors for electrode biofilm development, particularly species that can withstand direct current and strongly adhere to surfaces, such as *Sphingomonas* spp. and *Mycobacterium frederiksbergense* (Johnsen and Karlson 2004, Shi et al. 2008, Wick et al. 2004, Wick et al. 2007). Fermentative Bacteria that produce H₂ and CO₂ could potentially recycle cell lysis products into substrate for methanogens, thus improving CH₄ yield. Furthermore, some Bacteria may produce mediators that can act as electron shuttles (Logan 2009, Pham et al. 2008, Rabaey et al. 2005), potentially improving CH₄ production by biocathode methanogens. Bacteria may also be exoelectrogens capable of cathode biocatalytic H₂ formation (Geelhoed and Stams 2010). Although typically found in anodes, exoelectrogens could also potentially act as endogenous anodes that recycle electron equivalents from organic compounds within the biocathode.

Although many species may be beneficial to biocathode methanogenesis, some types of Bacteria could divert the electron flow within a system away from methanogenesis, reducing biocathode efficiency and CH₄ yield. If acetoclastic methanogens are not present and/or not active in the biocathode, acetogens may act as H₂/CO₂ scavengers and divert electron equivalents away from the desired product, CH₄. Although fermentative Bacteria can recycle cell lysis organic compounds and enhance methanogenesis if H₂ and/or CO₂ are produced, other species transfer electron equivalents to volatile fatty acids (VFAs) that must undergo further fermentation, thus slowing the

ultimate flow of electron equivalents to CH₄. For example, *Moorella thermoacetica* ferments glucose into acetate nearly stoichiometrically, without producing H₂ or CO₂ (Küsel and Drake 2011). Moreover, acetogens such as *Clostridium aceticum*, may convert H₂ and CO₂ into acetate, removing substrate from hydrogenotrophic methanogens (Küsel and Drake 2011). In addition, biofilm-forming Bacteria may physically impede the mass transfer of gases to and from methanogens. Bacteria may also affect methanogenesis in other ways that are not currently understood.

While several studies have examined the predominant Archaea in methanogenic biocathodes, little is known about the role of Bacteria. Using anaerobic digester sludge and bog sediment as separate inocula, Siegert et al. showed that the archaeal community of methanogenic biocathodes converged on hydrogenotrophic methanogens, *Methanobacterium* and *Methanobrevibacter* (Siegert et al. 2014). Other studies have reported similar results (Cheng et al. 2009, Siegert et al. 2014, Siegert et al. 2015, Zhen et al. 2015) Bacterial communities have also been reported in biocathodes (Li et al. 2016b, Siegert et al. 2014, Siegert et al. 2015), but it is not yet understood how the bacterial community of a culture changes through inoculum pre-enrichment for hydrogenotrophic methanogens or biocathode inoculation. Regardless of inoculum pre-enrichment, biocathode archaeal communities tend to converge on specific hydrogenotrophic species over time and, thus, differences in the performance of fully established biocathodes inoculated with a mixed culture and the mixed culture following a hydrogenotrophic pre-enrichment step (i.e., a subset of the mixed culture microorganisms) may be explained, in large part, by the difference in the biocathode bacterial communities. Therefore, to investigate the effect of the bacterial community composition on methanogenic biocathode

performance, two established biocathodes were compared: a biocathode inoculated with a mixed methanogenic (MM) culture, and a biocathode inoculated with an enriched hydrogenotrophic methanogenic (EHM) culture, developed from the MM culture by pre-enrichment with H₂ and CO₂ as the only, externally supplied electron donor and carbon source, respectively. By understanding microbial community changes during pre-enrichment and the establishment of cathode biofilm, insights may be gained on how Archaea and Bacteria affect cathodic CH₄ production and devise means to guide microbial selection for the development of efficient biocathodes.

5.2 Materials and Methods

5.2.1 BES Setup.

Each batch BES was a dual chamber, H-type with two 300-mL (250 mL liquid volume) modified square glass bottles separated by a proton exchange membrane (PEM; Nafion 117, 6.16 cm²; DuPont, Wilmington, DE). Each chamber was sealed with a butyl rubber stopper and initially flushed with nitrogen (N₂) (anode) or CO₂ (cathode) gas. All BESs were maintained at room temperature (22±2°C) under continuous mixing using magnetic stirrers. The anode and cathode electrodes were porous carbon felt (5 stripes, approximately 86 cm², 15 cm³; Alfa Aesar, Ward Hill, MA) attached to a stainless steel rod. An Ag/AgCl electrode (+0.199 V vs. SHE) was placed adjacent to the carbon felt electrode in each chamber to allow for voltage measurements. The cathode Ag/AgCl electrode acted as the reference electrode and the cathode and anode carbon felt electrodes were the working and counter electrodes, respectively. The working, counter and reference electrodes were attached to a Gamry Interface 1000 potentiostat (Warminster, PA) with

shielded cables and the cathode potential was poised at -0.8 V (vs. SHE). The anode compartment was filled with 250 mL anolyte, consisting of phosphate buffer medium (14.2 g/L; $\text{NaH}_2\text{PO}_4 \cdot \text{H}_2\text{O}$, 13.8 g/L; Na_2HPO_4 ; 0.31 g/L; NH_4Cl , 0.13 g/L; KCl), mineral stock 12.5 mL/L (Cheng et al. 2009) and vitamin stock 2.5 mL/L (Lovley and Phillips 1988). The cathode compartment was filled with 250 mL catholyte, consisting of phosphate buffer medium, mineral stock 12.5 mL/L and vitamin stock 5.0 mL/L (Cheng et al. 2009). Anolyte and catholyte were completely exchanged with freshly made solutions each week, for a hydraulic retention time (HRT) of 7 days. Bioanodes were fed sodium acetate at an initial concentration of 2.5 g COD/L, a model compound known to serve as an electron donor for exoelectrogenic bacteria such as *Geobacter sulfurreducens* sp. nov. (Geelhoed and Stams 2010). Biocathodes were fed by flushing the headspace with CO_2 and then pressurizing to an absolute pressure of 1.65 atm. Each BES was monitored for approximately one month until a consistent performance was achieved. Following the 7th consistent feeding cycle, determined by CH_4 production measurements and the current density profile, samples of catholyte and biocathode felt were removed and analyzed for protein to estimate biomass.

5.2.2 *Inocula.*

Bioanode inoculum was obtained from a stock microbial fuel cell (MFC) consisting of a carbon felt anode, 150 Ω resistor and Pt-coated air cathode. The MFC anode contained 250 mL anolyte, which was partially replaced weekly with fresh medium to achieve a HRT of 8.75 days. Sodium acetate was added weekly at an initial concentration of 1.2 g COD/L. Following a period of biofilm establishment (61 d, 7 HRTs), a piece of MFC bioanode felt was used as inoculum in the anode of the methanogenic BES.

Biocathode inoculum from two sources was used in this study: a mixed methanogenic (MM) culture and an enriched hydrogenotrophic methanogenic (EHM) culture. The MM culture was derived from a stock mixed methanogenic culture initially developed with inoculum from a mesophilic, municipal anaerobic digester, fed with a mixture of dextrin/peptone and maintained at 35°C for several years (Tugtas 2007). The MM culture (1.5 L) was developed with 500 mL of stock mixed methanogenic culture and 1 L reduced medium and was maintained at 22°C for 2 weeks before was used as biocathode inoculum. Like the stock culture, the MM culture was maintained with a HRT of 27 d fed with a mixture of dextrin/peptone, along with reduced medium (Tugtas 2007).

A 1.5 L sample of the MM culture was used to develop the EHM culture, which was fed 5 times per week by adding a mixture of H₂ and CO₂ (80:20; v/v) to the headspace (0.7 L) of a glass reactor, pressurized to an absolute pressure of 1.65 atm. The EHM culture was partially wasted once per week for a HRT of 21 d and the wasted culture volume replaced by catholyte. BES biocathode inoculation was conducted by anaerobically transferring 200 mL of MM or EHM suspended growth culture samples to the cathode and then adding 50 mL of catholyte medium.

5.2.3 *Microbial Community Analysis.*

Bacterial DNA was extracted from the suspended growth cultures and biocathode felts using the UltraClean Soil DNA Kit and PowerSoil DNA Isolation Kit (Mo Bio Laboratories, Carlsbad, CA), respectively, according to the manufacturer's instructions. Following extraction, all DNA was quantified using Nanodrop 3300 (Thermo Scientific, Wilmington, DE) and stored at -20°C until sequencing was performed. Bacterial DNA was amplified using the 16S rRNA gene primers 28F (5'-GAGTTTGATCNTGGCTCAG-3')

and 388R (5'-TGCTGCCTCCCGTAGGAGT-3'). The analysis of archaeal communities is strongly dependent on cell lysis efficiency during extraction and primer set selection (Klindworth et al. 2012, Salonen et al. 2010). Two methods of DNA analysis were used for the archaeal communities. In the first method (M1), archaeal DNA was extracted from suspended growth cultures and biocathode carbon felts using the UltraClean Soil DNA Kit and PowerSoil DNA Isolation Kit, respectively, according to the manufacturer's instructions, and amplified using the 16S rRNA gene primers 519wF (5'-CAGCMGCCGCGGTAA-3') and 909R (5'-TTTCAGYCTTGCGRCCGTAC-3'). In the second method (M2), archaeal DNA was extracted from suspended growth cultures and biocathode carbon felts according to the DNA extraction kit's manufacturer's instructions, with an additional step to enhance cell lysis that consisted of two cycles of heating at 70°C for 5 min and then vortexing for 5 min. Archaeal DNA was amplified using the 16S rRNA gene primers 519wF (5'-CAGCMGCCGCGGTAA-3') and 1017R (5'-GGCCATGCACCWCCTCTC).

Amplified DNA was sequenced using the Illumina MiSeq platform (Research and Testing Laboratory, Lubbock, TX). Forward and reverse reads were merged with PEAR Illumina paired-end read merger and trimmed for quality. Clustering was performed at a 4% divergence using the USEARCH clustering algorithm and the UPARSE OTU selection algorithm was utilized to classify clusters into OTUs. Chimera checking of selected OTUs was performed with UCHIME software. Phylogenetic analysis was conducted by comparing sequences that had a relative abundance $\geq 1\%$ with the closest 16S rRNA gene matches in GenBank (National Center for Biotechnology Information; Bethesda, MD). Using Mega 7.0 software, sequences were aligned with ClustalW and trimmed. A

maximum likelihood phylogenetic tree was constructed using the Tamura-Nei model, 100 bootstrap replications and the Nearest-Neighbor-Interchange heuristic method. Unique sequences have been deposited in GenBank (NCBI) with accession numbers KU597425-KU597475 and KX587564-KX587568. To compare community structure, all representative sequences of detected OTUs were trimmed, aligned and a maximum likelihood phylogenetic tree and rarefaction curves using alpha diversity were constructed using QIIME 1.9.0. Principal Coordinate Analysis (PCA) was then conducted and plotted in 2-D with QIIME 1.9.0, and 3-D with Emperor. Redundancy analysis and canonical correspondence analysis (CCA) were conducted using R (Team 2014) and vegan 2.4-1 community ecology package (Oksanen et al. 2016).

5.2.4 *Analytical Methods.*

pH was measured as described in Section 3.1.1. Total suspended solids (TSS) and volatile suspended solids (VSS) were measured as described in Section 3.1.5. Total gas production and gas composition were measured as described in Sections 3.1.6 and 3.1.7, respectively. Volatile fatty acids were measured as described in Section 3.1.8. Biofilm and suspended biomass protein was extracted and measured as described in Section 3.1.10. Biomass was estimated by assuming cell protein was 63% of the cell dry weight (Simon and Azam 1989).

5.3 Results and Discussion

5.3.1 *Performance of BES with MM- and EHM-inoculated Biocathodes.*

The suspended growth EHM culture was developed as described in Section 4.2.2; methane production over three, representative feeding cycles is shown in Figure 5.1. Two BESs were developed to compare the performance of an EHM-inoculated cathode with that of a MM-inoculated cathode, while each was paired with the same acetate-fed, pre-established bioanode. The EHM-inoculated biocathode was set up first with a 50 mM buffered anolyte and catholyte, which was insufficient to maintain a stable pH, necessitating an increase of the buffer concentration to 300 mM. Subsequently, the BES with the MM-biocathode was set up with 300 mM buffered anolyte and catholyte, which maintained a nearly constant pH of 6.8 in both the anode and cathode throughout each feeding cycle. Following buffer strength adjustment, the EHM-inoculated biocathode experienced temporary pH fluctuations before maintaining a nearly constant pH of 6.8 in the anode and a pH of 6.8-7.2 in the cathode for the duration of each feeding cycle during steady BES operation. Although ammonia was not measured in this study, the anode and cathode of a similar system had an ammonia concentration in the range of 67 to 73 mg N/L, (see Section 4.3.1) an ammonia level that is not expected to be inhibitory to exoelectrogens (Nam et al. 2010) nor to methanogens (Yenigün and Demirel 2013).

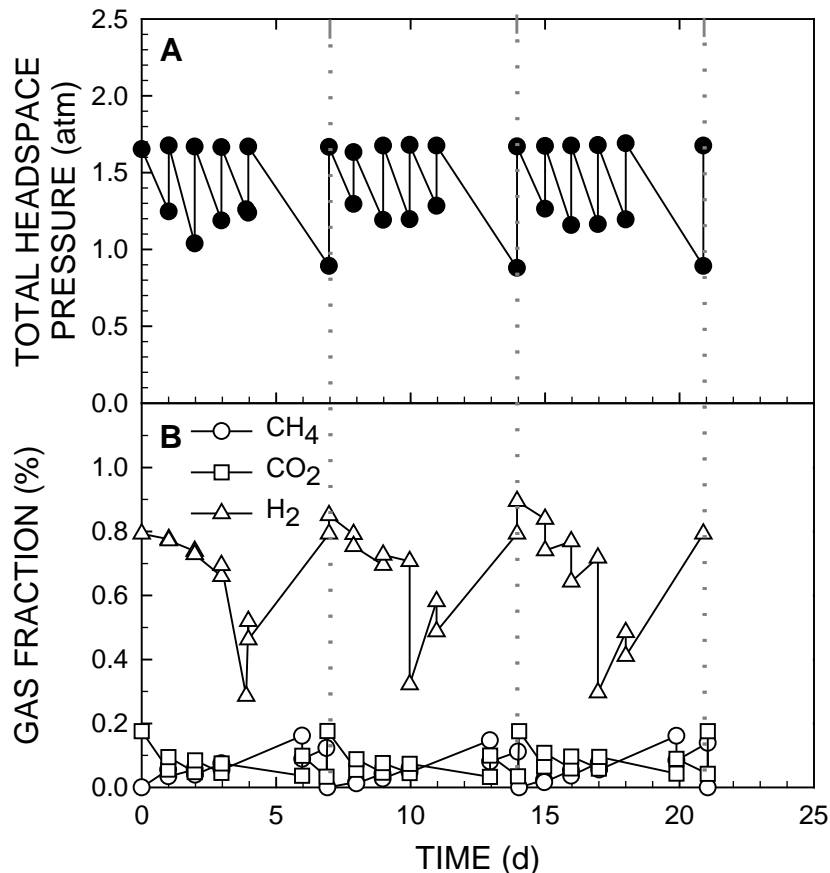


Figure 5.1 - Headspace gas pressure (A) and gas composition (B) of the EHM suspended growth culture over three, representative feeding cycles. Dashed vertical lines indicate the wasting of a portion of the culture and replacement with fresh medium, accompanied by the complete flushing of the headspace with H₂/CO₂ (80:20 v:v). The increase in total headspace pressure on days other than those at the end of a 7-d feeding cycle (i.e., days not indicated by dashed vertical lines), was due to the addition of H₂/CO₂ without any gas release.

Initially, the mean anode acetate removal over the first four feeding cycles was $83\pm 5\%$ and $81\pm 6\%$ while paired with the EHM- and MM-biocathodes, respectively. After establishing steady operation (6-8 cycles for each biocathode), the anode acetate removal was $81\pm 7\%$ over three typical feeding cycles when paired with the MM-biocathode (Figure 5.2A). In contrast, the anode acetate removal was $69\pm 2\%$ over three typical feeding cycles when paired with the EHM-biocathode (Figure 5.2A). VFAs were not detected in the

biocathodes, with the exception of trace levels of acetate (≤ 25 mg COD/L), which could have originated from acetogenesis (see Section 4.3.5), fermentation of cell lysis products, or the transport of acetate from the anode across the PEM to the cathode (Chae et al. 2008). Immediately after inoculation, the BES current density was higher with the EHM-biocathode than with the MM-biocathode (Figure 5.3A). Following biofilm development, the current density in the BES with EHM-biocathode increased dramatically upon feeding (Figure 5.2B). In contrast, the BES with MM-biocathode maintained a relatively low current density upon feeding (Figure 5.2B). The BES Coulombic efficiency during a typical cycle was substantially lower with the MM-biocathode (11%) than with the EHM-biocathode (39%). Regardless, these Coulombic efficiency values are likely underestimated because they are based on an assumption of complete acetate oxidation, which does not account for acetate used for microbial growth in the anode and/or possible conversion of acetate to microbial carbon storage molecules in the anode biofilm as has been previously observed (Freguia et al. 2007).

Transient H_2 was observed in the headspace of the MM-inoculated cathode, peaking at 24% v/v on day 4 of the first feeding cycle and 9% on day 2 of the second feeding cycle; after the second feeding cycle, H_2 was not detected in the cathode headspace. In the EHM-inoculated cathode, H_2 was not detected in the headspace, even during start-up. Previous work has shown that although H_2 is not detected in the headspace of a biocathode, H_2 may still be available in the liquid phase, as evidenced by continued transport of H_2 across the PEM from cathode to anode (see Section 4.3.3). Thus, H_2 may have contributed to the biocathode CH_4 production from the reduction of CO_2 even though it was not detected in the headspace.

Headspace CH₄ in the MM- and EHM-inoculated cathodes during the first three feeding cycles following start-up is shown in Figure 5.3B. The EHM-biocathode was very active upon inoculation and, during the initial three feeding cycles, produced 1.24±0.16 mmol CH₄ per cycle. In contrast, the MM-biocathode produced 0.83±0.33 mmol CH₄ per cycle during the first three feeding cycles and its CH₄ yield declined following the second cycle. Thus, as the microbial community developed in the biocathodes, CH₄ production by the EHM-inoculated biocathode community increased, while CH₄ production by the MM-inoculated community decreased. Biocathode CH₄ production may occur through direct electron transfer or through H₂ production, which can be catalyzed by extracellular enzymes or other cell products (Deutzmann et al. 2015). A wide-range cyclic voltammetry scan of the BES with enriched biocathode under inactive, unfed conditions (Figure 5.4) showed that abiotic H₂ evolution, catalyzed by the presence of inactive biomass and/or bioproducts on the cathode, occurred at -1.1 V, a more negative applied potential than that used in this study (-0.8 V). Furthermore, our previous work with a similar system showed that the biocathode produced over five-fold higher total CH₄ than the CH₄ equivalents of H₂ produced by an uninoculated, abiotic cathode (see Section 4.3.1). Therefore, direct electron transfer was likely one mechanism of CH₄ production in the enriched biocathode, alongside hydrogenotrophic methanogenesis with biologically-catalyzed H₂.

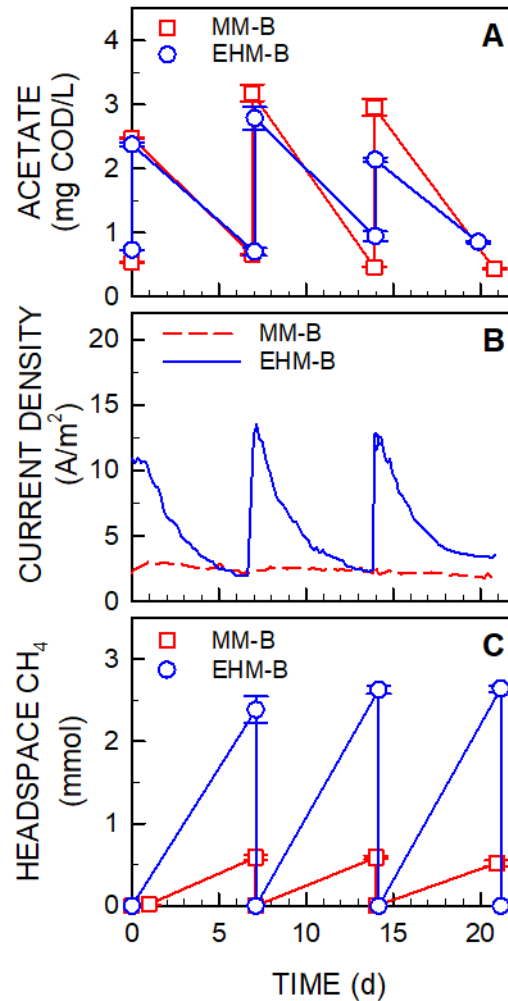


Figure 5.2 - Time course of anode acetate concentration (A), BES current density normalized to the PEM surface area (B), and cathode headspace methane (C) during three representative feeding cycles following 56 d of cathode biofilm establishment; MM-B, MM-inoculated biocathode; EHM-B, EHM-inoculated biocathode. Error bars represent mean values \pm one standard deviation, $n = 3$.

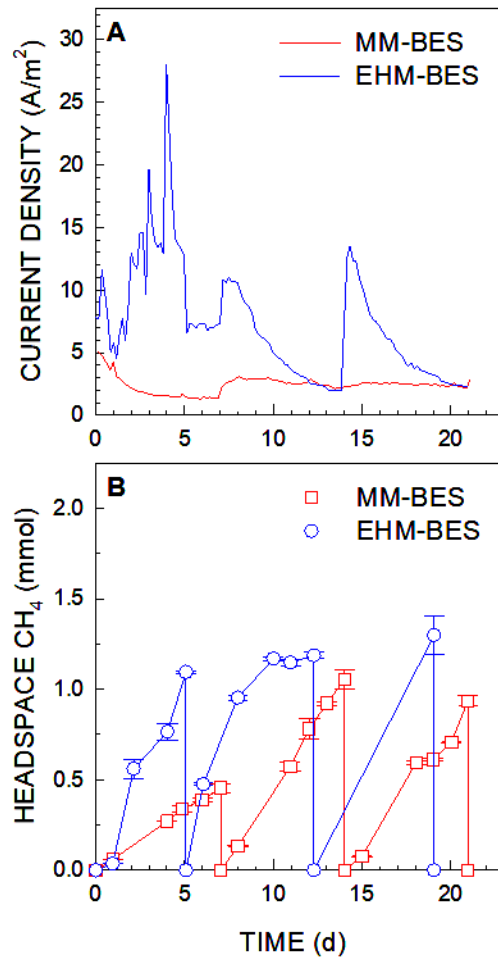


Figure 5.3 - Time course of BES current density (A) and headspace methane (B) over the course of the first three feeding cycles for the MM-inoculated biocathode BES (MM-BES) and the EHM-inoculated biocathode BES (EHM-BES).

At the end of experimentation, total biomass on the MM- and EHM-inoculated carbon felt biocathodes was 0.540 ± 0.067 and 0.639 ± 0.189 mg, respectively. Total suspended biomass, estimated by protein measurement, was also similar between the MM- and EHM-biocathode chambers, with 0.067 ± 0.006 and 0.078 ± 0.022 mg, respectively. Thus, the biofilm biomass made up 88.9% and 89.2% of the total biomass in the MM- and EHM-biocathodes, respectively. The headspace CH₄ in the MM- and EHM-biocathodes

during three typical cycles following 56 d of cathode biofilm establishment is shown in Figure 5.2C. Over the course of three cycles, the CH₄ production rate in the MM- and EHM-biocathode was 0.083±0.006 and 0.375±0.019 mmol CH₄/d, respectively. Normalizing to cathode biofilm biomass, the MM- and EHM-biocathode CH₄ production rate was 0.153±0.010 and 0.586±0.029 mmol CH₄/mg biomass-d, respectively. Thus, the EHM-biocathode produced CH₄ at a rate 3.8 times higher than that of the MM-biocathode, indicating a far more productive biofilm in the EHM-biocathode. However, both CH₄ production rates were much higher than that of the EHM suspended growth culture (4.22 x 10⁻³ mmol CH₄/mg biomass-d). Compared with reported CH₄ production rates for the anaerobic digestion of mixed food waste (6.76 x 10⁻⁴ mmol CH₄/mg biomass-d) (Zhang et al. 2007) or municipal solid waste (2.06 x 10⁻³ mmol CH₄/mg biomass-d) (Nopharatana et al. 2007), the biomass-normalized rate of biocathode CH₄ production in the present study was relatively high. When normalized to the PEM surface area, the MM- and EHM-biocathode mean CH₄ production rate over the course of a typical feeding cycle was 142±21 and 603±28 mmol/m²-d, respectively. Previously reported values of biocathode CH₄ production rates vary widely due to differences in system setups (i.e., BES geometry, electrode material, applied potential, etc.). One study with a biocathode poised at -0.8 V, the same potential used in the present study, produced CH₄ at a mean rate of 200 mmol/m²-d (Cheng et al. 2009). More recently, a thermophilic biocathode poised at -0.8 V produced 1,103 mmol CH₄/m²-d (Fu et al. 2015). Other studies have reported higher biocathode CH₄ production rates but at higher poised potentials or over shorter periods of operation (e.g., -0.9 V, 5 h) (Villano et al. 2010, Zhen et al. 2015). Compared to the initial feeding cycle, the established EHM-biocathode produced twice the CH₄ but the MM-biocathode

produced only 3% more CH₄ than it did during the initial start-up cycle and substantially less than in the initial second and third cycles (Figure 5.3B). This pattern in the CH₄ production in the MM-biocathode could be explained by the early enrichment of methanogens capable of utilizing H₂ and/or electrons directly from the cathode, followed by the growth of bacterial species that interfere with methanogenesis. In contrast, the EHM-biocathode community, which was pre-enriched under hydrogenotrophic methanogenic conditions, did not experience a later decline in CH₄ production. Thus, an enrichment step may be useful in not only selecting for hydrogenotrophic methanogens but also selecting for a bacterial community that is complimentary and supports electromethanogenesis, as further discussed below. Indeed, the current capture efficiency (CCE), a measure of how efficiently the cathode biofilm uses electron equivalents from the cathode to reduce CO₂ to CH₄, was 98% during a typical BES feeding cycle with the EHM-biocathode. In contrast, the BES CCE with the MM-biocathode was only 62%, indicating a far less efficient biofilm. Cyclic voltammetry also confirmed a greater catalytic activity with the EHM-biocathode than with the MM-biocathode (Figure 5.4). The ionic strength of anolyte and catholyte may affect the shape and current magnitude of the BES voltammogram, as shown in Figure 5.6. Although a trend of increasing current with increasing ionic strength was observed in CVs conducted with an abiotic (i.e., uninoculated BES) at increasing anolyte and catholyte ionic strength from 1.21 to 1.41 M, the current increase at an applied potential of -0.8 V was 0.108±0.003 mA in both the increasing (more positive) and decreasing (more negative) potential scan direction (Figure 5.6). In addition to the relatively low impact of ionic strength within the ionic strength range tested, all voltammograms in the present

study were conducted under similar conditions (i.e., ionic strength, scan rate, temperature, etc.).

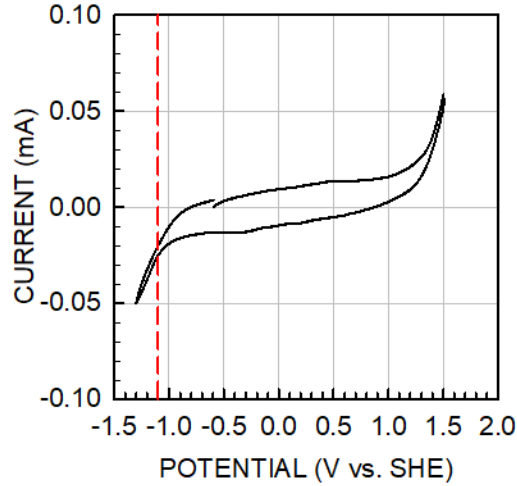


Figure 5.4 - Cyclic voltammetry scan of inactive BES after the EHM-biocathode was maintained unfed in fresh catholyte and a N₂-filled headspace for 24 h. Scan conducted at a rate of 50 mV/s. Vertical broken line denotes an applied potential of -1.1 V which H₂ evolution was noted.

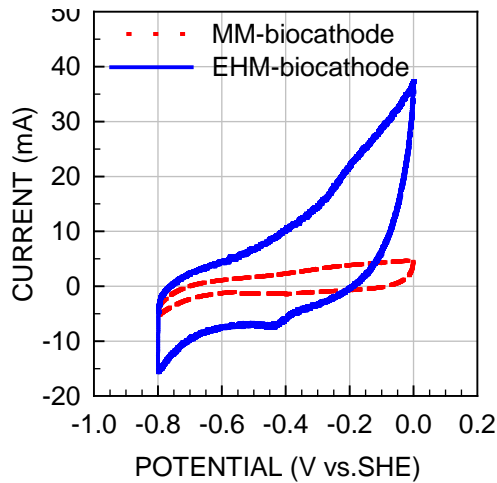


Figure 5.5 - Cyclic voltammograms of the MM-BES and EHM-BES. Scans were conducted at the end of a feeding cycle at a scan rate of 100 mV/s.

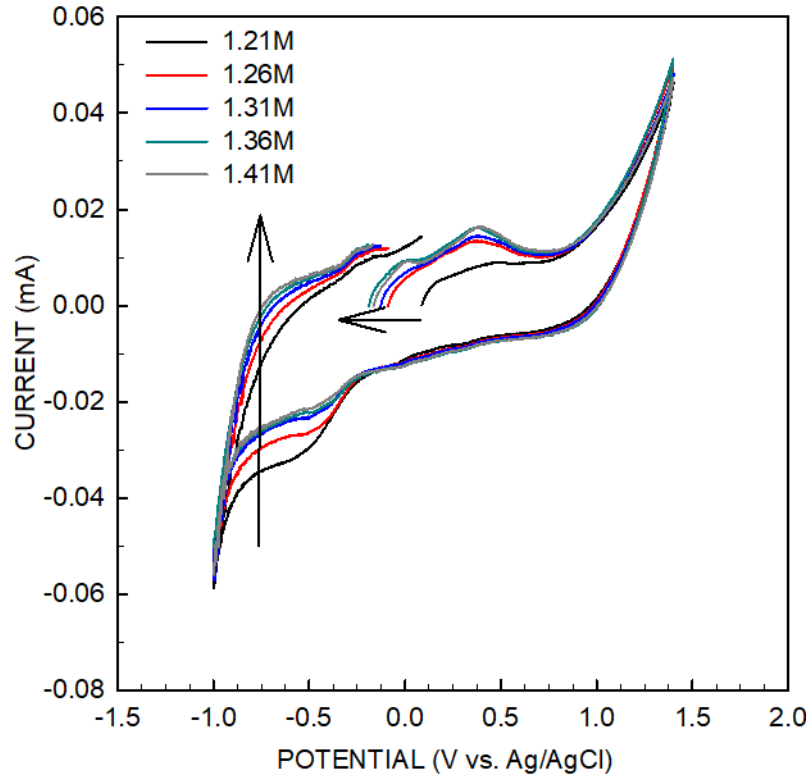


Figure 5.6 - Cyclic voltammograms of an abiotic (i.e., uninoculated) BES with anolyte and catholyte at various ionic strengths (1.21, 1.26, 1.31, 1.36 and 1.41 M), starting at open circuit potential. Scans conducted at a scan rate of 50 mV/s. The vertical arrow shows how the CV curve shifts due to double layer compression, while the horizontal arrow shows how the open circuit potential shifts due to decreasing ohmic resistance.

Overall, the pre-enrichment step selecting for hydrogenotrophic methanogens increased the methanogenic biocathode productivity over the use of a non-enriched, mixed methanogenic inoculum. Furthermore, inoculum enrichment allowed for faster BES start-up because of the greater abundance of hydrogenotrophic methanogens.

5.3.2 *Change in Microbial Community Structure.*

The total number of OTUs detected in the MM culture, EHM culture, MM-biocathode and EHM-biocathode was 285,968, 268,884, 216,080 and 278,850, respectively. A rarefaction

curve for each community sample (Figure 5.7) indicates that most of the OTUs in each sample were sequenced. The bacterial Shannon indices (Table 5.1) for the suspended growth cultures, MM and EHM, were lower than that of their respective biocathode communities, more likely the result of a much higher biomass retention time in the biofilm, as well as less homogeneity in the biocathodes than in the well-mixed suspended growth cultures. The carbon felt and biofilm affect mass-transfer and may allow for the development of microenvironments with conditions that can host a more diverse bacterial community. One study of a MFC anode found the bacterial community in the biofilm had a higher Shannon index (3.34) than that of the activated sludge used as inoculum (2.85) (Ki et al. 2008). In contrast, inocula with highly diverse bacterial communities (Shannon indices of 4.7 and 4.9) used by another study to setup microbial electrolysis cells (MECs) resulted in lower cathode biofilm bacterial diversity (Shannon index of 2.0) (Siegert et al. 2015). Principal Coordinate Analysis (PCA; Figure 5.8 and Figure 5.9) indicated a greater shift in bacterial community composition occurred due to biofilm development and/or increased buffer strength with the EHM-biocathode (EHM culture vs. EHM-biocathode) than with the MM-biocathode (MM culture vs. MM-biocathode). A redundancy analysis and Canonical Correspondence Analysis (CCA) was performed to reveal the factors that most contributed to the change in microbial community (Figure 5.10). Redundancy analysis (Figure 5.10A) indicated that large changes in microbial community structure occurred during enrichment from MM culture to EHM culture (i.e., change to a lower temperature and a different, simple substrate) and with inoculation of biocathodes (i.e., biofilm development and higher buffer strength). CCA analysis (Figure 5.10B) indicated

that substrate type and biofilm development were likely to be primary factors in the microbial community change.

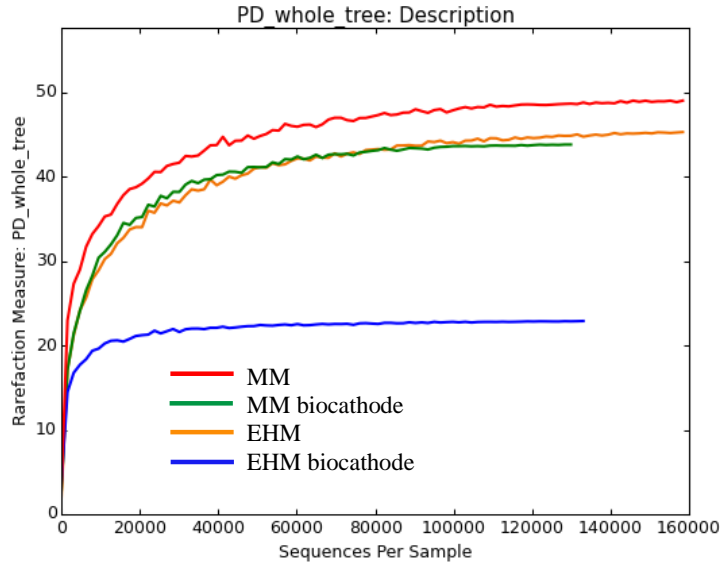


Figure 5.7 - Rarefaction curves for the EHM culture, EHM biocathode, MM culture and MM biocathode. Lower and upper limits of rarefaction depths were 10 and 100, respectively, and the number of steps (i.e., rarefied OTU table sizes) was 100.

Table 5.1 - Bacterial and Archaeal Shannon Diversity Indices for Suspended Growth Cultures and Biocathode Biofilms

Culture ^a	Bacterial	Archaeal	Archaeal
	Community	Community (M1) ^b	Community (M2) ^b
MM	1.466	1.132	1.578
MM-biocathode	2.120	0.114	0.035
EHM	2.033	0.240	0.007
EHM-biocathode	2.684	0.047	0.047

^a Abbreviations: MM, mixed methanogenic suspended growth culture; EHM, enriched methanogenic suspended growth culture; MM-biocathode, MM-inoculated biocathode; EHM-biocathode, EHM-inoculated biocathode.

^b M1, M2, DNA analysis method 1, method 2, respectively.

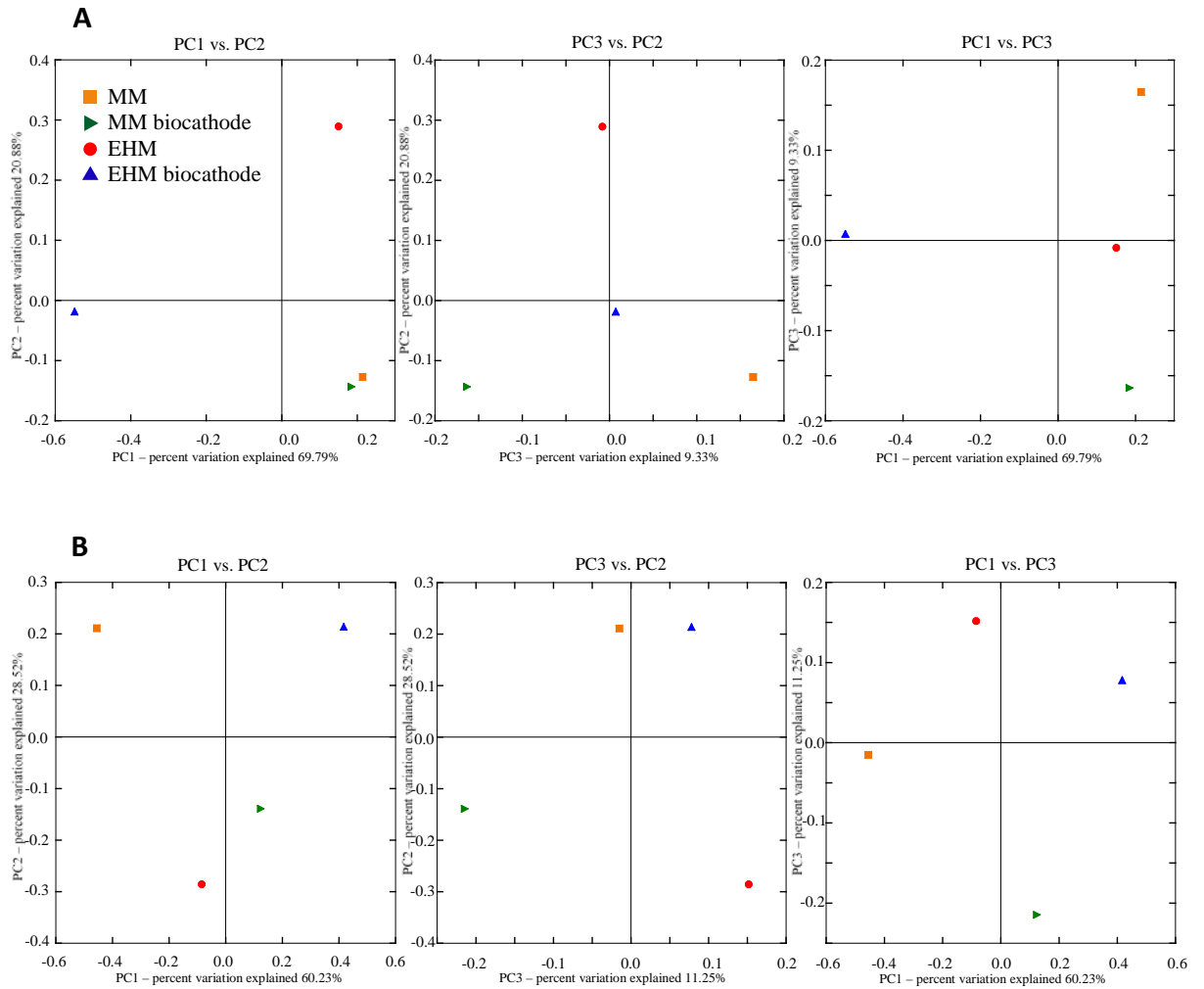


Figure 5.8 - 2-D Principal Coordinate Analysis (PCA) plots for bacterial communities (A) and archaeal communities (B) of the MM suspended growth, MM biocathode, EHM suspended growth and EHM biocathode cultures.

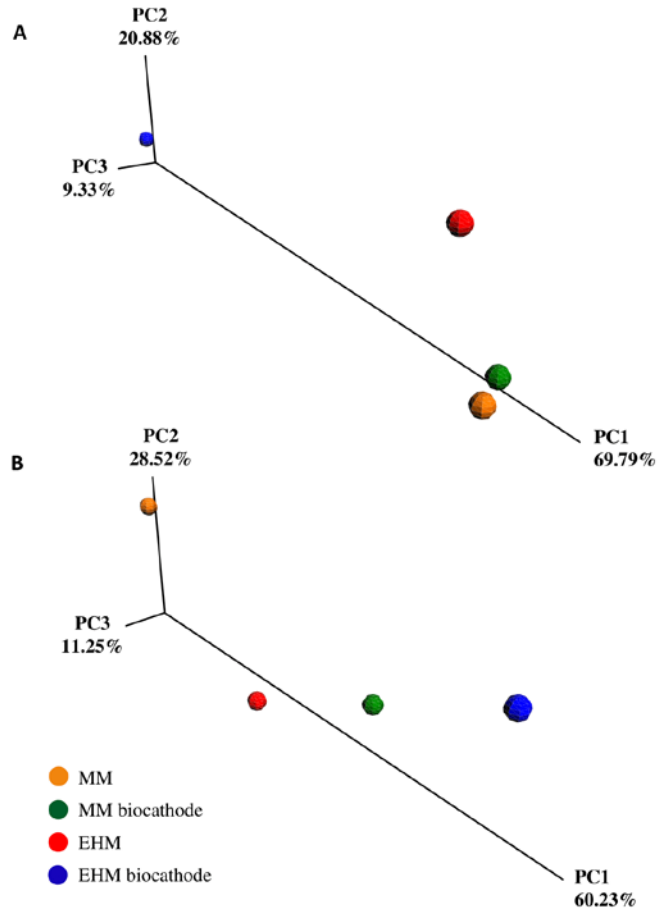


Figure 5.9 - 3-D Principal Coordinate Analysis (PCA) plots for bacterial communities (A) and archaeal communities (B) of the MM suspended growth, MM biocathode, EHM suspended growth and EHM biocathode cultures. Axes are scaled to the percent variation explained by the principal coordinates.

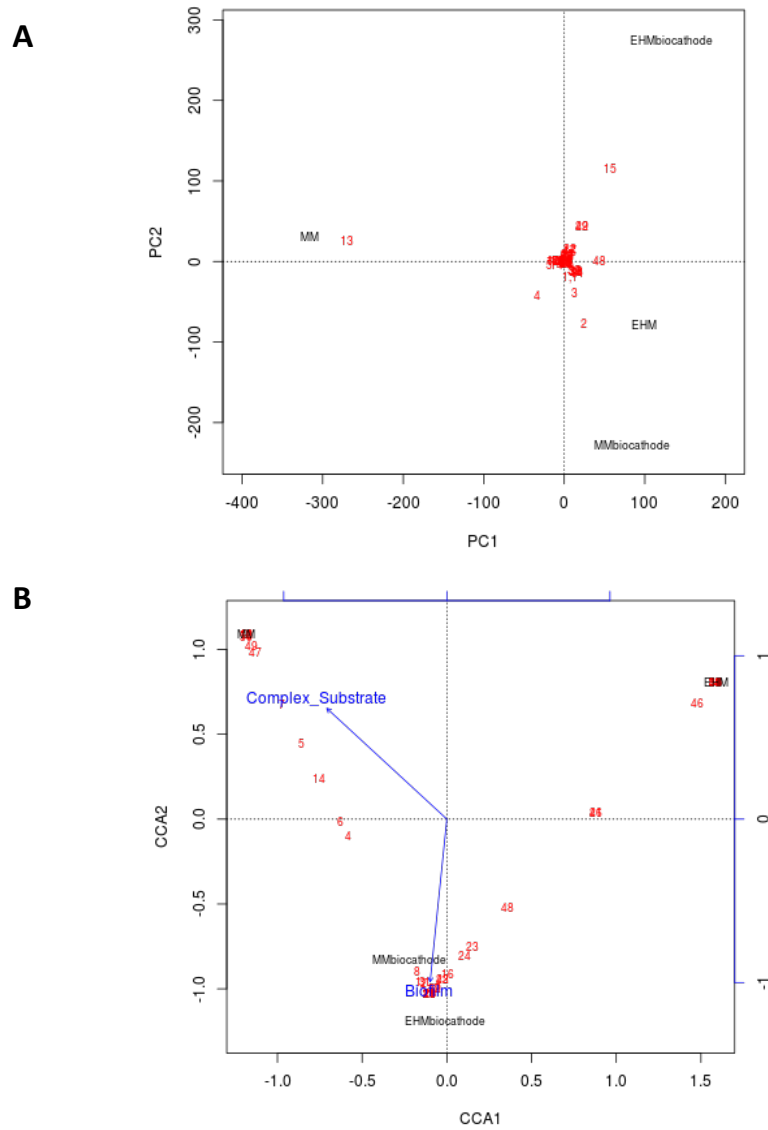


Figure 5.10 - Redundancy analysis (A) and canonical correspondence analysis (B) plots to determine changes in OTU abundance attributed to biofilm development and higher buffer strength (MM Biocathode and EHM Biocathode), or higher temperature (35 vs. 22°C) with a more complex (dextrin and peptone) substrate (MM culture). EHM was maintained with a lower buffer strength (100 vs. 300 mM) and a simple (CO₂/H₂) substrate.

The archaeal Shannon index for DNA samples extracted using method 1 (M1), which represented the hydrogenotrophic methanogen diversity, decreased between the

suspended growth cultures and the resulting cathode biofilms (Table 5.1). This result is likely due to enrichment of methanogens capable of utilizing H₂ and/or electrons originating from the cathode. Thus, the bacterial diversity may have increased due to biofilm formation but the archaeal diversity (M1 DNA extraction method) may have decreased because of electrochemical enrichment of hydrogenotrophic methanogens at the cathode. The archaeal diversity for DNA samples extracted using method 2 (M2), which represented acetoclastic methanogen diversity, declined substantially between the MM suspended growth culture, in which acetate would be available from dextrin/peptone fermentation, and the MM-biocathode biofilm, which was not fed complex organic substrates. As expected, the M2 archaeal Shannon indices were low in both the EHM suspended growth culture and EHM-biocathode biofilm; the EHM-biocathode had a slightly higher index than the EHM suspended growth culture, which could be due to minor diffusion of acetate across the PEM from the anode to the cathode, as has been previously reported. (Chae et al. 2008) PCA showed that the MM culture and EHM culture archaeal community composition shifted similarly following biofilm development on the MM- and EHM-biocathodes (Figure 5.8 and Figure 5.9).

5.3.3 *Phylogeny of Suspended Growth Cultures and Cathode Biofilms.*

The most abundant ($\geq 1\%$ relative abundance) bacterial and archaeal OTUs were placed with their closest defined species matches in GenBank into phylogenetic trees (Figure 5.11, Figure 5.12 and Figure 5.13). The relative abundance of Archaea in the MM and EHM suspended growth cultures and biocathode biofilms is given in Table 5.2. The first method of DNA analysis, M1, was more effective at detecting hydrogenotrophic methanogens, particularly *Methanoculleus*, *Methanolinea* and *Methanobacterium*, whereas the second

method of DNA analysis, M2, was more effective at detecting acetoclastic methanogens such as *Methanosaeta*. For the DNA samples extracted using method 1 (M1), *Methanomicrobiaceae* and *Methanoregulaceae* together represented 97% of sequenced Archaea in the MM culture. In contrast, *Methanobacteriaceae* represented 95% of sequenced Archaea in the EHM culture. This result indicates that the enrichment conditions in the EHM culture altered the hydrogenotrophic methanogen community composition. For example, in the MM culture, *Methanoculleus* was the most abundant genus of the sequenced Archaea (77%, M1) but was the least abundant of detected Archaea in the EHM culture (4%, M1). Similarly, *Methanolinea*, which had the second greatest abundance in the MM culture sequenced Archaea (20%, M1), was undetected in the EHM culture. Although *Methanoculleus* and *Methanolinea* are hydrogenotrophic methanogens capable of converting H₂ and CO₂ to CH₄, some species are known to require acetate as a carbon source and/or peptone as a growth factor (Ferry 1993, Mikucki et al. 2003, Sakai et al. 2012). Thus, the EHM culture's enrichment conditions favored the growth of other hydrogenotrophic methanogens, such as *Methanobrevibacter* and *Methanobacterium*, which do not require complex carbon sources/growth factors (Ferry 1993). Indeed, the most abundant M1 phylotype in the EHM culture was most closely related to *Methanobrevibacter arboriphilus*, a species that grows autotrophically and only requires B vitamins as growth factors (Ferry 1993).

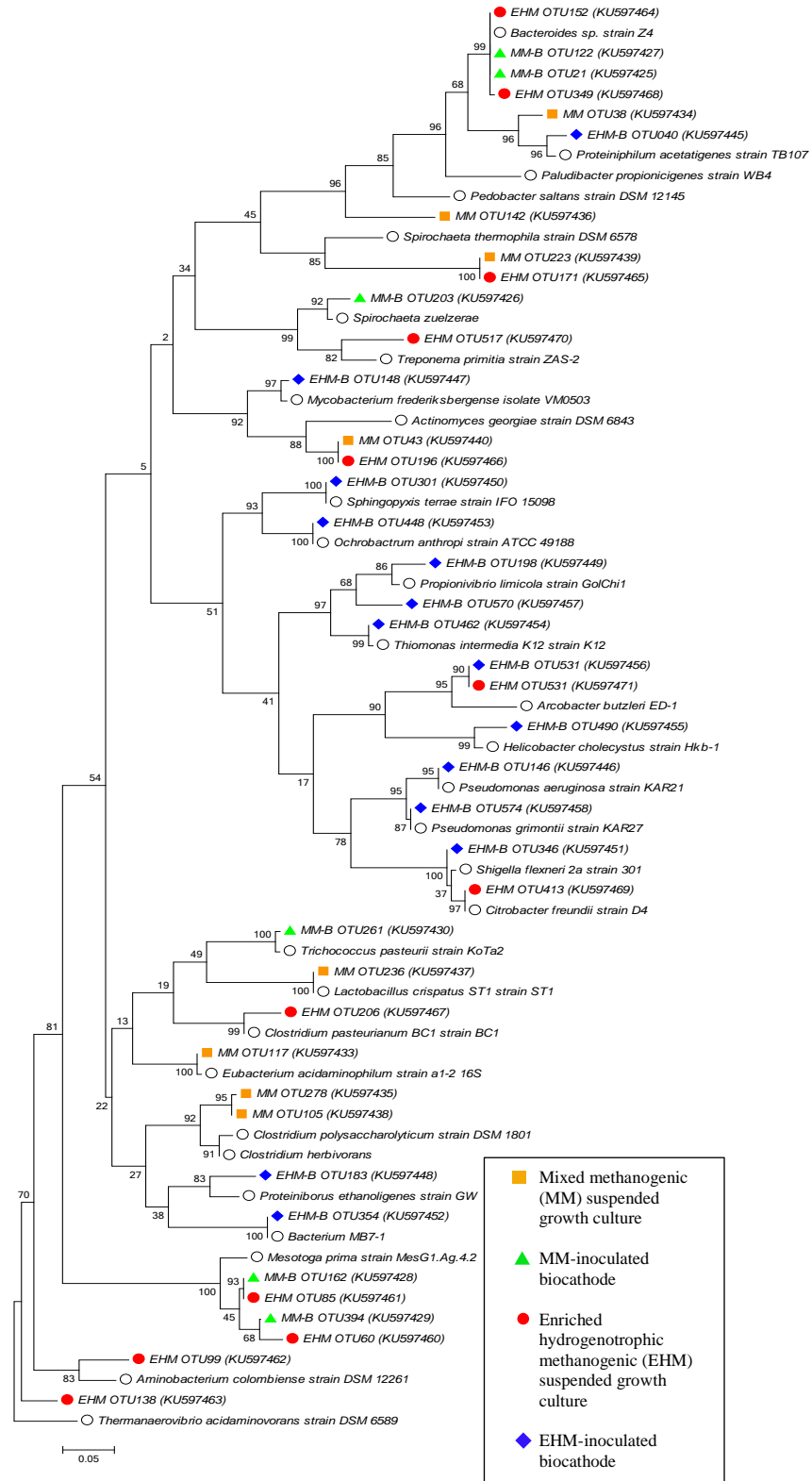


Figure 5.11 - Phylogenetic Tree showing the relationship of suspended growth cultures and BES biocathodes Bacteria OTUs ($\geq 1\%$ relative abundance) to their closest matched species in GenBank.

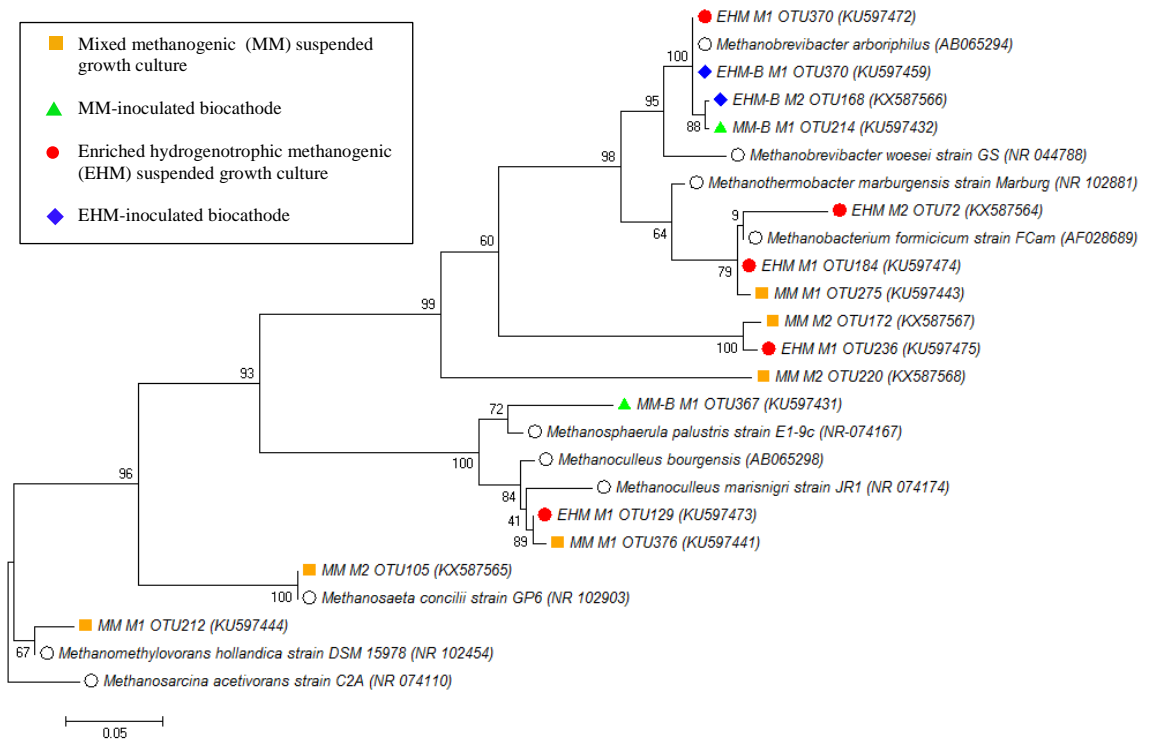


Figure 5.12 - Phylogenetic tree showing the relationship of suspended growth cultures and BES biocathodes Archaea OTUs ($\geq 1\%$ relative abundance) to their closest matched species in GenBank.

Methanosarcinales is an order consisting of methylotrophic and acetoclastic methanogens, such as *Methanomethylovorans* and *Methanosaeta*. Despite feeding a complex substrate (dextrin/peptone) to the MM culture, *Methanosaeta* was only detected at trace levels and the methylotrophic genus *Methanomethylovorans* represented just 2% of sequenced Archaea (M1 DNA extraction method). However, using method 2 for DNA extraction, *Methanosaeta* was the most abundant identified genus in the MM culture (Table 5.2), illustrating the large bias that may be introduced based on the choices of the DNA extraction method and primers. As expected, due to a lack of complex substrate,

Methanosarcinales was not detected in the EHM culture with either M1 or M2 DNA extraction method.

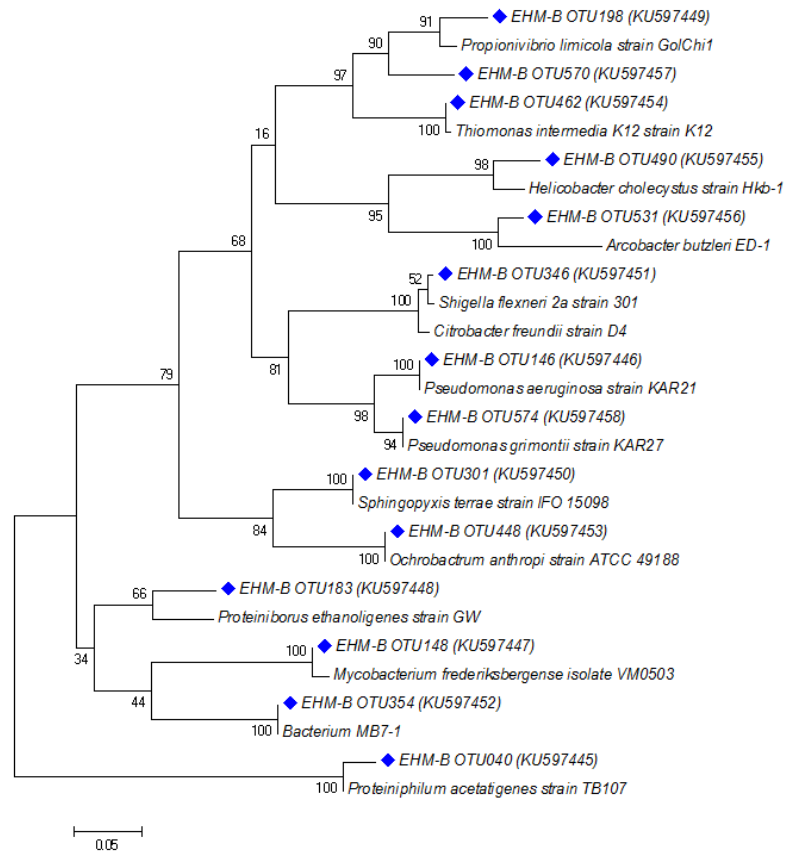


Figure 5.13 - Phylogenetic tree showing the relationship of EHM-biocathode (EHM-B; blue diamond) Bacteria OTUs (≥1% relative abundance) to their closest matched species in GenBank.

Table 5.2 - Relative Abundance (%) of Archaeal Community Members in Suspended Growth Cultures and Biocathode Biofilms

Family	Genus	Suspended Culture ^a				Biocathode Biofilm ^a			
		MM		EHM		MM-B		EHM-B	
		M1	M2	M1	M2	M1	M2	M1	M2
<i>Methanomicrobiaceae</i>	<i>Methanoculleus</i>	77	13	4	ND ^b	T ^c	TT ^d	ND	ND
<i>Methanoregulaceae</i>	<i>Methanolinea</i>	20	ND	ND	ND	12	ND	ND	ND
<i>Methanobacteriaceae</i>	<i>Methanobacterium</i>	1	ND	25	TT	T	ND	TT	TT
	<i>Methanobrevibacter</i>	T	TT	70	100	86	100	100	99
<i>Methanosarcinaceae</i>	<i>Methanomethylovorans</i>	2	ND	ND	ND	TT	ND	ND	ND
<i>Methanosaetaceae</i>	<i>Methanosaeta</i>	TT	19	ND	ND	TT	TT	ND	T
Unclassified		-	68	1	-	1	T	-	T

^a Abbreviations: MM, mixed methanogenic suspended growth culture; EHM, enriched methanogenic suspended growth culture; MM-B, MM-inoculated biocathode; EHM-B, EHM-inoculated biocathode; M1, M2, DNA analysis method 1, method 2, respectively.

^b ND, not detected.

^c T, trace with relative abundance < 1%.

^d TT, trace with relative abundance ≤ 0.1%.

In both the MM- and EHM-biocathodes, the genus *Methanobrevibacter* was highly enriched following inoculation. *Methanobrevibacter* spp. increased from 70% (M1) of detected Archaea in the EHM suspended growth inoculum to 100% (M1) in the established EHM cathode biofilm. Similarly, in the MM suspended growth culture, *Methanobrevibacter* spp. represented only 0.5% (M1) of all detected Archaea but, following biocathode biofilm establishment, it represented 86% (M1) of detected Archaea

in the MM cathode biofilm. Thus, *Methanobrevibacter* was highly enriched under biocathode conditions, regardless of the level of initial abundance in the two inocula. Furthermore, the dominant phylotype in the MM- and EHM-biocathodes was most closely related to *M. arboriphilus*, representing 86% and 100% (M1) of detected Archaea in the MM- and EHM-biocathodes, respectively. In comparison, this phylotype represented only 0.003% and 68% of detected Archaea in the MM and EHM suspended growth inoculum, respectively. Biocathode enrichment of *M. arboriphilus* has also been noted in other studies (Jiang et al. 2014, Siegert et al. 2015, Zeppilli et al. 2015). Because complex substrates were not added to the cathodes, *Methanosarcinales* were either not detected or present only in trace amounts (<1% relative abundance) using M1 and M2 DNA extraction methods.

The bacterial microbial community composition and relative abundance of phyla and selected species detected in the MM and EHM suspended growth cultures and biocathode biofilms are shown in Figure 5.14 and listed in Table 5.3 and Table 5.4. Enrichment of the suspended growth culture had a substantial impact on the bacterial community structure, which was also illustrated with PCA (Figure 5.8 and Figure 5.9). *Bacteroidetes*, *Proteobacteria*, *Thermotogae* and *Actinobacteria* were enriched in the EHM suspended growth culture, relative to the MM culture. Similarly, *Bacteroidetes* and *Proteobacteria* were enriched following biofilm development in both the MM-biocathode and EHM-biocathode. However, *Thermotogae* increased in relative abundance between the MM culture (16%) and MM-biocathode (24%), but decreased from 53% in the EHM culture to below detection in the EHM-biocathode.

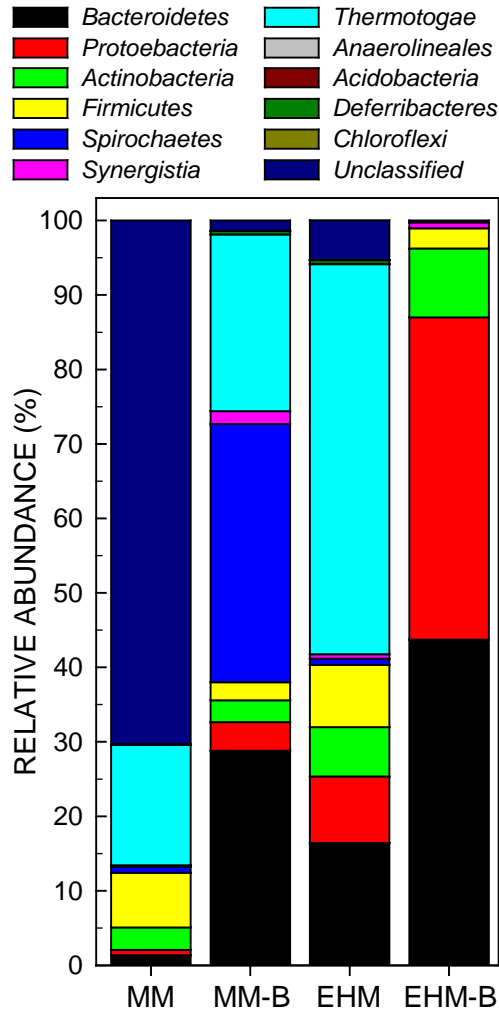


Figure 5.14 - Bacterial community structure in suspended growth culture and biofilm samples. MM, mixed methanogenic suspended growth culture; MM-B, MM-inoculated biocathode; EHM, enriched methanogenic suspended growth culture; EHM-B, EHM-inoculated biocathode.

Bacteroidetes, which increased in relative abundance following H₂/CO₂ enrichment and cathode biofilm formation, are capable of utilizing many different complex polysaccharides and are highly adaptable in changing environments due to their ability to widely regulate gene expression (Krieg et al. 2010). While complex substrates were not added to the EHM culture or MM- and EHM-biocathodes, lysed microbial cells release

organic substrates, which may be utilized by *Bacteroidetes*. Phylotypes in the EHM suspended growth culture and MM-biocathode biofilm were most closely related to *Bacteroides* sp. strain Z4 (Table 5.3). A similar strain, *Bacteroides* sp. W7, has previously been isolated from an anode biofilm (Wang et al. 2010). In the MM-biocathode, the composition of *Bacteroidetes* was similar to that of the MM suspended growth culture *Bacteroidetes*, indicating the enrichment primarily affected the abundance of *Bacteroidetes* as a whole relative to total Bacteria. In contrast, *Bacteroidetes* in the EHM-biocathode were different in both bacterial relative abundance and composition from the EHM suspended growth culture. The EHM suspended growth culture *Bacteroidetes* consisted predominantly of two phylotypes: *Bacteroides* sp. (49%) and *Parabacteroides* sp. (40%). Following biofilm development in the EHM-biocathode, a phylotype similar to *Proteiniphilum* sp. made up 98% of *Bacteroidetes*. In fact, this phylotype alone made up 43% of all detected Bacteria in the EHM cathode biofilm, yet was undetected in the EHM suspended growth culture used as inoculum (Table 5.3). In contrast, the *Proteiniphilum* phylotype made up only 2% of *Bacteroidetes* and 0.4% of all Bacteria in the MM cathode biofilm as well as 1% of *Bacteroidetes* and 0.06% of Bacteria in the MM suspended growth culture used as inoculum. *Proteiniphilum* spp. is not well-studied, although two strains have been isolated from the granular sludge of an upflow anaerobic sludge blanket reactor treating brewery wastewater (Chen and Dong 2005). *Proteiniphilum* spp. is known to ferment amino acids (Chen and Dong 2005) and anaerobically degrade polycyclic aromatic hydrocarbons (PAHs) (Larsen et al. 2009). Considering its substantial presence in the EHM-biocathode, *Proteiniphilum* spp. is a noteworthy candidate for future study as to its role in the cathode biofilm community.

Proteobacteria were also detected with a greater relative abundance in the EHM culture than the MM culture, and were also present at a greater relative abundance in the two biocathodes than in their respective inocula (Table 5.3; Figure 5.14). Members of the phylum *Proteobacteria* are highly diverse in their morphology, phenotype and metabolism, with no one class serving as a model of the entire phylum (Kersters et al. 2006). Because the *Proteobacteria* phylum consists of such diverse classes, a further analysis of the relative class abundance was conducted, as discussed in more detail in Section 5.3.4 (Figure 5.15). The most abundant *Proteobacteria* in the MM culture were δ -*Proteobacteria*, while in the EHM culture γ -*Proteobacteria* were most abundant, each representing 64% of their respective *Proteobacteria*. The MM and EHM cathode biofilms contained more α -*Proteobacteria*, β -*Proteobacteria* and *Campylobacterales*, and less δ -*Proteobacteria* than in their respective MM and EHM suspended culture inocula. However, γ -*Proteobacteria*, which were enriched in the MM-biocathode, declined between the EHM inoculum and the EHM-biocathode.

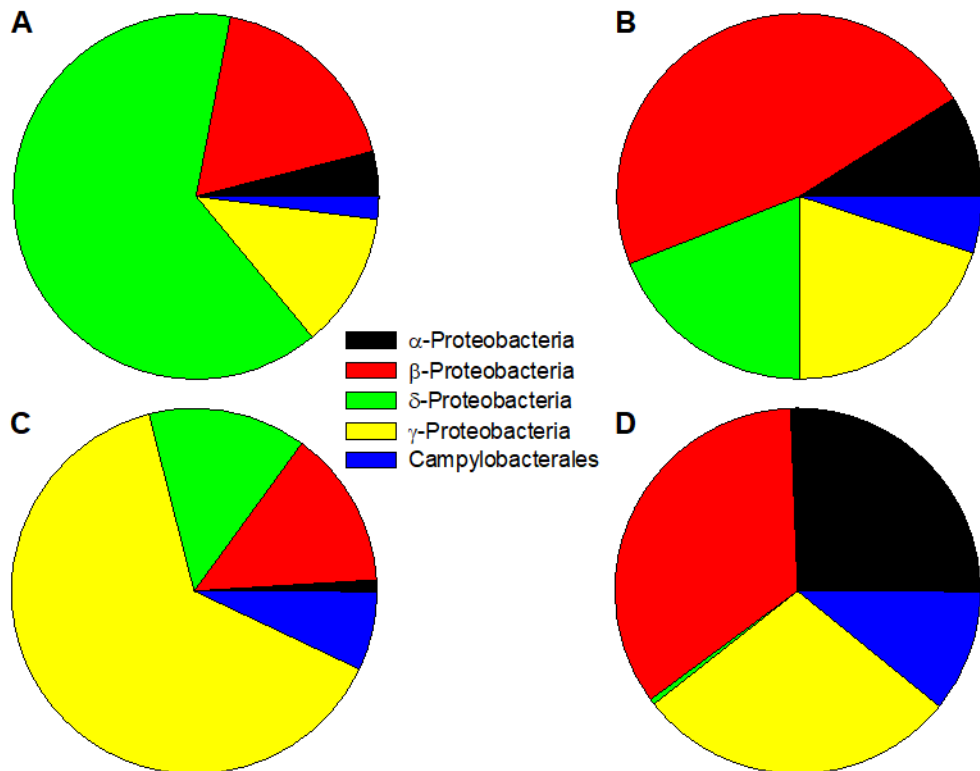


Figure 5.15 - Relative abundance of classes within the phylum Proteobacteria for MM suspended growth culture (A), MM-inoculated biocathode BES (B), EHM suspended growth culture (C) and EHM-inoculated biocathode BES (D).

Table 5.3 - Relative Abundance, Closest GenBank Relatives and Roles of Related Bacterial Species for OTUs in Suspended Growth Cultures and Biocathode Biofilms.

Closest GenBank Match / Accession No.	Relative Abundance ^a (%)				Roles ^b	Ref.
	MM	MM-B	EHM	EHM-B		
<i>Actinomyces georgiae</i> strain DSM 6843 (NR_026182)	2	2	5	0	CF; BF	
<i>Aminobacterium colombiense</i> strain DSM 12261 (NR_074624)	0	0	1	0	AF; HP	77
<i>Anaerolinea thermophila</i> strain UNI-1 (NR_074383)	9	0	0	0	CF; AF	78
<i>Arcobacter mytili</i> strain T234 (FJ156092)	0	0	2	2	BF; CB	79, 80
<i>Bacterium</i> MB7-1 (DQ453797)	0	0	0	6	Unk	
<i>Bacteroides</i> sp. strain Z4 (AY949860)	0	21	15	0	CF; AB	46
<i>Citrobacter amalonaticus</i> Y19 (LN564018)	0	0	0	3	EE; AB	54, 55
<i>Cloacibacillus evryensis</i> strain 158 (NR_115465)	0	0	1	0	AF	81
<i>Clostridium herbivorans</i> (L34418)	3	0	0	0	CF; HP; EE; AB	72, 73
<i>Clostridium pasteurianum</i> BC1 strain BC1 (NR_103938)	0	0	1	0	CF; HP; EE; AB	72, 73
<i>Clostridium polysaccharolyticum</i> strain DSM 1801 (NR_119085)	1	0	0	0	CF; HP; EE; AB	72, 73
<i>Eubacterium acidaminophilum</i> strain a1-2 (NR_121725)	1	0	0	0	AF; HP	82
<i>Helicobacter cholecystus</i> strain Hkb-1 (NR_118812)	0	0	0	3	HS	83
<i>Lactobacillus crispatus</i> ST1 strain ST1 (NR_074986)	2	0	0	0	CF; AB	75
<i>Mesotoga prima</i> strain MesG1.Ag.4.2 (NR_102952)	5	20	53	0	CF; AF; HP	65-67
<i>Mycobacterium frederiksbergense</i> isolate VM0503 (AF544628)	0	0	0	5	HD; BF	71
<i>Ochrobactrum anthropi</i> strain ATCC 49188 (NR_074243)	0	0	0	3	EE; AB	50
<i>Pedobacter saltans</i> strain DSM 12145 (NR_074586)	3	0	0	0	Unk	
<i>Propionivibrio limicola</i> strain GolChi1 (NR_025455)	0	0	0	6	HD	51
<i>Proteiniborus ethanoligenes</i> strain GW (NR_044093)	0	0	0	1	AF; HP	84
<i>Proteiniphilum acetatigenes</i> strain TB107 (NR_043154)	0	1	0	43	AF; HD	47, 48
<i>Pseudomonas aeruginosa</i> strain KAR21 (KR054983)	0	0	0	5	MP; BF	56, 57
<i>Pseudomonas grimontii</i> strain KAR27 (KR054989)	0	0	0	1	CF; MP	58
<i>Sphingopyxis terrae</i> strain IFO 15098 (NR_115618)	0	0	0	2	Unk	
<i>Spirochaeta thermophila</i> strain DSM 6578 (NR_074795)	0	0	2	0	CF	85
<i>Thiomonas intermedia</i> K12 strain K12 (NR_074593)	0	0	0	1	BF	52, 53
<i>Treponema primitia</i> strain ZAS-2 (NR_074169)	0	0	6	0	Ac; HS	62, 63
<i>Treponema</i> sp. I:K:T3 (AF023060)	1	34	0	0	Ac; HS	62, 63
<i>Trichococcus pasteurii</i> strain KoTa2 (NR_036793)	0	1	0	0	CB	76
Minor species (< 1% relative abundance)	72	21	12	18	Unk	

^a Abbreviations: MM, mixed methanogenic suspended growth culture; EHM, enriched methanogenic suspended growth culture; MM-B, MM-inoculated biocathode; EHM-B, EHM-inoculated biocathode.

^b Known roles of related Bacteria: Carbohydrate fermenter (CF); Amino acid fermenter (AAF); Hydrogen producer (HP); Hydrogen scavenger (HS); Acetogen (Ac); Exoelectrogen (EE); Hydrocarbon degrader (HD); Mediator producer (MP); Implicated in biofilm formation (BF); Found in anode biofilm (AB); Found in cathode biofilm (CB); Unknown function (Unk).

Table 5.4 - Closest GenBank Match and Relative Abundance of Identified Bacterial OTUs in the MM and EHM Suspended Growth and Biofilm Cultures

OTU	ID		Relative Abundance ^a (%)			
	(%)	Closest GenBank Match	MM	MM-B	EHM	EHM-B
KU597466	90	NR_026182 <i>Actinomyces georgiae</i> strain DSM 6843	0	0	5	0
KU597440	90	NR_026182 <i>Actinomyces georgiae</i> strain DSM 6843	2	2	0	0
KU597462	86	NR_074624 <i>Aminobacterium colombiense</i> strain DSM 12261	0	0	1	0
KU597439	87	NR_074383 <i>Anaerolinea thermophila</i> strain UNI-1	9	0	0	0
KU597471	88	FJ156092 <i>Arcobacter mytili</i> strain T234	0	0	1	1
KU597456	89	FJ156092 <i>Arcobacter mytili</i> strain T234	0	0	1	1
KU597452	99	DQ453797 <i>Bacterium</i> MB7-1	0	0	0	6
KU597464	99	DQ453797 <i>Bacterium</i> MB7-1	0	0	8	0
KU597468	97	AY949860 <i>Bacteroides</i> sp. strain Z4	0	0	7	0
KU597425	98	AY949860 <i>Bacteroides</i> sp. strain Z4	0	9	0	0
KU597427	100	AY949860 <i>Bacteroides</i> sp. strain Z4	0	12	0	0
KU597451	99	LN564018 <i>Citrobacter amalonaticus</i> Y19	0	0	0	3
KU597463	86	NR_115465 <i>Cloacibacillus evryensis</i> strain 158	0	0	1	0
KU597438	88	L34418 <i>Clostridium herbivorans</i>	3	0	0	0
KU597467	90	NR_103938 <i>Clostridium pasteurianum</i> BC1 strain BC1	0	0	1	0
KU597435	88	NR_119085 <i>Clostridium polysaccharolyticum</i> strain DSM 1801	1	0	0	0
KU597433	99	NR_121725 <i>Eubacterium acidaminophilum</i> strain a1-2	1	0	0	0
KU597455	92	NR_118812 <i>Helicobacter cholecystus</i> strain Hkb-1	0	0	0	3
KU597437	100	NR_074986 <i>Lactobacillus crispatus</i> ST1 strain ST1	2	0	0	0
KU597460	93	NR_102952 <i>Mesotoga prima</i> strain MesG1.Ag.4.2	0	0	1	0
KU597461	95	NR_102952 <i>Mesotoga prima</i> strain MesG1.Ag.4.2	0	0	52	0
KU597428	95	NR_102952 <i>Mesotoga prima</i> strain MesG1.Ag.4.2	0	17	0	0
KU597429	94	NR_102952 <i>Mesotoga prima</i> strain MesG1.Ag.4.2	5	3	0	0
KU597447	98	AF544628 <i>Mycobacterium frederiksbergense</i> isolate VM0503	0	0	0	5
KU597453	100	NR_074243 <i>Ochrobactrum anthropi</i> strain ATCC 49188	0	0	0	3
KU597436	79	NR_074586 <i>Pedobacter saltans</i> strain DSM 12145	3	0	0	0
KU597449	92	NR_025455 <i>Propionivibrio limicola</i> strain GolChi1	0	0	0	3
KU597457	92	NR_025455 <i>Propionivibrio limicola</i> strain GolChi1	0	0	0	3
KU597448	90	NR_044093 <i>Proteiniborus ethanoligenes</i> strain GW	0	0	0	1
KU597445	96	NR_043154 <i>Proteiniphilum acetatigenes</i> strain TB107	0	0	0	43
KU597434	94	NR_043154 <i>Proteiniphilum acetatigenes</i> strain TB107	0	1	0	0
KU597446	100	KR054983 <i>Pseudomonas aeruginosa</i> strain KAR21	0	0	0	5
KU597458	100	KR054989 <i>Pseudomonas grimonii</i> strain KAR27	0	0	0	1
KU597450	100	NR_115618 <i>Sphingopyxis terrae</i> strain IFO 15098	0	0	0	2
KU597465	77	NR_074795 <i>Spirochaeta thermophila</i> strain DSM 6578	0	0	2	0
KU597454	99	NR_074593 <i>Thiomonas intermedia</i> K12 strain K12	0	0	0	1
KU597469	88	NR_074169 <i>Treponema primitia</i> strain ZAS-2	0	0	5	0
KU597470	88	NR_074169 <i>Treponema primitia</i> strain ZAS-2	0	0	1	0
KU597426	89	AF023060 <i>Treponema</i> sp. I:K:T3	1	34	0	0
KU597430	99	NR_036793 <i>Trichococcus pasteurii</i> strain KoTa2	0	1	0	0
Other	NA	Minor species (< 1% relative abundance)	72	21	12	18

^a Abbreviations: MM, mixed methanogenic suspended growth culture; EHM, enriched methanogenic suspended growth culture; MM-B, MM-inoculated biocathode; EHM-B, EHM-inoculated biocathode.

In the EHM-biocathode, a phylotype was identified that was most closely related to *Ochrobactrum anthropi*, a species of α -*Proteobacteria* that has been reported to have exoelectrogenic properties and was isolated from an MFC anode (Zuo et al. 2008). Two phylotypes related to β -*Proteobacteria* species *Propionivibrio limicola* were also identified in the EHM-biocathode. *P. limicola* is an aerotolerant anaerobe known to ferment hydroaromatic compounds, producing only acetate and propionate. However, *P. limicola* does not ferment sugars, amino acids or aromatic compounds (Brune et al. 2002). The EHM-biocathode also had a phylotype related to *Thiomonas intermedia* strain K12, a species capable of fermenting tetrathionate under anoxic conditions or oxidizing sulfur species under aerobic conditions (Wentzien and Sand 2004). A relative, *Thiomonas arsenivorans*, is known to excrete exopolymeric substances that enhance biofilm stability. (Michel et al. 2011) Three phylotypes of γ -*Proteobacteria* were also observed in the EHM-biocathode, most closely related to *Citrobacter amalonaticus*, *Pseudomonas aeruginosa* and *Pseudomonas grimontii*. Several *Citrobacter* species are exoelectrogens capable of using a wide range of substrates (Huang et al. 2015, Xu and Liu 2011). *P. aeruginosa* has been isolated from the microbial community of a MFC anode, found to produce pyocyanin, a redox mediator that facilitated electrochemical activity (Rabaey et al. 2004). *P. aeruginosa* may also produce extracellular polymeric substances that assist in biofilm formation (Harimawan and Ting 2016). However, less is known about the related *P. grimontii* (Baïda et al. 2002).

While *Proteobacteria* were enriched in the EHM-biocathode, *Spirochaetes* were similarly enriched in the MM-biocathode to 35% of total detected Bacteria. In contrast, *Spirochaetes* represented less than 1% of the total detected Bacteria in the MM culture,

EHM culture and EHM-biocathode. *Spirochaetes* are Bacteria that utilize carbohydrates and produce H₂ and CO₂, along with other fermentation products such as acetate, lactate and ethanol (Leschine et al. 2006, Veldkamp 1960). *Spirochaetes* are normally low in abundance in most anaerobic reactors but have been found to persist under low-substrate conditions because of several mechanisms, including nutrient-seeking chemotaxis and the ability to derive energy from polymeric storage molecules, amino acids or intracellular RNA (Dollhopf et al. 2001). It is not likely that *Spirochaetes* were enriched in the MM-biocathode due to electrochemical conditions because a similar enrichment was not observed with the EHM-biocathode. Rather, it is probable that in the EHM-biocathode, *Spirochaetes* were outcompeted by other Bacteria such as *Proteobacteria*, which were more abundant in the EHM suspended growth culture than in the MM culture and include exoelectrogenic species. In the MM-biocathode, low substrate concentrations from cell lysis products and the relatively lower abundance of *Proteobacteria* in the MM suspended growth culture may have contributed to the enrichment of *Spirochaetes*. One phylotype, most closely related to *Treponema* spp., represented 34% of total Bacteria in the MM-biocathode. *Treponema* spp. are acetogens that use H₂ and CO₂ (Graber and Breznak 2004, Graber et al. 2004) and could theoretically divert electron equivalents away from the desired product, CH₄. Therefore, the substantial presence of acetogens in the MM-biocathode biofilm may have contributed to lower CH₄ production, relative to the EHM-biocathode.

Thermotogae increased in relative abundance between the MM and EHM suspended growth cultures and was the most abundant phylum in the EHM culture (53%). Despite the high abundance in the EHM culture, *Thermotogae* were undetected in the

EHM-biocathode. In contrast, the relative abundance of *Thermotogae* increased between the MM culture (16%) and MM-biocathode (24%). *Thermotogae* are anaerobic Bacteria that ferment a wide array of carbohydrates and amino acids, known to produce H₂ (Bhandari and Gupta 2014, Cappelletti et al. 2014, Nesbø et al. 2012, Zhaxybayeva et al. 2012). While most known *Thermotogae* are thermophilic, some, such as *Mesotoga prima*, are mesophilic and grow at the temperature conditions of this study (Bhandari and Gupta 2014). Indeed, phylotypes most closely related to *M. prima* represented 31% and 99% of the total *Thermotogae* detected in the MM and EHM cultures, respectively. Furthermore, in the EHM culture, *M. prima* phylotypes represented 52% of the total Bacteria (Table 5.3), indicating H₂/CO₂ enrichment conditions favored *M. prima* growth. MM-biocathode conditions also appeared to favor *M. prima* growth (20% relative abundance; 84% of total *Thermotogae*), but this phylotype was not detected in the EHM-biocathode.

Actinobacteria were slightly more abundant in the EHM and EHM-biocathode cultures than in the MM and MM-biocathode cultures (Figure 5.14). Phylotypes related to *Actinomyces georgiae* were identified in the MM, EHM and MM-biocathode cultures. *A. georgiae* is a carbohydrate fermenter (Johnson et al. 1990), and similar species have been implicated in biofilm formation processes (Paddick et al. 2003). In contrast, the EHM-biocathode had a phylotype most closely related to *Mycobacterium frederiksbergense*, a PAH-degrader (Willumsen et al. 2001). A relative, *Mycobacterium* sp. LB501T, was capable of growing on solid anthracene as a sole carbon source (Wick et al. 2002).

Firmicutes had a similar relative abundance in each suspended growth culture and a similar, albeit smaller, relative abundance in each cathode biofilm. The EHM and MM suspended growth cultures, but not the respective biofilms, contained several phylotypes

related to carbohydrate-fermenting, H₂-producing *Clostridium* spp., which are exoelectrogenic (Kumar et al. 2015, Park et al. 2001). The MM culture contained a phylotype related to *Lactobacillus crispatus*, a carbohydrate fermenter and close relative to a species found within a MFC (van der Wielen et al. 2002, Vega and Fernández 1987). A phylotype in the MM-biocathode was most closely related to *Trichococcus pasteurii*, which has previously been observed in the biofilm of a chromium (Cr(VI)) reduction cathode (Tandukar et al. 2009).

The relative abundance of total identified OTUs that were closely related to a bacterial species with one of several known functions was presented in a heatmap for the EHM, MM and biocathode cultures (Figure 5.16). While the function of many bacterial species within a methanogenic biocathode is not clear, this analysis suggests that amino acid fermenters, exoelectrogens, hydrocarbon degraders and redox mediator producers may be the most beneficial to methanogenic biocathode performance. Further study is needed to understand how the members of the biocathode microbial communities interact to influence CH₄ production. By understanding how to select for beneficial biocathode Bacteria, more effective enrichment techniques may be developed to enhance biocathode CH₄ production for use in BES-based biogas upgrading.

Culture	Relative Abundance of OTUs Related to Species of Various Categories (%)											
	CF	AAF	HP	HS	Ac	EE	HD	MP	BF	AB	CB	Unk
MM	22	15	10	1	1	4	0	0	2	6	0	75
MM-B	43	21	20	34	34	0	1	0	2	21	1	21
EHM	76	55	55	7	7	1	0	0	8	16	2	12
EHM-B	1	44	1	4	0	6	48	6	13	6	2	20

Figure 5.16 - Relative abundance heatmap of OTUs most closely related to species classified as a carbohydrate fermenter (CF); amino acid fermenter (AAF); hydrogen producer (HP); hydrogen scavenger (HS); acetogen (Ac); exoelectrogen (EE); hydrocarbon degrader (HD); mediator producer (MP); implicated in biofilm formation (BF); found in anode biofilm (AB); found in cathode biofilm (CB); and unknown function (Unk). Mixed methanogenic suspended growth culture (MM); MM-inoculated biocathode (MM-B); Enriched hydrogenotrophic methanogenic suspended growth culture (EHM); EHM-inoculated biocathode (EHM-B). Note that most identified OTUs were related to species that belong to more than one class and, therefore, the row total for each culture exceeded 100%.

5.3.4 *Proteobacteria in Suspended Growth and Cathode Biofilm Cultures.*

α-Proteobacteria represented 2% and 4% of all *Proteobacteria* in the MM and MM-biocathode communities, respectively. In contrast, *α-Proteobacteria* increased from 1% to 26% of *Proteobacteria* between the EHM culture and EHM-biocathode. Within *α-Proteobacteria*, a phylotype similar to *Ochrobactrum* sp. was enriched on both the EHM- and MM-biocathodes. In the EHM and MM suspended growth cultures, this phylotype made up 17% and 77% of the *α-Proteobacteria*, respectively, but represented a respective 25% and 83% of EHM- and MM-biocathode *α-Proteobacteria*. *Ochrobactrum* species are known exoelectrogens capable of producing current from volatile fatty acids, sugars and alcohols (Liu et al. 1999, Logan 2009, Matias et al. 2005).

β-Proteobacteria represented similar fractions of *Proteobacteria* in the MM and EHM cultures (18% and 14%, respectively) and each biocathode achieved similar

enrichment to 47% and 35% of *Proteobacteria* in the MM- and EHM-biocathodes, respectively. Within β -*Proteobacteria*, a phylotype similar to *Achromobacter* sp. was enriched on both the EHM- and MM-biocathodes. In the EHM and MM suspended growth cultures, this phylotype made up 9% and 28% of the β -*Proteobacteria*, respectively, but represented a respective 39% and 55% of EHM- and MM-biocathode β -*Proteobacteria*. In fact, in the EHM-biocathode, the *Achromobacter* phylotype alone made up 6% of total Bacteria. *Achromobacter* enrichment on a biocathode with CO₂ as a sole external carbon source has previously been reported (Bond et al. 2002).

The δ -*Proteobacteria* composition differed between the MM and EHM suspended growth cultures (Table 5.5), with a greater relative abundance of phylotypes related to *Smithella* sp., *Desulfovibrionales* spp., and *Geobacter* sp. in the EHM culture than in the MM culture. *Smithella propionica* are syntrophic Bacteria that ferment propionate in association with methanogens that consume H₂ (McLennan et al. 2008). *Desulfovibrio* spp. are anaerobic Bacteria that are also capable of fermentation in association with methanogens during anaerobic digestion (Gölz et al. 2012). *Geobacter* species are well known exoelectrogens capable of utilizing organics such as acetate to produce current and CO₂ (Huang et al. 2015). δ -*Proteobacteria* represented a far smaller fraction of *Proteobacteria* in the MM- and EHM-biocathodes (19% and 0.5%, respectively) than in the MM and EHM inocula (64% and 14%, respectively). δ -*Proteobacteria* contains many sulfate- and iron-reducing species (Jeon et al. 2012), which require oxidized electron acceptors unlikely to be abundant near a highly-reduced cathode. In contrast, *Campylobacteriales*, an order of ϵ -*Proteobacteria*, represented a moderately higher fraction of *Proteobacteria* in the MM- and EHM-biocathodes (5% and 11%, respectively) than in

the MM and EHM inocula (2% and 7%, respectively). Many species of *Campylobacteriales* possess surface polysaccharides that have been implicated in biofilm formation (Savelieva et al. 2004, Xu and Liu 2011).

Table 5.5 - Composition of δ -Proteobacteria in the MM and EHM Suspended Growth Cultures

Closest Matching Species	MM Culture		EHM Culture	
	Fraction of δ -Proteobacteria	Fraction of Total Bacteria	Fraction of δ -Proteobacteria	Fraction of Total Bacteria
Unclassified <i>Syntrophobacteriales</i>	58	0.8	19	0.2
<i>Smithella</i> sp.	26	0.4	49	0.6
<i>Syntrophus</i> spp.	7	0.1	7	0.09
<i>Syntrophorhabdus</i> sp.	6	0.08	3	0.04
<i>Syntrophus buswelli</i>	1	0.01	ND	ND
<i>Geobacter</i> sp.	2	0.02	4	0.05
<i>Desulfovibrionales</i> sp.	0.3	0.005	17	0.2
<i>Desulfobulbus</i> sp.	0.2	0.003	ND	ND
<i>Sorangium cellulosum</i>	ND ^a	ND	0.3	0.004
<i>Desulfofaba</i> sp.	ND	ND	0.2	0.003

^a ND, not detected

γ -Proteobacteria (64%) were the most abundant *Proteobacteria* in the EHM culture but made up only 12% of the MM culture *Proteobacteria* (Figure 5.15). Additionally, the γ -Proteobacteria composition was markedly different between the two cultures. In the EHM culture, 93% of γ -Proteobacteria was made up of a phylotype similar to *Citrobacter freundii*. In both biocathodes, a phylotype similar to *Citrobacter* sp. dominated the *Enterobacteriaceae*, making up 97% and 99% of the *Enterobacteriaceae* in the EHM- and MM-biocathodes, respectively. This phylotype made up 3% of total Bacteria in the EHM-biocathode but only 0.5% of total Bacteria in the MM-biocathode. *Citrobacter*

spp. have been shown to be exoelectrogens capable of utilizing a wide range of substrates and producing current in an MFC (Bouvet et al. 1995, Yong et al. 2011). In one study, a strain of *C. freundii* exhibited high electrochemical activity and was thought to transfer electrons through extracellular mediators (Bouvet et al. 1995), suggesting a potentially useful role in bioelectrochemical systems. *C. freundii* can ferment pyruvate, producing acetate, CO₂ and H₂, as well as small amounts of lactate, succinate and formate (Price-Whelan et al. 2007, Seviour et al. 2015). In the EHM culture, cell lysis products may have supplied fermentation substrates for *C. freundii*. However, it is not clear why *C. freundii* comprised such a large fraction (93%) of the γ -*Proteobacteria* in the EHM culture or what role it played in the microbial community.

The γ -*Proteobacteria* families represented in the MM culture were more diverse: *Enterobacteriaceae* (33%), *Vibrionaceae* (24%), *Xanthomonadaceae* (13%), *Pseudomonaceae* (12%) and unclassified (19%). In the MM culture, the most abundant family, *Enterobacteriaceae*, was dominated by a phylotype related to *Citrobacter* sp. (29% of *Enterobacteriaceae*), indicating a significant presence of *Citrobacter* phylotypes in both the MM and EHM cultures. Other families, such as the *Xanthomonadaceae*, *Pseudomonadaceae* and *Vibrionaceae* fell in relative abundance over the course of enrichment to 3%, 2% and below detection, respectively, in the EHM culture. Thus, enrichment conditions favored the growth of *Enterobacteriaceae*, in particular *Citrobacter*, over the growth of other types of γ -*Proteobacteria*.

The γ -*Proteobacteria* fraction of *Proteobacteria* increased between the MM inoculum (12%) and the MM-biocathode (20%), but decreased between the EHM inoculum (64%) and the EHM-biocathode (29%). The family composition of γ -

Proteobacteria was also substantially different between the suspended growth cultures and the cathode biofilms. The family *Enterobacteriaceae* represented 69% of γ -*Proteobacteria* in the MM-biocathode but only 33% in the MM suspended growth culture. In contrast, *Enterobacteriaceae* represented 9% and 27% of the γ -*Proteobacteria* in the EHM and EHM-biocathode, respectively. Instead, *Pseudomonas* and *Xanthomonadales*, which represented only 2% and 3% of the γ -*Proteobacteria* in the EHM suspended growth culture, respectively, made up 54% and 19% in the EHM-biocathode, respectively.

Within the family of γ -*Proteobacteria*, the genus *Pseudomonas* was enriched on both biocathodes. *Pseudomonas* represented only 0.1% of the total Bacteria in the EHM suspended growth culture but made up 7% of all Bacteria in the EHM-biocathode biofilm. In the MM suspended growth culture, *Pseudomonas* made up only 0.03% of all Bacteria, which increased to 0.1% in the MM cathode biofilm. A previous study observed the enrichment of *Pseudomonas* on a cathode with CO₂ as a sole external carbon source (Bond et al. 2002). Within the genus, a phylotype similar to *Pseudomonas aeruginosa* represented 26% and 30% of *Pseudomonas* in the MM suspended growth culture and MM-biocathode biofilm, respectively, indicating not much change in *Pseudomonas* composition due to biofilm development. In contrast, the *P. aeruginosa* phylotype made up 100% of *Pseudomonas* in the EHM suspended growth culture and 70% of *Pseudomonas* in the EHM-biocathode. *P. aeruginosa* produces compounds, such as pyocyanin and phenazine, which are capable of acting as electron shuttles that can be utilized by other species for electron transfer in BESs (Logan 2009, Pham et al. 2008). Indeed, phenazine has been shown to increase electron transfer in the anode of a MFC (Rabaey et al. 2005). Excretion of electron shuttles by *P. aeruginosa* appears to be associated with quorum sensing. In a

study of a *P. aeruginosa* strain in which the *rhl* quorum sensing system was overexpressed, pyocyanin and phenazine-1-carboxylate were produced, with reduction potentials of -0.37 V and -0.48 V, respectively (Leschine et al. 2006). Thus, excreted phenazines may act as mediators between a cathode surface poised at -0.80 V and the terminal electron acceptor, CO₂ ($E^0 = -0.24$ V for CO₂/CH₄). Furthermore, another study showed *P. aeruginosa*-excreted pyocyanin concentrations were higher at more negative working electrode potentials (Veldkamp 1960), although the tested potentials were not as negative as the cathode potential used in the present study (i.e., -0.8 V). Finally, phenazines are known to be produced when cell densities are high (Dollhopf et al. 2001), which is also consistent with microbial growth as a biofilm on the cathode. Thus, it is possible that the greater abundance of the *P. aeruginosa* phylotype in the EHM-biocathode contributed to the observed higher CH₄ production than in the MM-biocathode.

5.4 Summary

The cathode microbial community of a methanogenic bioelectrochemical system (BES) is key to efficient conversion of carbon dioxide (CO₂) to methane (CH₄) with application to biogas upgrading. The objective of this study was to compare the performance and microbial community composition of a biocathode inoculated with a mixed methanogenic (MM) culture to a biocathode inoculated with an enriched hydrogenotrophic methanogenic (EHM) culture, developed from the MM culture following pre-enrichment with H₂ and CO₂ as the only externally supplied electron donor and carbon source, respectively. Using an adjacent Ag/AgCl reference electrode, biocathode potential was poised at -0.8 V (vs. SHE) using a potentiostat, with the bioanode acting as the counter electrode. When normalized to cathode biofilm biomass,

the methane production in the MM- and EHM-biocathode was 0.153 ± 0.010 and 0.586 ± 0.029 mmol CH₄/mg biomass-d, respectively. This study showed that H₂/CO₂ pre-enriched inoculum enhanced biocathode CH₄ production, although the archaeal communities in both biocathodes converged primarily (86-100%) on a phylotype closely related to *Methanobrevibacter arboriphilus*. The bacterial community of the MM-biocathode was similar to that of the MM inoculum but was enriched in *Spirochaetes* and other non-exoelectrogenic, fermentative Bacteria. In contrast, the EHM-biocathode bacterial community was enriched in *Proteobacteria*, exoelectrogens and putative producers of electron shuttle mediators. Similar biomass levels were detected in the MM- and EHM-biocathodes. Thus, although the archaeal communities were similar in the two biocathodes, the difference in bacterial community composition was likely responsible for the 3.8-fold larger CH₄ production rate observed in the EHM-biocathode. Roles for abundant OTUs identified in the biofilm and inoculum cultures were highlighted based on previous reports.

CHAPTER 6. ZERO VALENT IRON-AMENDED BIOCATHODE

6.1 Introduction

Biogas produced by anaerobic digestion contains a mixture of carbon dioxide (CO₂) and methane (CH₄), along with other trace gases. Current methods of biogas upgrading separate or sequester CO₂, but a methanogenic bioelectrochemical system (BES) is capable of directly converting CO₂ to CH₄, improving both biogas energy content and CH₄ yield (Geppert et al. 2016, Muñoz et al. 2015) In a methanogenic BES, a low applied potential (<1 V) drives an oxidation reaction in the bioanode and the reduction of CO₂ to CH₄ in the biocathode (Cheng et al. 2009). While direct electron transfer from the cathode to methanogens may occur ($\text{CO}_2 + 8\text{H}^+ + 8\text{e}^- \rightleftharpoons \text{CH}_4 + 2\text{H}_2\text{O}$; $E_{\text{H}}^{\circ} = -0.244 \text{ V vs. SHE}$), hydrogen (H₂) may also be produced at the cathode from the reduction of protons ($2\text{H}^+ + 2\text{e}^- \rightleftharpoons \text{H}_2$; $E_{\text{H}}^{\circ} = -0.421 \text{ V vs. SHE}$) and utilized by hydrogenotrophic methanogens to reduce CO₂ ($\text{CO}_2 + 4\text{H}_2 \rightleftharpoons \text{CH}_4 + 2\text{H}_2\text{O}$; $\Delta E_{\text{H}}^{\circ} = 0.170 \text{ V}$) (Cheng et al. 2009, Rosenbaum et al. 2011). Alternately, mediators may accept electrons from the cathode and, in turn, act as electron donors for the reduction of CO₂ (Rosenbaum et al. 2011).

Iron is an important trace metal for methanogens and is a central element in hydrogenases, ferredoxin, polyferredoxin and other iron-sulfur proteins (Ferry 1993). Of particular importance are NiFe and FeFe hydrogenases, which catalyze the production of H₂ from protons and electrons, as well as the reverse reaction. Carbon monoxide and cyanide ligands stabilize the iron center of these enzymes (Kuchenreuther et al. 2013, Reissmann et al. 2003). A number of methanogens are capable of producing CH₄ from

CO₂, using zero-valent iron (ZVI) as the sole electron donor (Belay and Daniels 1990, Daniels et al. 1987, Lorowitz et al. 1992, Mayhew et al. 2016). ZVI undergoes cathodic depolarization under anaerobic conditions, resulting in metal oxidation and the formation of H₂ ($\text{Fe}^0 + 2\text{H}^+ \rightleftharpoons \text{Fe}^{2+} + \text{H}_2$; $\Delta E_{\text{H}^0} = 0.026 \text{ V}$), which in turn may be used by methanogens for CO₂ reduction to CH₄ (Daniels et al. 1987, Kato 2016). It is also known that in anaerobic environments rich in dissolved CO₂ species, ZVI corrosion is accelerated by H₂CO₃ and HCO₃⁻ (Agrawal et al. 2002). Additionally, by maintaining a low localized H₂ partial pressure, methanogens create conditions that are more thermodynamically favorable for ZVI corrosion. Some evidence also exists for direct electron transfer from ZVI without intermediate H₂ formation (Dinh et al. 2004, Kato 2016). Indeed, the addition of ZVI to anaerobic digesters has been shown to improve biogas CH₄ content (Feng et al. 2014, Huang et al. , Karri et al. 2005). Although it is not clear whether methanogens increase the rate of iron corrosion, research into *Methanococcus maripaludis* found the ability to corrode iron was strain-specific, suggesting that certain methanogens may accelerate iron corrosion (Dinh et al. 2004, Uchiyama et al. 2010).

In addition to H₂, the anaerobic corrosion of ZVI also produces Fe²⁺, which may complex with other ions to form precipitates (Agrawal et al. 2002, Bonin et al. 2000), and OH⁻ ions that may increase pH and result in the precipitation of carbonates (Reardon 1995). A number of precipitates have been observed in ZVI permeable reactive barriers, including iron (hydr)oxides, iron carbonates, iron sulfides, green rusts, siderite, ferrihydrite, vivianite and magnetite (Henderson and Demond 2007, Phillips et al. 2010). Although some precipitates, such as magnetite, are electrically conductive, iron (hydr)oxides, carbonates and other precipitates may passivate ZVI and decrease the rate of corrosion (Henderson

and Demond 2007). In one study, methanogenic cultures fed with acetate or ethanol displayed accelerated methanogenesis when semi-conductive iron-oxide minerals hematite or magnetite were added (Kato et al. 2012). Furthermore, iron-supplemented cultures had a higher abundance of exoelectrogenic *Geobacter* spp. (Kato et al. 2012). Fe^{2+} ions, a product of ZVI anaerobic corrosion, have also been found to improve the production of biogas and increase its CH_4 content during anaerobic digestion, although the mechanism was not identified (Zhang et al. 2016). Thus, ZVI and/or its products may affect the microbial community of a biocathode and alter microbial metabolism. Moreover, in a biocathode, iron precipitates resulting from ZVI corrosion and ion complexation could coat the cathode surface, potentially affecting biofilm development and/or electron transfer.

Although ZVI addition has been previously examined in the context of electrochemical systems for copper(II), nitrate and arsenite removal (Kim et al. 2015, Li et al. 2016a, Xue et al. 2013), reports on the effect of ZVI addition to a methanogenic biocathode could not be found. Thus, the objective of this study was to assess how the addition of ZVI to a CO_2 -fed methanogenic biocathode would affect: i) CH_4 production at a fixed cathode potential over several feeding cycles; ii) CH_4 production at different cathode potentials; and iii) the cathode microbial community.

6.2 Materials and Methods

6.2.1 BES Setup.

A batch BES was setup as a dual chamber, H-type with two 300-mL (250 mL liquid volume) modified square glass bottles separated by a proton exchange membrane (PEM; Nafion 117, 6.16 cm^2 ; DuPont, Wilmington, DE). Each chamber was sealed with a butyl

rubber stopper and initially flushed with nitrogen (N₂) (anode) or CO₂ (cathode) gas. The BES was maintained at room temperature (22±2°C) under continuous mixing using a magnetic stirrer. The anode and cathode electrodes were porous carbon felt (4 strips, approximately 86 cm², 15 cm³; Alfa Aesar, Ward Hill, MA) attached to a stainless steel rod. An Ag/AgCl electrode (+0.199 V vs. standard hydrogen electrode, SHE) was placed adjacent to the carbon felt electrode in each chamber to allow for voltage measurements. The cathode Ag/AgCl electrode acted as the reference electrode and the cathode and anode carbon felt electrodes were the working and counter electrodes, respectively. The working, counter and reference electrodes were connected to a Gamry Interface 1000 potentiostat (Warminster, PA) with shielded cables and the cathode potential was poised at -0.8 V (vs. SHE) for the fixed-potential tests. The BES bioanode was inoculated with felt from an established, stock microbial fuel cell (MFC) consisting of a carbon felt bioanode, 150 Ω resistor and Pt-coated air cathode, as previously described in Section 5.2.2. The MFC was fed acetate weekly at an initial concentration of 1.2 g COD/L and maintained with hydraulic retention time (HRT) of 8.75 days. The BES biocathode was inoculated with felt from an established, stock methanogenic biocathode that had been initially inoculated with an enriched, hydrogenotrophic methanogenic suspended-growth culture (see Section 5.2.2). The stock biocathode was fed weekly by flushing the headspace with CO₂ and then pressurizing to an absolute pressure of 1.65 atm. The BES anode was filled with 250 mL anolyte, consisting of phosphate buffer medium (NaH₂PO₄·H₂O, 14.2 g/L; Na₂HPO₄, 13.8 g/L; NH₄Cl, 0.31 g/L; KCl, 0.13 g/L), mineral stock (Cheng et al. 2009) 12.5 mL/L, and anode vitamin stock 2.5 mL/L. (Lovley and Phillips 1988) The cathode was filled with 250 mL catholyte, consisting of phosphate buffer medium, mineral stock 12.5 mL/L and

cathode vitamin stock 5.0 mL/L.(Cheng et al. 2009) Anode and cathode liquid was completely replaced with fresh anolyte or catholyte each week, for a HRT of 7 days. The bioanode was fed sodium acetate at an initial concentration of 2.5 g COD/L and the biocathode was fed by flushing the headspace with CO₂ and then pressurizing to an absolute pressure of 1.65 atm.

6.2.2 *Zero-Valent Iron Biocathode.*

ZVI filings (40 mesh) were obtained from ThermoFisher Scientific (Waltham, MA). Following biofilm establishment, ZVI was added to the bottom of the cathode compartment to initial concentrations of 1 or 2 g/L at the beginning of a feeding cycle using a syringe. ZVI filings initially adhered to the magnetic stir bar but gradually dissipated as the ZVI corroded; ZVI filings were not noticeable at the end of a 7-d feeding cycle. BES performance was monitored for four feeding cycles in which no new ZVI was added and all catholyte was exchanged for fresh medium each cycle. Similarly, a BES with a ZVI-free biocathode was maintained and served as the bioactive control. Two abiotic cathode controls (0 and 1 g/L ZVI) were also set up and compared with the biocathodes. Then, the biocathode performance was compared in which the initial ZVI concentration was 1 g/L and the cathode potential was -0.80, -0.75, -0.70 or -0.65 V. Between tests, the biocathode was rinsed with catholyte to remove residual ZVI or iron precipitates. Iron (II) ions (Fe²⁺) were measured as described in Section 3.1.11.

6.2.3 *Precipitate Analysis.*

A precipitate, which formed in the biocathode following ZVI addition, was collected in a N₂-flushed bottle and rinsed 5 times with 500 mL deoxygenated DI water to

remove all soluble substances. The precipitate was then dried under a N₂ stream and the resulting powder was analyzed using cyclic voltammetry and scanning electron microscopy with energy-dispersive X-ray spectroscopy (SEM-EDS). SEM-EDS was conducted with a Zeiss Ultra 60 FE-SEM from 0 to 9 keV and AZtecTEM software.

6.2.4 *Microbial Community Analysis.*

Bacterial DNA was extracted from the biocathode felt using the PowerSoil DNA Isolation Kit (Mo Bio Laboratories, Carlsbad, CA) according to manufacturer's instructions. Following extraction, all DNA was quantified using a Nanodrop 3300 (Thermo Scientific, Wilmington, DE) and stored at -20°C until sequencing was performed. Bacterial DNA was amplified using the 16S rRNA gene primers 28F (5'-GAGTTTGATCNTGGCTCAG-3') and 388R (5'-TGCTGCCTCCCGTAGGAGT-3'). Archaeal DNA was amplified using the 16S rRNA gene primers 519wF (5'-CAGCMGCCGCGGTAA-3') and 1017R (5'-GGCCATGCACCWCCTCTC). Amplified DNA was sequenced using the Illumina MiSeq platform (Research and Testing Laboratory, Lubbock, TX). Forward and reverse reads were merged with PEAR Illumina paired-end read merger and trimmed for quality. Clustering was performed at a 4% divergence using the USEARCH clustering algorithm and the UPARSE OTU selection algorithm was utilized to classify clusters into OTUs. Chimera checking of selected OTUs was performed with UCHIME software. A phylogenetic analysis was conducted by comparing sequences that had a relative abundance $\geq 1\%$ with the closest 16S rRNA gene matches in GenBank (National Center for Biotechnology Information; Bethesda, MD). Using Mega 7.0 software, sequences were aligned with ClustalW and trimmed. A maximum likelihood phylogenetic tree was constructed using the Tamura-Nei model, 100 bootstrap replications

and the Nearest-Neighbor-Interchange heuristic method. Unique sequences have been deposited in GenBank (NCBI) with accession numbers KX587566 and KX759042-KX759087.

6.2.5 *Analytical Methods.*

pH was measured as described in Section 3.1.1. Total suspended solids (TSS) and volatile suspended solids (VSS) were measured as described in Section 3.1.5. Total gas production and gas composition were measured as described in Sections 3.1.6 and 3.1.7, respectively. Volatile fatty acids were measured as described in Section 3.1.8. Biofilm and suspended biomass protein was extracted and measured as described in Section 3.1.10. Biomass was estimated by assuming cell protein was 63% of the cell dry weight (Simon and Azam 1989).

6.3 **Results and Discussion**

6.3.1 *ZVI-Free Biocathode.*

The performance of a BES with an established methanogenic biocathode (BC0) was compared with that of the abiotic cathode control BES (AC0) (Table 1). The anolyte and catholyte pH remained between 6.7 and 6.8. During a feeding cycle, the clear anolyte gradually turned brown (Figure 6.1), due to the production of a dark-colored soluble substance, likely an oxidation product of an anolyte component (e.g., vitamin, mineral, etc.). Anode acetate removal ranged from 85.8 to 98.9% over the course of the feeding cycles. At the end of a typical cycle, the anode headspace gas consisted of $18.3 \pm 5.0\%$ CO₂, $4.9 \pm 1.3\%$ CH₄, $0.9 \pm 0.5\%$ H₂ and $76.0 \pm 5.5\%$ N₂. The observed CH₄ and H₂ was consistent

with the transport of dissolved gases across the membrane from cathode to anode (Chae et al. 2008, Jiang and Chu 2002, Ma et al. 2005).

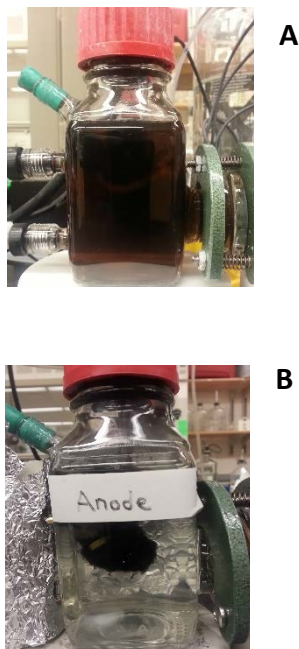


Figure 6.1 - Anolyte at the end of a feeding cycle prior to the addition of ZVI to the cathode (A) and at the end of a feeding cycle after ZVI addition to the cathode (B).

Compared to the abiotic cathode (AC0), the BES with the BC0 biocathode produced a greater number of electron equivalents as gas (H_2 or CH_4) (Table 6.1). The AC0 cathode produced H_2 from water electrolysis at a linear rate of 493 ± 6 mmol/m²-d ($R^2 = 0.998$; normalized to the PEM surface area) (Figure 6.2B); CH_4 was not detected in the AC0 cathode headspace (Figure 6.3B). In contrast, the BC0 cathode headspace CH_4 increased linearly at a rate of 169 ± 6 mmol/m²-d ($R^2 = 0.9918$) (Figure 6.3B) and H_2 was not detected (Figure 6.2B). The linear rate of CH_4 production indicates that methanogenesis

was not CO₂-limited during the feeding cycle. H₂ was not detected in the BC0 cathode headspace due to fast and efficient hydrogenotrophic methanogenesis.

Table 6.1 - BES Performance under Different Cathode Conditions

Setup	Cathode Type	Cathode Potential ^a (V)	Cycle ^b	ZVI ^c (g/L)	Anode	Cathode Gas Production		
					Acetate Removal (%)	H ₂ (mmol)	CH ₄ (mmol)	eeq ^d (meeq)
AC0	Abiotic	-0.80	1	-- ^e	81.9	2.08	ND ^f	4.17
AC1	Abiotic	-0.80	1	1	87.3	11.68	ND	23.35
BC0	Biotic	-0.80	1	--	86.0	ND	0.78	6.22
			2	--	85.8	ND	0.60	4.77
			3	--	90.5	ND	0.77	6.14
			4	--	98.9	ND	0.69	5.54
BC1	Biotic	-0.80	1	1	90.1	0.01	2.67	21.34
			2	--	90.9	ND	2.21	17.67
			3	--	93.6	ND	1.71	13.69
			4	--	95.2	ND	1.58	12.62
BC2	Biotic	-0.80	1	2	89.7	0.08	2.73	22.02
			2	--	96.8	0.01	1.63	13.01
			3	--	96.8	ND	2.22	17.78
			4	--	80.7	ND	2.57	20.57

^a V versus SHE.

^b Number of consecutive 7-d feeding cycles.

^c Initial concentration of ZVI added to the cathode at the start of a feeding cycle.

^d Electron equivalents.

^e Not added.

^f Not detected.

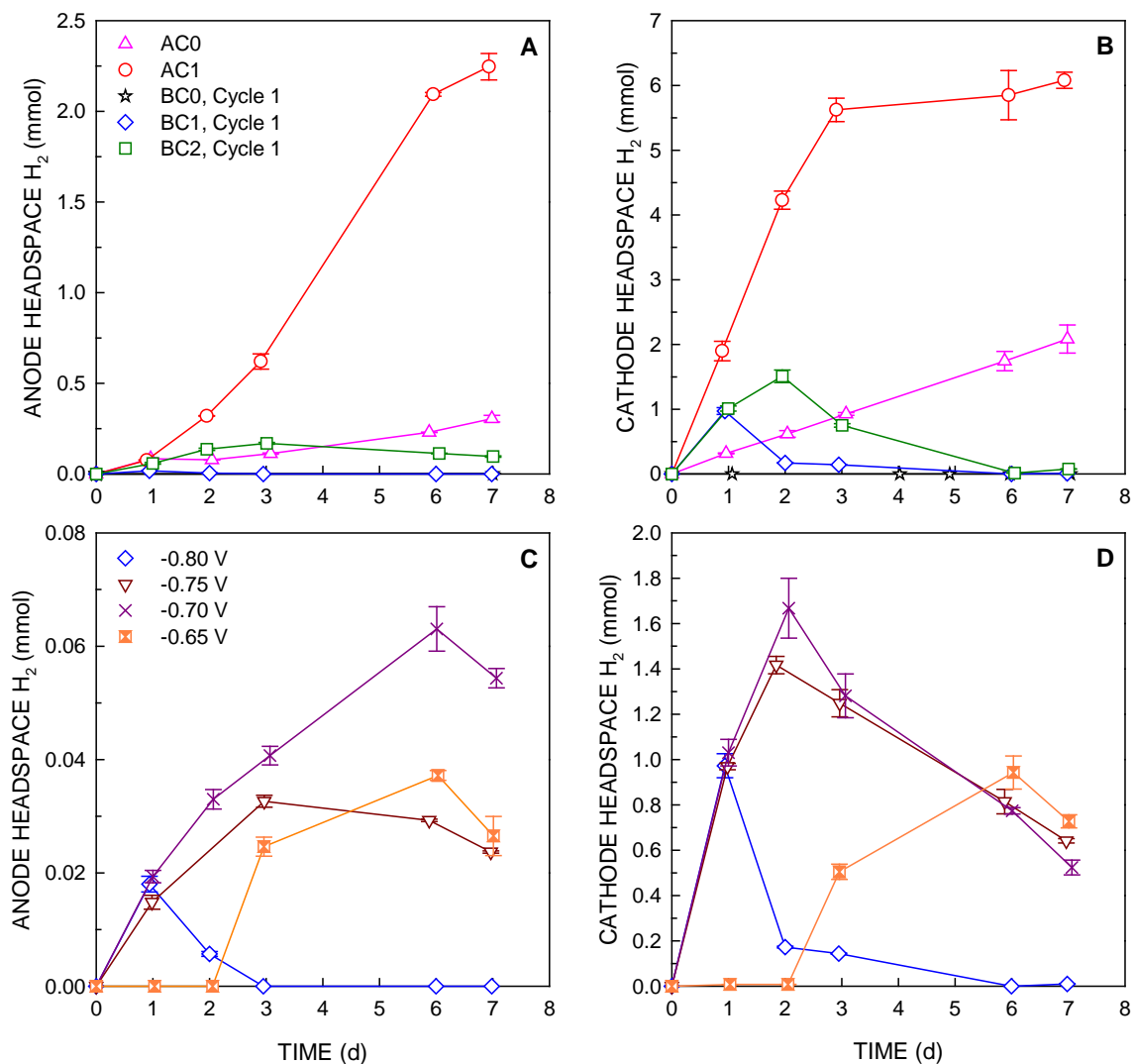


Figure 6.2 - Time course of headspace hydrogen in the anode (A) and cathode (B) for various BES configurations (ZVI-free abiotic cathode, AC0; abiotic cathode with 1 g/L ZVI, AC1; ZVI-free biocathode, BC0; biocathode with 1 g/L ZVI, BC1; biocathode with 2 g/L ZVI, BC2), and in the anode (C) and cathode (D) of the BC1 system at various applied potentials (-0.65 to -0.80 V vs. SHE).

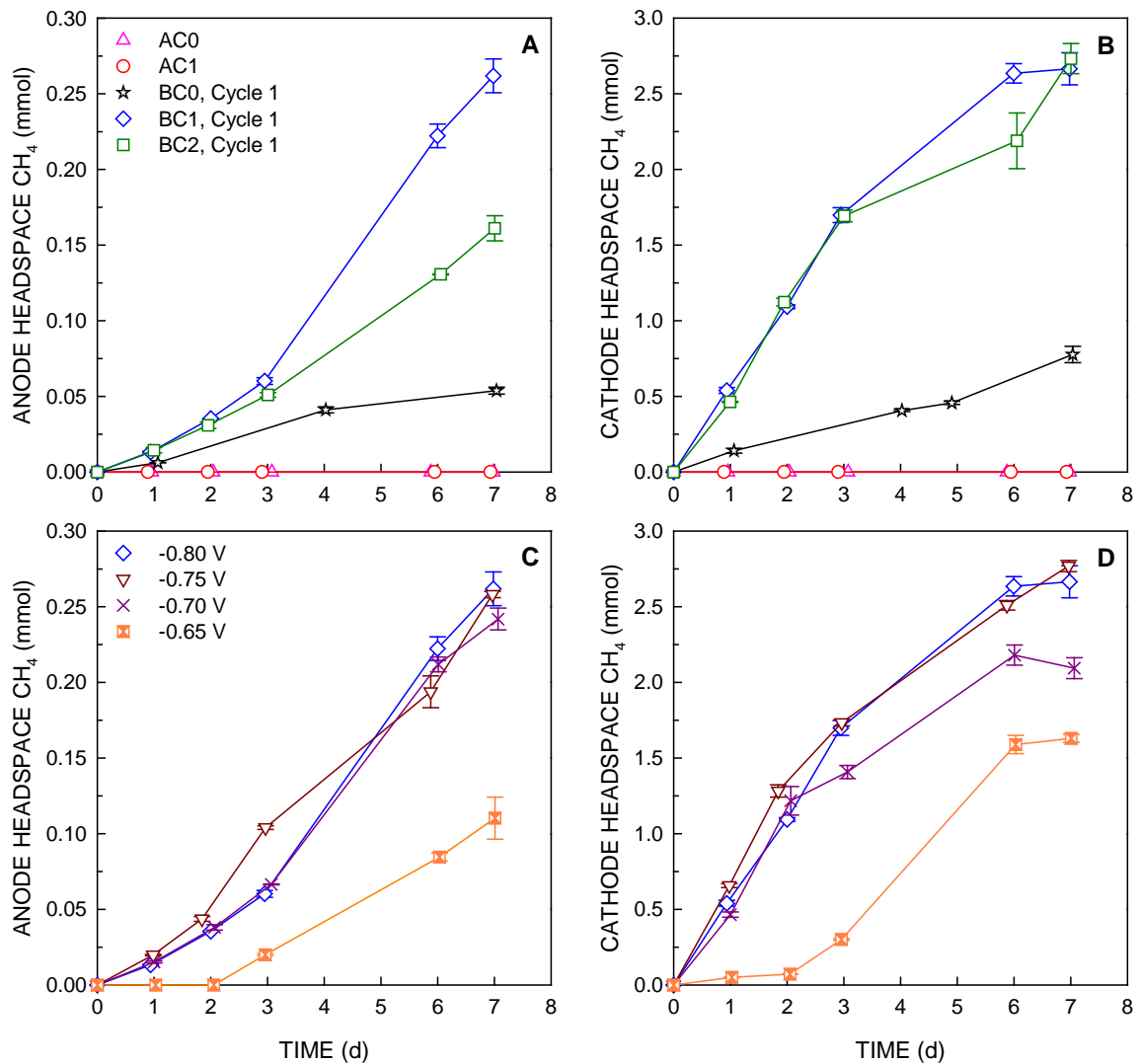


Figure 6.3 - Time course of headspace methane in the anode (A) and cathode (B) for various BES configurations (ZVI-free abiotic cathode, AC0; abiotic cathode with 1 g/L ZVI, AC1; ZVI-free biocathode, BC0; biocathode with 1 g/L ZVI, BC1; biocathode with 2 g/L ZVI, BC2), and in the anode (C) and cathode (D) of the BC1 system at various applied potentials (-0.65 to -0.80 V vs. SHE).

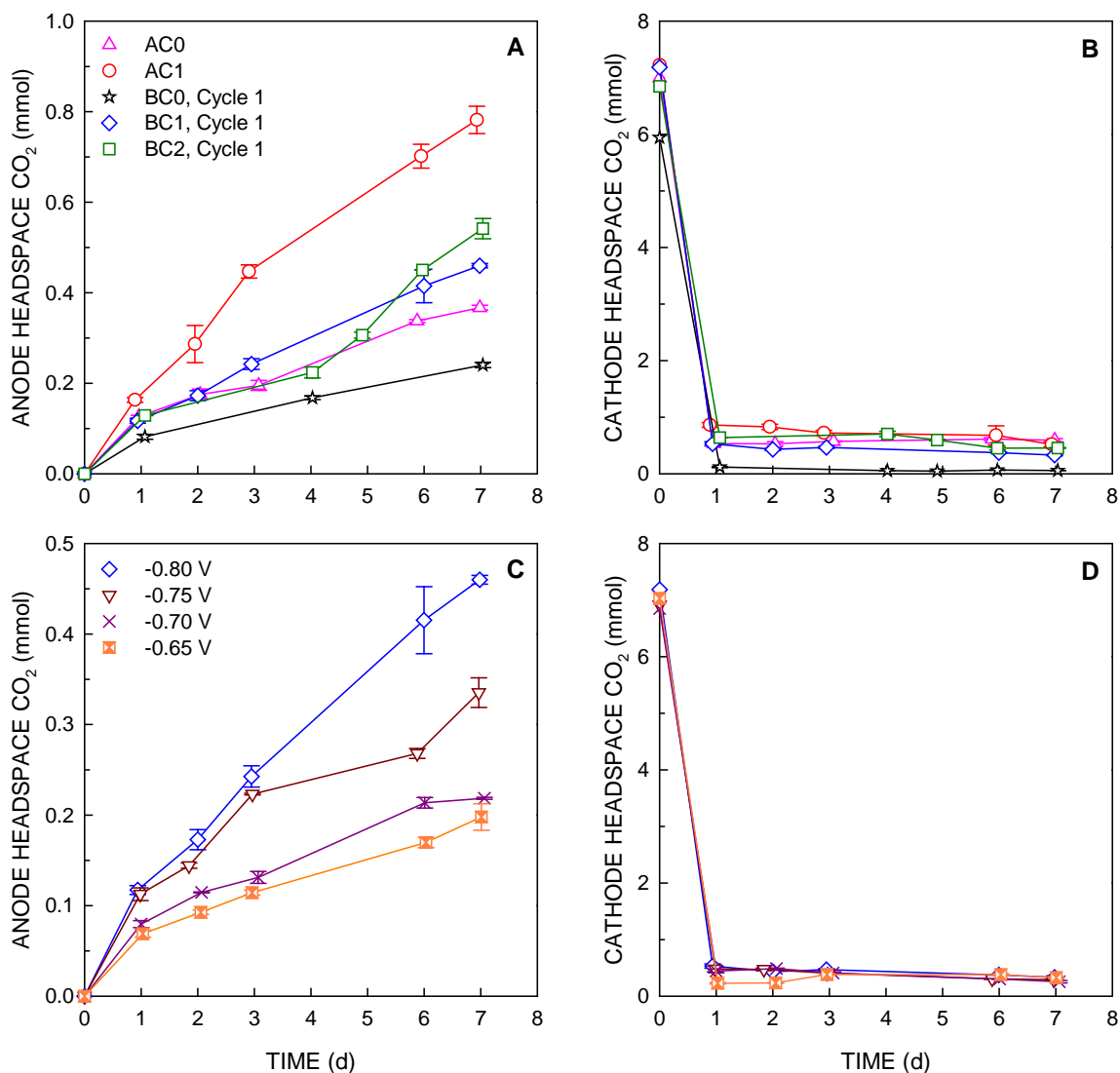


Figure 6.4 - Time course of headspace carbon dioxide in the anode (A) and cathode (B) for various BES configurations (ZVI-free abiotic cathode, AC0; abiotic cathode with 1 g/L ZVI, AC1; ZVI-free biocathode, BC0; biocathode with 1 g/L ZVI, BC1; biocathode with 2 g/L ZVI, BC2), and in the anode (C) and cathode (D) of the BC1 system at various applied potentials (-0.65 to -0.80 V vs. SHE).

6.3.2 *ZVI-Amended Biocathode.*

The performance of the BES with the BC0 biocathode was compared with that following the addition of 1 g/L initial ZVI (BC1) or 2 g/L initial ZVI (BC2) to the cathode (Table 1). The performance of a BES with an abiotic cathode control with 1 g/L initial ZVI (AC1) was also compared with the performance of the BES with the ZVI-amended biocathodes. BC1 and BC2 were monitored over four feeding cycles in which the catholyte was completely replaced with fresh one and CO₂ was resupplied to the headspace, but new ZVI was not added. The pH of the anolyte and catholyte remained between 6.5 and 7.0 throughout each 7-day feeding cycle. Anode acetate removal following cathode ZVI addition was similar to acetate removal in the cycles prior to cathode ZVI addition (Table 1). However, the Coulombic efficiency was significantly lower in the bioanode with ZVI-amended biocathodes (11-19%) than in the preceding ZVI-free cycle (34%). Notably, after the addition of ZVI to the biocathode, the anolyte did not undergo a color change and remained clear throughout each cycle (Figure 6.1B). It is possible that ZVI-produced H₂ diminished the cathodic demand for electrons, allowing the anode to oxidize primarily acetate or carbon storage compounds, without oxidizing anolyte components.

The overall removal of initial cathode headspace CO₂ during a feeding cycle was similar across all biocathodes (94-96%), with most (91-95%) of the headspace CO₂ removed within the first 24 hours (Figure 6.4B), largely due to CO₂ dissolution into the catholyte, as previously described in Section 4.3.4. Therefore, the similar headspace CO₂ removal between the ZVI-free (BC0) and ZVI-amended cathodes (BC1, BC2) indicates that the addition of ZVI did not appreciably affect the dissolution of CO₂.

Unlike the ZVI-free cathode (BC0), significant quantities of H₂ were observed in the ZVI-amended cathode headspace (Figure 6.6B), resulting from anaerobic oxidation of the added ZVI (Figure 6.7). The BC1 cathode headspace H₂ content peaked on day 1, amounting to up to 7% of the gas volume. In the BC2 cathode, the headspace H₂ peaked on day 2 at 40% of the gas volume, indicating significant H₂ release from ZVI oxidation. Upon the second feeding following the replacement of the catholyte, there was a minor increase in headspace H₂ in both BC1 and BC2 cathodes, possibly from the oxidation of ZVI particles that remained within the biofilm after catholyte exchange. Cathode and anode headspace H₂ remained low in subsequent feedings (Figure 6.6).

The concentration of Fe²⁺, which is released during anaerobic corrosion of ZVI, was significantly higher in the BC1 catholyte than in the AC1 catholyte (Figure 6.5), which indicated that the biological activity may have increased the rate of ZVI corrosion. In both the AC1 and BC1 catholyte, the Fe²⁺ concentration increased rapidly following feeding, due to the rapid corrosion of ZVI upon the application of reducing potential. In AC1, the Fe²⁺ concentration peaked within the first day following feeding and then began to slowly decline throughout the remainder of the feeding cycle (Figure 6.5). Within 4 h of feeding, the Fe²⁺ in the catholyte of the AC1 and BC1 cathodes represented 10% and 25%, respectively, of the total added ZVI. In the AC1 catholyte, from the observed Fe²⁺ peak at 4 h to the end of the feeding cycle, the Fe²⁺ concentration declined by 69 mg Fe²⁺/L. The Fe²⁺ concentration in the AC1 anolyte gradually increased throughout the cycle to 7 mg Fe²⁺/L, indicating some minor transport of Fe²⁺ through the proton exchange membrane. However, this minor transport could not fully explain the decline in Fe²⁺ concentration in the AC1 cathode. Thus, it is likely that Fe²⁺ complexed with other ions in the system over

time. The BC1 catholyte Fe^{2+} concentration peaked at 1.8 d into the feeding cycle, at which time the Fe^{2+} in the catholyte represented 45% of the total added ZVI. Decline in Fe^{2+} was also observed in the BC1 catholyte (Figure 6.5), indicating the complexation of Fe^{2+} with other ions in solution. Indeed, precipitate formation was observed in the BC1 cathode, as discussed further in Section 6.3.6.

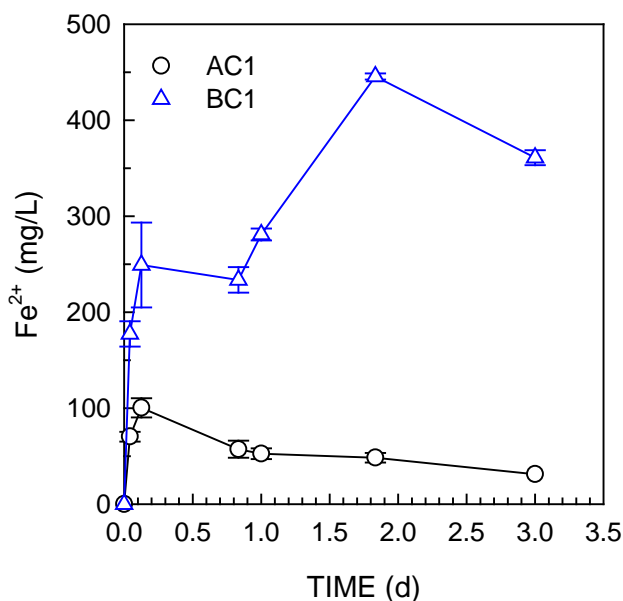


Figure 6.5 - Time course of Fe^{2+} concentration in the catholyte of the abiotic cathode (AC1) and biocathode (BC1) when initially amended with 1 g/L ZVI.

Over the course of four feeding cycles, BC1 and BC2 cathodes produced over twice the CH_4 compared to the BC0 cathode in the four cycles preceding ZVI addition (Table 6.1, Figure 6.8). Despite different initial ZVI concentrations (1 and 2 g/L), BC1 and BC2 produced a similar amount of CH_4 , which is likely due to the ZVI reaching a maximum rate of oxidation. Indeed, BC1 and BC2 biocathodes produced H_2 at nearly the same rate over the first day following feeding (Figure 6.2). The maximum rate of CH_4 production in

each cathode occurred during the first day following feeding and, in the case of BC1 and BC2, during the first cycle following ZVI addition (Figure 6.8). The maximum rate of CH₄ production in BC0, BC1 and BC2 was 393±12, 877±31, and 754±6 mmol/m²-d, respectively, normalized to the PEM surface area. Thus, the initial CH₄ production in BC1 was 16% larger than in BC2 (p<0.001).

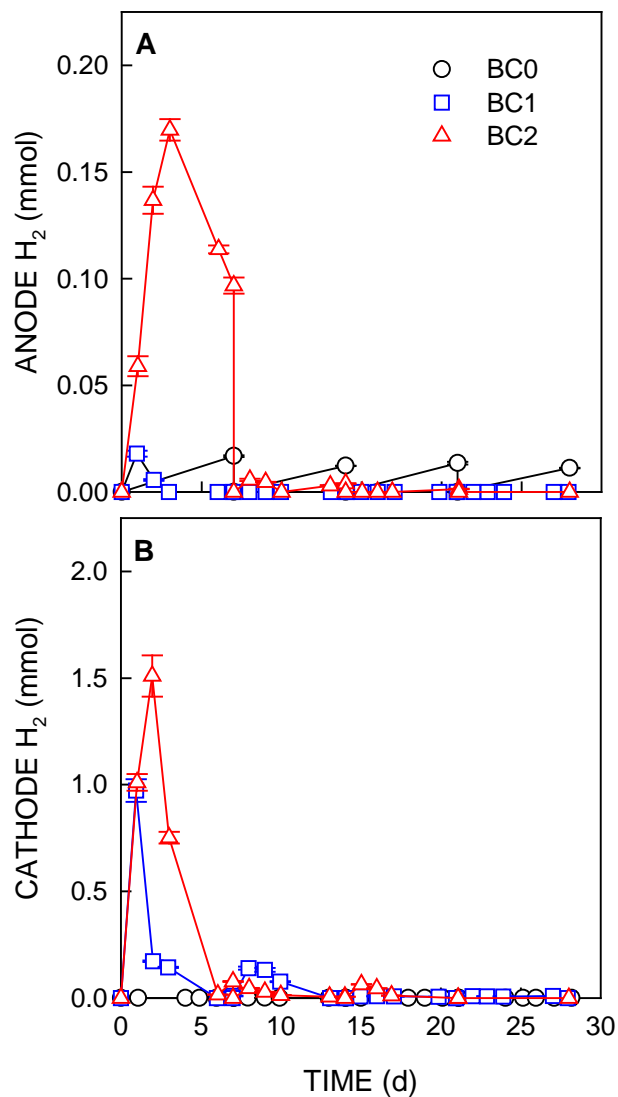


Figure 6.6 - Time course of hydrogen in the headspace of the anode (A) and cathode (B) over the course of four feeding cycles in which 0 g/L (BC0), 1 g/L (BC1) or 2 g/L (BC2) ZVI was added at the start of the first cycle.

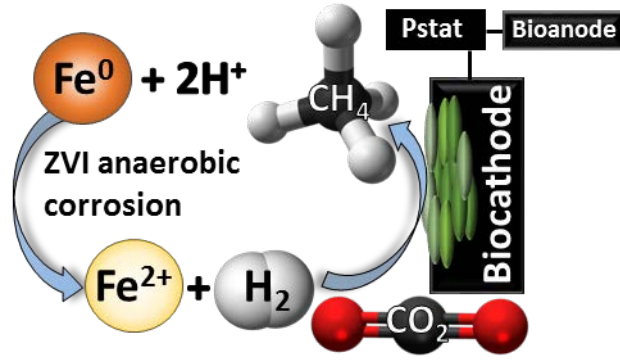


Figure 6.7 - Diagram showing the anaerobic corrosion of ZVI, which produces Fe^{2+} and H_2 . Methanogens use the H_2 resulting from ZVI corrosion to reduce CO_2 to CH_4 , in addition to utilizing electron equivalents directly from the biocathode.

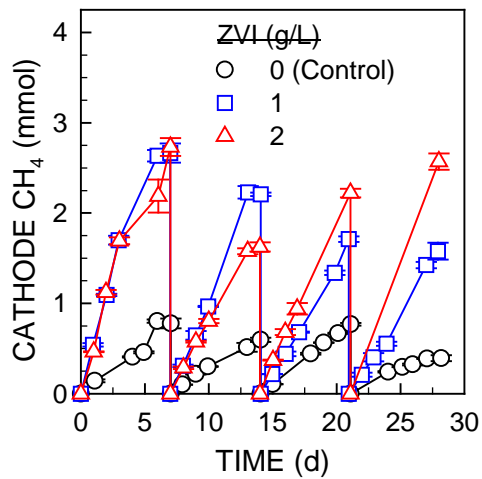


Figure 6.8 - Time course of cathode headspace CH_4 over the course of four feeding cycles during which 0, 1 or 2 g/L ZVI was added only at the start of the first feeding cycle. Error bars represent mean values \pm one standard deviation, $n = 3$.

In the initial 7-d feeding cycle, the BC1 cathode produced 2.03 mmol CH_4 above the mean CH_4 produced in the four previous feeding cycles without ZVI, which would

correspond to the oxidation of 0.45 g ZVI. However, only 0.25 g ZVI was added to the 1 g/L ZVI cathode, indicating that the increase in CH₄ production was not due solely to the production of H₂ from ZVI oxidation. Thus, the addition of ZVI also enhanced the cathode-dependent production of CH₄. At the same time, ZVI addition decreased current consumption, a trend observed in both abiotic and biotic cathodes (Figure 6.9). When ZVI was added to the abiotic cathode, the total charge transferred over the course of a feeding cycle decreased by 96%. When 1 g/L ZVI was added to the ZVI-free biocathode, the total feeding cycle charge transfer decreased by 69%. This result could be due to additional H₂ resulting from ZVI oxidation, which may decrease the water electrolysis rate at the cathode. Given that ZVI addition enhanced the cathode-dependent production of CH₄ while at the same time decreased current production, it follows that ZVI increased the cathode capture efficiency (CCE), which is a measure of how efficiently electrons from the cathode electrode are converted to CH₄. Actual CCE could not be determined due to the two sources of reducing power (ZVI-derived H₂ and the cathode). If the partial pressure of H₂ was elevated at the cathode and slowed the water electrolysis reaction, direct electron transfer from the cathode electrode to methanogens may have increased. Direct electron transfer may be more efficient than diffusion-dependent mediated electron transfer (e.g., with H₂ or another mediator) (Shi et al. 2016). Thus, a shift toward direct electron transfer in the presence of elevated H₂ from ZVI oxidation may increase the CCE and CH₄ production and decrease current density. However, further study is needed to determine which mechanism(s) of electron transfer actually occur in ZVI-amended biocathodes.

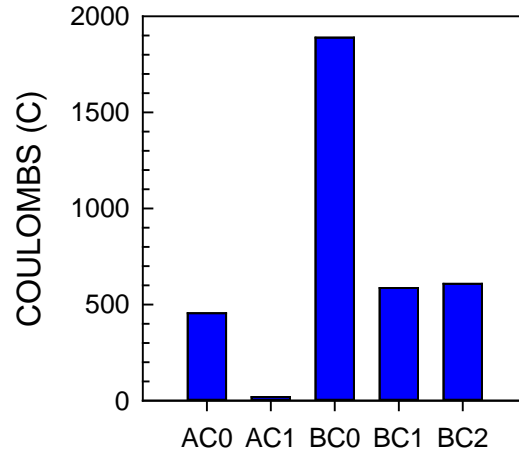


Figure 6.9 - Charge transferred during a 7-d feeding cycle in various BES configurations (AC0, ZVI-free abiotic cathode; AC1, abiotic cathode with 1 g/L ZVI; BC0, ZVI-free biocathode; BC1, biocathode with 1 g/L ZVI; BC2, biocathode with 2 g/L ZVI).

There are several plausible explanations for the long-term effect of ZVI on biocathodic CH₄ production. First, ZVI particles within the biofilm and/or the felt electrode matrix may not be completely removed with the catholyte replacement, thus improving CH₄ production in subsequent cycles as the ZVI oxidizes. However, this effect cannot account for the observed improved CH₄ yield. Over four cycles, the cumulative electron equivalents of gas produced in the ZVI-free biocathode (BC0) were 22.7 meeq. In BC1 and BC2 BES configuration, the cumulative gas equivalents produced were 65.3 and 73.4 meeq, respectively. Complete ZVI oxidation in BC1 and BC2 would have contributed only 9.0 and 17.9 meeq, respectively. Therefore, if all ZVI was oxidized and the produced H₂ were to be used for methanogenesis with 100% efficiency, the cumulative gas equivalents in BC1 and BC2 would have still been 107 and 81% higher than expected, respectively. Thus, another effect must have contributed to the observed higher CH₄ yield following ZVI

exposure. A second possibility is that ZVI exposure increased biomass growth in the cathode. However, protein measurements of the biofilm and suspended biomass before and after ZVI exposure indicated that total biomass and biofilm biomass were 6% and 5% lower, respectively, in the ZVI-amended biocathode. However, protein measurements do not distinguish between active and inactive biomass. A third possible cause for the observed increased CH₄ production in the ZVI-amended biocathode is the ZVI itself, which could potentially act as an electrically-conductive material to enhance electron transfer between the cathode electrode and methanogens. To test this possible effect, a ZVI-free biocathode was amended with powdered magnetite (Fe²⁺Fe³⁺₂O₄; Ward's Science, Rochester, NY) at the same molar iron concentration as in the BC1 ZVI-amended biocathode (17.9 mM). However, over the course of a 7-d feeding cycle, the magnetite-amended biocathode produced 8% less CH₄ than in the previous magnetite-free cycle, suggesting that conductivity or magnetic properties were not involved in the ZVI-enhanced CH₄ production. Then, to test whether the Fe²⁺ released from ZVI oxidation played a role in the observed enhanced CH₄ production, a solution of FeCl₂ (Fisher Scientific, Pittsburg, PA) was added to the biocathode at the same molar iron concentration as in the BC1 ZVI-amended biocathode (17.9 mM). A green precipitate formed that coated the biocathode but the 7-d CH₄ production remained within 2% of the previous FeCl₂-free cycle.

Another possible explanation for the higher CH₄ production in the ZVI-amended biocathode could be a change in the biocathode microbial community composition following exposure to ZVI, which is further discussed below. Finally, the ZVI-induced development of redox-active compounds or precipitates may facilitate electron transfer and improve CH₄ production. Although most compounds would be removed through weekly

catholyte replacement, some may be retained within the cathode carbon felt. This possibility was explored in more depth, as discussed below.

6.3.3 *ZVI-Amended Biocathode at Various Potentials.*

ZVI provides an additional source of reducing power to a biocathode and, thus, may support methanogenesis at a lower applied potential, decreasing external energy input. To test this possibility, 1 g/L ZVI was added to the biocathode and four feeding cycles were monitored with the cathode potential at -0.80, -0.75, -0.70 and -0.65 V. The cathode was rinsed with fresh catholyte in between feeding cycles to remove remaining ZVI and/or precipitate. The pH of the anolyte and catholyte remained between 6.7 and 6.8 during all cycles. The highest anode acetate removal (89.7%) was observed at the -0.80 V cathode potential (Table 6.2), with similar removal at the -0.75 V (88.6%) and -0.65 V (87.7%) cycles. However, at a cathode potential of -0.70 V, a lower acetate removal (80.3%) was observed, which could be explained by differences in the uptake and conversion of acetate to carbon storage compounds. Indeed, bioanode acetate removal comprises both acetate oxidation to CO₂ and conversion to carbon storage compounds;(Freguia et al. 2007) thus, anode acetate removal is an unreliable measure of overall carbon oxidation. Accordingly, final anode headspace CO₂, a measure of the carbon oxidized in the anode and the relatively constant transport of CO₂ from the cathode, decreased with decreasing applied potential (Figure 6.4A). The CO₂ profile in the cathode headspace was similar at all cathode potentials with 1 g/L ZVI (Figure 6.4B), indicating the removal of cathode CO₂ was independent of the cathodic electrochemical reaction and instead depended on the catholyte capacity to dissolve CO₂.

Table 6.2 - BES Performance at Various Applied Potentials

Cathode Potential^a (V)	Initial ZVI (g/L)	Anode Acetate Removal (%)	Cathode Final H₂ (mmol)	Cathode Final CH₄ (mmol)	Cathode Total Gas Electron Equivalents^b (meeq)
-0.80	1	90.1	0.01	2.67	21.34
-0.75	1	88.6	0.64	2.77	23.44
-0.70	1	80.3	0.52	2.09	17.80
-0.65	1	87.7	0.73	1.63	14.49

^a Cathode potential versus SHE.

^b Electron equivalents (eeq) of gas in the cathode headspace at the end of a feeding cycle; 8 eeq/mol CH₄ and 2 eeq/mol H₂.

At all applied voltage values, anode headspace H₂ remained low (Figure 6.2C), although the highest amount of H₂ was observed at -0.80 V. Cathode headspace H₂ increased similarly over the first day at all voltage values tested, except at -0.65 V. At these applied voltage values, cathode H₂ peaked on day 1 or 2, and then declined throughout the remainder of the feeding cycle (Figure 6.2D). The cathode headspace H₂ declined at a faster rate at -0.80 V than at -0.75 V or -0.70 V, indicating more robust methanogenic consumption of H₂ at a more negative cathode potential. Thus, the applied potential influenced biocathodic methanogenesis, even with H₂ resulting from ZVI corrosion. At -0.65 V, cathode H₂ was detected at low levels until day 3, indicating a negative cathode potential was significant for both cathode-dependent methanogenesis and ZVI corrosion.

Cathode headspace CH₄ was similar at a cathode potential of -0.80 and -0.75 V (Figure 2). However, total CH₄ production declined by 24% when the cathode potential was changed from -0.75 to -0.70 V (Table 6.2). The lowest total CH₄ production was observed at -0.65 V (Table 6.2), where a lag period of 2 days was observed before

significant CH₄ production occurred (Figure 6.10). Furthermore, the CH₄ lag period corresponded to a lag in cathode headspace H₂, which only increased after day 2 (Figure 6.2B). At a more positive cathode potential, fewer electron equivalents are transferred from anode to cathode and ZVI corrosion may have proceeded at a lower rate, producing less H₂. Thus, the addition of ZVI may allow a methanogenic biocathode to maintain performance at both -0.80 and -0.75 V, increasing overall energy efficiency, but more positive cathode potentials result in lower total CH₄ production.

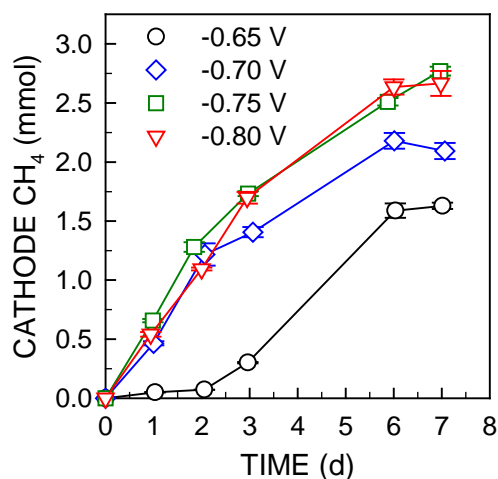


Figure 6.10 - Time course of cathode headspace CH₄ over the course of four feeding cycles with 1 g/L initial ZVI and cathode potential at -0.65, -0.70, -0.75 or -0.80 V vs. SHE, respectively. Error bars represent mean values \pm one standard deviation, $n = 3$.

6.3.4 *BES Performance with Mid-Cycle ZVI Addition and Short-Term Open Circuit Conditions.*

To better understand the effect of ZVI on biocathode performance, the ZVI-exposed biocathode was fed and operated at -0.80 V cathode potential for 3 d without ZVI, after which 1 g/L ZVI was added. Throughout the duration of the cycle, the pH of the anolyte and catholyte remained in the range of 6.6-6.8. Acetate removal in the anode over the entire cycle was 92.8% (Table 6.3), with 80.4% acetate removed by day 3, when the ZVI was added. The high initial removal reflects both acetate oxidation and rapid acetate uptake and conversion to carbon storage compounds (Freguia et al. 2007).

Table 6.3 - BES Performance with Mid-Cycle ZVI Addition and Voltage Application

Cathode Potential^a (V)	Initial ZVI (g/L)	Anode Acetate Removal (%)	Cathode Final H₂ (mmol)	Cathode Final CH₄ (mmol)	Cathode Total Gas Electron Equivalents^b (meeq)
-0.80	-- ^c ,1 ^d	92.8	0.50	1.78	20.94
OCC ^e , -0.80	1	83.0	ND ^f	2.49	14.21

^a Cathode potential versus SHE.

^b Electron equivalents (eeq) of gas in the cathode headspace at the end of a feeding cycle; 8 eeq/mol CH₄ and 2 eeq/mol H₂.

^c ZVI-free abiotic cathode.

^d 1 g/L ZVI added to the biocathode on day 3 of the 7-d feeding cycle.

^e OCC, open circuit condition for 2 days, followed by application of -0.80 V cathode potential for the remainder of the 7-d feeding cycle.

^f ND, not detected.

The cathode CO₂ removal was similar to previous cycles, with 95% removal within 24 h and 96% overall removal (Figure 6.11A). H₂ was barely above the method detection limit (0.1%, v/v) until the addition of ZVI on day 3, which generated H₂ via anaerobic oxidation (Figure 6.11B). H₂ levels peaked on day 4 and then slowly declined until the end of the cycle. As expected, the production of CH₄ increased in response to the newly available H₂ (Figure 6.11C). Prior to the addition of ZVI, CH₄ was produced at a nearly linear rate of 433±2 mmol/m²-d (R² = 0.999). After ZVI addition, the mean CH₄ production rate increased to 524±16 mmol/m²-d (R² = 0.999) between days 4-7, a 21% increase (p<0.001).

To better understand how a ZVI-amended biocathode would perform during a short-term power disruption, the biocathode was fed, supplemented with 1 g/L g ZVI, and operated under open circuit conditions for 2 d. The pH of both anolyte and catholyte remained constant at 6.7. Despite open circuit conditions, the anode acetate declined by 65% over the 2-d incubation period. In comparison, in the first cycle of BC1, 82% acetate removal was achieved after 2 d. During the 2-d incubation under open circuit conditions, low levels of CH₄ (< 0.03 mmol) were detected in the anode, which was consistent with CH₄ transport across the membrane from the cathode (see Section 4.3.3). However, if the observed CH₄ was the result of anode methanogenesis, it would only represent conversion of 0.2% of the removed acetate. Therefore, the initial 2-d observed anode acetate removal in the BC1 system could have been due primarily to bacterial uptake and storage, with less of the removed acetate undergoing complete oxidation. Indeed, microbial carbon storage in an acetate-fed batch MFC has been previously described (Freguia et al. 2007). Over the

course of the full 7-d feeding cycle, 83% of the initial acetate in the anode was removed (Table 6.3).

As in other configurations used in this study, most of the initial CO₂ in the cathode headspace (93%) was removed within 1 d due to CO₂ dissolution in the catholyte (Figure 6.11A). H₂ was detected in the cathode headspace, with a peak level of 0.176 mmol on day 2 (Figure 6.11B). In comparison, when the same amount of ZVI was added on the third day of a cycle with the cathode potential at -0.80 V, the peak headspace H₂ was 0.637 mmol, almost 4 times higher than under open circuit conditions. Instead, once the applied voltage was restored on day 2, H₂ declined and remained near the detection limit (0.1%, v/v) for the remainder of the cycle.

Over the course of the first 2 d under open circuit conditions, the biocathode CH₄ production was nearly linear at a rate of 397±10 mmol/m²-d (R²=0.993) utilizing H₂ produced by ZVI oxidation. This rate was similar to that of the biocathode at -0.80 V before ZVI addition. Following the application of -0.8 V cathode potential (days 2-7), the mean CH₄ production rate increased to 430±5 mmol/m²-d (R²=0.959). However, this rate was slower than the mean rate observed in the -0.80 V biocathode following ZVI addition on day 3 of the cycle (643±81 mmol/m²-d; R²=0.969). In contrast, the BC1 biocathode with both applied potential and ZVI upon feeding, resulted in an initial 2-d CH₄ production rate of 896±13 mmol/m²-d (R² = 0.999). Therefore, the order in which electrochemical potential and ZVI are applied to the biocathode appears to influence the resulting CH₄ production rate. Further study is needed to determine what mechanism(s) underlie the observed difference in biocathode performance.

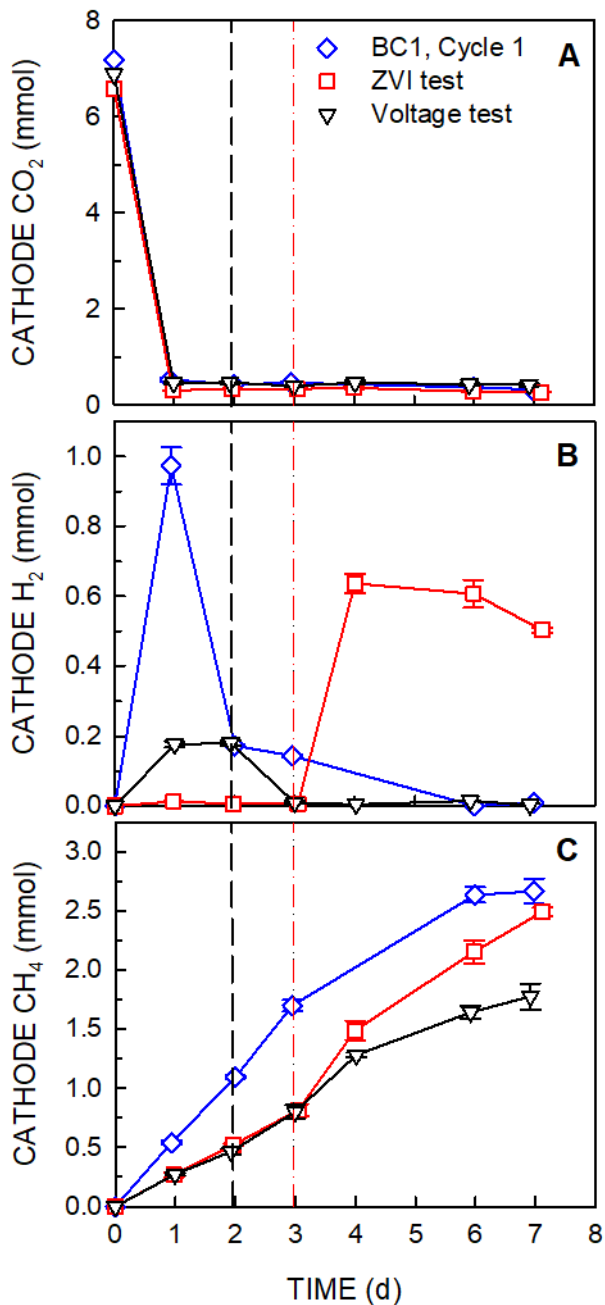


Figure 6.11 - Time course of CO₂ (A), H₂ (B) and CH₄ (C) in the cathode headspace during the first feeding cycle of BC1 and two later tests using the same biocathode: a ZVI addition test in which 1 g/L ZVI was added on the third day of a feeding cycle (red dash-dot line), and a voltage test in which 1 g/L ZVI was added on the first day of a feeding cycle under open circuit conditions and -0.80 V was applied on the second day of the feeding cycle (black dashed line).

6.3.5 *Phylogeny and Microbial Community Diversity of ZVI Biocathode.*

The microbial community of the biocathode biofilm was analyzed following exposure to ZVI over a period of 24 feeding cycles (>170 days) and compared with the community structure prior to ZVI addition. A phylotype most closely related to *Methanobrevibacter arboriphilus* represented 99% and 100% of the Archaea detected in the original, ZVI-free biocathode and ZVI-amended biocathode, respectively. The remaining 1% of detected archaeal OTUs in the original biocathode belonged to *Methanobacterium* and *Methanosaeta*. Thus, the archaeal community did not undergo a significant change following ZVI exposure.

However, the biocathode bacterial community changed significantly following ZVI exposure. Relative to the original biocathode, the ZVI-amended biocathode bacterial community had a slightly lower Shannon diversity index (2.32) than that of the original biocathode (2.68). The most abundant ($\geq 1\%$ relative abundance) bacterial OTUs were placed with their closest defined species matches in GenBank into a phylogenetic tree (Figure 6.12), and the phylum relative abundance was compared between the ZVI-free and ZVI-amended biocathodes (Figure 6.13). The ZVI-amended biocathode had a substantially higher relative abundance of *Proteobacteria* and lower relative abundance of *Bacteroidetes* than did the ZVI-free biocathode. Indeed, in a previous study comparing two methanogenic biocathodes with a similar archaeal community, the biocathode with the higher relative abundance of *Proteobacteria* produced CH₄ at a rate nearly 4-fold higher than that of the other biocathode (see Section 5.3.3). In the present study, fewer abundant ($\geq 1\%$ relative abundance) phylotypes were detected in the ZVI-amended biocathode (9 OTUs) than in the ZVI-free biocathode (14 OTUs). Three of the phylotypes identified in the ZVI-amended

biocathode did not have a closely-related phylotype in the ZVI-free biocathode at a relative abundance higher than 1%. The closest relatives to the three phylotypes were: *Achromobacter* sp. BP3, *Nitrobacter winogradskyi* and *Oligotropha carboxidovorans*. Both *Achromobacter* sp. and *Nitrobacter winogradskyi* have been found in the biocathode of a MFC (Zhang et al. 2011), and *Achromobacter* sp. has been identified in a MFC biocathode capable of decolorizing textile azo dyes (Kumru et al. 2012). *Oligotropha carboxidovorans*, a chemoautotrophic bacterium, was also found in a MFC biocathode that performed H₂-supported autotrophic denitrification (Puig et al. 2011). Although the addition of ZVI to the biocathode changed the bacterial community composition, it is not clear to what extent the community change contributed to the observed higher CH₄ production rate in the ZVI-amended biocathode.

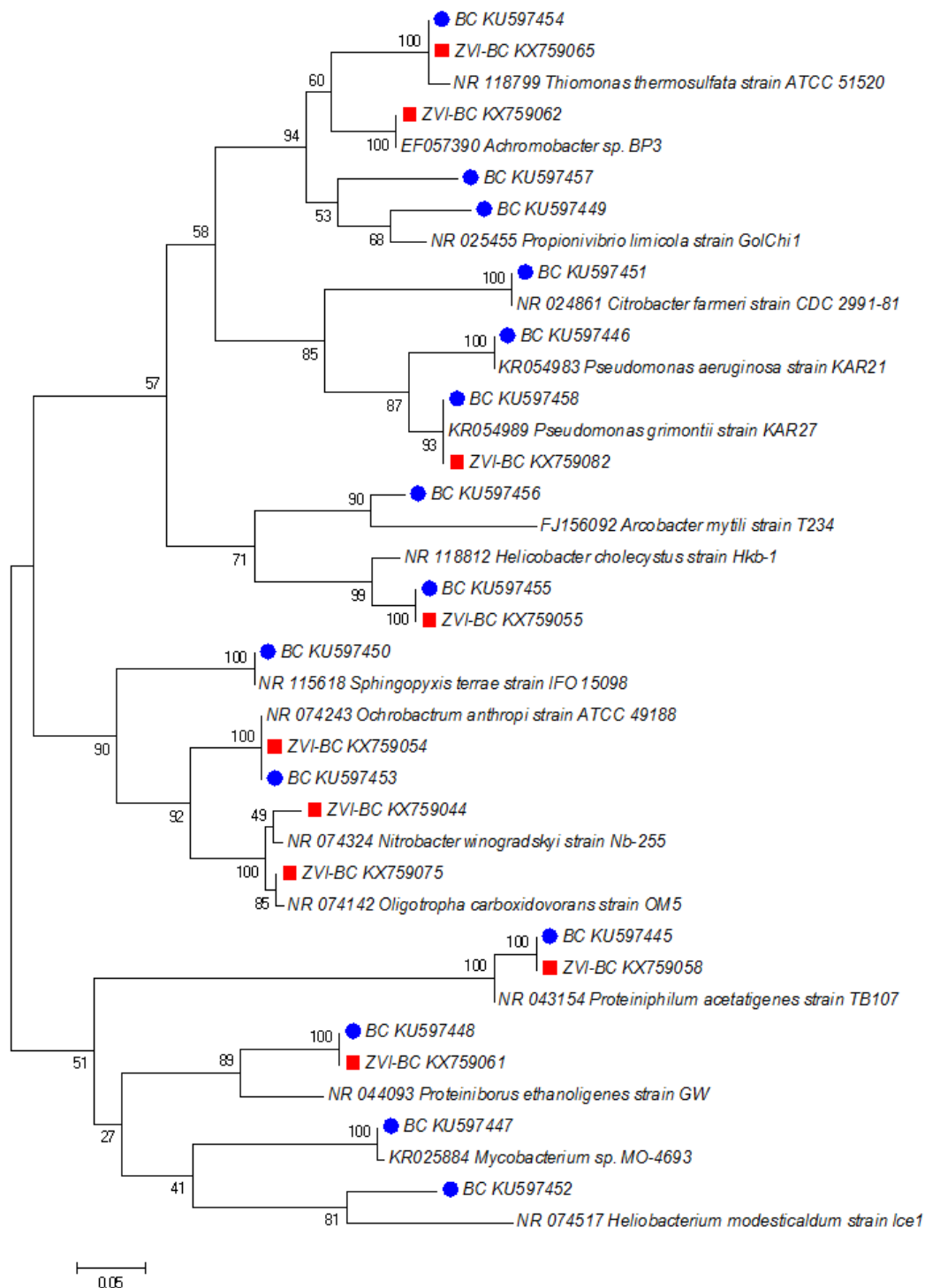


Figure 6.12 - Phylogenetic tree showing the relationship of the biocathode (BC; blue circle) and ZVI biocathode (ZVI-BC; red square) Bacteria OTUs ($\geq 1\%$ relative abundance) to their closest matched species in GenBank.

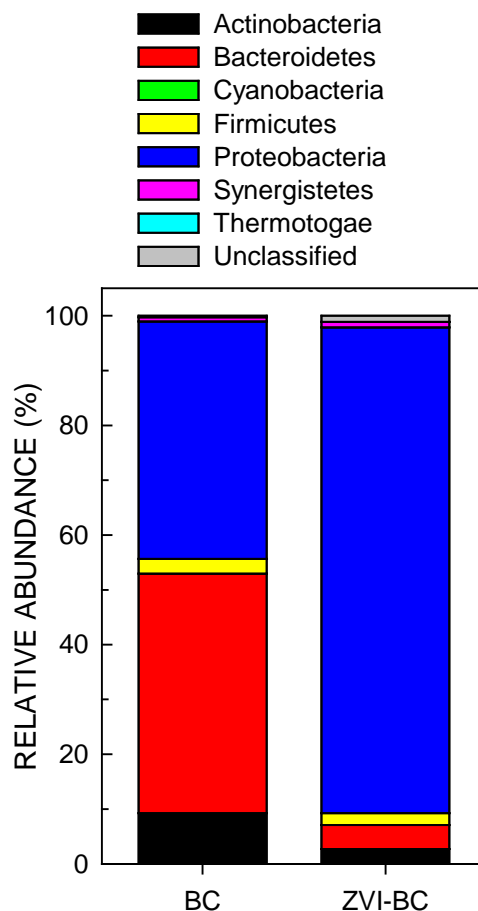


Figure 6.13 - Relative abundance of bacterial phyla in the ZVI-free biocathode (BC) and ZVI-exposed biocathode (ZVI-BC).

6.3.6 *Precipitate Formation and Characterization.*

In addition to the above-discussed change in bacterial community structure, formation of a precipitate was observed that may have contributed to the increased CH₄ production by the ZVI-amended biocathodes. As the ZVI filings were oxidized, the catholyte turned opaque and a white precipitate formed (Figure 6.14A). When the precipitate was removed from the biocathode and then exposed to air, its color turned blue (Figure 6.14B). The blue precipitate turned orange-yellow upon further oxidation in the

anode of an abiotic electrochemical cell at a cathode potential of 1.2 V (vs. Ag/AgCl) (Figure 6.14C). SEM-EDS analysis showed that the primary elements in the blue precipitate were C, O, Fe, P and N (Table 6.4; Figure 6.15). Trace amounts of Ca, Mg and Na were observed at only one of the five analyzed sites. Because the catholyte consisted of a sodium phosphate buffer, the relative lack of Na in comparison to P indicated that soluble Na was successfully removed during rinsing, while the detected P remained as part of, or sorbed to, the precipitate. It is likely that the precipitate was a mixture of several compounds. A similar white precipitate, determined to be siderite (FeCO_3), was observed in an anaerobic system with ZVI and aqueous CO_2 species during the dechlorination of 1,1,1-trichloroethane (Agrawal et al. 2002). While the precipitate identified in the present study likely contained siderite, the distinct color change upon air contact suggests the presence of vivianite ($\text{Fe}^{2+}_3(\text{PO}_4)_2 \cdot 8\text{H}_2\text{O}$) (Grodzicki and Amthauer 2000, Nanzyo et al. 2013). Indeed, vivianite formation has been observed under reducing conditions in soil, sediments, sludge and anaerobic digesters (Nanzyo et al. 2013, Singer 1972). Vivianite was also observed in a study that used nano-ZVI for abiotic phosphate removal from aqueous solutions (Wu et al. 2013). Nitrogen was also detected in the precipitate, indicating unidentified compound(s) were present, which could have also contributed to the precipitate's redox activity.

Cyclic voltammetry of the blue, oxidized form of the precipitate was conducted in an abiotic BES (Figure 6.16). Adjusting the scan rate from 50 to 200 mV/s did not cause a horizontal shift in redox peaks, indicating the reactions were reversible. Oxidation peaks occurred at 0.85 and -0.16 V (vs. Ag/AgCl), with reduction peaks at 0.09 V and -0.55 V (vs. Ag/AgCl) (Figure 6.16B). Then, the blue precipitate was reduced by applying a

cathode potential of -1.0 vs. Ag/AgCl, and turned white. Cyclic voltammetry of the reduced precipitate resulted in a new oxidation peak at -0.61 V vs. Ag/AgCl and the peak current was higher after longer periods of applied potential (Figure 6.17). Without an applied potential, the reduced precipitate was readily oxidized, but could be reduced again following the resumption of applied potential (Figure 6.18). Thus, the precipitate redox reaction was easily reversed. This property, along with the multiple reversible redox peaks, indicate that the precipitate may have acted as a redox mediator in the ZVI-amended biocathode. Furthermore, as the blue precipitate turned white, it began to sorb to the abiotic carbon felt electrode. Thus, within 90 min of adding the precipitate to the cathode, the catholyte was clear (Figure 6.19) and the white precipitate was observed on the carbon felt. Indeed, in the ZVI-amended biocathode, the white precipitate was observed to be within the carbon felt electrode (Figure 6.20), thus promoting close contact with both the electrode and the biofilm. Therefore, the ability of the precipitate to act as a redox mediator and its close association with the electrode and biofilm indicate its potential beneficial role in the ZVI-enhanced cathodic CH₄ production rate. Because of the long-lasting effect of ZVI on the performance of a methanogenic biocathode, periodic addition of ZVI may be a cost-effective means to increase BES CH₄ output. Additionally, ZVI could be used to assist in the start-up of an electromethanogenic biocathode or to maintain microbial activity during voltage interruptions.

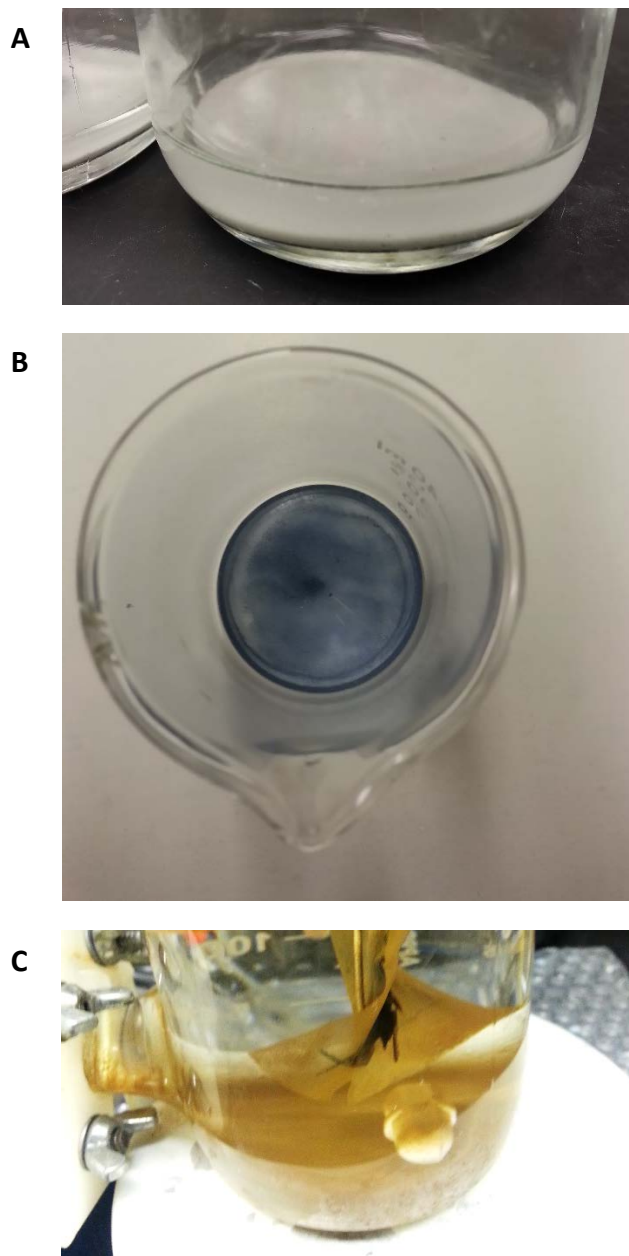


Figure 6.14 - Precipitate formed in the cathode after the addition of ZVI was white under reducing conditions (A), spontaneously turned blue when exposed to air (oxygen) (B), and turned orange-yellow when electrochemically oxidized (abiotically) with a platinum electrode poised at +1.2 V vs. Ag/AgCl, with 50 mM NaCl as anolyte (C).

Table 6.4 - Elemental Composition of the Biocathode Precipitate (SEM-EDS)

Element	Weight Range (%) ^a	Molar Range (%) ^b
Carbon	58.9 – 82.0	70.2 – 87.7
Oxygen	13.9 – 28.9	11.1 – 25.9
Iron	3.1 – 10.6	0.7 – 2.7
Phosphorus	1.0 – 2.7	0.4 – 1.3
Nitrogen	0.0 – 0.2	0.0 – 0.3

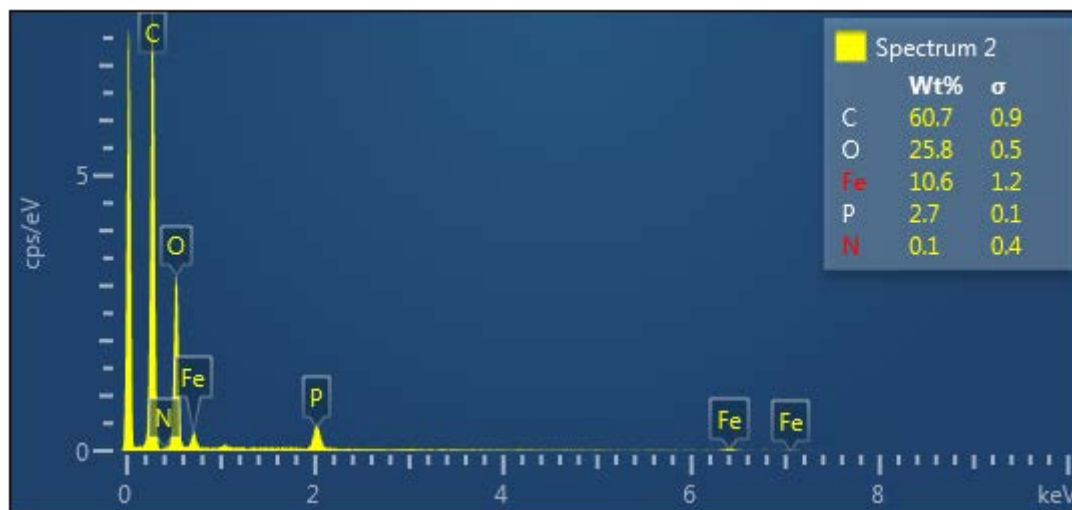


Figure 6.15 - SEM-EDS analysis of a blue powder precipitate sample collected from the biocathode following ZVI addition and exposure to air.

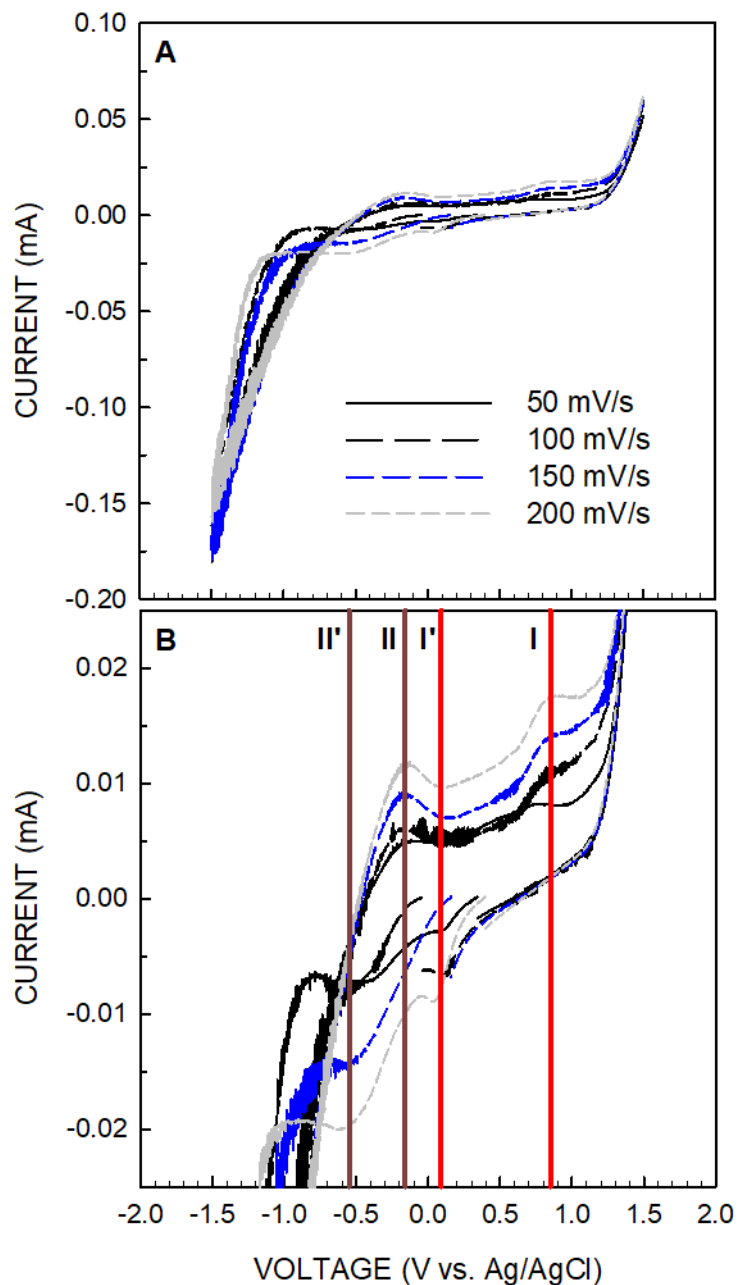


Figure 6.16 - Cyclic voltammogram of biocathode precipitate (A) magnified from -0.025 to +0.025 V (B) to highlight two oxidation peaks (I at 0.85 V and II at -0.16 V vs. Ag/AgCl) and two reduction peaks (I' at 0.09 V and II' at -0.55 V vs. Ag/AgCl). The scan rate was varied from 50 to 200 mV/s to determine reaction reversibility and identify redox pairs.

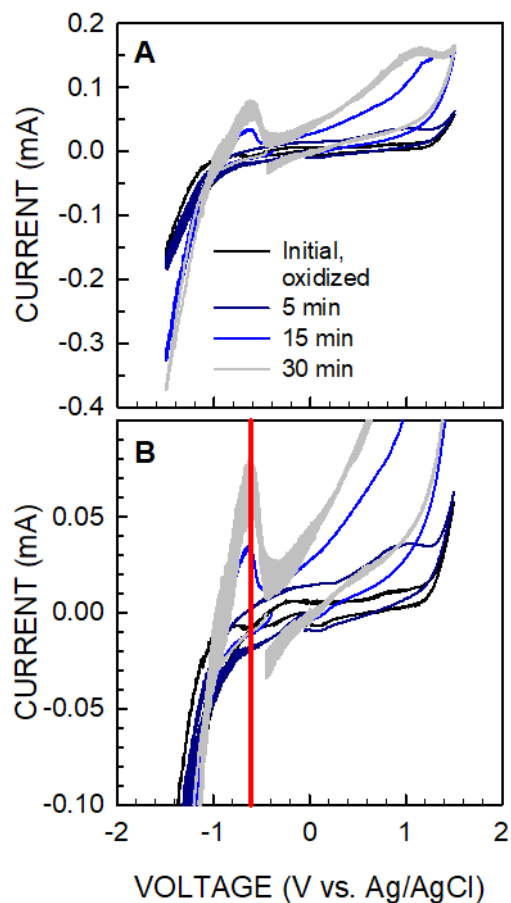


Figure 6.17 - Cyclic voltammogram of biocathode precipitate (A) magnified from -0.10 to +0.10 V (B). The red line indicates a redox peak at -0.61 V versus Ag/AgCl (-0.41 V versus SHE) that became more pronounced as the precipitate was progressively reduced. Scans were conducted on the oxidized precipitate and then at intervals of 5, 15, and 30 min at a cathode potential of -0.8 V versus SHE (Scan rate 100 mV/s).

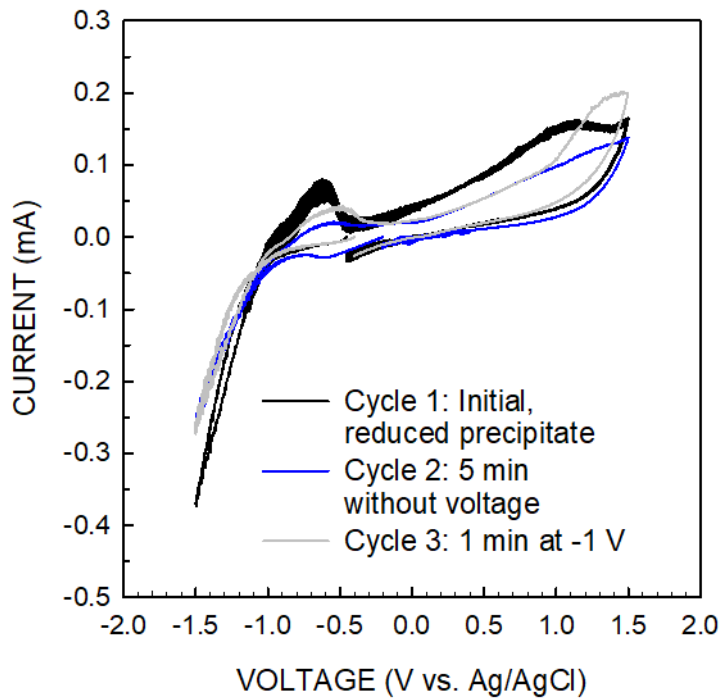


Figure 6.18 - Cyclic voltammogram of the precipitate following pre-reduction for 30 min at -1 V (vs. Ag/AgCl). After 5 min without an applied voltage, the peak current of the redox peak at -0.61 V (vs. Ag/AgCl) was lower, indicating a lower concentration of the reduced species. After applying a voltage of -1 V (vs. Ag/AgCl) for 1 additional min, the peak current increased, indicating a higher concentration of the reduced species (Scan rate 100 mV/s).

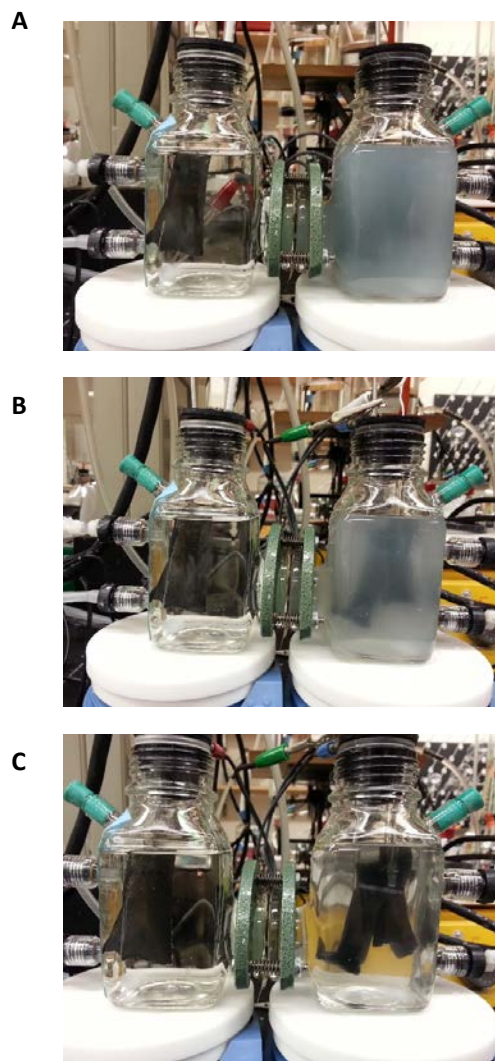


Figure 6.19 - Abiotic electrochemical reduction of blue precipitate (A) to white precipitate (B) by applying -1 V (vs. Ag/AgCl) cathode potential, followed by precipitate sorption to the carbon felt electrode, yielding a clear catholyte (C).

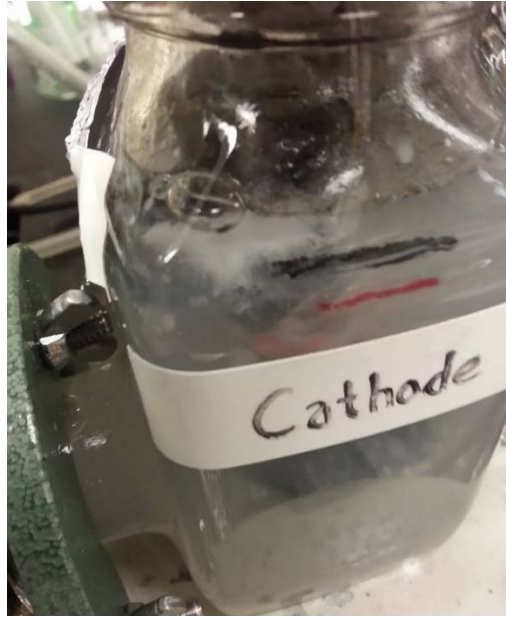


Figure 6.20 - White precipitate in close association with the carbon felt electrode and biofilm in the ZVI-amended biocathode.

6.4 Summary

Methanogenic bioelectrochemical systems (BESs), which convert carbon dioxide (CO_2) directly to methane (CH_4), promise to be an innovative technology for anaerobic digester biogas upgrading. Zero-valent iron (ZVI), which has previously been used to improve CH_4 production in anaerobic digesters, has not been explored in methanogenic biocathodes. Thus, the objective of this study was to assess the effect of biocathode ZVI on BES performance at 1 and 2 g/L initial ZVI concentrations and at various cathode potentials (-0.65 to -0.80 V vs. SHE). The total CH_4 produced during a 7-day feeding cycle with 1 and 2 g/L initial ZVI was 277% and 285% higher, respectively, than the mean CH_4 production in the four prior cycles without ZVI addition. Furthermore, CH_4 production by the ZVI-amended biocathodes remained elevated throughout three subsequent feeding cycles, despite catholyte replacement and no new ZVI addition. The fourth cycle following

a single ZVI addition of 1 g/L and 2 g/L yielded 123% and 231% more total CH₄ than in the non-ZVI cycles, respectively. The higher CH₄ production could not be fully explained by complete anaerobic oxidation of the ZVI and utilization of produced H₂ by hydrogenotrophic methanogens. Microbial community analysis showed that the same phylotype, most closely related to *Methanobrevibacter arboriphilus*, dominated the archaeal community in the ZVI-free and ZVI-amended biocathodes. However, the bacterial community experienced substantial changes following ZVI exposure, with more *Proteobacteria* and fewer *Bacteroidetes* in the ZVI-amended biocathode. Furthermore, it is likely that a redox-active precipitate formed in the ZVI-amended biocathode, which sorbed to the electrode and/or biofilm, acted as a redox mediator, and enhanced electron transfer and CH₄ production. Thus, ZVI may be used to increase biocathode CH₄ production, assist in the start-up of an electromethanogenic biocathode and/or maintain microbial activity during voltage interruptions.

CHAPTER 7. THE EFFECT OF HYDROGEN SULFIDE ON BES PERFORMANCE

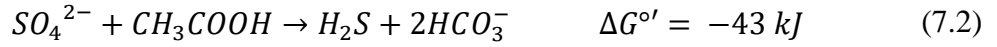
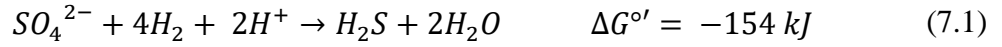
7.1 Introduction

Hydrogen sulfide (H_2S) is a toxic gas that is highly corrosive and is converted to environmentally-hazardous sulfur dioxide upon combustion (Singhal et al. 2017). H_2S is also a common trace contaminant in biogas from anaerobic digestion, which is primarily composed of CO_2 and CH_4 . Because biogas is often burned to recover energy, H_2S must be removed from the biogas prior to combustion to prevent corrosive damage to the equipment. The concentration of H_2S in biogas depends on the sulfur content of the anaerobic digestion feedstock. Thus, for biogas from municipal anaerobic digestion, the H_2S concentration typically ranges from 0.6% to 1.9% (v/v) (Peu et al. 2012). Anaerobic digestion of alternative feedstocks (e.g., agricultural residue, algae, seaweed, etc.) is gaining interest because of the potential for energy recovery combined with solids destruction (Ge et al. 2016). However, alternative feedstocks may contain a lower carbon-to-sulfur ratio than typical municipal sludge, and, therefore, the biogas H_2S concentration will be higher. For example, a typical carbon-to-sulfur ratio for pig bristles and harvested green seaweed is estimated to result in a biogas with 2.0-4.9% and 5.5-17.7% H_2S , respectively (Peu et al. 2012).

H_2S is formed during anaerobic digestion mainly when sulfate reducing bacteria (SRB) reduce sulfate to H_2S . SRB include two main groups: complete oxidizers that convert acetate to $\text{CO}_2/\text{HCO}_3^-$; and incomplete oxidizers that convert more complex molecules like lactate to acetate and CO_2 (Chen et al. 2008). During anaerobic digestion,

high concentrations of sulfate can stimulate SRB growth and complete oxidizers can compete with acetoclastic methanogens for acetate, thereby indirectly inhibiting methanogenesis (Choi and Rim 1991). Sulfate reduction (Equations 7.1-7.2) yields more energy than methanogenesis (Equations 7.3-7.4) and thus, SRB are able to outcompete methanogens when sulfate is readily available (Karhadkar et al. 1987). Furthermore, the sulfide produced by SRB may be toxic to bacteria and archaea, directly inhibiting anaerobic digestion and methanogenesis (Chen et al. 2008), as discussed further below.

H_2S is highly soluble in water ($K_{\text{H}} = 9.37 \pm 0.39 \text{ atm/M}$ at 22°C) (Sander 2015), where it undergoes dissociation into the species H_2S , HS^- and S^{2-} according to Equations 7.5-7.6. At equilibrium, the molar fraction of each sulfide species can be described with Equations 7.7-7.9. Using these equations, the equilibrium molar fraction of each sulfide species can be determined at various pH values (Figure 7.1). Thus, when at equilibrium in a medium with pH 7.0, half of the total sulfide in the aqueous phase is present as H_2S and half as HS^- . Reports conflict as to whether sulfide inhibition of methanogenesis correlates to the un-ionized form of sulfide (H_2S) or to total sulfide (H_2S , HS^- and S^{2-}) (Chen et al. 2008, Hilton and Oleszkiewicz 1988, Karhadkar et al. 1987, McCartney and Oleszkiewicz 1991). Hilton and Oleszkiewicz (1988) reported that sulfide inhibition of acetoclastic methanogenesis was pH-dependent and that the un-ionized form of sulfide (H_2S) was inhibitory, independent of total sulfide. However, McCartney and Oleszkiewicz (1991) reported that acetoclastic methanogenesis was inhibited in proportion to the un-ionized sulfide and was independent of total sulfide only when H_2S concentrations were less than 2.5 mM (80 mg S/L). When H_2S concentrations were larger, sulfide inhibition depended on total sulfide concentration. While the exact mechanism(s) of sulfide inhibition in



$$K_{a1} = \frac{[H^+][HS^-]}{[H_2S]} = 10^{-7} \quad (7.5)$$

$$K_{a2} = \frac{[H^+][S^{2-}]}{[HS^-]} = 10^{-13} \quad (7.6)$$

$$\alpha_{H_2S} = \frac{[H^+]^2}{[H^+]^2 + [H^+]K_{a1} + K_{a1}K_{a2}} \quad (7.7)$$

$$\alpha_{HS^-} = \frac{[H^+]K_{a1}}{[H^+]^2 + [H^+]K_{a1} + K_{a1}K_{a2}} \quad (7.8)$$

$$\alpha_{S^{2-}} = \frac{K_{a1}K_{a2}}{[H^+]^2 + [H^+]K_{a1} + K_{a1}K_{a2}} \quad (7.9)$$

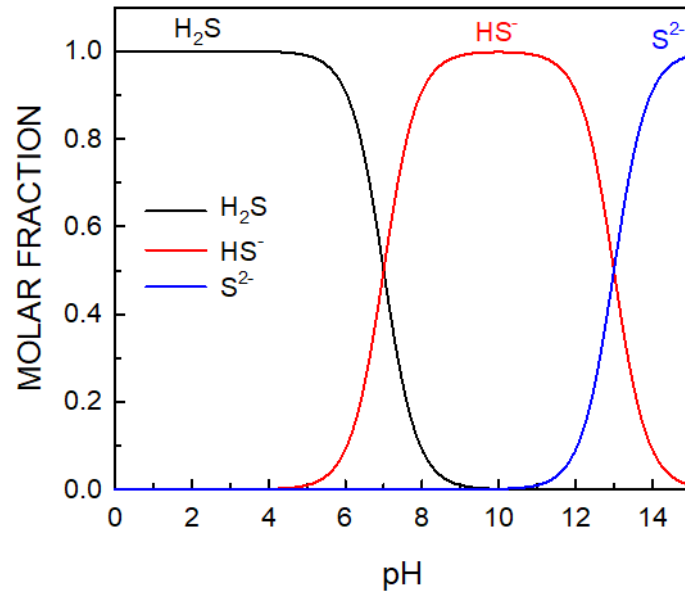


Figure 7.1 - Molar Fraction of Sulfide Species versus pH

anaerobic digestion and methanogenesis are not clear, studies suggest that a higher pH, which shifts sulfide species equilibrium towards S²⁻, can be partially protective against sulfide inhibition (Chen et al. 2008, Hilton and Oleszkiewicz 1988, McCartney and Oleszkiewicz 1991).

H₂S is highly corrosive and therefore must be removed from biogas prior to use downstream. One traditional method of H₂S removal is the use of chemical absorption using either the oxidation of S²⁻ to S⁰ or the precipitation of metal-sulfur complexes in aqueous solutions. Dry sorbents, such as an iron oxide sponge, are also used for small-scale sulfide removal but require non-regenerable and relatively short-lived adsorbents (Abatzoglou and Boivin 2009). Following desulfurization of biogas, CO₂ is often removed to increase the biogas energy (i.e., CH₄) content in a process termed “biogas upgrading”. Anaerobic digester biogas may contain 30-40% CO₂ and 60-70% CH₄ (Petersson and Wellinger 2009), which often limits energy recovery to combined heat and power (CHP)

units. Biogas upgrading to high-quality CH₄ ($\geq 95\%$ CH₄ v/v) allows biogas to be used in a far wider range of applications without requiring a CHP unit. Bioelectrochemical systems are capable of upgrading biogas without requiring expensive consumables or large amounts of energy like traditional biogas upgrading methods.

Although H₂S has been well-studied relative to anaerobic digestion, it is not known how H₂S affects the performance of a BES for biogas upgrading. Therefore, the objective of this study was to: i) assess the effect on BES performance of various H₂S concentrations in the biocathode headspace; and ii) assess the effect of cathode H₂S on suspended growth and biofilm microbial communities within the BES anode and cathode.

7.2 Materials and Methods

7.2.1 Serum Bottle Tests.

Although H₂S is inhibitory to methanogenesis during anaerobic digestion (Chen et al. 2008), it is not known how H₂S affects biocathode CH₄ production. As a preliminary test, two series of serum bottles were set up to separately test the effect of H₂S on the CH₄ production by hydrogenotrophic methanogens and acetoclastic methanogens. To set up the test, 50 mL of active culture, obtained from the waste of a mixed methanogenic (acetoclastic tests) or enriched hydrogenotrophic methanogenic (hydrogenotrophic tests) stock cultures at the end of a feeding cycle, was added anaerobically to a 160 mL serum bottle pre-flushed with N₂ (for acetoclastic tests) or a H₂/CO₂ mixture (80% H₂, 20% CO₂; for hydrogenotrophic tests). In the first series, a mixed methanogenic culture developed from the stock methanogenic culture discussed in Section 5.2.2 was used, which was treated identically but acclimated to 22°C, instead of 35°C. Because this culture was fed a

more complex substrate (dextrin and peptone), it was used to test the sensitivity of acetoclastic methanogens to H₂S. In the second series, an enriched hydrogenotrophic methanogenic (EHM) culture, as described in Section 5.2.2, was used. Because of the rich media carried with the waste of the culture and concern over low biomass concentration in the EHM culture, no additional media was added to the serum bottles. Triplicate serum bottles were maintained as controls (i.e., no H₂S addition) and the two series (acetoclastic and hydrogenotrophic) of triplicate serum bottles were supplied with H₂S using a locking, gas-tight glass syringe with Teflon-lined plunger to a H₂S concentration in the headspace of 1%. In the acetoclastic series, sodium acetate was added to each serum bottle to approximately 600 mg COD/L and the bottles were flushed with N₂. In the hydrogenotrophic series, no acetate was added and the H₂/CO₂ flushing gas mixture was added to 1.25 atm (absolute). All serum bottles were incubated at 22°C for 14 days and were hand-shaken once per day.

Headspace pressure and gas composition were monitored over time and the maximum rate of CH₄ production, which occurred during the first 7 d following feeding, was calculated. However, as the acetoclastic and hydrogenotrophic cultures had significantly different quantities of biomass, the maximum CH₄ production rate was normalized to the biomass present in the system at the end of the experiment (14 d), as measured by VSS. In the acetoclastic series, acetate was measured at the beginning and end of the 14 d incubation period. For all series, pH was also measured at the beginning and end of incubation.

Next, five sets of triplicate serum bottles were set up as described above using the mixed methanogenic culture. However, unlike the previous acetoclastic test, a mixture of

H₂ (80%) and CO₂ (20%) was added to stimulate the hydrogenotrophic methanogens within the mixed culture. No acetate was added to preclude acetoclastic methanogenesis. One set was kept as a control (i.e., no H₂S added) and the other sets were given 0.38%, 0.75%, 1.5% and 3.0% H₂S in the headspace. CH₄ production was monitored by gas pressure and composition over the course of a 7-d incubation at 22°C.

7.2.2 Measurement of Sulfide Transport.

When sulfide is introduced into the cathode headspace of a BES, its transport within the system may be described by two processes: transfer of sulfide between gas and liquid phases towards equilibrium; and transfer of sulfide across the proton exchange membrane towards equilibrium between anolyte and catholyte sulfide concentrations. First, to better understand the initial rate of dissolution of H₂S from the cathode headspace into the catholyte, cyclic voltammetry (CV) was periodically conducted to measure the concentration of sulfide dissolved in the catholyte. Sulfide ions may be measured electrochemically using a platinum electrode (Al Kharafi et al. 2010). Therefore, the cathode consisted of a carbon cloth (2 inches x 2 inches) coated with platinum on one side, and the anode consisted of an uninoculated carbon felt electrode, as described in Section 5.2.1. The anode and cathode were filled with phosphate buffer-based anolyte and catholyte (see Section 5.2.1), respectively. Using a Ag/AgCl reference electrode adjacent to the cathode, the cathode potential was swept from -1.2 to 0.2 V (vs. Ag/AgCl) at 100 mV/s. CV was performed immediately prior to H₂S addition to the cathode headspace (3% H₂S v/v), immediately after H₂S addition, and at 5, 10, 15 and 30 min following H₂S addition. The maximum current at -0.2 V (vs. Ag/AgCl), which is on the shoulder of the sulfide peak, was used to predict the sulfide concentration because it produced a more linear

calibration curve when tested with a sodium sulfide standard than the maximum current at the sulfide peak. This result could be due to side reactions that may occur within the media at or near the potential of the sulfide peak. Thus, the maximum current at -0.2 V (vs. Ag/AgCl) was plotted over time to assess the dissolution of sulfide from the cathode headspace into the catholyte.

The proton exchange membrane used in this study (Nafion 117) is permeable to dissolved gases (see Section 4.3.3). Therefore, to demonstrate the transport of sulfide from the cathode compartment to the anode compartment, an abiotic (i.e., uninoculated) BES was set up. The cathode was a carbon felt cathode, as described in Section 6.2.1, and the anode was a carbon cloth (2 inches x 2 inches) coated on one side with platinum. A Ag/AgCl reference electrode was placed adjacent to the platinum electrode in the anode compartment. To exclude other electrochemical reactions, the anolyte and catholyte consisted of a NaCl solution (0.58 M). The anode and cathode headspaces were flushed with N₂ and CO₂, respectively, and equilibrated to atmospheric pressure.

Sulfide ions donate electrons to the anode and increase the observed maximum current during cyclic voltammetry (CV). Thus, a calibration curve may be created to relate the maximum current to the concentration of sulfide ions (Al Kharafi et al. 2010). Using the abiotic BES at room temperature (22°C), CV was performed by sweeping the anode voltage from -0.5 V to 1.1 V (vs. Ag/AgCl) and back to -0.5 V (vs. Ag/AgCl) at 10 mV/s. Using a syringe, 3 g Na₂S was added to the anode while under magnetic mixing, to a total sulfide ion concentration of 0.05 mM. Immediately following dissolution of the Na₂S into the anolyte, CV was again performed. The sequential addition of 3 g Na₂S and CV was repeated twice to measure the maximum current at 0.10 and 0.15 mM sulfide ions. The

resulting voltammograms are shown in Figure 7.2. The maximum observed current, which occurred at 1.1 V (vs. Ag/AgCl) in each voltammogram, was plotted versus the total sulfide ion concentration in the anode to create a calibration curve (Figure 7.3).

Next, the abiotic BES was rinsed and reset, as previously described. Using a locking, gas-tight syringe with Teflon-lined plunger, gaseous H₂S was added to the cathode headspace to a total initial headspace concentration of 3% H₂S (v/v). Immediately upon injection of the H₂S, CV was performed. The BES was then incubated at room temperature (22°C) under magnetic mixing. CV was performed every 5 minutes for 85 minutes. The maximum current in each CV was converted to the analyte sulfide ion concentration and plotted over time to illustrate the transport of H₂S from the cathode headspace to the anolyte.

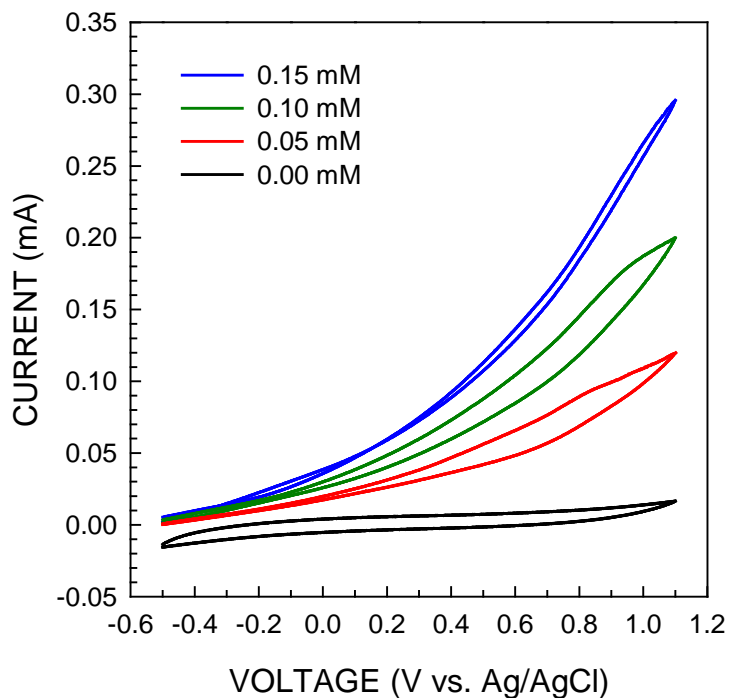


Figure 7.2 - Cyclic voltammograms of an abiotic anode with total sulfide ion concentrations of 0.00, 0.05, 0.10 and 0.15 mM

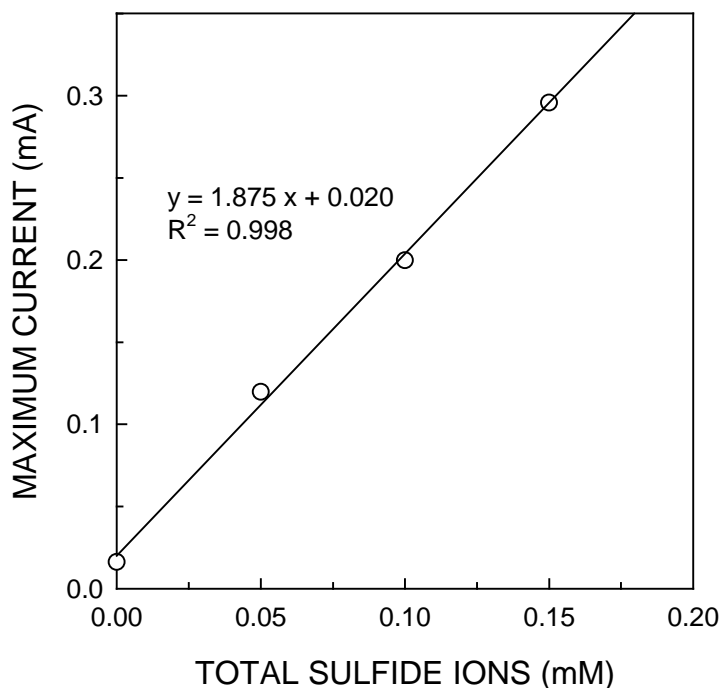


Figure 7.3 - Cyclic voltammetry maximum current versus total sulfide ion concentration

7.2.3 BES Performance with Cathode H_2S .

Two identical BESs (BES1 and BES2) were set up as previously described (see Section 5.2.1) and each inoculated with felt cuttings from the anode and cathode of a stock methanogenic BES. The stock methanogenic BES had an established anode fed with acetate to 1200 mg COD/L and an established methanogenic cathode fed with CO_2 to an absolute pressure of 1.6 atm. Anolyte and catholyte, as previously described (see Section 5.2.1) were completely exchanged at the end of each 7-d feeding cycle. The stock BES was incubated at 22°C under continuous magnetic mixing. BES1 and BES2 were maintained in

the same manner as the stock BES for approximately 8 cycles until a stable performance was achieved, as defined by a consistent current and CH₄ profile following feeding.

Following biofilm development, BES1 (control) and BES2 were maintained in the same manner, with the exception that BES1 was not exposed to H₂S. BES1 and BES2 were monitored for 1 d following a feeding without H₂S to illustrate similar performance. After 1 d incubation, a locking, gas-tight syringe with Teflon plunger was used to add H₂S to the BES2 cathode headspace to an initial concentration of 1% H₂S (v/v). The pH of the catholyte and anolyte was measured as described in Section 3.1.1, and the anode acetate was measured as described in Section 3.1.8. Cathode and anode gas production and gas composition was measured as described in Sections 3.1.6-3.1.7. System current was measured as described in Section 3.2.1.

BES1 and BES2 were monitored for the remainder of a 7-d feeding cycle, at which time the anode and cathode were flushed with N₂ and CO₂, respectively, and the anolyte and catholyte were completely replaced. BES1 and BES2 were fed as previously described and 1% H₂S was added to the BES2 cathode at the start of the new feeding cycle. The BESs were monitored and, on day 15, the feeding was repeated with the addition of 1% H₂S to the BES2 cathode headspace. The BESs were then incubated and monitored for a 3-d cycle. Based on the data collected during monitoring of the previous 7-d and 8-d cycles, the highest rate of current and CH₄ production occurred during the first 3 d of a feeding cycle, during which CH₄ production was linear (Figure 7.4). After 3 d, substrate limitations became evident, particularly in the BES2 anode. Thus, BES1 and BES2 were converted to a 3-d feeding cycle.

Next, H₂S was added at increasing concentrations to the cathode headspace of BES2, according to the schedule described in Table 7.1. The mean CH₄ production rate over each 3-d feeding cycle was calculated. Multiple 3-d cycles were conducted at 0%-3% H₂S (v/v) (Table 7.1) but only one cycle was conducted at 4-6% H₂S (v/v) because of observed inhibition. The mean value was then taken of the 3-d CH₄ production rates for the 3 cycles conducted under 1%, 2% and 3% H₂S (v/v).

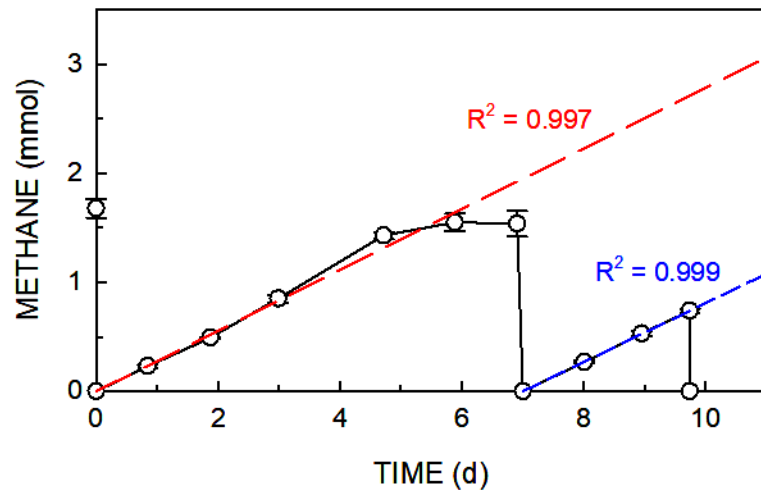


Figure 7.4 - Linear biocathode CH₄ production during the first 3 days of two feeding cycles

Table 7.1 - BES2 Feeding Schedule

Cycle	Initial cathode headspace H ₂ S (% v/v)	Cycle length (d)
1	1	7
2	1	8
3	1	3
4	2	3
5	2	3
6	2	3
7	3	3
8	3	3
9	3	3
10	4	3
11	5	3
12	6	3

7.2.4 Carbon Balance.

To determine if the introduction of H₂S to the cathode headspace affects the flow of carbon within the system, various forms of carbon in the anode and cathode were measured and compared between BES1 and BES2 following a 3-d feeding cycle. Anolyte and catholyte were replaced at the beginning of the cycle in both systems. BES1 and BES2 anodes were fed with acetate to 700 and 790 mg COD/L, respectively. Although the same amount of acetate was added to each anode, the difference in initial acetate concentrations was due to the retention of acetate-containing interstitial water in the carbon felt electrode; because the BES1 anode was less efficient at acetate removal, the interstitial water retained a larger amount of acetate into the following cycle than in the BES2 anode. Each cathode was pressurized to 1.6 atm (absolute pressure) with CO₂. Using a locking, gas-tight syringe with Teflon-lined plunger, H₂S was added to the BES2 cathode headspace to an initial

concentration of 3% H₂S (v/v). The BESs were incubated at 22°C under continuous magnetic mixing for 3 d.

At the end of incubation, gaseous CH₄ and CO₂ were measured in the headspace of the anode and cathode as described in Sections 3.1.6 and 3.1.7. Total dissolved CO₂ was measured as described in Section 3.1.9. Dissolved CH₄ was calculated using the Henry's law constant (K_H) for the phosphate buffer medium used for anolyte and catholyte, corrected for ionic strength and 22°C (1,424.6±14.5 atm/M) (Sander 2015, Weisenberger and Schumpe 1996), and assuming equilibrium between the liquid and headspace gas. Acetate was measured in the anolyte and catholyte as described in Section 3.1.8. Protein measurements (Section 3.1.10) of the anolyte and catholyte following 3 d incubation were used to estimate the amount of suspended biomass in the anode and cathode with the assumption that 52.4% of the dry weight of each cell was made up of protein (Stouthamer 1973) and that the formula C₅H₇O₂N was representative of microbial biomass (Rittmann and McCarty 2001). Thus, protein measurements of suspended biomass in the anolyte and catholyte were converted into the total mass of carbon as suspended biomass. To understand the biomass distribution between suspended growth and biofilm, felt was removed from the anode and cathode of each system and the protein content was measured (Section 3.1.10). Biofilm growth in the anode was assumed to follow the observed yield coefficient for exoelectrogenic Bacteria (0.02 g VSS/g COD) (Wilson and Kim 2016). Using the acetate consumption (in terms of COD) in the anode, the amount of anode biofilm growth as carbon was calculated. Biofilm growth in the cathode was estimated using the yield coefficient for hydrogenotrophic methanogens (0.45 g VSS/g H₂) and a decay coefficient of 0.03 d⁻¹, which is common for anaerobic microorganisms (Rittmann and

McCarty 2001). Assuming growth and decay followed first-order kinetics, the growth of the cathode biofilm biomass over the 3-d cycle was calculated.

7.3 Results and Discussion

7.3.1 Serum Bottle Tests.

Two series of serum bottles were set up to compare the response of acetoclastic and hydrogenotrophic methanogenic cultures to 1% H₂S (v/v). A mixed methanogenic (MM) culture was used for the acetoclastic methanogenesis test and an enriched hydrogenotrophic methanogenic culture (EHM) was used for the hydrogenotrophic methanogenesis test. In all serum bottles, the pH remained between 6.8 and 7.0 during incubation. Over the 14 d incubation, the MM control and MM with H₂S removed 96.8% and 97.1% of the acetate, respectively, indicating the presence of sulfide did not significantly affect acetate removal. The time series of CH₄ production for the MM bottles with and without H₂S is shown in Figure 7.5. The maximum rate of CH₄ production in the MM control serum bottles, normalized to the biomass in the system (0.629 ± 0.016 mmol/d-g biomass; $R^2=0.986$), occurred during the first 11 days following feeding, after which CH₄ production decreased. The rate of CH₄ production in the MM bottles with H₂S was similar to the control during the first day after feeding but the mean rate of CH₄ production over the duration of the incubation (0.480 ± 0.019 mmol/d-g biomass; $R^2=0.963$) was 24% slower than that of the MM control. However, the extent of CH₄ production in the MM with H₂S over the 14 d incubation was similar to the MM control. At the end of incubation, the CH₄ in the MM control and MM with H₂S bottles represented 62% and 77%, respectively, of the theoretical CH₄ production based on stoichiometric conversion of the removed acetate to CH₄.

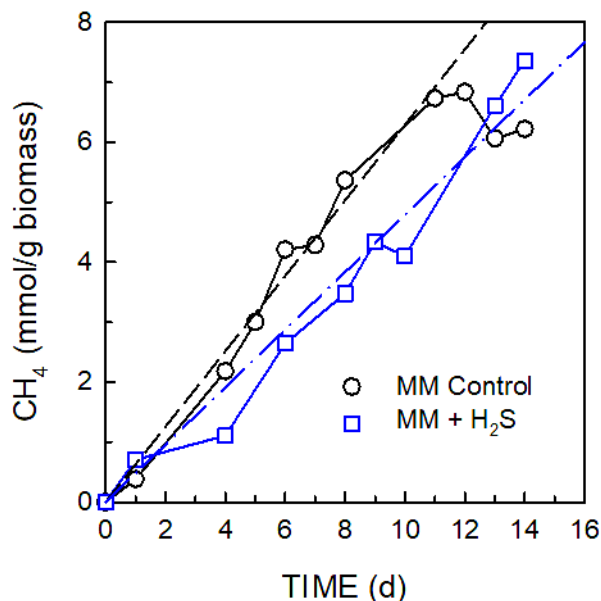


Figure 7.5 - Time course of MM serum bottle CH₄ production with 0% H₂S (MM control) and 1% initial H₂S in the headspace (MM + H₂S)

The EHM control (no H₂S) produced CH₄ at a mean rate of 0.237 ± 0.015 mmol CH₄/d-g biomass (Figure 7.6). Although normalized to the biomass, the slower rate of CH₄ production in the EHM control as compared to the MM control may be due to the less active status of the stock EHM culture, which was fed less often (once per week) than the MM culture (fed twice per week). In the EHM bottles with H₂S, some CH₄ was produced over the first 2 d following feeding but CH₄ production was completely inhibited over the remainder of the incubation. The significant inhibition of the EHM culture by 1% H₂S is likely due to the low biomass concentration in the EHM culture. While the MM bottle with H₂S had 0.25 g biomass at the end of incubation, the EHM bottle with H₂S had only 0.06 g biomass. The extent of microbial inhibition is affected by both the concentration of the inhibiting substance (e.g., sulfide) and the concentration of the biomass present (Rozzi and

Remigi 2004). Assuming equilibrium between the gas and liquid phase, the ratio of total dissolved sulfide to biomass in the MM and EHM sulfide bottles was 0.03 and 0.18 g-S/g-biomass, respectively. Thus, the biomass in the EHM sulfide bottles had a 5-fold greater ratio of sulfide to biomass in the MM sulfide bottles. Therefore, further testing is needed to directly compare the response of acetoclastic and hydrogenotrophic methanogens to sulfide.

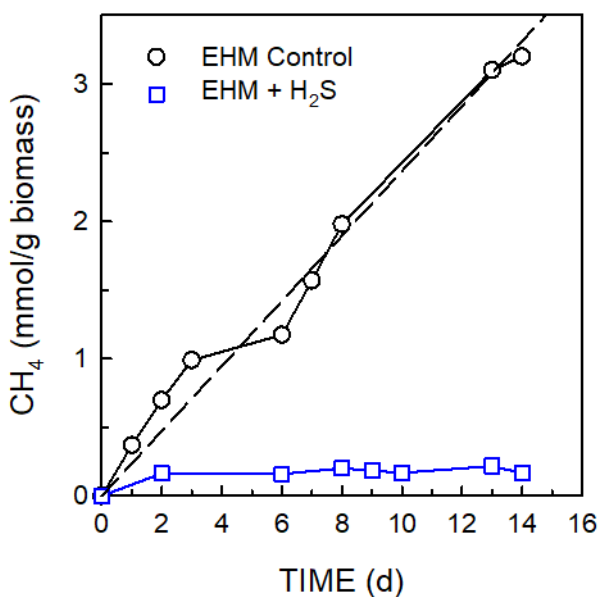


Figure 7.6 - Time course of EHM serum bottle CH₄ production with 0% H₂S (EHM Control) and 1% initial H₂S in the headspace (EHM + H₂S)

Although the MM culture was used to assess acetoclastic methanogens by feeding acetate, the culture also contained hydrogenotrophic methanogens (see Section 5.3.3). Therefore, to assess the response of the hydrogenotrophic methanogens in the MM culture to sulfide exposure, five series of serum bottles were set up with the MM culture, flushed with H₂/CO₂ (80:20) and added 0%, 0.38%, 0.75%, 1.5% and 3.0% H₂S (v/v). No acetate

or other organics were added to discourage acetoclastic methanogenesis. The time course of CH₄ production in each series is shown in Figure 7.7. Unlike the acetoclastic test with the MM culture, under hydrogenotrophic conditions, the MM culture did not display any inhibition up to 3% H₂S. No significant difference was observed in the CH₄ production at any of the H₂S concentrations, indicating that the hydrogenotrophic methanogens in the MM culture were less susceptible to H₂S inhibition than the acetoclastic methanogens in the MM culture. The difference in response to H₂S between the MM culture and the EHM culture could be due to differences in hydrogenotrophic methanogens (see Section 5.3.3), a greater diversity in the MM culture, and a greater abundance of non-methanogenic biomass that may decrease methanogen contact with sulfide.

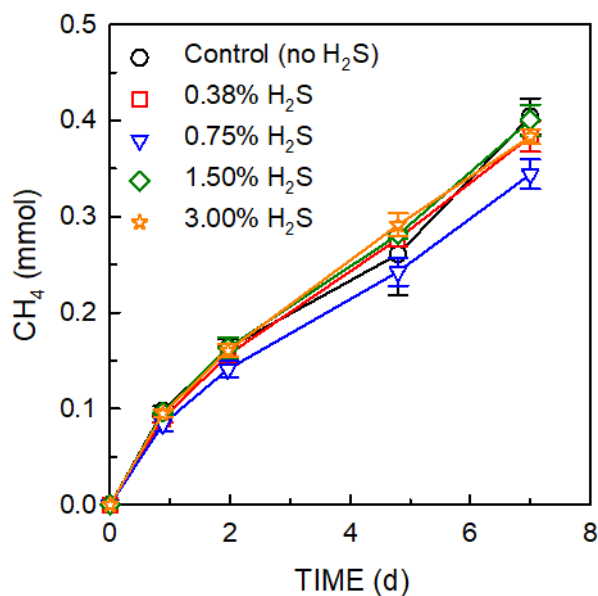


Figure 7.7 - Time course of CH₄ production by the MM culture under hydrogenotrophic conditions with 0% (Control), 0.38%, 0.75%, 1.50% and 3.00% H₂S in the headspace

7.3.2 Sulfide Transport within a BES.

CV with a platinum cathode can indicate the concentration of sulfide ions as a peak near -0.1 V vs. Ag/AgCl, and the maximum current produced at the sulfide peak can be correlated to the concentration of sulfide ions in solution in the catholyte (Al Kharafi et al. 2010). In the present system, H₂S was added to the headspace of a Pt-coated cathode and periodic CV revealed a growing oxidation peak at -0.2 V vs. Ag/AgCl (-0.14 V vs. Ag/AgCl when measured at 30 min) (Figure 7.8). The difference in applied voltage at the reported and observed sulfide peak is likely due to differences in electrochemical cell architecture. In the present study, no significant difference existed between the voltammograms prior to and immediately after H₂S addition. Thus, gaseous H₂S in the cathode headspace had little, if any, effect on system current. However, as the sulfide dissolved into the catholyte, the system current increased, resulting in the appearance of a peak at -0.2 V vs. Ag/AgCl, as previously mentioned. To assess the rate of sulfide dissolution into the cathode, the current at the identified sulfide peak (-0.2 V vs. Ag/AgCl) and the current at the most oxidizing applied potential (0.2 V) were used as surrogates for the sulfide ion concentration and plotted over time (Figure 7.9). Both current profiles indicated that the dissolution of sulfide occurred rapidly and approached an equilibrium concentration within 10 min of being introduced to the system.

As H₂S dissolves into the catholyte, it may also begin to be transported across the proton exchange membrane into the anode compartment. A similar membrane, Nafion 112, is permeable to dissolved H₂S (Sethuraman et al. 2009) and the membrane in the present study, Nafion 117, is permeable to several other dissolved gases (see Section 4.3.3). Therefore, to assess the transport of H₂S across the Nafion 117 membrane, the anode

concentration of sulfide ions was measured by adjusting the BES configuration such that the anode contained the platinum-coated carbon cloth electrode and the cathode contained the abiotic carbon felt electrode. Following the addition of 3% H₂S (v/v) to the cathode headspace, CV was performed at increments of 5 min for a period of 85 min (Figure 7.10). The maximum current for each voltammogram was used to calculate the total sulfide ions in solution in the anolyte (Figure 7.11). The measurements indicate that the transport of sulfide ions to the anode does not occur in a linear manner but that most transport occurs within the first 60 min following H₂S addition. A study of the diffusion coefficient and solubility of H₂S in a similar membrane, Nafion 112, at 35°C, reported that the initial transport of H₂S was faster than that predicted by the mathematical model, although equilibrium predictions were accurate (Sethuraman et al. 2009). In the present study, the sulfide ion concentration in the anolyte reached a maximum around 0.12 mM, where it remained for approximately 20 min before slightly declining. At the maximum sulfide ion concentration, the anolyte was estimated to contain 48% of the total amount of sulfur initially added to the cathode headspace as H₂S. Thus, the measurements indicate the equilibration of H₂S between anode and cathode occurred quickly and, under the conditions of the present study, was complete within 60 min. After reaching the maximum concentration of sulfide in the anolyte, the concentration began to decline. This observation may be explained by losses of sulfide due to irreversible oxidation during CV, sorption to the synthetic rubber stoppers or deposition of sulfur on the electrode or sulfide. For example, a platinum electrode may react with H₂S (aq), as given in equation 7.10. The solid product, PtS, may reduce the available electrode surface area for electrochemical reactions to occur.

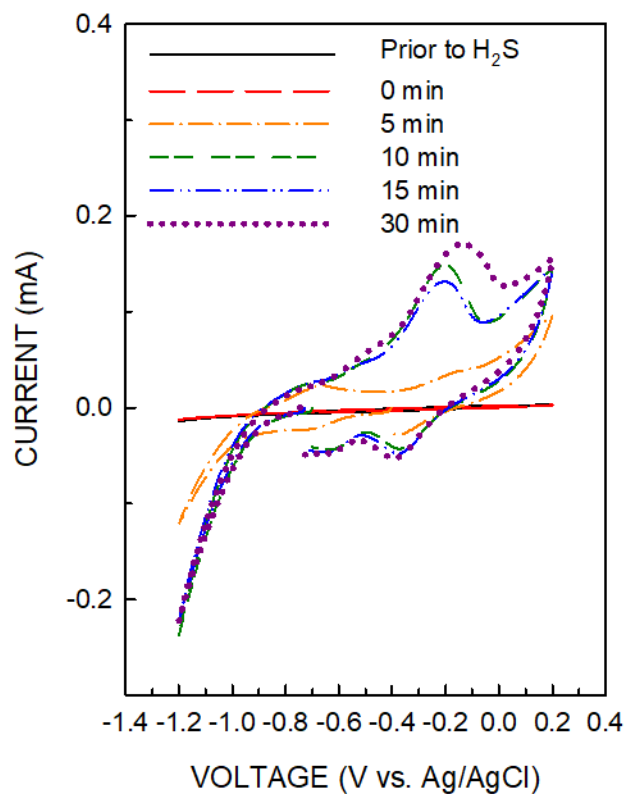
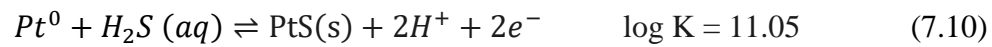


Figure 7.8 - Cyclic voltammetry conducted on the cathode over time following the addition of 3% H₂S (v/v) to the cathode headspace

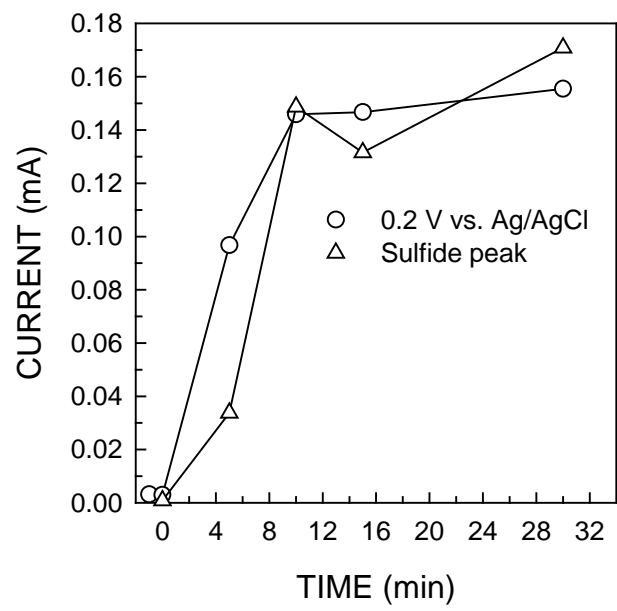


Figure 7.9 - Time course of maximum current during CV from -1.2 V to 0.2 V (vs. Ag/AgCl) and system current at the applied cathode voltage of 0.2 V (vs. Ag/AgCl).

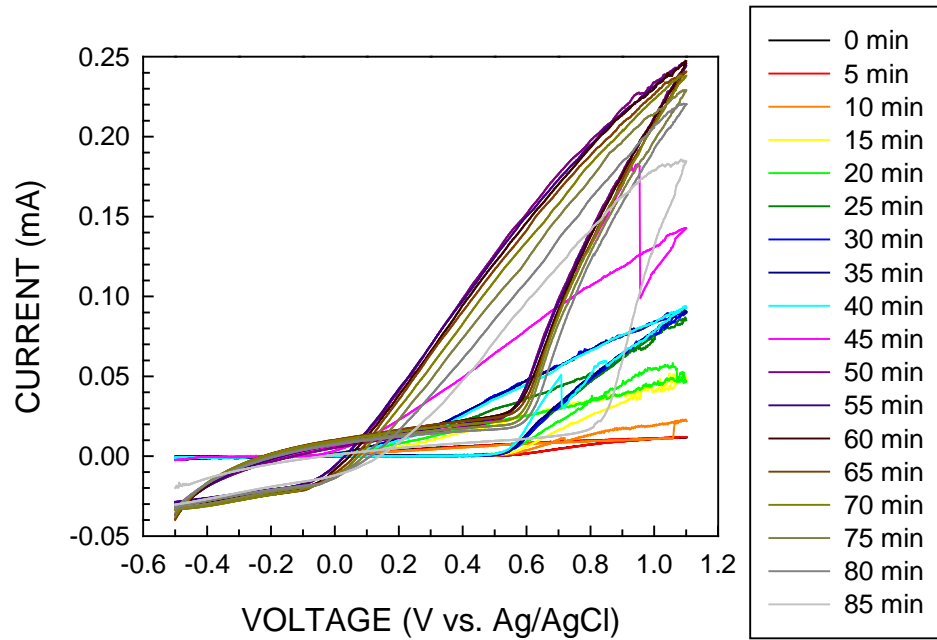


Figure 7.10 - Anode cyclic voltammety conducted over time following the addition of 3% H₂S (v/v) to the cathode headspace

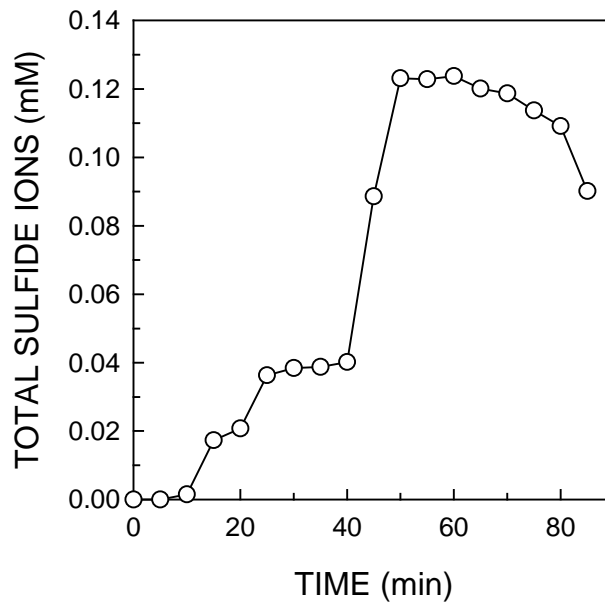


Figure 7.11 - Time sequence of anolyte total sulfide ion concentration following the addition of 3% H₂S (v/v) to the headspace of the cathode.

7.3.3 Effect of H₂S on BES Performance.

Following the development of anode and cathode biofilm in the parallel reactors BES1 and BES2, each system reached a steady operation, as defined by consistent bioanode acetate removal (69-72%), biocathode CH₄ production and current production over the course of three consecutive 7-d feeding cycles. Similar performance was observed in BES1 and BES2 in the feeding cycle prior to the addition of H₂S to the BES2 biocathode (Table 7.2).

Table 7.2 - Comparison of BES1 and BES2 prior to H₂S Addition

Parameter	BES1	BES2
Cell voltage, start of cycle prior to H ₂ S addition (V)	3.02	2.89
Cell voltage, end of cycle prior to H ₂ S addition (V)	2.06	2.01
Mean CH ₄ production per 7-d cycle (mmol)	1.61±0.10 ^a	1.54±0.14
Mean anode acetate removal per 7-d cycle (%)	69.3±2.8	70.4±1.6
Coulombic efficiency, cycle prior to H ₂ S addition (%)	51.2	47.8
Cathode capture efficiency, cycle prior to H ₂ S addition (%)	73.9	79.8

^a Mean ± standard deviation, *n* = 3.

BES1 and BES2 were fed and monitored for 1 day before the first addition of H₂S to the headspace of the BES2 cathode. While the current density was slightly lower in BES2 than in BES1 for the first day (Figure 7.12), the CH₄ production was similar, with BES1 and BES2 producing 0.230±0.015 and 0.222±0.014 mmol, respectively, over the first day. Using a locking, gas-tight syringe, H₂S was added to the BES2 cathode headspace to an initial concentration of 1% H₂S (v/v) on day 1. The observed current density in BES2 almost immediately increased (Figure 7.12) and remained above the BES1 current density for the remainder of the feeding cycle, despite an initial lower current density prior to H₂S addition. Thus, the addition of H₂S to the cathode had a rapid effect on the system current

that was sustained throughout the cycle. On day 7, the anolyte and catholyte was replaced, BES1 and BES2 were fed and 1% H₂S was added to the BES2 cathode headspace. Upon feeding, the peak current density observed in BES2 was nearly twice as large as the current density in BES1, a pattern that was repeated at the next feeding on day 15 (Figure 7.12).

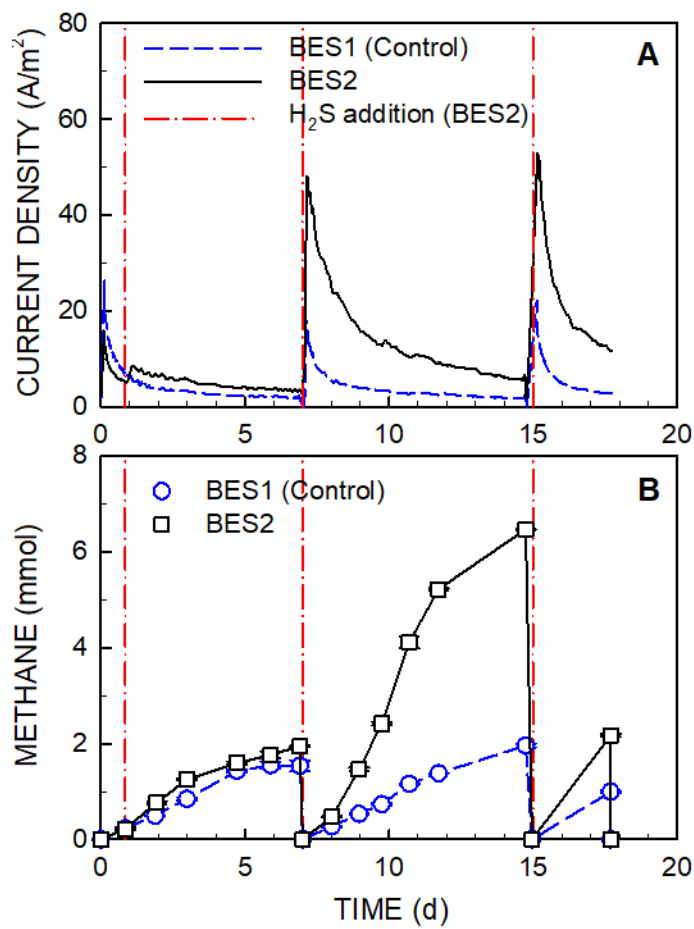


Figure 7.12 - Time course of current density in BES1 (control) and BES2, during which H₂S was added to 1% H₂S (v/v) in the cathode headspace on days 1, 7 and 15.

7.3.1 Biocathode Methane Production at Various Initial Hydrogen Sulfide Concentrations

To test the effect of various initial H₂S concentrations in the cathode headspace, a series of 3-d feeding cycles were monitored in which the initial H₂S concentration was incrementally increased from 1% to 6%. The initial 3-d mean rate of CH₄ production was assessed over several cycles, as shown in Figure 7.13. The highest CH₄ production rate was observed at 2% and 3% initial H₂S (0.889±0.091 and 0.889±0.044 mmol/d, respectively), which represented a nearly two-fold increase over the mean rate prior to H₂S exposure. Above 3% initial H₂S in the cathode headspace, the rate of CH₄ production decreased significantly. At 5% and 6% initial H₂S, the rate of CH₄ production was 43% and 24% lower, respectively, than the mean rate prior to H₂S exposure. A previous study reported a 50% inhibition of methanogenesis from synthetic distillery waste when the produced gas contained 5% H₂S (v/v) (Karhadkar et al. 1987). Fewer feeding cycles with an initial H₂S concentration above 3% were assessed due to the clear inhibition of CH₄ production at relatively high sulfide concentrations.

The bell-shaped profile of the CH₄ production rates versus initial H₂S concentration (Figure 7.13) indicates that H₂S exerted at least two competing effects on the system performance. Abiotic tests show that H₂S will dissolve quickly and be transported to the anode, where it contributes to current by donating electrons to the electrode. Thus, sulfide can increase cathodic CH₄ production by increasing current in the system and increasing the electrons available at the cathode for CO₂ reduction. Alternately, H₂S is inhibitory to enriched hydrogenotrophic methanogens used as the stock biocathode inoculum, as shown

with serum bottle tests (see Section 7.3.1). However, at relatively low H₂S concentrations, biocathode biofilm can help protect against sulfide inhibition by creating microenvironments with a lower sulfide concentration where methanogenic activity can occur. Furthermore, the local pH near the biofilm surface at the cathode is higher than the pH of the well-mixed catholyte because protons are consumed at the cathode surface in either the reduction of CO₂ to CH₄ or the reduction of H⁺ to H₂. Therefore, the sulfide species present near the cathode surface will shift towards HS⁻ and S²⁻, and away from H₂S, which is considered to be involved in sulfide inhibition of methanogenesis (Chen et al. 2008, Hilton and Oleszkiewicz 1988, McCartney and Oleszkiewicz 1991). Thus, at relatively low H₂S concentrations ($\leq 3\%$ H₂S, v/v), the cathode biofilm was able to resist sulfide inhibition and, in fact, activity was increased because sulfide donated electrons to the anode and increased current. However, as H₂S concentrations increased above 3% H₂S (v/v), the inhibition of methanogens resulted in a decrease in CH₄ production.

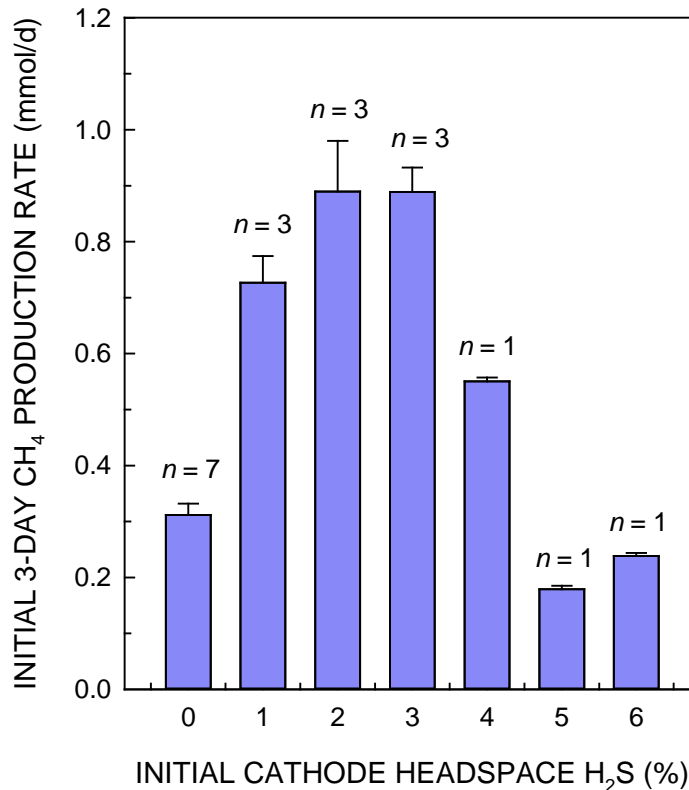


Figure 7.13 - Comparison of the initial 3-day methane production rate at initial cathode headspace hydrogen sulfide concentrations of 0-6% (v/v); *n* is the number of feeding cycles represented.

7.3.2 Carbon Balance

To determine whether the addition of H₂S to the cathode headspace affects the carbon flow within the system, various forms of carbon (i.e., dissolved and gaseous CO₂ and CH₄, acetate and biomass as both suspended and biofilm) were measured or estimated (see Section 7.2.4) in BES1 and BES2 (3% H₂S v/v in cathode headspace) at the beginning and end of a 3-d feeding cycle. A comparison of the carbon forms is shown in Figure 7.14. Enhanced microbial activity in the anode of BES2 may be seen by the acetate and CO₂ (gaseous and dissolved) at the end of the cycle. The BES1 anode removed 54.7% of the

initial acetate over 3 d. In contrast, acetate was not detected in the BES2 anode at the end of 3 d, indicating a higher rate of acetate uptake and metabolism in the BES2 anode. Acetate is converted to CO₂ by exoelectrogens but may also be utilized as an electron donor by SRB if oxidized sulfur electron acceptors (e.g., SO₄²⁻) are available. In the BES2, H₂S is transported from the cathode to the anode through the proton exchange membrane, where it may become oxidized at the anode (see Section 7.3.2), providing an electron acceptor for SRB. Thus, by acting as an alternative electron acceptor to the anode, the oxidized sulfur species may divert acetate electron equivalents away from exoelectrogens at the anode.

Total biomass growth was significantly larger in the anode and cathode of BES2 than in BES1 (Figure 7.14). At the end of the 3 d feeding cycle, protein measurements of the suspended and biofilm biomass in each system indicated that the anode and cathode of BES2 had a substantially larger amount of biofilm biomass than in BES1 (Figure 7.15). The BES2 anode had less suspended biomass than the BES1 anode but had 128% more biofilm biomass, which resulted in an overall larger net biomass quantity in the BES2 anode than the BES1 anode. In the BES2 cathode, the suspended biomass was similar to that of the BES1 cathode but the biofilm biomass was over 16-fold larger than the biofilm biomass in the BES1 cathode (Figure 7.15). A thicker biofilm coverage was indeed visible on the cathode of BES2 when compared to BES1 (Figure 7.16). Thus, the presence of H₂S likely stimulated biofilm biomass development in the cathode, while transported H₂S and/or its resulting oxidized compounds stimulated biofilm biomass development in the anode. Sulfur was provided in the anolyte and catholyte to a concentration of 6.4 mg S/L, which was replenished prior to each feeding. This concentration is within the recommended range of 1 to 25 mg S/L (Chen et al. 2008). Thus, the increase in biomass observed in BES2

was not likely due to the relief of a sulfur deficiency but was more likely due to the promotion of bacteria involved in the cycling of sulfur (see Section 7.3.3).

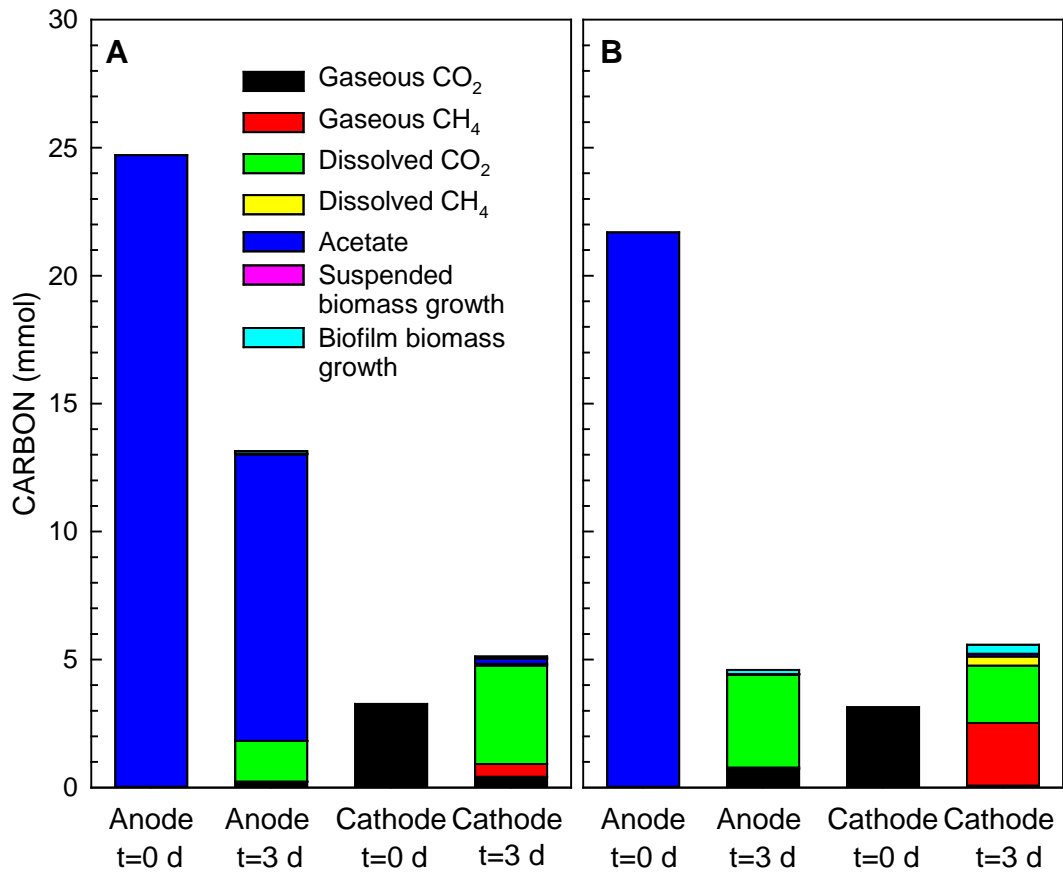


Figure 7.14 - Carbon balance of BES1 (control), A; and BES2 with 3% initial H₂S (v/v) in the cathode headspace, B.

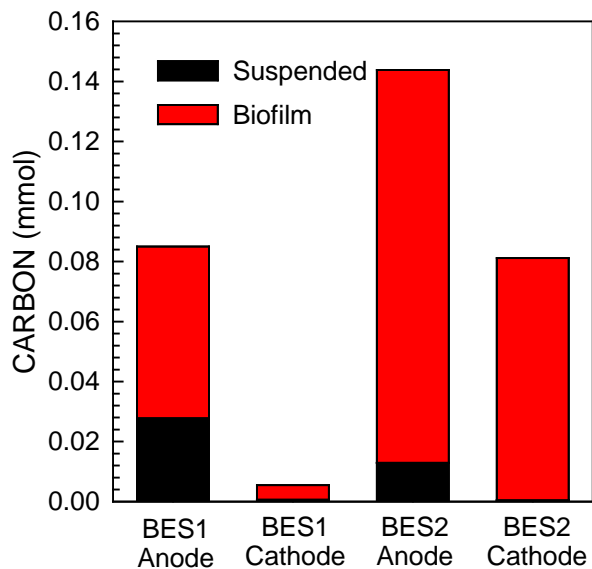


Figure 7.15 - Biomass distribution between suspended and biofilm biomass in the anode and cathode of BES1 and BES2 after 3-d incubation.

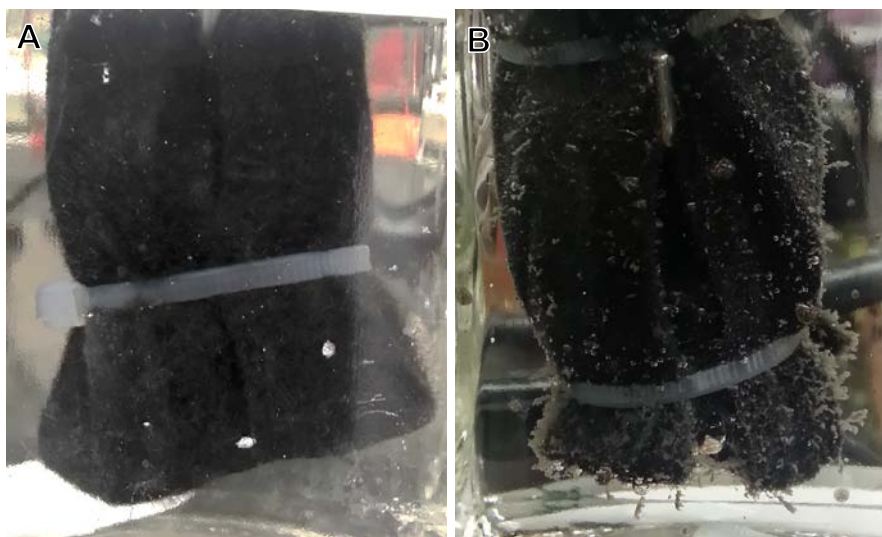


Figure 7.16 - Biofilm growth on the BES1 cathode (A) was visibly thinner than the biofilm growth on the BES2 cathode (B).

At the beginning of incubation, the cathodes of BES1 and BES2 only contained gaseous CO₂ as a carbon source. At the end of incubation, both cathodes contained a larger

amount of total carbon than at the beginning of incubation, indicating an overall transport of carbon from anode to cathode, as has previously been described (see Section 4.3.4). Acetate was observed as a minor component of cathode carbon in the BES1 and BES2 following incubation (0.2 and 0.1 mmol C, respectively). Acetate may be produced through acetogenesis in the cathode or through the diffusion of acetate through the proton exchange membrane (Chae et al. 2008, Nevin et al. 2011). Conversion of the initial CO₂ to CH₄ in the BES1 cathode was 17% over the 3-d incubation. In contrast, 89% of the initial CO₂ in the BES2 cathode was converted to CH₄ over the same length of time. Thus, the addition of 3% H₂S to the BES2 cathode resulted in a nearly five-fold increase in the amount of CH₄ produced over the 3-d incubation. By increasing system current, H₂S increased the rate of CO₂ conversion to CH₄ in the cathode, while also shifting more carbon to biomass growth.

7.3.3 Phylogeny and Microbial Community Assessment

The bacterial and archaeal communities of the BES anodes and cathodes were analyzed using 16S rRNA gene sequencing. OTU counts are given in Table 7.3. The BES1 anode biofilm and BES2 anode suspended biomass samples had very low archaeal counts and relatively low archaeal counts were also obtained in the BES1 anode suspended biomass and BES2 anode biofilm. Despite low abundances of Archaea in the BES anodes, the fraction of bacterial OTUs detected in the BES2 anode biofilm was 45% (Table 7.3), indicating the majority of detected OTUs for that sample were Archaea. In contrast, the bacterial fraction of total OTUs in the BES1 anode biofilm was 97%. Thus, the sulfide-exposed anode appeared to favor archaeal growth.

A larger number of archaeal OTUs were detected in the cathodes than in the anodes, which was expected due to methanogenic activity. However, the bacterial OTUs in the BES1 cathode biofilm represented 85% of the total OTUs, indicating a significant role for Bacteria in a methanogenic biocathode. Archaeal OTUs represented 65% of the total OTUs in the BES1 cathode suspended biomass, which suggests that mediated methanogenesis occurred in the catholyte at a distance from the cathode surface. In contrast, the sulfide-exposed BES2 had a slightly lower archaeal fraction in the suspended biomass (51%) than in BES1 (65%). Furthermore, BES2 had a greater archaeal fraction in the biofilm (48%) than in BES1 (15%), which indicates that sulfide encouraged biofilm archaeal growth.

Table 7.3 - BES1 and BES2 OTU Counts

Sample	Bacteria	Archaea	Bacterial Fraction ^a (%)
BES1 Anode Biofilm	20,094	657	97
BES1 Anode Suspended Biomass	21,353	12,384	63
BES1 Cathode Biofilm	133,547	24,258	85
BES1 Cathode Suspended Biomass	18,245	33,318	35
BES2 Anode Biofilm	14,336	17,775	45
BES2 Anode Suspended Biomass	12,042	1 ^b	100
BES2 Cathode Biofilm	24,328	22,524	52
BES2 Cathode Suspended Biomass	21,605	22,390	49

^a Fraction of the sample's total OTU count (Bacteria plus Archaea) that consists of bacterial OTUs.

^b Insignificant. DNA sequencing yielded too few archaeal reads.

A single phylotype, most closely related to *Methanobrevibacter arboriphilus*, dominated the archaeal community in the BES1 cathode biofilm and suspended growth

(Table 7.4). The enrichment of *M. arboriphilus* on a biocathode has also been noted in other studies (Jiang et al. 2014, Siegert et al. 2015, Zeppilli et al. 2015). The present study shows that the archaeal community in the suspended biomass was similar in composition to that of the biofilm archaeal community. Considering that a similar amount of biomass was present in the cathode suspended biomass of both BES1 and BES2, but a significantly larger amount of biomass was present in the BES2 cathode biofilm (Figure 7.15), the analysis of BES2 cathode archaeal OTU counts indicates that biocathode exposure to H₂S may promote archaeal biofilm development.

Table 7.4 - Archaeal Community Analysis (Relative Abundance, %)

OTU Accession No. / Closest GenBank Relative	BES1 Anode		BES1 Cathode		BES2 Anode		BES2 Cathode	
	B ^a	S ^b	B	S	B	S	B	S
KU597459 & MF512189 / <i>Methanobrevibacter</i> <i>arboriphilus</i>	2	6	100	99	72	NA ^c	100	100
MF12188 / <i>Methanobacterium</i> <i>formicum</i>	2	90	0	1	0	NA	0	0
MF512192 / <i>Methanobacterium</i> <i>formicum</i>	5	0	0	0	23	NA	0	0
MF512190 / <i>Methanothermobacter</i> <i>marburgensis</i>	0	0	0	0	1	NA	0	0
MF12191 / <i>Methanosaeta</i> <i>concilii</i>	0	0	0	0	3	NA	0	0

^a Biofilm.

^b Suspended biomass.

^c Not available. DNA sequencing yielded too few archaeal reads to be significant.

The bacterial communities of the BES1 and BES2 anode biofilm and suspended biomass were also compared (Figure 7.17A). In BES1, the anode biofilm and suspended bacterial communities were similar, with *Proteobacteria* as the predominant class of Bacteria. However, the BES2 anode biofilm and suspended bacterial community had a substantially larger relative abundance of *Actinobacteria* than in the BES1 anode communities. The BES2 anode biofilm also contained *Bacteroidetes*, *Firmicutes* and other unclassified Bacteria at a greater relative abundance than in the BES1 anode biofilm, indicating a larger diversity in the bacterial community. Indeed, the Shannon diversity indices (Table 7.5) show that the BES2 anode biofilm had a significantly greater bacterial diversity (2.76 Shannon index) than the BES1 anode biofilm (1.35 Shannon index). Thus, the presence of sulfide and/or sulfur cycling in the anode likely contributed to the increased diversity observed in the BES2 anode. The bacterial and archaeal diversity was lower in the BES2 cathode biofilm than in the BES1 cathode biofilm, but the suspended biomass in the BES2 cathode had a slightly greater diversity than in the BES1 cathode. The diversity indices were similar between other samples in BES1 and BES2; therefore, the greatest effect of H₂S on community diversity was on the Bacteria in the anode biofilm. The oxidation of H₂S at the anode likely encouraged growth of a more diverse bacterial community.

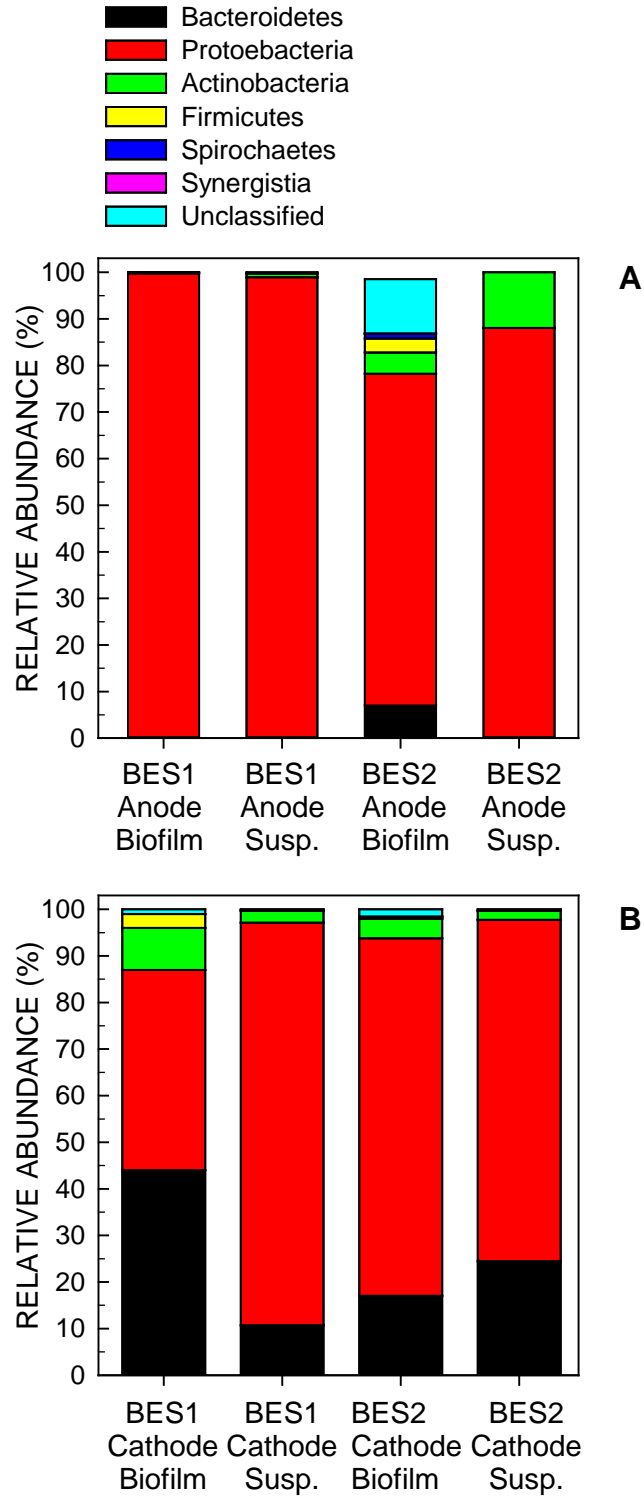


Figure 7.17 - Bacterial community of BES1 and BES2 anode (A) and cathode (B) biofilm and suspended biomass

Table 7.5 - Bacterial and Archaeal Shannon Diversity Indices

Sample	Bacteria	Archaea
BES1 Anode Biofilm	1.35	0.93
BES1 Anode Suspended Biomass	1.01	0.39
BES1 Cathode Biofilm	2.68	0.05
BES1 Cathode Suspended Biomass	1.73	0.04
BES2 Anode Biofilm	2.76	0.79
BES2 Anode Suspended Biomass	1.04	NA ^a
BES2 Cathode Biofilm	2.12	0.002
BES2 Cathode Suspended Biomass	1.89	0.0005

^a Not Available. OTU counts were too low for analysis.

The cathode bacterial communities also differed between BES1 and BES2 (Figure 7.17B). Unlike in the anode, the cathode biofilm bacterial community in BES2 had a lower relative abundance of *Bacteroidetes*, *Actinobacteria* and *Firmicutes* than the BES2 biofilm. Instead, the BES2 cathode biofilm had a larger relative abundance of *Proteobacteria* than in the BES1 cathode biofilm. In contrast, the BES2 cathode suspended biomass contained a lower relative abundance of *Proteobacteria* and a greater abundance of *Bacteroidetes* than the BES1 cathode suspended biomass. Therefore, exposure to H₂S may promote *Bacteroidetes* suspended growth over biofilm growth, and promote *Proteobacteria* biofilm growth over suspended growth.

All OTUs detected at $\geq 1\%$ relative abundance were assessed for their relative abundance in the anode and cathode of BES1 and BES2 (Table 7.6). In the cathode of BES1, a phylotype most closely related to *Proteiniphilum acetatigenes* represented 43% of the biofilm bacterial OTUs and 11% of the suspended growth bacterial OTUs. In contrast, this phylotype represented 17% and 24% of the BES2 biofilm and suspended growth, respectively. Two strains of *Proteiniphilum* spp. have been isolated from the granular sludge of an upflow anaerobic sludge blanket reactor treating brewery wastewater (Chen

and Dong 2005). *Proteiniphilum* spp. is able to ferment amino acids (Chen and Dong 2005) and anaerobically degrade polycyclic aromatic hydrocarbons (PAHs) (Larsen et al. 2009). *Proteiniphilum* spp. was also noted to be enriched under biocathode conditions, as discussed in Section 5.3.3.

A phylotype most closely related to *Achromobacter* sp. was observed at a similar relative abundance in both the BES1 and BES2 biofilm (6% and 10%, respectively), and suspended biomass (25% and 21%, respectively). *Achromobacter* sp. has previously been observed in the biocathode of MFCs (Kumru et al. 2012, Zhang et al. 2011) but its role in biocathode processes is unknown. Regardless, the biocathode exposure to H₂S did not appear to affect the relative abundance of *Achromobacter* sp. in either the biofilm or suspended biomass.

Another phylotype, which was most closely related to *Ochrobactrum anthropi*, was observed across all cathode samples. In the BES1 biofilm, 3% of the bacterial OTUs were represented by this phylotype. However, in the BES2 biofilm, this phylotype represented 43% of bacterial OTUs, indicating an enrichment in the presence of H₂S. A slight enrichment also occurred in the suspended biomass. While the *Ochrobactrum* sp. phylotype represented 29% of the bacterial OTUs in the BES1 suspended biomass, it represented 34% of bacterial OTUs in the BES2 suspended biomass. Thus, cathode *Ochrobactrum* sp. growth might be stimulated by H₂S addition. *Ochrobactrum anthropi* is a known exoelectrogen and has been observed in MFCs (Jayashree et al. 2014, Kumru et al. 2012, Zuo et al. 2008). Although typically found under anodic conditions, the enrichment of exoelectrogens on biocathode surfaces may facilitate the recycling of lysed cells and cellular products into electron equivalents that may be donated back to

electrotrophic microorganisms, like methanogens. Some evidence suggests that exoelectrogens are beneficial to biocathode CH₄ production due to cellular recycling, as discussed in Section 5.3.3.

The same *Ochrobactrum* sp. phylotype was also identified in the BES1 and BES2 anode. This phylotype represented 7% of the bacterial OTUs in the BES1 anode biofilm and 4% in the BES2 anode biofilm. However, in the suspended growth, the *Ochrobactrum* sp. phylotype represented 21% and 72% of the BES1 and BES2 bacterial OTUs, respectively. Thus, the *Ochrobactrum* sp. phylotype was enriched in the anode suspended biomass when H₂S was added to the biocathode. As an exoelectrogen, it is possible that *Ochrobactrum* sp. contributed to the increased current observed in BES2 through indirect electron transfer (Logan 2009, Zuo et al. 2008). A phylotype related to *Shigella dysenteriae* was present in the BES1 and BES2 anode biofilm at a relative abundance of 34% and 23%, respectively. In contrast, the BES1 and BES2 anode suspended biomass contained this phylotype at a relative abundance of 3% and undetected, respectively. Thus, the *Shigella* sp. phylotype appeared to prefer biofilm growth. Indeed, *Shigella dysenteriae* is known to produce lipopolysaccharides that assist with bacterial adhesion and may assist in biofilm formation (Qadri et al. 1994).

SRB typically belong to the *Deltaproteobacteria* class of *Proteobacteria*. When the BES1 and BES2 anode and cathode suspended biomass and biofilm biomass were analyzed, only the BES2 anode biofilm contained *Deltaproteobacteria*. Within this class, SRB phylotypes represented 32% of the *Deltaproteobacteria* and made up 1% of total Bacteria in the biofilm. The most abundant SRB phylotypes were closely related to *Desulfobulbus propionicus*, *Desulfovibrio* sp. and *Syntrophobacterales* spp., indicating

that sulfate reduction occurred in the anode biofilm. Thus, sulfur cycling likely occurred at the anode surface and within the biofilm instead of in the suspended biomass. Further study is needed to better understand bioanode sulfur cycling.

Table 7.6 – Bacterial OTUs with a Relative Abundance $\geq 1\%$

OTU Accession No. / Closest GenBank Relative	BES1		BES1		BES2		BES2	
	Anode		Cathode		Anode		Cathode	
	B ^a	S ^b	B	S	B	S	B	S
MF512155 / <i>Proteiniphilum acetatigenes</i>	0	0	0	11	T ^c	0	17	24
MF512156 / <i>Rhodopseudomonas palustris</i>	T	T	0	1	T	0	2	1
MF512157 / <i>Xanthobacter autotrophicus</i>	0	0	0	1	0	0	T	T
MF512158 / <i>Bacillus pseudofirmus</i>	0	0	0	0	0	0	0	0
MF512159 / <i>Syntrophus aciditrophicus</i>	0	0	0	0	3	0	T	0
MF512160 / <i>Achromobacter</i> sp.	27	69	0	25	18	14	10	21
MF512161 / <i>Mycobacterium</i> sp.	T	T	0	T	0	4	T	T
MF512162 / <i>Gordonia rubripertincta</i>	T	T	0	1	1	6	T	T
MF512163 / <i>Mycobacterium</i> sp.	T	T	0	T	0	1	1	T
MF512164 / <i>Geobacter sulfurreducens</i>	0	0	0	0	2	0	0	0
MF512165 / <i>Burkholderia lata</i>	0	0	0	0	T	0	T	0
MF512166 / <i>Citrobacter gillenii</i>	0	T	0	0	T	0	T	0
MF512167 / <i>Actinomyces georgiae</i>	0	T	0	T	T	0	1	T
MF512168 / <i>Thiomonas thermosulfata</i>	0	0	0	T	0	0	T	T
MF512169 / <i>Aminobacterium colombiense</i>	0	0	0	0	1	0	T	0
MF512170 / <i>Eubacterium acidaminophilum</i>	0	0	0	0	1	0	T	0
MF512171 / <i>Pseudomonas aeruginosa</i>	31	3	0	T	22	1	2	T
MF512172 / <i>Pseudomonas grimontii</i>	T	T	0	29	T	0	T	9
MF512173 / <i>Burkholderia tropica</i>	0	0	0	T	T	0	T	0
MF512174 / <i>Propionibacterium acnes</i>	0	0	0	0	2	0	0	0
MF512175 / <i>Leifsonia</i> sp.	0	T	0	0	T	T	0	0
MF512176 / <i>Adhaeribacter</i> sp.	0	0	0	0	1	0	T	0
MF512177 / <i>Proteiniphilum acetatigenes</i>	0	0	0	0	2	0	0	0
MF512178 / <i>Gordonia</i> sp.	0	T	0	T	0	0	T	T
MF512179 / <i>Ochrobactrum anthropi</i>	7	21	0	29	4	72	43	34
MF512180 / <i>Shigella dysenteriae</i>	34	3	0	T	23	0	13	T
MF512181 / <i>Magnetospirillum gryphiswaldense</i>	0	0	0	T	0	0	T	3
MF512182 / <i>Rhodococcus fascians</i>	0	0	0	T	0	0	T	T
MF512183 / <i>Propionicimonas paludicola</i>	0	0	0	0	1	0	0	0
MF512184 / <i>Rhodococcus</i> sp.	T	T	0	1	0	T	T	1
MF512185 / <i>Bacteroides</i> sp.	0	0	0	0	3	0	0	0
MF512186 / <i>Pseudomonas knackmussii</i>	T	T	0	T	T	T	1	T
MF512187 / <i>Adhaeribacter</i> sp.	0	0	0	0	1	0	T	0
KU597442 / <i>Proteiniphilum acetatigenes</i>	0	0	43	0	0	0	0	0
KU597446 / <i>Pseudomonas aeruginosa</i>	0	0	5	0	0	0	0	0
KU597447 / <i>Mycobacterium conceptionense</i>	0	0	5	0	0	0	0	0
KU597448 / <i>Sedimentibacter hydroxybenzoicus</i>	0	0	1	0	0	0	0	0
KU597449 / <i>Propionivibrio limicola</i>	0	0	3	0	0	0	0	0
KU597450 / <i>Sphingopyxis terrae</i>	0	0	2	0	0	0	0	0
KU597451 / <i>Citrobacter farmerii</i>	0	0	3	0	0	0	0	0
KU597452 / <i>Achromobacter</i> sp.	0	0	6	0	0	0	0	0
KU597453 / <i>Ochrobactrum anthropi</i>	0	0	3	0	0	0	0	0
KU597454 / <i>Thiomonas thermosulfata</i>	0	0	1	0	0	0	0	0
KU597455 / <i>Wolinella succinogenes</i>	0	0	3	0	0	0	0	0
KU597456 / <i>Arcobacter thereius</i>	0	0	1	0	0	0	0	0
KU597457 / <i>Neisseria animaloris</i>	0	0	3	0	0	0	0	0
KU597458 / <i>Pseudomonas cedrina</i>	0	0	1	0	0	0	0	0

^a Biofilm; ^b Suspended biomass; ^c Trace amounts (<1% relative abundance).

7.4 Summary

Methanogenic BESs, which convert CO_2 directly to CH_4 , are an innovative technology for anaerobic digester biogas upgrading. However, the effect on BES performance of H_2S , a common contaminant of anaerobic digester biogas, is unknown. Thus, the objectives of this study were to assess the effect of biocathode H_2S on BES performance at various initial H_2S concentrations (0-6% H_2S v/v), compare the flow of carbon between BESs with and without cathode H_2S addition, and assess the effect of cathode H_2S amendment on anode and cathode microbial communities. Although inhibitory to methanogenesis in anaerobic digestion, the addition of up to 3% H_2S initial concentration (v/v) to the cathode headspace resulted in improved CH_4 production and system current. The largest 3-d CH_4 production rates were observed at 2% and 3% initial H_2S (0.889 ± 0.091 and 0.889 ± 0.044 mmol/d, respectively), which represented a nearly two-fold increase over the CH_4 production rate prior to H_2S exposure. Using an abiotic setup, the transport of H_2S across the proton exchange membrane into the anode compartment and its subsequent oxidation was demonstrated. Thus, H_2S added to the cathode headspace travels to the anode, where it donates electrons and increases system current. However, the 3-d rate of CH_4 production declined above 3% H_2S , indicating an inhibitory effect at relatively large concentrations. At 3% initial H_2S , in addition to the increased CH_4 production rate, a carbon balance of the sulfide-exposed BES showed a faster acetate removal rate in the anode and a larger increase in biofilm biomass growth in the anode and cathode than observed in the non-sulfide BES. The microbial community of the suspended biomass and biofilm in the anode and cathode of the control (non-sulfide) BES and the sulfide-exposed BES were analyzed and compared. In all cathode samples, a phylotype

most closely related to *Methanobrevibacter arboriphilus* was predominant (99%-100% relative archaeal abundance); fewer total archaeal counts were found in the anode samples. The bacterial community analysis indicated enrichment of a phylotype similar to the exoelectrogen *Ochrobactrum anthropi* in both the anode and cathode of the sulfide-exposed BES, which may have also contributed to the observed increased current in the system. Further research is necessary to determine which sulfur-related processes may occur in the anode and cathode compartments of a methanogenic BES.

CHAPTER 8. EFFECT OF HYDROGEN SULFIDE AND ZERO VALENT IRON ON BES PERFORMANCE AND MICROBIAL COMMUNITIES

8.1 Introduction

Anaerobic digester biogas contains a mixture of CO₂, CH₄ and trace gases (e.g., H₂S, N₂, H₂) and typically undergoes biogas upgrading prior to certain downstream uses such as automobile fuel (Sun et al. 2015). Bioelectrochemical systems are a promising technology to convert biogas CO₂ to CH₄ and upgrade biogas without expensive consumables or large energy inputs. Moderate amounts (up to 3% v/v) of H₂S has been shown to improve biocathode CH₄ production by donating electrons to the anode following transport through the proton exchange membrane (see Section 7.3.3). Furthermore, the addition of H₂S to the cathode headspace resulted in changes in the microbial communities of both the cathode and anode (see Section 7.3.3).

A zero-valent iron- (ZVI-) amended biocathode was developed that utilized iron filings in the cathode as an additional source of H₂ for methanogenesis (see Section 6.2.2). Under anaerobic conditions, ZVI undergoes corrosion, resulting in the formation of H₂ ($\text{Fe}^0 + 2\text{H}^+ \rightleftharpoons \text{Fe}^{2+} + \text{H}_2$; $\Delta E_{\text{H}^0} = 0.026 \text{ V}$), which in turn may be used by methanogens for CO₂ reduction to CH₄ (Daniels et al. 1987, Kato 2016). Furthermore, the release of Fe²⁺ ions during anaerobic oxidation may lead to the precipitation of a redox-active substance that enhances CH₄ production (see Section 6.2.2). When biogas carries H₂S into the ZVI-amended cathode during biogas upgrading, it is possible that the Fe²⁺ released during

anaerobic oxidation may combine with sulfide to produce insoluble $\text{FeS}_{(s)}$, which may be removed through settling. Thus, a ZVI-amended biocathode may be capable of removing H_2S through precipitation. However, the effect of H_2S on the performance of a ZVI-amended biocathode has previously been unexplored.

Three mechanisms of CH_4 production have been proposed. The first mechanism is the production of H_2 at the cathode, which is then utilized by hydrogenotrophic methanogens to reduce CO_2 , as given in Equation 2.4 of Table 2.4 (Chapter 2). The reaction at the cathode surface is water electrolysis, represented by Equation 2.5 (Table 2.4, Chapter 2), and may be catalyzed by viable or non-viable biomass on the electrode (Yates et al. 2014). CH_4 production may also result from the transfer of electrons between the cathode and methanogens via electron shuttles, or mediators. Biocathode methanogenesis may also proceed through direct electron transfer from the cathode to the methanogens, resulting in the cathodic reaction given as Equation 2.6 (Table 2.4, Chapter 2) (Cheng et al. 2009, Costa et al. 2013, Lohner et al. 2014). However, it is currently unknown how much each mechanism contributes to biocathode methanogenesis when the cathode is amended with H_2S and/or ZVI.

Previous work shows that the application of ZVI to a biocathode changes the cathode biofilm bacterial community. However, the effect of ZVI on the microbial communities of the anode biofilm and suspended biomass in both anode and cathode has been unexplored. Furthermore, while H_2S is known to affect the microbial communities of both anode and cathode, its effect on the communities in a BES with a ZVI-amended biocathode is unknown. By examining the changes to the microbial communities associated with various environmental conditions, the processes occurring in the BES

anode and cathode may be better understood. Therefore, the objective of this study was to: i) evaluate the effect of biocathode H₂S on the performance of a BES with a ZVI-amended biocathode; ii) probe the electron transfer mechanisms involved in biocathode processes in H₂S- and ZVI-amended biocathodes; and iii) assess the effect of biofilm formation, biocathode H₂S, and biocathode ZVI on the microbial communities of the anode and cathode biofilm and suspended biomass.

8.2 Materials and Methods

8.2.1 Effect of H₂S on BES Performance with a ZVI-Amended Biocathode

Four BESs were developed as described in Sections 5.2.1, 6.2.1, 7.2.3 with the parameters given in Table 8.1. Each BES bioanode was filled with 250 mL anolyte media (see Section 4.2.1), flushed with N₂ and fed with sodium acetate to a concentration of 1,500 mg COD/L at the start of each 3-d feeding cycle. Each biocathode was filled with 250 mL catholyte media (see Section 4.2.1) and fed with 100% CO₂ to 1.6 atm (absolute pressure). The biocathodes of BES2 and BES3 were supplemented with 3% H₂S (v/v) and 1 g/L ZVI, respectively, at the beginning of each feeding cycle. BES4 was supplemented with both 3% H₂S and 1 g/L ZVI. Gas pressure and gas composition measurements were taken as described in Sections 3.1.6 and 3.1.7, respectively. Each cathode was maintained at -0.8 V vs. SHE using a Gamry Interface 1000 potentiostat (Warminster, PA).

Table 8.1 - BES Setups

BES	Cathode H ₂ S (3% v/v)	Cathode ZVI (1 g/L)
BES1	- ^a	-
BES2	+ ^b	-
BES3	-	+
BES4	+	+

^a Not Added. ^b Added.

8.2.1 Electron Transfer Mechanisms

The electron transfer mechanisms in BES1-4 were explored by observing the H₂ production rate while the biocathode was deprived of CO₂ by using CO₂-free catholyte media (see Section 4.2.1) and the headspace was flushed with N₂. Without CO₂ available as an electron acceptor, the cathodic reaction must shift to water electrolysis, producing H₂ as given by Equation 2.5 (Table 2.4, Chapter 2). This reaction may be catalyzed by cell debris and biomass present on the electrode, whether or not the biomass is active (Yates et al. 2014). Thus, the measurement of H₂ evolution under CO₂-deprived conditions reflects the rate of hydrogen-mediated methanogenesis alone. H₂ evolution was measured over 2 h to minimize disruptive effects to the biofilm. Next, CO₂ was added by flushing the biocathode with CO₂ and pressurizing to 1.6 atm (absolute pressure). The initial 3-d CH₄ production rates, which were linear for each biocathode, were then compared with the H₂ production rate in terms of CH₄ equivalents, assuming that 100% of the produced H₂ was converted to CH₄ according to Equation 2.4 (Table 2.4, Chapter 2).

In each BES, the bioanode was filled with 250 mL anolyte media (see Section 4.2.1), flushed with N₂ and fed with sodium acetate to 1,500 mg COD/L. Each BES was incubated under continuous magnetic mixing at room temperature (22±2°C) for a total of

7 d. Gas pressure and gas composition measurements were taken as described in Sections 3.1.6 and 3.1.7, respectively. Each cathode was maintained at -0.8 V vs. SHE.

8.2.2 *Microbial Community Analysis*

Bacterial and archaeal DNA was extracted from the suspended growth cultures and biocathode felts using the UltraClean Soil DNA Kit and PowerSoil DNA Isolation Kit (Mo Bio Laboratories, Carlsbad, CA), respectively, according to the manufacturer's instructions. Following extraction, all DNA was quantified using Nanodrop 3300 (Thermo Scientific, Wilmington, DE) and stored at -20°C until sequencing was performed. Bacterial DNA was amplified using the 16S rRNA gene primers 28F (5'-GAGTTTGATCCTGGCTCAG-3') and 388R (5'-TGCTGCCTCCCGTAGGAGT-3'). Archaeal DNA was amplified using the 16S rRNA gene primers 519wF (5'-CAGCMGCCGCGGTAA-3') and 1017R (5'-GGCCATGCACCCWCCTCTC). DNA sequencing and analysis was performed as described in Section 5.2.3. Unique sequences have been deposited in GenBank (NCBI) with accession numbers MF512155- MF512192. Principal Coordinate Analysis (PCA) was then conducted and plotted in 2-D with QIIME 1.9.0, and 3-D with Emperor. Redundancy analysis and canonical correspondence analysis (CCA) were conducted using R (Team 2014) and vegan 2.4-1 community ecology package (Oksanen et al. 2016).

8.3 Results and Discussion

8.3.1 *Effect of H₂S on BES Performance with a ZVI-Amended Biocathode*

To evaluate how cathode H₂S would affect the performance of a ZVI-amended biocathode, four BESs were developed with the parameters described in Table 8.1. The BES4 cathode biofilm was developed initially as a ZVI-amended biocathode. Over the course of a typical 3-d feeding cycle prior to H₂S addition, the BES4 biocathode removed 88.9% of the initial CO₂, with 86.9% removal within 1 d. In contrast, during a 3-d feeding cycle with 3% v/v H₂S initially added to the biocathode headspace, 100% CO₂ removal was achieved, with 99.7% removal within 1 d. Cathode H₂S may be transported across the permeable exchange membrane to the anode, where it can donate electrons, increase current and, in turn, increase biocathode CH₄ production (see Sections 7.3.2 and 7.3.3). Therefore, the increased CO₂ removal observed following H₂S addition is likely due to increased conversion of CO₂ to CH₄. Indeed, a significantly higher CH₄ production was observed following H₂S addition (Figure 8.1B). Prior to H₂S addition, the 3-d mean rate of CH₄ production was 0.342±0.018 mmol/d (R²=0.977). With the addition of 3% H₂S, the 3-d mean rate of CH₄ production increased by 61% to 0.870±0.057 mmol/d (R²=0.960). In addition, biocathode H₂ production was significantly greater during the first day of the feeding cycle after H₂S was added (Figure 8.1A). However, between days 1 and 3 of the feeding cycle, the H₂ in the H₂S-amended biocathode headspace declined until it was nearly the same as the final (day 3) H₂ in the biocathode prior to H₂S addition (Figure 8.1A). The additional H₂ observed in the middle of the cycle when H₂S was added to the cathode could be due to increased water electrolysis at the cathode due to increased current, or from the acceleration of ZVI corrosion. H₂S is known to accelerate the corrosion of iron under most

conditions (Ma et al. 2000). Therefore, the addition of H₂S to the biocathode headspace of the ZVI-amended biocathode increased the availability of electron equivalents in the biocathode, stimulating increased methanogenesis.

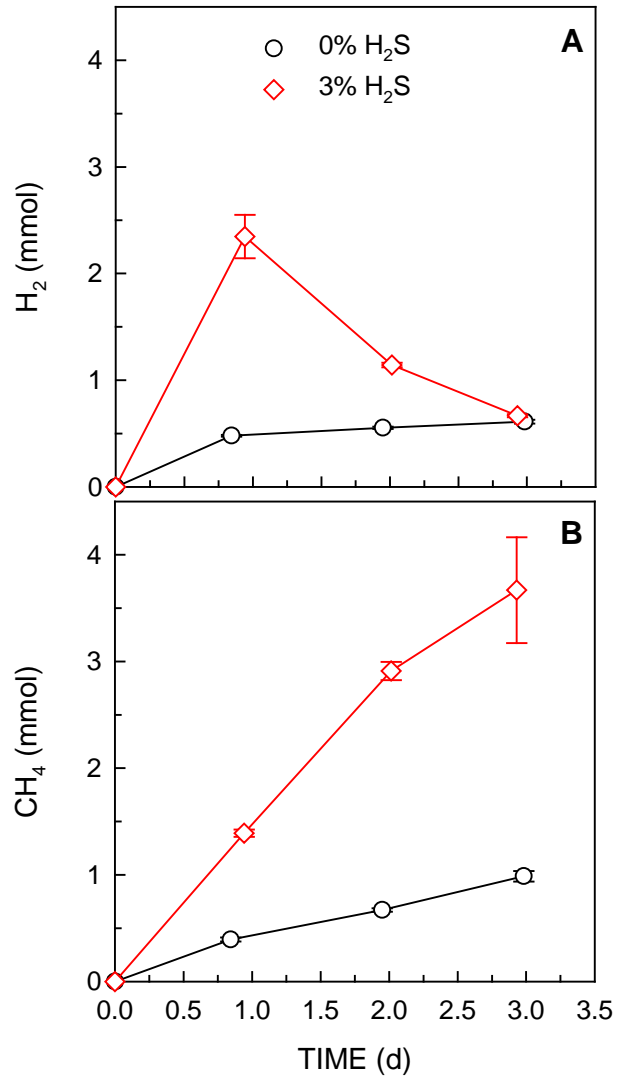


Figure 8.1 - Time course of biocathode headspace H₂ (A) and CH₄ (B) in BES4 during a 3-day feeding cycle before and after 3% v/v H₂S addition. Error bars represent mean \pm standard deviation; $n = 3$.

In the BES4 catholyte, the concentration of Fe^{2+} was significantly lower than in the BES3 catholyte throughout the feeding cycle. The lower catholyte Fe^{2+} concentration in BES4 may be due to the formation of iron sulfides. Indeed, the BES4 biocathode removed H_2S from the gas to below the odor threshold ($< 0.01\text{--}1.54$ ppm). In contrast, the BES2 biocathode removed H_2S to below the detection limit ($<1\%$ H_2S v/v) but not below the odor threshold. The additional removal of H_2S in the BES4 biocathode was likely due to the formation of iron sulfides. The relatively stable concentration of Fe^{2+} in the BES4 catholyte, as compared to BES3, may represent the solubility limit before iron sulfide precipitation occurs.

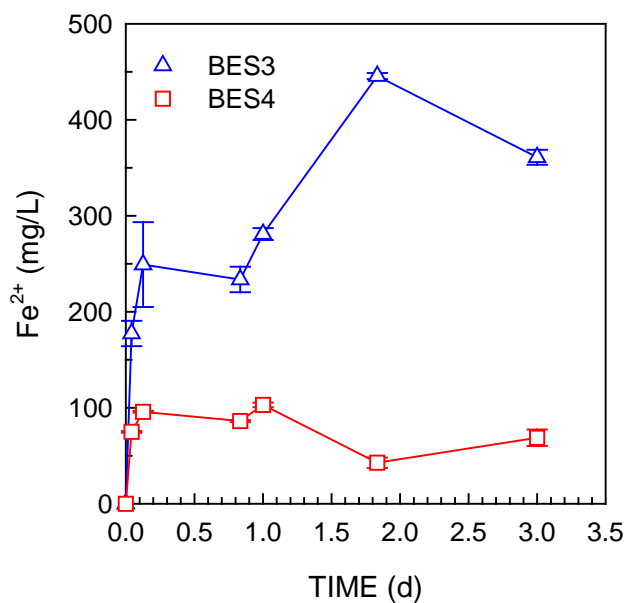


Figure 8.2 - Time course of Fe^{2+} concentration in the BES3 and BES3 catholyte.

The performance of the BES4 biocathode was then compared with the performance of the biocathodes in BES1, BES2 and BES3 (Figure 8.3). The BES4 biocathode removed 100% of the CO_2 over the course of a typical 3-d feeding cycle (Figure 8.3). BES3, which

had a H₂S-amended biocathode, removed 97% of the total CO₂ in the 3-d cycle. In contrast, the ZVI-amended biocathode in BES3 and the control biocathode in BES1 removed only 90% and 87% , respectively, of the initial cathode CO₂ over the course of the feeding cycle. These results suggest that, in a biocathode, reducing equivalents in the form of cathode-provided electrons (e.g., from H₂S oxidation at the anode) can increase CO₂ removal to a larger extent than reducing equivalents in the form of H₂ from ZVI corrosion. However, further study is needed to determine if the type of reducing equivalents affect CO₂ removal.

The mean 3-d CH₄ production for the BES4 biocathode was 0.870±0.057 mmol/d (R²=0.960), which was 663% higher than the mean CH₄ production rate in the BES1 biocathode (0.114±0.002 mmol/d; R²=0.997). The BES2 H₂S-amended biocathode produced CH₄ at a mean rate (0.348±0.008 mmol/d; R²=0.995) that was 205% higher than the BES1 biocathode. The mean CH₄ production rate in the ZVI-amended biocathode (0.207±0.015 mmol/d; R²=0.964) in BES3 was 81% higher than the rate in the BES1 biocathode. Therefore, the addition of H₂S appeared to have a larger effect on the increase of CH₄ production than the addition of ZVI. However, the combination of ZVI and H₂S in the biocathode led to the production of the largest amount of total CH₄ and the fastest rate of CH₄ generation of all the biocathodes in this study.

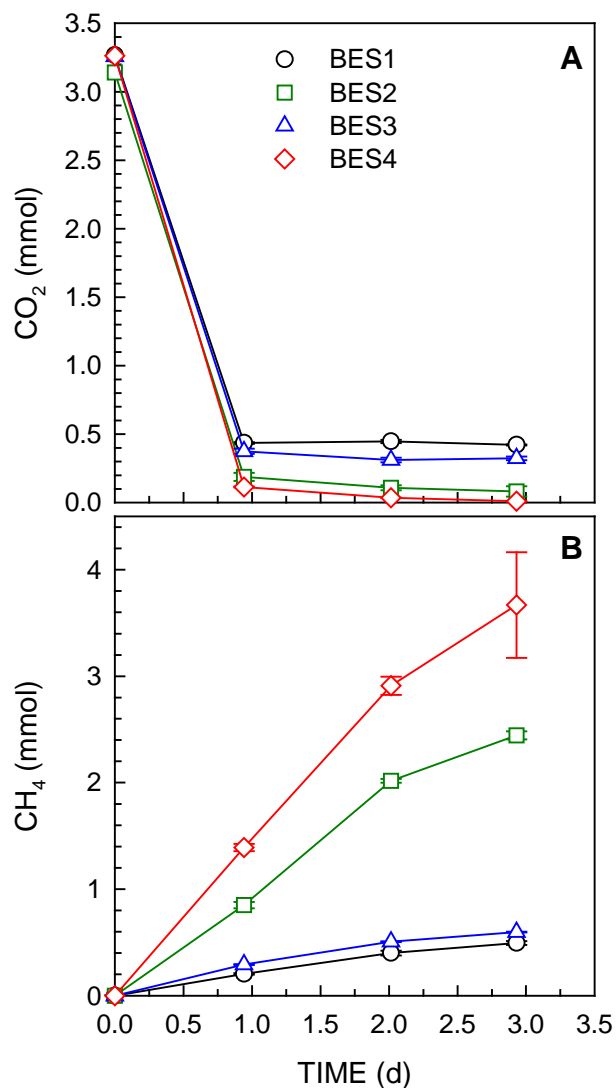


Figure 8.3 - Time course of biocathode headspace CO₂ (A) and CH₄ (B) in BES1-BES4 during a 3-day feeding cycle. Error bars represent mean \pm standard deviation; $n = 3$.

8.3.2 *Electron Transfer Mechanisms*

To better understand the electron transfer mechanisms that take place in the biocathodes of BES1-BES4, several tests were used to determine where electron equivalents for CH₄ originated from. First, to determine the abiotic contribution of ZVI

corrosion, an abiotic (i.e., uninoculated) BES was set up, a cathode potential of -0.8 V (vs. SHE) was applied and H₂ production was measured over time without ZVI and with 1 g/L ZVI (Table 8.2). The abiotic biocathode without ZVI produced H₂ at a mean rate of 0.30±0.01 mmol H₂/d. When ZVI was added, the abiotic biocathode produced H₂ at a mean rate of 2.01±0.04 mmol H₂/d. Thus, without the presence of biofilm in a ZVI-amended cathode, 15% of the total H₂ produced was due to water electrolysis at the cathode and 85% was produced by the anaerobic corrosion of ZVI.

Next, to understand how biofilm affected cathode H₂ evolution, a test was performed on BES1-4 for 2 hr following a feeding, in which each biocathode was deprived of CO₂ and the rate of H₂ evolution was quantified (Figure 8.4A; Table 8.2). After the test was completed, the biocathodes were flushed with CO₂ and the CH₄ production rate was measured. By comparing the actual CH₄ production with the theoretical CH₄ equivalents of H₂ produced in the H₂-evolution test (assuming the stoichiometric ratio of 4 mol H₂:1 mol CH₄), the fraction of CH₄ produced by H₂-mediated methanogenesis may be estimated.

During the H₂-evolution test, the rate of H₂ evolution in the BES1 biocathode was 23% higher than the rate of H₂ evolution in the abiotic biocathode, indicating the biofilm catalyzed the water electrolysis reaction at the cathode. Indeed, a study by Yates et al. (2014) showed that biomass and cell debris may catalyze water electrolysis. The rate of H₂ evolution in the BES2 biocathode was 335% higher than the rate in the BES1 biocathode, indicating that H₂S had a significant effect on biocathode output. Although the abiotic BES with a ZVI-amended biocathode had a significantly higher rate of H₂ production than the abiotic BES without ZVI, the BES3 ZVI-amended biocathode produced H₂ at a rate that was 30% lower than the rate in the BES1 biocathode. One possible reason for this

observation may be that the mature biofilm had accumulated a precipitate coating from previous feedings with ZVI (see Section 6.3.6), which may have created mass transfer limitations that slowed the water electrolysis reaction. The biocathode of BES4 produced H₂ at a rate 591% higher than the rate in the BES1 biocathode, and 59% higher than the rate in the BES2 biocathode. Therefore, the combination of ZVI and H₂S in the biocathode increased the rate of H₂ evolution over the rate of H₂ evolution with either ZVI or H₂S alone.

Table 8.2 - Mean Biocathode H₂ and CH₄ Production Rates

BES	H ₂ -production rate ^a (mmol H ₂ /d)	H ₂ -production CH ₄ - equivalent rate ^b (mmol CH ₄ /d)	CH ₄ -production rate ^c (mmol CH ₄ /d)
Abiotic BES	0.30 ± 0.01 R ² = 0.999	0.075 ± 0.002	None
Abiotic BES with ZVI	2.01±0.04 R ² = 0.997	0.503 ± 0.010	None
BES1	0.37 ± 0.02 R ² = 0.959	0.093 ± 0.006	0.114 ± 0.002 R ² = 0.997
BES2	1.63 ± 0.12 R ² = 0.937	0.405 ± 0.030	0.348 ± 0.008 R ² = 0.995
BES3	0.26 ± 0.01 R ² = 0.968	0.065 ± 0.003	0.207 ± 0.015 R ² = 0.964
BES4	2.57 ± 0.10 R ² = 0.981	0.643 ± 0.025	0.870 ± 0.057 R ² = 0.960

^a Mean rate over two hours, with standard deviation; *n* =6.

^b Equivalent CH₄ estimated based on H₂ produced at the biocathode without CO₂ present, and the stoichiometric ratio of 4 mol H₂:1 mol CH₄.

^c Mean rate over 3 d, with standard deviation; *n* =4.

Once CO₂ was added to the biocathodes following the H₂-evolution test, CH₄ immediately began to be produced (Figure 8.4B). As previously observed, the highest rate of CH₄ production in all cases occurred within 3 days of the 7-d feeding cycle.

Therefore, mean rates of CH₄ production were compared over the first 3 d following CO₂ feeding (Table 8.2). The mean CH₄ production rate in the BES3 cathode was 0.093 mmol/d higher than the mean CH₄ production rate in the BES1 cathode, indicating the effect of ZVI alone on the biocathode. If the effect is applied to the BES2 biocathode, which was exposed to H₂S, the total predicted CH₄ production rate for the BES4 biocathode is 0.441 mmol/d. However, the BES4 biocathode actually produced 0.870 mmol/d, indicating that the H₂S and ZVI effect on biocathode performance is not an additive effect, but synergistic. In other words, the CH₄ production rate in the BES4 biocathode is higher than the predicted rate if the ZVI and H₂S affected the biocathode independently. Thus, the CH₄ rate measurements suggest that the H₂S and ZVI interact to improve CH₄ production. However, the elucidation of mechanism(s) responsible for improved CH₄ production were beyond the scope of this study.

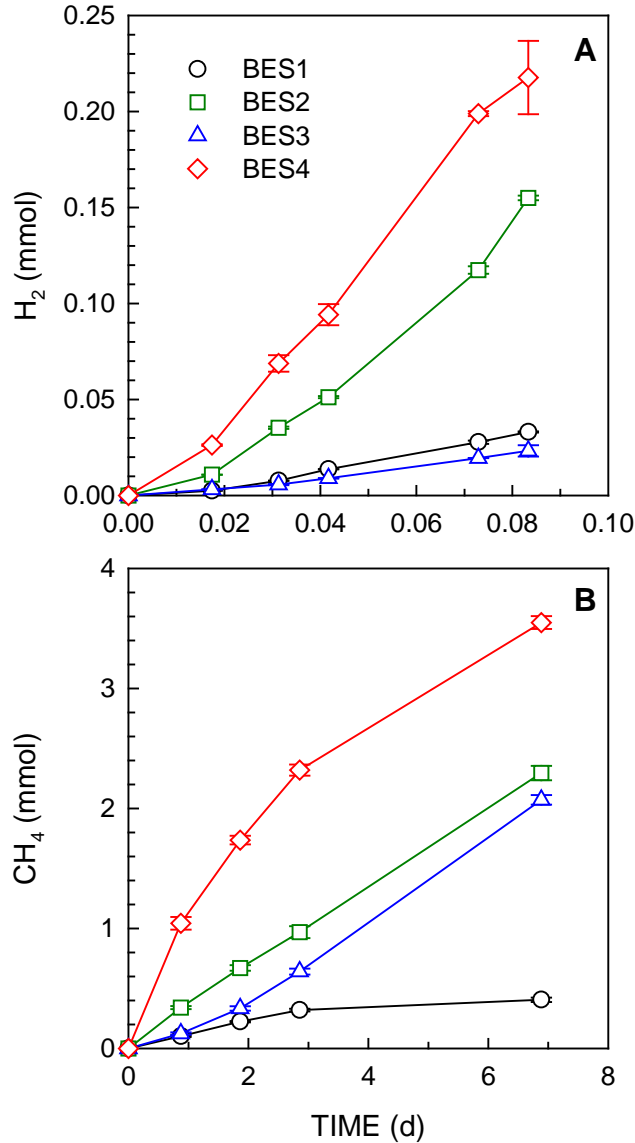


Figure 8.4 - Time course of BES1, BES2, BES3 and BES4 biocathode H₂ production (A) and CH₄ production (B). Error bars represent mean \pm standard deviation; $n = 3$.

The rate of biocathode H₂ production, as equivalents of CH₄ (assuming the stoichiometric ratio of 4 mol H₂:1 mol CH₄), was compared to the actual rate of CH₄ production by the biocathodes (Figure 8.5). In the BES1 biocathode, the H₂-mediated methanogenesis was estimated to represent 82% of the total CH₄ produced. The remainder of the CH₄ (18%) was produced through one or a combination of the following

mechanisms: direct electron transfer from the cathode, non-H₂ mediated methanogenesis, and methanogenesis mediated by H₂ produced from active cells that are not active under CO₂-limited conditions. In the BES2 biocathode, the production rate of H₂ as CH₄ equivalents was 14% lower than the actual rate of CH₄ production. It is possible that the BES2 biocathode experienced a larger loss of CH₄ to the bioanode than the other biocathodes due to anaerobic oxidation of CH₄ in the anode, which would create a larger CH₄ concentration gradient across the membrane and increase CH₄ transport from cathode to anode. The anaerobic oxidation of methane coupled with current production at an anode was recently described in a study in which the anode biofilm was dominated by *Methanobacterium* (67% of Archaea) and *Geobacter* (38% of Bacteria) (Gao et al. 2017). Indeed, the anode biofilm in BES2 was enriched in both *Methanobacterium* and *Geobacter*, as discussed further in Section 8.3.3. If significant amounts of CH₄ in the BES2 biocathode were lost to the anaerobic oxidation of CH₄ at the anode, the total CH₄ production rate might be lower than the H₂ production rate as CH₄ equivalents. Another possibility is that the efficiency of CH₄ production at the cathode was lower than the efficiency of H₂ production. However, when the cathode capture efficiency (CCE) was measured for each biocathode, the CCE was consistently lower for the water electrolysis reaction than for the CH₄ production reaction (Table 8.3). Therefore, the transport of H₂S to the anode and its effect on the anode microbial community might result in the loss of CH₄ to anaerobic oxidation, as discussed further in Sections 8.3.3 and 9.3.2.

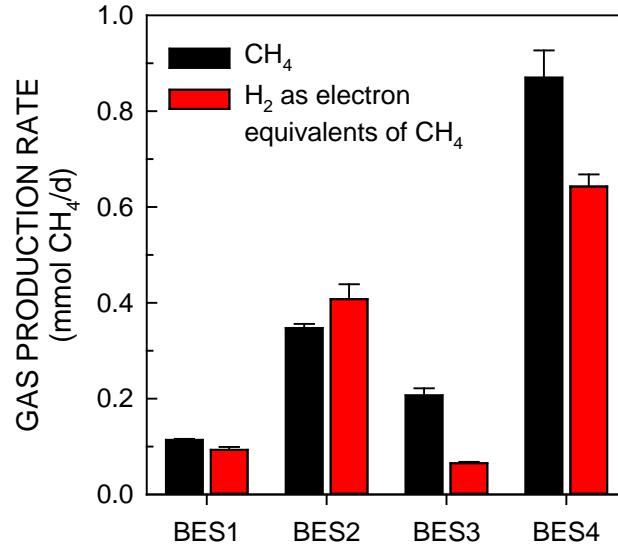


Figure 8.5 - Comparison of Biocathode CH₄ Production Rate with H₂ Production Rate as Electron Equivalents of CH₄ for BES1-BES4. Error bars represent mean \pm standard deviation; $n = 3$.

Table 8.3 - Cathode Capture Efficiency (CCE) During H₂ and CH₄ Production

BES	H ₂ -production CCE (%)	CH ₄ -production CCE (%)
BES1	53.1	99.8
BES2	52.7	89.0
BES3	118.2	305.6
BES4	40.2	1,424.0

8.3.3 Microbial Community Analysis

To better understand the effect of biofilm formation, ZVI exposure and H₂S exposure on the microbial communities in the anode and cathode, 16S rRNA gene analysis was conducted on the suspended and biofilm communities in the anode and cathode of BES1-4. The relative abundance of the most abundant ($\geq 1\%$ relative abundance) bacterial and archaeal OTUs were compared across all samples.

In all BESs, the archaeal community of the biocathode biofilm and suspended biomass was dominated (99-100% of all Archaea) by a single phylotype most closely related to *Methanobrevibacter arboriphilus* (Table 8.6 and Table 8.7). As previously discussed in Section 5.3.3, *M. arboriphilus* is a hydrogenotrophic methanogen that has been observed in other methanogenic biocathodes (Cheng et al. 2009, Siegert et al. 2014, Siegert et al. 2015, Zhen et al. 2015). *M. arboriphilus* was also identified in the anode biofilm of BES2, BES3 and BES4 at 72%, 95% and 99% relative abundance, respectively. However, in the anode biofilm of BES1, the *M. arboriphilus* phylotype only represented 2% of the total Archaea, with the majority (91%) of archaeal OTUs unclassified. Thus, the conditions in the cathode of each BES may affect the microbial community in each respective anode because of the potential for gas and ion transport between the anode and cathode. *Methanobacterium formicicum* was identified in trace amounts in the cathode biofilm and/or suspended biomass of each BES. *M. formicicum* is a hydrogenotrophic methanogen that was enriched when microbial electrolysis was applied to an anaerobic digester (Lee et al. 2017), indicating a possible role in biocathode methanogenesis. Although *M. formicicum* was detected in the anode biofilm and suspended biomass of the BESs (Table 8.6), the archaeal OTU counts in the anode samples were low or failed to

amplify, with the exception of the BES2 biofilm (Table 8.4). Acetoclastic methanogens were not detected in any of the anode samples, indicating that CH₄ in the anode chambers was likely due to transport across the membrane from the cathode, or from hydrogenotrophic methanogenesis using transported H₂ from the cathode. Along with containing the largest number of archaeal OTUs of all anode samples, the BES2 anode biofilm was also the only anode sample to contain *Geobacter sp.* (Table 8.8), which has been implicated in anaerobic CH₄ oxidation when coupled with *Methanobacterium spp.* (Gao et al. 2017). Thus, it is possible that the enrichment of *M. formicicum* on the BES2 anode biofilm could have been due to cooperation with *Geobacter sp.* in anaerobic CH₄ oxidation.

Table 8.4 - OTU Counts in Anode and Cathode Biofilm and Suspended Biomass Samples from BES1 – BES4

BES	Archaeal OTUs				Bacterial OTUs			
	Anode		Cathode		Anode		Cathode	
	B ^a	S ^b	B ^a	S ^b	B ^a	S ^b	B ^a	S ^b
BES1	657	12,384	24,258	33,318	20,094	21,353	133,547	18,245
BES2	17,775	F ^c	22,524	22,390	14,336	12,042	24,328	21,605
BES3	1,724	660	23,452	21,257	21,285	18,839	42,948	24,936
BES4	8,594	F ^c	20,815	24,184	17,938	23,163	23,631	20,047

^a Biofilm.

^b Suspended biomass.

^c Not detected.

The cathode bacterial community analysis indicated shifts in composition due to the various cathode conditions (Table 8.7). Two of the four most abundant phylotypes (*Achromobacter sp.* and *Ochrobactrum anthropi*) across all cathode samples were also among the most abundant phylotypes identified in the anode samples (Table 8.7 and Table

8.8). *O. anthropi* is a known exoelectrogen that has previously been identified in anode biofilm (Jayashree et al. 2014, Kokko et al. 2015) and *Achromobacter* sp. has also been identified in the anodes of microbial fuel cells (Yousaf et al. 2017, Yu et al. 2012, Zhang et al. 2011). The *O. anthropi* phylotype was enriched in the cathode biofilm of BES2, BES3 and BES4, relative to BES1. Although the *O. anthropi* phylotype only represented 3% of all Bacteria in the BES1 cathode biofilm, it represented 29% of all suspended biomass Bacteria. The *O. anthropi* phylotype was also enriched in the cathode suspended biomass of BES2 and BES3, relative to BES1; a similar relative abundance was observed in the BES4 suspended biomass as in the BES1 suspended biomass. As discussed in Section 5.3.3, exoelectrogens may be involved in recycling cell debris, releasing electron equivalents back to the methanogenic biofilm, improving CH₄ production. Indeed, the largest relative abundance of the *O. anthropi* phylotype was observed in the most productive biocathode (BES4), where it represented 66% of all Bacteria. The *O. anthropi* phylotype was also abundant in all cathode suspended biomass samples. Thus, exoelectrogens may serve an important function in a methanogenic biocathode.

The Shannon diversity index of the cathode bacterial communities was slightly lower in the biofilm of BES2 and BES3 than in the BES1 cathode biofilm (Table 8.9). However, the diversity index in the BES4 cathode biofilm (1.44) was significantly lower than in BES1 (2.68). Thus, the amendment of both ZVI and H₂S to the cathode reduced the biofilm bacterial diversity. In contrast, the BES4 suspended biomass bacterial diversity index (1.88) was similar to the BES1 suspended biomass diversity index (1.73) (Table 8.9), indicating the combined ZVI and H₂S had less of an effect on the suspended biomass bacterial diversity than on the biofilm bacterial diversity.

The anode bacterial communities were also compared for each sample (Table 8.8). Four phylotypes most closely related to *O. anthropi*, *Achromobacter* sp., *Pseudomonas aeruginosa* and *Shigella dysenteriae* were prominent components of the anode biofilm and suspended biomass. *O. anthropi* are known exoelectrogens capable of generating current at an anode (Jayashree et al. 2014, Kokko et al. 2015, Zuo et al. 2008). Interestingly, the suspended biomass had a larger relative abundance of the *O. anthropi* phylotype than the biofilm biomass in all anode samples (Table 8.8), indicating a role for exoelectrogens in the suspended biomass of the anodes. Thus, mediated electron transfer likely occurs in the anode. Indeed, *P. aeruginosa* is known to produce phenazines and other extracellular compounds that may be used as redox mediators in the anode of a microbial fuel cell (Pham et al. 2008). *Achromobacter* sp. has also been identified in the anodes of microbial fuel cells along with *O. anthropi*, suggesting that *Achromobacter* sp. may also play a role in current generation (Yousaf et al. 2017, Yu et al. 2012, Zhang et al. 2011). In the BES1 and BES3 anodes, the *Achromobacter* sp. phylotype was also more abundant in the suspended biomass than in the biofilm. However, the relative abundance of the *Achromobacter* sp. phylotype was lower in the anodes exposed to sulfide (BES2 and BES4), suggesting a possible inhibitory role of sulfide. Indeed, sulfide is known to have an inhibitory effect on some Bacteria (Chen et al. 2008).

Unlike the *O. anthropi* and *Achromobacter* sp. phylotypes, the *P. aeruginosa* phylotype was predominantly observed in the biofilm. *P. aeruginosa* produces extracellular polysaccharides and biosurfactants that assist in biofilm formation (Davey et al. 2003, Sauer et al. 2002). The *P. aeruginosa* phylotype represented 31%, 22% and 46% of all Bacteria in the BES1, BES2 and BES3 anode biofilms, respectively. However, the

phylotype was not detected in the anode biofilm of BES4. It is possible that the complexation of iron with sulfide in BES4 decreased the concentration of iron in both the anode and cathode, negatively affecting the growth of *P. aeruginosa* biofilm. Iron is used as a signal by *P. aeruginosa* for quorum sensing and biofilm development (Banin et al. 2005, Bollinger et al. 2001). A recent study found that production of the exopolysaccharide Psl, a biofilm matrix component produced by *P. aeruginosa*, was stimulated by iron, leading to increased biofilm formation (Yu et al. 2016). Furthermore, Psl is the only known exopolysaccharide that can bind with both ferrous (Fe^{2+}) and ferric (Fe^{3+}) ions, although it has a stronger affinity for ferrous ions (Yu et al. 2016). Indeed, the ZVI-amended BES bioanode had the largest relative abundance of the *P. aeruginosa* phylotype. Although ZVI was not added to the anode, small amounts of Fe^{2+} from the cathode may have been transported across the membrane to the anode. In an abiotic BES with an initial 1 g/L ZVI in the cathode, Fe^{2+} concentrations in the anode increased to 7 mg Fe^{2+} /L over the course of 3 d, indicating that Fe^{2+} may be slowly transported from the cathode to the anode through the proton exchange membrane. Other divalent cations have also been shown to be transported across a Nafion 117 proton exchange membrane (Chae et al. 2008, Chaudhury et al. 2015). However, it is not clear to what extent this transport may occur in a biological system.

A phylotype most closely related to *Shigella dysenteriae* represented 34%, 23%, 7% and 74% of all Bacteria in the BES1, BES2, BES3 and BES4 anode biofilms, respectively. Thus, the application of ZVI to the biocathode appeared to reduce biofilm *S. dysenteriae*. However, the application of both ZVI and H_2S to the biocathode increased the relative abundance of the *S. dysenteriae* phylotype in both the biofilm and the suspended

growth. *S. dysenteriae* causes bacillary dysentery in humans but has also been found in the anodes of microbial fuel cells (Kokko et al. 2015, Lenin et al. 2013). The role of *S. dysenteriae* in anodic systems is not clear but the abundant presence of this phylotype suggests a role in exoelectrogenesis.

Although one of the more well-described exoelectrogens, the phylotype related to *Geobacter sulfurreducens* was only detected in the BES2 anode biofilm. *G. sulfurreducens* is a bacterium capable of utilizing acetate as an electron donor and an anode surface or elemental sulfur as an electron acceptor (Caccavo et al. 1994, Logan 2009). However, *G. sulfurreducens* is not able to use sulfate, sulfite, or thiosulfate as electron acceptors with acetate as an electron donor (Caccavo et al. 1994). Thus, the growth of *G. sulfurreducens* on the BES2 anode biofilm may have been stimulated by the transport of H₂S from the cathode to anode, where it can be oxidized to elemental sulfur (Sun et al. 2009), thus providing an alternate electron acceptor for *G. sulfurreducens* besides the anode surface. Additionally, *G. sulfurreducens* may be involved in the anaerobic oxidation of CH₄ at the anode, which was recently described in an anode biofilm dominated by *Methanobacterium* (67% of Archaea) and *Geobacter* (38% of Bacteria) (Gao et al. 2017). Indeed, the anode biofilm in BES2 was enriched in both *Methanobacterium* and *Geobacter*. *Methanobacterium* represented 23% of total Archaea in the BES2 anode biofilm (Table 8.6) but only represented 5% and 1% of Archaea in the BES1 and BES3 anode biofilm. While the *G. sulfurreducens* phylotype represented only 2% of the BES2 biofilm Bacteria, it was not detected in any other anode sample. Therefore, as CH₄ may be transported across the membrane from the cathode to the anode, some CH₄ oxidation may occur at the anode,

thus contributing to current generation. In these ways, exoelectrogenic *Geobacter* species may have contributed to the increased current observed in BES2 relative to the control.

Table 8.5 - Closest GenBank Relatives and Archaeal Relative Abundance for Defined OTUs in Cathode Biofilm and Suspended Biomass

OTU Accession No. / Closest GenBank Match	BES1		BES2		BES3		BES4	
	B ^a	S ^b	B	S	B	S	B	S
MF512188, MF512192 / <i>Methanobacterium formicicum</i>	ND ^c	1	T ^d	T	ND	T	T	T
MF512189, KU597459 / <i>Methanobrevibacter arboriphilus</i>	100	99	100	100	100	100	100	100

^a Biofilm.

^b Suspended biomass.

^c Not detected.

^d Trace amounts ($\leq 1\%$ relative abundance).

Table 8.6 - Closest GenBank Relatives and Archaeal Relative Abundance for Defined OTUs in Anode Biofilm and Suspended Biomass

OTU Accession No. / Closest GenBank Match	BES1		BES2		BES3		BES4	
	B ^a	S ^b	B	S	B	S	B	S
MF512188, MF512192 / <i>Methanobacterium formicicum</i>	7	90	23	F ^c	1	ND ^d	1	F
MF512189, KU597459 / <i>Methanobrevibacter arboriphilus</i>	2	6	72	F	95	11	99	F
MF512190 / <i>Methanothermobacter marburgensis</i>	ND	ND	1	F	ND	ND	ND	F
MF512191 / <i>Methanosaeta concilii</i>	ND	ND	3	F	1	ND	ND	F

^a Biofilm.

^b Suspended biomass.

^c Failed; archaeal OTU counts were too low for analysis.

^d Not detected.

Table 8.7 - Closest GenBank Relatives and Bacterial Relative Abundance for Defined OTUs in Cathode Biofilm and Suspended Biomass

OTU Accession No.s / Closest GenBank Match	BES1		BES2		BES3		BES4	
	B ^a	S ^b	B	S	B	S	B	S
MF512155, MF512177, KU597442, KX759058, KX759061 / <i>Proteiniphilum acetatigenes</i>	43	11	17	24	4	2	3	T
MF512156 / <i>Rhodopseudomonas palustris</i>	ND ^c	1	2	1	ND	5	T	T
MF512157 / <i>Xanthobacter autotrophicus</i>	ND	1	T	T	ND	2	T	ND
MF512158 / <i>Bacillus pseudofirmus</i>	ND	ND	ND	ND	ND	ND	2	2
MF512159 / <i>Syntrophus aciditrophicus</i>	ND	ND	T	ND	ND	ND	T	ND
MF512160, KX759062 / <i>Achromobacter sp.</i>	ND	25	10	21	12	5	18	27
MF512161, MF512163 / <i>Mycobacterium sp.</i>	ND	T	1	T	ND	1	T	T
MF512162 / <i>Gordonia rubripertincta</i>	ND	1	T	T	ND	3	T	T
MF512165 / <i>Burkholderia lata</i>	ND	ND	T	ND	ND	ND	ND	ND
MF512166 / <i>Citrobacter gillenii</i>	ND	ND	T	ND	ND	ND	T	2
MF512167 / <i>Actinomyces georgiae</i>	ND	T	1	T	ND	T	1	T
MF512168 / <i>Thiomonas thermosulfata</i>	ND	T	T	T	ND	1	T	T
MF512169 / <i>Aminobacterium colombiense</i>	ND	ND	T	ND	ND	ND	T	ND
MF512170 / <i>Eubacterium acidaminophilum</i>	ND	ND	T	ND	ND	ND	T	ND
MF512171, KU597446, / <i>Pseudomonas aeruginosa</i>	5	T	2	T	ND	T	T	T
MF512172, KX759082 / <i>Pseudomonas grimontii</i>	ND	29	T	9	21	3	T	ND
MF512173 / <i>Burkholderia tropica</i>	ND	T	T	ND	ND	T	T	ND
MF512174 / <i>Propionibacterium acnes</i>	ND	ND	ND	ND	ND	T	ND	ND
MF512175 / <i>Leifsonia sp.</i>	ND	ND	ND	ND	ND	ND	T	T
MF512176 / <i>Adhaeribacter sp.</i>	ND	ND	T	ND	ND	ND	T	ND
MF512178 / <i>Gordonia sp.</i>	ND	T	T	T	ND	1	T	T
MF512179, KU597453, KX759054 / <i>Ochrobactrum anthropi</i>	3	29	43	34	39	70	66	29
MF512180 / <i>Shigella dysenteriae</i>	ND	T	13	T	ND	T	T	12
MF512181 / <i>Magnetospirillum gryphiswaldense</i>	ND	T	T	3	ND	T	T	ND
MF512182 / <i>Rhodococcus fascians</i>	ND	T	T	T	ND	T	T	19
MF512183 / <i>Propionicimonas paludicola</i>	ND	ND	ND	T	ND	ND	T	ND
MF512184 / <i>Rhodococcus sp.</i>	ND	1	T	ND	ND	T	T	19
MF512185 / <i>Bacteroides sp.</i>	ND	ND	ND	1	ND	ND	T	ND
MF512186 / <i>Pseudomonas knackmussii</i>	ND	T	1	ND	ND	1	T	5
MF512187 / <i>Adhaeribacter sp.</i>	ND	ND	T	T	ND	ND	T	ND

OTU Accession No.s / Closest GenBank Match	BES1		BES2		BES3		BES4	
	B ^a	S ^b	B	S	B	S	B	S
KU597447 / <i>Mycobacterium conceptionense</i>	5	ND	ND	ND	ND	ND	ND	ND
KU597448 / <i>Sedimentibacter hydroxybenzoicus</i>	1	ND	ND	ND	ND	ND	ND	ND
KU597449, KX759048 / <i>Propionivibrio limicola</i>	3	ND	ND	ND	1	ND	ND	ND
KU597450 / <i>Sphingopyxis terrae</i>	2	ND	ND	ND	ND	ND	ND	ND
KU597451 / <i>Citrobacter farmerii</i>	3	ND	ND	ND	ND	ND	ND	ND
KU597452 / <i>Thermincola carboxydiphila</i>	6	ND	ND	ND	ND	ND	ND	ND
KU597454 / <i>Thiomonas thermosulfata</i>	1	ND	ND	ND	ND	ND	ND	ND
KU597455 / <i>Wolinella succinogenes</i>	3	ND	ND	ND	ND	ND	ND	ND
KU597456 / <i>Arcobacter thereius</i>	1	ND	ND	ND	ND	ND	ND	ND
KU597457 / <i>Neisseria animaloris</i>	3	ND	ND	ND	ND	ND	ND	ND
KU597458 / <i>Pseudomonas cedrina</i>	1	ND	ND	ND	ND	ND	ND	ND
KX759044 / <i>Nitrobacter hamburgensis</i>	ND	ND	ND	ND	1	ND	ND	ND
KX759055 / <i>Helicobacter cholecystus</i>	ND	ND	ND	ND	1	ND	ND	ND
KX759061 / <i>Proteiniborus ethanoligenes</i>	ND	ND	ND	ND	1	ND	ND	ND
KX759065 / <i>Thiomonas thermosulfata</i>	ND	ND	ND	ND	3	ND	ND	ND
KX759075 / <i>Oligotropha carboxidovorans</i>	ND	ND	ND	ND	2	ND	ND	ND

^a Biofilm.

^b Suspended biomass.

^c Not detected.

^d Trace amounts ($\leq 1\%$ relative abundance).

Table 8.8 - Closest GenBank Relatives and Bacterial Relative Abundance for Defined OTUs in Anode Biofilm and Suspended Biomass

OTU Accession No. / Closest GenBank Match	BES1		BES2		BES3		BES4	
	B ^a	S ^b	B	S	B	S	B	S
MF512155 / <i>Proteiniphilum acetatigenes</i>	ND ^c	ND	T ^d	ND	ND	ND	ND	T
MF512156 / <i>Rhodopseudomonas palustris</i>	T	T	T	ND	T	ND	ND	T
MF512157 / <i>Xanthobacter autotrophicus</i>	ND	ND	ND	ND	ND	T	ND	ND
MF512159 / <i>Syntrophus aciditrophicus</i>	ND	ND	3	ND	ND	ND	ND	ND
MF512160 / <i>Achromobacter sp.</i>	27	69	18	14	23	37	18	18
MF512161 / <i>Mycobacterium sp.</i>	T	T	ND	4	T	T	T	1
MF512162 / <i>Gordonia rubripertincta</i>	T	T	1	6	1	2	1	T
MF512163 / <i>Mycobacterium sp.</i>	T	T	ND	1	T	T	T	ND
MF512164 / <i>Geobacter sulfurreducens</i>	ND	ND	2	ND	ND	ND	ND	ND
MF512165 / <i>Burkholderia lata</i>	ND	ND	T	ND	ND	ND	T	1
MF512166 / <i>Citrobacter gillenii</i>	ND	T	T	ND	ND	T	ND	T
MF512167 / <i>Actinomyces georgiae</i>	ND	T	T	ND	ND	ND	ND	ND
MF512169 / <i>Aminobacterium colombiense</i>	ND	ND	1	ND	ND	ND	ND	ND
MF512170 / <i>Eubacterium acidaminophilum</i>	ND	ND	1	ND	ND	ND	ND	ND
MF512171 / <i>Pseudomonas aeruginosa</i>	31	3	22	1	46	2	ND	1
MF512172 / <i>Pseudomonas grimontii</i>	T	T	T	ND	ND	ND	ND	1
MF512173 / <i>Burkholderia tropica</i>	ND	ND	T	ND	ND	ND	5	22
MF512174 / <i>Propionibacterium acnes</i>	ND	ND	2	ND	ND	ND	ND	ND
MF512175 / <i>Leifsonia sp.</i>	ND	T	T	T	T	T	2	10
MF512176 / <i>Adhaeribacter sp.</i>	ND	ND	1	ND	ND	ND	ND	ND
MF512177 / <i>Proteiniphilum acetatigenes</i>	ND	ND	2	ND	ND	ND	ND	ND
MF512178 / <i>Gordonia sp.</i>	ND	T	ND	ND	ND	ND	ND	ND
MF512179 / <i>Ochrobactrum anthropi</i>	7	21	4	72	20	36	1	19
MF512180 / <i>Shigella dysenteriae</i>	34	3	23	ND	7	20	74	25
MF512183 / <i>Propionicimonas paludicola</i>	ND	ND	1	ND	ND	ND	ND	ND
MF512184 / <i>Rhodococcus sp.</i>	T	T	ND	T	T	T	T	2
MF512185 / <i>Bacteroides sp.</i>	ND	ND	3	ND	ND	ND	ND	ND
MF512186 / <i>Pseudomonas knackmussii</i>	T	T	T	T	3	1	ND	ND
MF512187 / <i>Adhaeribacter sp.</i>	ND	ND	1	ND	ND	ND	ND	ND

^a Biofilm.

^b Suspended biomass.

^c Not detected.

^d Trace amounts ($\leq 1\%$ relative abundance).

Table 8.9 - Bacterial and Archaeal Shannon Diversity Indices

Sample	Bacteria	Archaea
BES1 Anode Biofilm	1.35	0.93
BES1 Anode Suspended Biomass	1.01	0.39
BES1 Cathode Biofilm	2.68	0.05
BES1 Cathode Suspended Biomass	1.73	0.04
BES2 Anode Biofilm	2.76	0.79
BES2 Anode Suspended Biomass	1.04	NA ^a
BES2 Cathode Biofilm	2.12	0.002
BES2 Cathode Suspended Biomass	1.89	0.0005
BES3 Anode Biofilm	1.43	0.45
BES3 Anode Suspended Biomass	1.43	1.05
BES3 Cathode Biofilm	2.32	0.001
BES3 Cathode Suspended Biomass	1.52	0.001
BES4 Anode Biofilm	0.85	0.15
BES4 Anode Suspended Biomass	1.88	NA ^a
BES4 Cathode Biofilm	1.44	0.003
BES4 Cathode Suspended Biomass	1.88	0.003

^a Not Available. OTU counts were too low for analysis.

To better understand the effects of biofilm formation (i.e., biofilm versus suspended biomass), biocathode ZVI exposure and biocathode H₂S exposure on the cathode bacterial communities, a principal coordinate analysis was conducted (Figure 8.6 and Figure 8.7). The results show that the BES1 cathode biofilm had a bacterial community that was significantly different than the suspended biomass and biofilm in the other BES cathodes. The bacterial communities in the suspended biomass samples of BES1, BES2 and BES4 were more similar to each other than to that of BES3, suggesting the presence of ZVI had the greatest effect on the suspended biomass bacterial community.

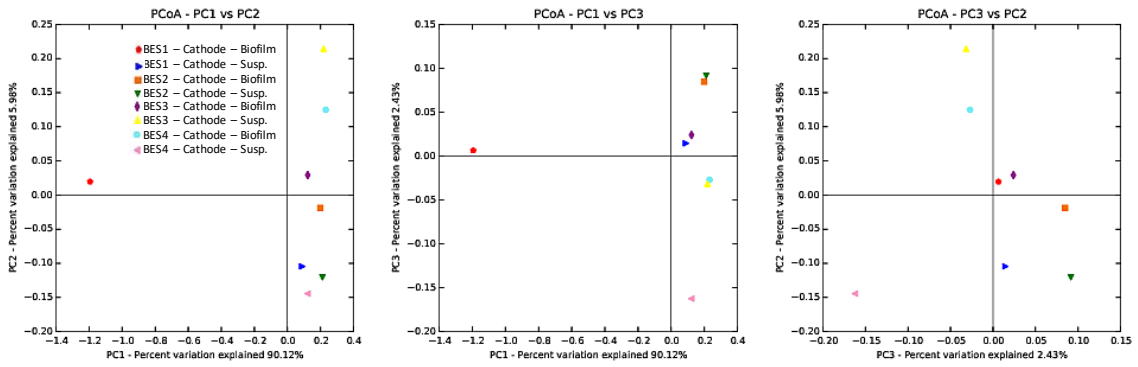


Figure 8.6 - 2D Principal coordinate analysis plots for the cathode biofilm and suspended biomass in BES1, BES2, BES3 and BES4.

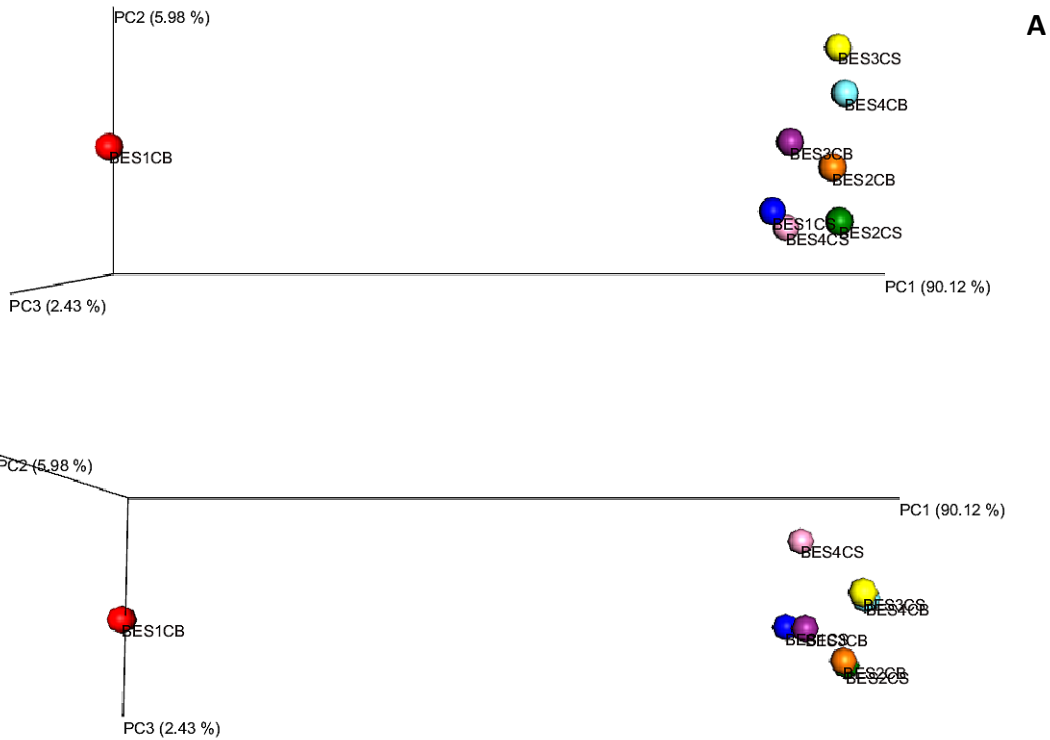


Figure 8.7 - 3D Principal coordinate analysis plots for the cathode biofilm and suspended biomass in BES1, BES2, BES3 and BES4; Front view (A), Overhead view (B). Cathode suspended biomass, -CS; Cathode biofilm, -CB.

To determine which factors (biofilm development, ZVI amendment and H₂S amendment) had the greatest effect on the biocathode bacterial community, a canonical correspondence analysis and redundancy analysis was performed (Figure 8.8). In both analyses, the effect of the H₂S amendment was nearly opposite to that of the effect of biofilm development. In contrast, the effect of ZVI amendment shifted communities in a different direction, indicating that ZVI affected a different set of Bacteria than the amendment of H₂S or the development of biofilm.

The anode bacterial communities were similarly analyzed using principal coordinate analysis (Figure 8.9 and Figure 8.10), canonical correspondence analysis and redundancy analysis (Figure 8.11). The principal coordinate analysis showed that the BES2 anode biofilm and suspended biomass bacterial communities were significantly different from the other biofilm and suspended biomass communities. This result is likely due to the ability of H₂S to be transported from the cathode to the anode, unlike ZVI. Unlike in the cathode bacterial communities, the effect of biofilm development had a greater effect on the bacterial community composition than the cathode addition of ZVI or H₂S (Figure 8.11). In other words, the difference between biofilm and suspended biomass bacterial communities was greater than the difference between bacterial communities due to ZVI or H₂S addition.

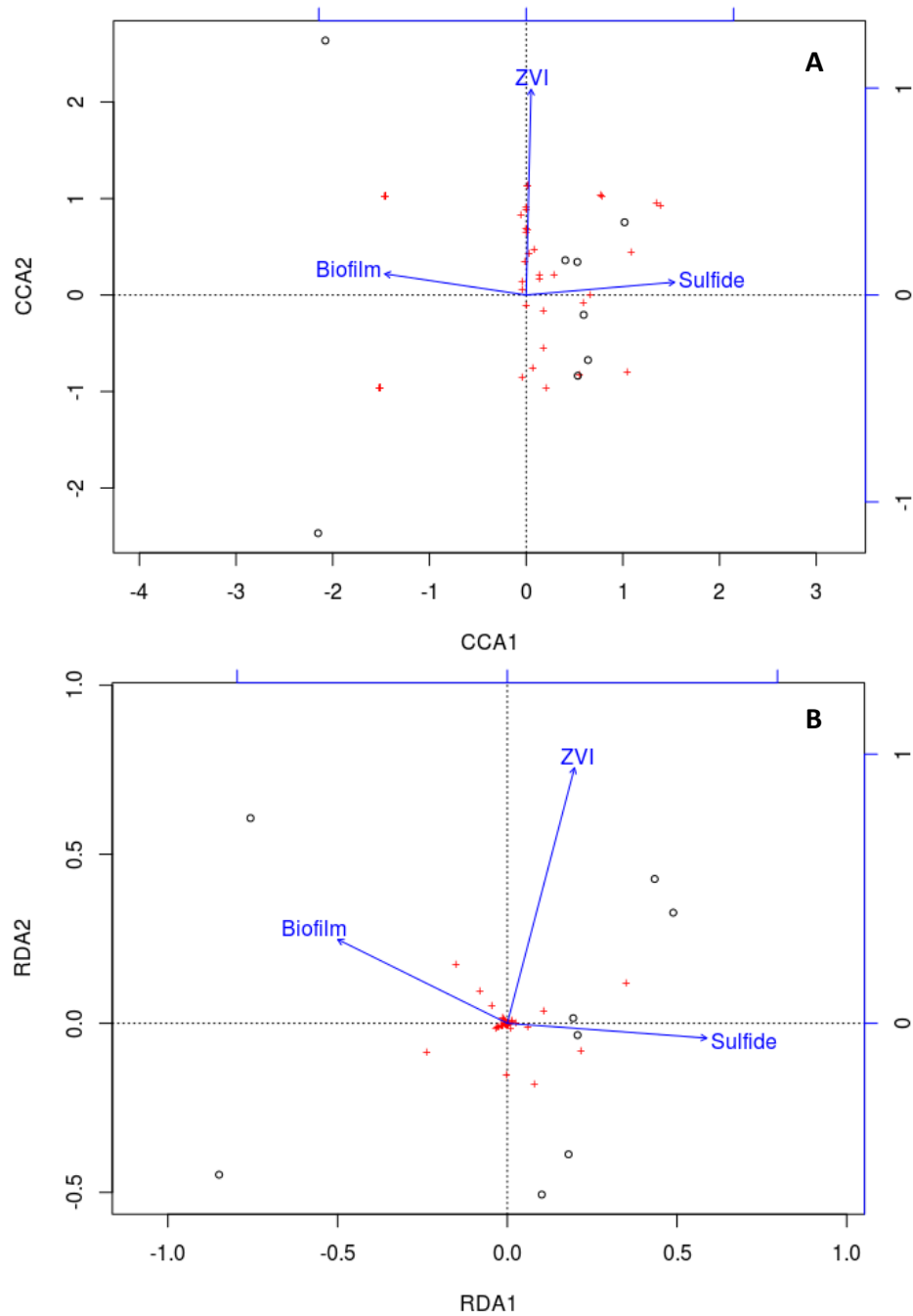


Figure 8.8 - Canonical correspondence analysis plot (A) and redundancy analysis plot (B) for the cathode biofilm and suspended biomass in BES1, BES2, BES3 and BES4.

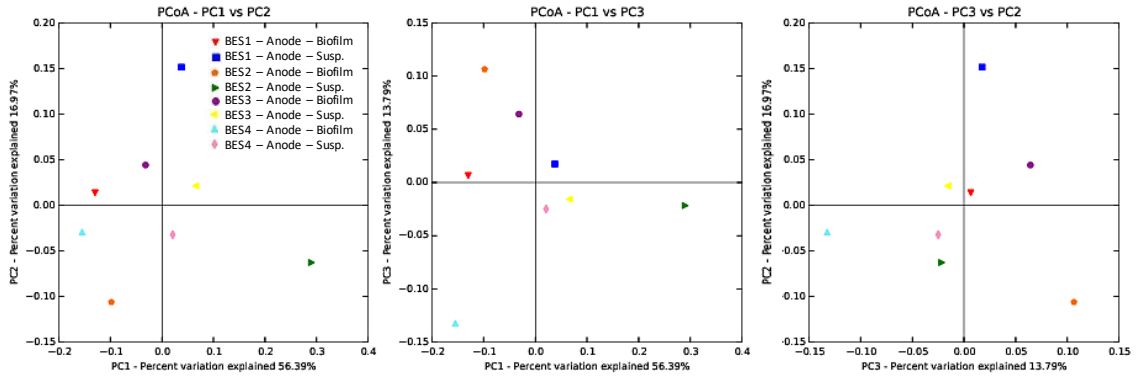


Figure 8.9 - 2D Principal coordinate analysis plots for the anode biofilm and suspended biomass in BES1, BES2, BES3 and BES4.

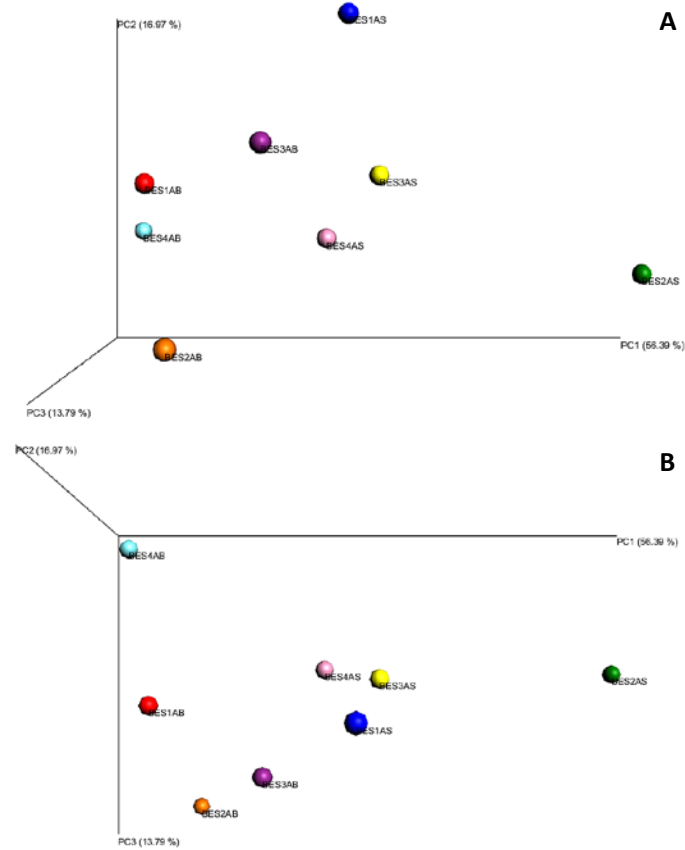


Figure 8.10 - 3D Principal coordinate analysis plots for the anode biofilm and suspended biomass in BES1, BES2, BES3 and BES4; Front view (A), Overhead view (B). Anode suspended biomass, -AS; Anode biofilm, -AB.

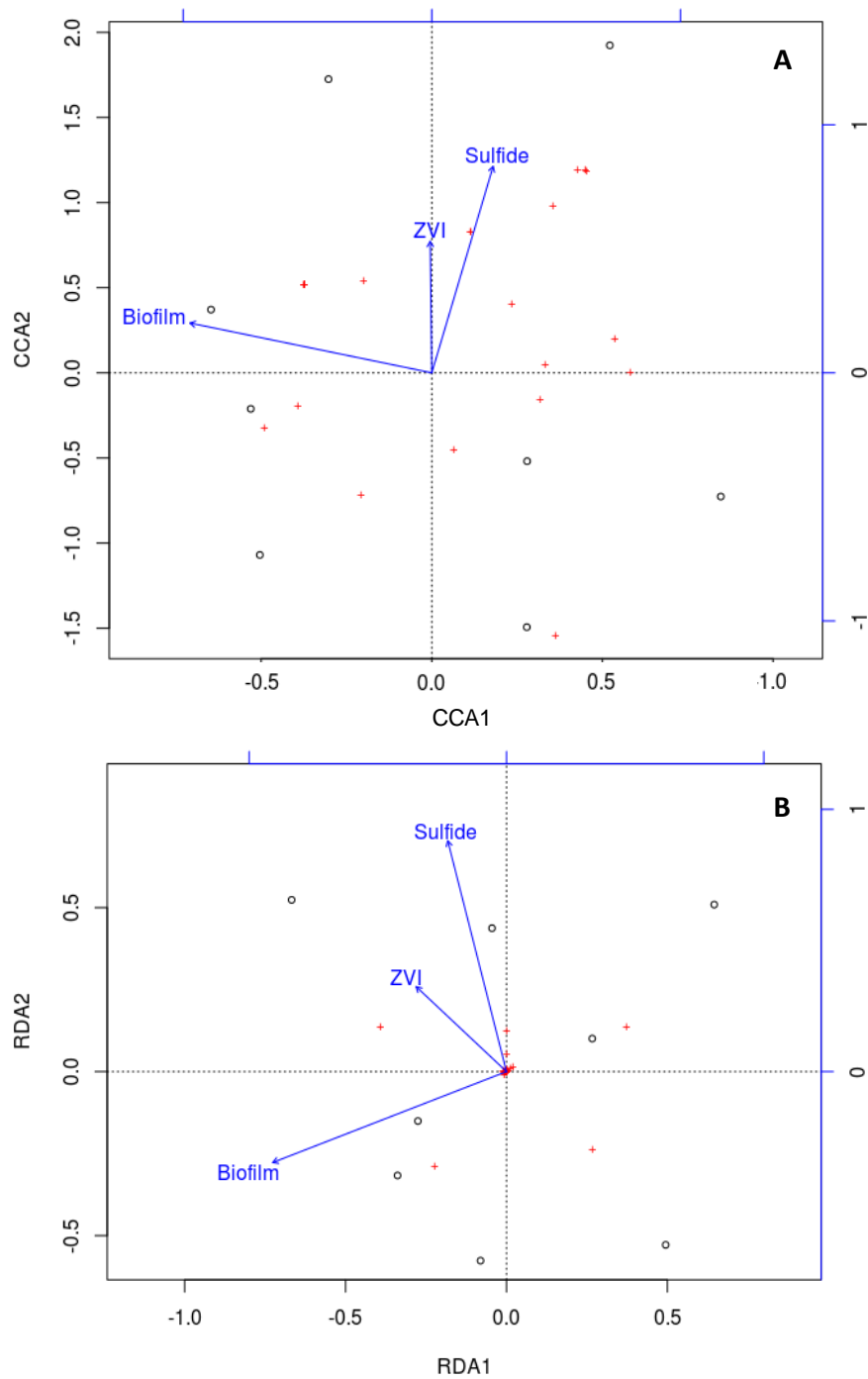


Figure 8.11 - Canonical correspondence analysis plot (A) and redundancy analysis plot (B) for the anode biofilm and suspended growth in BES1, BES2, BES3 and BES4.

8.4 Summary

Anaerobic digester biogas contains a mixture of CO₂, CH₄ and trace gases (e.g., H₂S, N₂, H₂). A ZVI-amended biocathode has been developed for the upgrading of biogas (i.e., conversion of CO₂ to CH₄ to increase energy content) but the effect of H₂S, a common biogas contaminant, on a BES with ZVI-amended biocathode is unknown. Thus, the objective of this research was to i) evaluate the effect of biocathode H₂S on the performance of a BES with a ZVI-amended biocathode; ii) probe the electron transfer mechanisms involved in biocathode processes in H₂S- and ZVI-amended biocathodes; and iii) assess the effect of biofilm formation, biocathode H₂S, and biocathode ZVI on the microbial communities of the anode and cathode biofilm and suspended biomass. Following amendment with H₂S, the ZVI-amended biocathode removed more headspace CO₂ (100% vs. 89% previously) over the course of a 3-d incubation and produced CH₄ at a 61% faster rate of production. Electron transfer mechanisms were explored by measuring the amount of H₂-mediated CH₄ production in the biocathode. The majority of the CH₄ produced by the control BES and BES with H₂S-amended biocathode could be explained by H₂-mediated CH₄ production. However, in the BES4 and BES3 biocathodes, 74% and 32% of the CH₄ produced could be attributed to H₂-mediated CH₄ production. This suggests that in the presence of ZVI, the modes of electron transfer shift away from H₂-mediated transfer and possibly towards more direct electron transfer. An analysis across the anode and cathode biofilm and suspended biomass communities indicated exoelectrogens were enriched in the anode and cathode of better performing systems. H₂S amendment to the cathode stimulated *Geobacter* sp. growth in the anode but this effect was not observed in the ZVI-biocathode amended with H₂S. Of the three factors (biofilm development,

biocathode ZVI amendment and biocathode H₂S amendment) analyzed with principal coordinate analysis, canonical correspondence analysis and redundancy analysis, ZVI had the greatest effect on the cathode bacterial community, while biofilm growth had the greatest effect on the anode bacterial community.

CHAPTER 9. BIOELECTROCHEMICAL BIOGAS UPGRADING

9.1 Introduction

Anaerobic digester biogas contains a mixture of CO₂, CH₄ and trace gases (e.g., H₂S, N₂, H₂, etc.). After collection, the biogas must undergo processing to make it suitable for its final use. Different biogas processing requirements must be met depending on how the biogas will be used. If the biogas is used for heating in an onsite boiler or with combined heat and power (CHP) systems, only impurities such as H₂S, NH₃, siloxanes, halocarbons and water must be removed prior to combustion (Muñoz et al. 2015, Sun et al. 2015). However, in order to use biogas as a vehicle fuel or to inject into natural gas pipelines, the biogas must be processed to meet more rigorous requirements. In order to expand the use of biogas to the vehicle fuel and natural gas markets, biogas must be processed such that CH₄ concentration is larger than 80-96%, CO₂ concentrations are below 2-3% and H₂S is below 5 mg/m³, along with requirements for O₂, NH₃ and siloxanes (Sun et al. 2015). The processing of biogas to increase energy content and remove impurities is referred to as “biogas upgrading”.

Traditional biogas upgrading methods include water scrubbing, physical/chemical absorption, pressure swing absorption, membrane technology and cryogenic separation. These technologies often require expensive consumables (e.g., membranes, sorbents), energy-intensive processes (e.g., pressurization, sorbent regeneration) or produce a CO₂ waste stream (e.g., membrane separation) (Abdeen et al. 2016, Bauer et al. 2013, Muñoz et al. 2015, Petersson and Wellinger 2009, Sun et al. 2015, Weiland 2010). Instead, bioelectrochemical systems (BESs) are able to convert CO₂ into CH₄ without these

disadvantages. The addition of zero valent iron (ZVI) increases methanogenesis in a biocathode (see Section 6.3.2). Furthermore, the addition of pure H₂S to the headspace of a methanogenic biocathode led to an increase in system current and an increase in CH₄ output up to 3% initial H₂S (v/v) (see Section 7.3.3). However, trace gases other than H₂S (e.g., NH₃, siloxanes, etc.) may also affect BES operation. Yet, BES biogas upgrading studies have typically used commercial gases, such as CO₂ and N₂.

In order to scale up a BES for biogas upgrading, a continuous-flow system will be required. One method of continuously introducing CO₂ to the cathode biofilm is through the pumping of pre-carbonated catholyte into the cathode. After delivering CO₂ to the biofilm, the catholyte (carrying CH₄ and some CO₂) is returned to a gas collection chamber where gases are stripped and the catholyte is mixed and returned to the cathode. However, such a system is untested and it is not known if the rate of biocathode CH₄ production observed in batch studies would be sustained with a continuous supply of CO₂. Therefore, the objective of this study was to test BESs under more applied conditions by: i) testing a catholyte recycle system to approximate a continuous supply of CO₂; and ii) testing the performance of four developed BESs (control BES, BES with ZVI-amended biocathode, BES with H₂S-amended biocathode and BES with H₂S/ZVI-amended biocathode; see Chapter 8) when the biocathode was fed with biogas produced by a stock mesophilic anaerobic digester.

9.2 Materials and Methods

9.2.1 Catholyte Recycle System

One of the current engineering challenges of BES biogas upgrading technology is the development of a system that can treat biogas in a continuous-flow system. Although reactor architecture is beyond the scope of this study, some of the processes that may be applied to continuous-flow systems can be described using the H-style reactor configuration used in this research. To assess if the biocathode CH_4 production rate could be sustained with a nearly-continuous supply of CO_2 , a typical 7-d batch cycle without catholyte recycle was compared with three subsequent 7-d feeding cycles with catholyte recycle in the configuration shown in Figure 9.1. Although the initial total carbonate species in the catholyte in all feedings was the same, the catholyte recycling system employed a larger catholyte volume and, hence, a larger reservoir of CO_2 . The volume of catholyte in the cathode was 250 mL, and the total volume of catholyte in the catholyte-recycle system (cathode and catholyte recycle bottle) was 1 L. Thus, the catholyte-recycle system catholyte contained fourfold more CO_2 but delivered the CO_2 to the biofilm at the same initial concentration than in the non-recycle batch cycle and, thus, more closely approximated a continuous-flow system. In all cases, the catholyte was amended with sodium bicarbonate solution to 26.3 mM total carbonate species at the beginning of a feeding. Bicarbonate solution was added directly to the cathode in the non-recycle batch cycle and was added to the catholyte recycle bottle (Figure 9.1) in the catholyte-recycle system.

Prior to implementing the catholyte recycle, the biocathode was fed in three 7-d batch feeding cycles at the same bicarbonate concentration (26.3 mM total carbonate species) and monitored to determine a mean CH_4 production rate. In the subsequent recycling feeding cycles, catholyte was pumped at a rate of 0.5 mL/min using a dual-head Masterflex peristaltic pump (Cole Parmer; Vernon Hills, IL). The catholyte was dripped into the headspace of a catholyte recycle bottle, which was pre-flushed with N_2 prior to the start of the cycle. The dripped catholyte released dissolved gases into the headspace of the catholyte recycle bottle and the liquid phase collected in the bottom of the bottle, where it was continuously mixed. In turn, a second head on the pump returned the catholyte from the bottom of the catholyte recycle bottle to the bottom of the cathode compartment. Gas pressure and composition in the headspace of the cathode recycle bottle were measured as described in Sections 3.1.6 and 3.1.7.

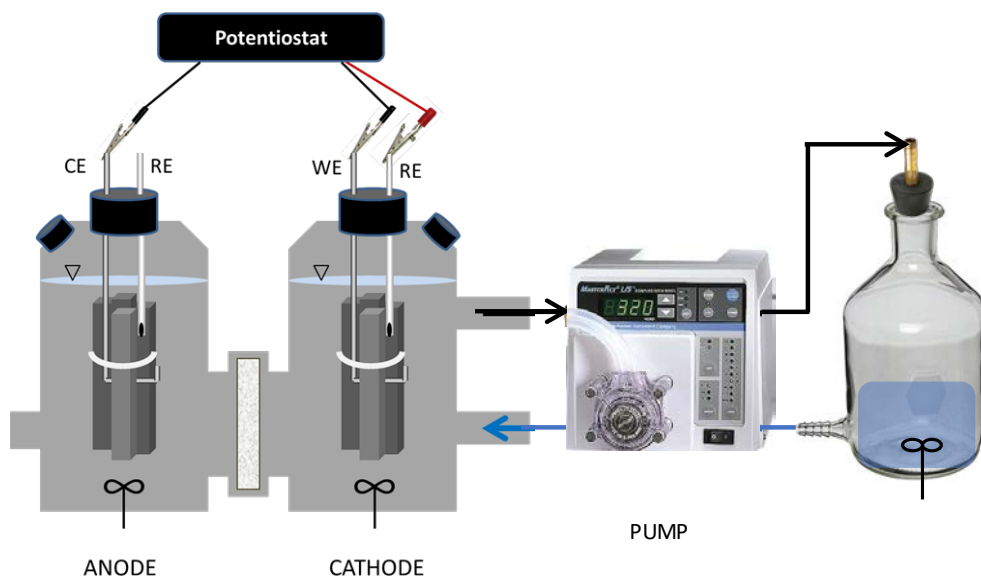


Figure 9.1 - Schematic of catholyte recycle system

9.2.2 BES Biogas Upgrading with Anaerobic Digester Biogas

A stock anaerobic digester was developed with inoculum from a mesophilic, municipal anaerobic digester, fed with a mixture of dextrin/peptone and anaerobic media (Tugtas 2007), and maintained at 35°C under continuous mixing for over 10 years. The digester was maintained with a hydraulic retention time (HRT) of 31.5 d and was fed twice per week to a concentration of 1 g COD/L. Gas produced by the anaerobic digester was continuously collected in an acid-brine displacement system to facilitate a low pressure in the headspace of the reactor.

Three BESs were developed as described in Sections 5.2.1, 6.2.1 and 7.2.3 with the parameters given in Table 9.1. Each BES bioanode was filled with 250 mL anolyte media (see Section 4.2.1), flushed with N₂ and fed with sodium acetate to a concentration of 1,500 mg COD/L at the start of each 3-d feeding cycle. Initially, each biocathode was fed with 100% CO₂ to 1 atm (absolute pressure). BES performance during the CO₂-fed cycle was compared with BES performance when the biocathode was fed with anaerobic digester biogas (to 1 atm absolute pressure), as discussed further below. BES1 was operated as a control. The biocathodes of BES2 and BES3 were supplemented with 3% H₂S (v/v) and 1 g/L ZVI, respectively, at the beginning of each feeding cycle.

Table 9.1 - BES Setups

BES	Cathode H ₂ S (3% v/v)	Cathode ZVI (1 g/L)
BES1	- ^a	-
BES2	+ ^b	-
BES3	-	+

^a Not Added. ^b Added.

To test how the three BESs would perform when fed with biogas, each cathode compartment was flushed with biogas from the anaerobic digester at 35°C. Room temperature (22°C) cathode media (see Section 4.2.1) was then added to each cathode and the initial gas composition in the headspace was immediately measured. The cathodes were then incubated at room temperature (22±2°C), allowing the gas to cool in the cathode. BES bioanodes were prepared at room temperature; anodes were flushed with N₂, filled with fresh anode media (see Section 4.2.1) and fed with sodium acetate to an initial reactor concentration of 1.5 g COD/L. The BESs were incubated under mixing at 22±2°C for 3 d. Gas pressure and gas composition measurements were taken as described in Sections 3.1.6 and 3.1.7, respectively. Each cathode was maintained at -0.8 V vs. SHE using a Gamry Interface 1000 potentiostat (Warminster, PA).

9.3 Results and Discussion

9.3.1 Catholyte Recycle System

In the two batch cycles prior to implementing the catholyte recycle, the cathode was filled with 250 mL catholyte and fed with bicarbonate to the same concentration used in the subsequent catholyte recycle feedings (26.3 mM total carbonate species). Over the course of a 7-d cycle, the anolyte pH declined from 7.0 to 6.4 and the catholyte pH increased from 7.0 to 7.1. Mean 7-d anode acetate removal over the two cycles was 98.7±0.1%. In the cathode, headspace CO₂ increased over the course of the first day following feeding due to the equilibration of the added bicarbonate between the liquid and gas phases (Figure 9.2). By the end of the 7-d feeding cycle, the cathode headspace gas consisted of 1.9±0.1% CO₂ (v/v). The biocathode produced CH₄ at a nearly linear rate of

0.387 ± 0.012 mmol/d ($R^2 = 0.991$), despite the relatively low headspace CO_2 concentrations.

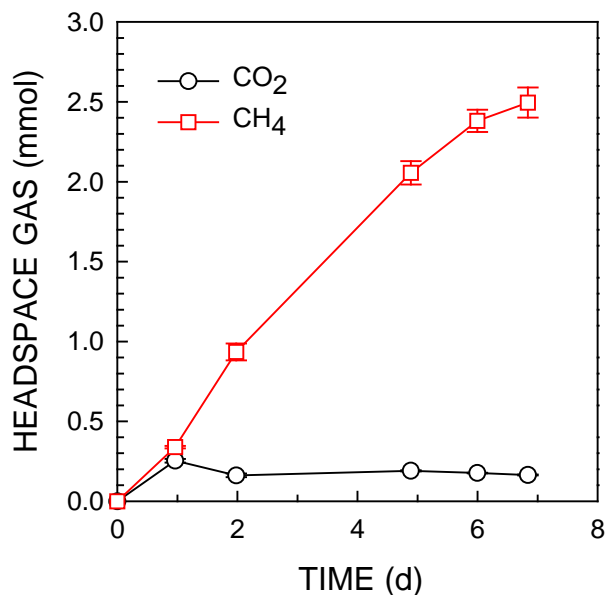


Figure 9.2 - Time course of CO_2 and CH_4 in the cathode headspace in the feeding cycle prior to implementing catholyte-recycle. Error bars represent mean \pm standard deviation; $n = 3$.

To better approximate a continuous-flow system, a catholyte recycle system was set up as shown in Figure 9.1. Three 7-d feeding cycles were monitored in which the anolyte was completely exchanged and batch-fed with sodium acetate; the catholyte was not exchanged and only bicarbonate was added to the catholyte recycle bottle. During each of the three feeding cycles, the anolyte pH declined from 7.0 to 6.2. The 7-d mean acetate removal across the three cycles was $99.1 \pm 0.5\%$, which was similar to the mean acetate removal prior to catholyte recycle ($98.7 \pm 0.1\%$). The catholyte pH, which was not

exchanged during feedings, gradually increased from 7.0 to 7.2 by the end of the three cycles.

Cathode gas was collected in the catholyte recycle bottle, for which the headspace CO_2 and CH_4 is shown in Figure 9.3. Initially, the headspace contained only N_2 but, after adding bicarbonate to the cathode recycle bottle, CO_2 evolved into the headspace, resulting in a sharp increase of headspace CO_2 over the first day following each feeding. Between days 2-7 of each feeding cycle, the headspace CO_2 declined at a nearly linear rate of 0.629 ± 0.027 mmol/d ($R^2=0.979$) during all three cycles, indicating a steady rate of CO_2 uptake in the biocathode. In comparison, the CH_4 in the cathode recycle bottle headspace increased at a nearly linear rate of 0.710 ± 0.010 mmol/d ($R^2=0.987$) across the full 21 days of incubation. Assuming a 1:1 molar ratio of CO_2 to CH_4 , the slightly higher rate of CH_4 production than CO_2 removal from the headspace suggests that some CO_2 from the anode crossed the membrane and was utilized by the biocathode for CH_4 production. Indeed, this phenomenon has been previously noted (see Section 4.3.4). Compared with the previous cycles, catholyte recycling increased the mean 7-d CH_4 production rate by 45%.

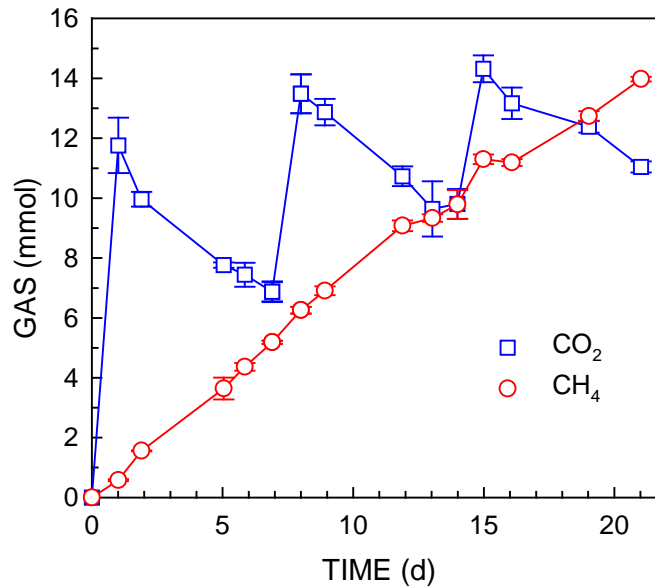


Figure 9.3 - Time course of headspace CO₂ and CH₄ in the catholyte recycle bottle. Error bars represent mean ± standard deviation; $n = 3$.

Significant CO₂ substrate limitations were not observed in the feeding cycle without catholyte recycle, as indicated by the nearly linear CH₄ production ($R^2 = 0.991$). Therefore, the increase in the rate of CH₄ production with catholyte recycle was not likely due to the relief of substrate limitations (i.e., declining catholyte CO₂ concentration). Rather, the rate increase was likely due to the relief of mass-transfer limitations at the interface of the cathode biofilm and liquid catholyte. When CH₄ is produced by the biocathode, small bubbles develop at the cathode surface. Without catholyte recycle, two forces act on a bubble: buoyancy and surface tension. A bubble must accumulate enough gas for the buoyancy force to overcome the surface tension holding the bubble to the cathode surface before it will detach and rise to the headspace. However, in the cathode with catholyte recycle, the bubble at the cathode surface also has a drag force acting on it as the liquid flows across the cathode surface in an upward direction (Al-Hayes and Winterton 1981).

In this case, the drag and buoyancy forces combined must overcome the surface tension to cause bubble detachment. Therefore, upward catholyte flow from catholyte recycling would cause bubbles to detach at a smaller diameter than without catholyte recycling (Al-Hayes and Winterton 1981). Stripping bubbles away from the cathode surface more quickly makes more surface area of the cathode available for CO₂ and proton mass transport into the biofilm. In this way, the catholyte recycle likely reduced mass transfer limitations at the cathode surface and increased the CH₄ production rate.

9.3.2 *BES Biogas Upgrading with Anaerobic Digester Biogas*

To examine the effect of feeding real digester biogas to biocathodes, a typical 3-d batch feeding cycle in BES1 (control), BES2 (3% v/v H₂S-amended biocathode) and BES3 (1 g/L ZVI-amended biocathode) was observed, in which the cathodes were initially fed with 100% CO₂ (g). At the next feeding, on day 3, the biocathodes were fed with anaerobic digester biogas, obtained from a stock anaerobic digester. BES2 was supplemented with 3% v/v H₂S and BES3 was supplemented with 1 g/L ZVI. The BESs were then monitored for 3 days. The pH of the anolyte and catholyte in all systems remained between 6.8 and 7.3 in both the CO₂-fed cycle and the biogas-fed cycle. In all cycles, the current density increased immediately upon feeding (Figure 9.4A) and then declined over the remainder of the feeding cycle. The maximum current density values observed for BES1, BES2 and BES3 under the CO₂-fed conditions were substantially different from each other (Table 9.2). BES3 had a 66% lower maximum current density than BES1, which is likely due to the alternative source of reducing power (H₂ produced from ZVI anaerobic corrosion) that reduced demand for electrons from the cathode. In contrast, BES2 had a maximum current density that was over three-fold higher than the maximum current density in BES1. The

higher current density in BES2 is indicative of H₂S transport across the proton exchange membrane into the anode chamber, where it donates electrons to the anode.

When anaerobic digester biogas was fed to the biocathodes instead of 100% CO₂, the maximum current density in each of the systems changed. In BES1, the maximum current density increased by 13%, which could be due to the presence of trace H₂S in the anaerobic digester biogas. H₂S can contribute to current by migrating to the anode through the proton exchange membrane and donating electrons to the anode (see Section 7.3.2). Indeed, the anaerobic digester biogas did have a sulfide odor but H₂S was below the detection limit (1% v/v) for GC-TCD measurement. In BES2, the maximum current density in the biogas-fed cycle was 35% higher than the maximum current density in the CO₂-fed cycle. While the increase may be due, in part, to the presence of H₂S, other cause(s) are likely. One possible reason for increased current could be the anaerobic oxidation of CH₄ at the anode, coupled to current production, which has recently been described (Gao et al. 2017). This possibility is discussed in more detail at the end of this section. The cathode capture efficiency (CCE), which is defined as the percentage of the cumulative equivalents transferred as electric charge that are recovered as cumulative equivalents of CH₄, was assessed over the 3-d incubation period, with the exception of BES2 during the biogas-fed cycle. In that case, due to the decline in CH₄ at the end of the incubation period, the CH₄ production could not be accurately measured. Thus, the BES2 CCE was measured over the first day following feeding with biogas, during which CH₄ production could be assessed. The CCE for BES1 declined by 51% between the CO₂-fed cycle and the biogas-fed cycle. In BES2, the CCE declined by 76%, although the quantification of CH₄ production may not be accurate due to the suspected loss of CH₄ to anaerobic oxidation in the anode. In

BES3, the CCE is not an accurate representation of the cathode biofilm efficiency because the produced CH_4 may originate from methanogenesis with ZVI-derived H_2 , in addition to electron equivalents from the cathode. However, the CCE measurement may be used as a relative measurement to evaluate the effect of a change in conditions on both methanogenic processes relative to the electric charge transferred. Therefore, the CCE for BES3 indicates that the efficiency of all methanogenic processes in the cathode declined by 67% between the CO_2 -fed cycle and the biogas cycle.

In all cases, CO_2 removal primarily occurred within the first day (Figure 9.4B). BES1, BES2 and BES3 removed 89.4%, 87.9% and 93.7% of the initial CO_2 during the first day of the CO_2 -feeding cycle. In comparison, when fed with anaerobic digester biogas, the cathodes of BES1, BES2 and BES3 removed 89.9%, 100.0% and 96.8% of the initial CO_2 , respectively. The initial quantity of CO_2 in the biogas-fed cycle was approximately 82-84% less than in the CO_2 -fed cycle and, thus, the amount of CO_2 removed between days 3 and 4 by BES1-3 was 82-86% lower on a molar mass basis than during the CO_2 -fed cycle (days 1-2). However, at the end of the biogas-fed cycle, the amount of CO_2 in the BES1, BES2 and BES3 headspace was 82%, 100% and 92% (v/v), which was lower than at the end of the CO_2 -fed cycle.

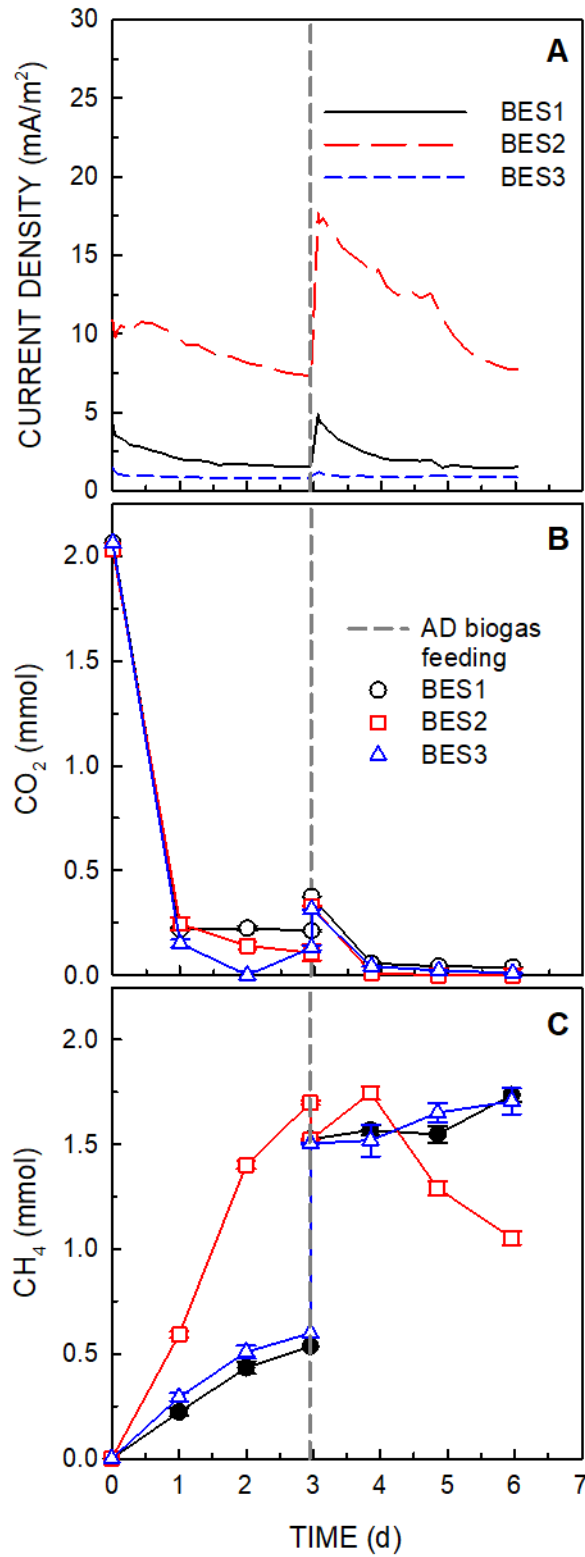


Figure 9.4 - Time course of current density (A), cathode headspace CO₂ (B) and cathode headspace CH₄ (C) when fed with 100% CO₂ (days 1-3) and anaerobic digester biogas (days 3-6). Error bars represent mean \pm standard deviation; $n = 3$.

Table 9.2 - Maximum Current Density and Cathode Capture Efficiency under Various Configurations

BES	CO ₂ -fed Biocathode		Biogas-fed Biocathode	
	Max. Current		Max. Current	
	Density (mA/m ²)	CCE (%)	Density (mA/m ²)	CCE (%)
BES1	4.33	99.8	4.90	48.5
BES2	13.1	88.2	17.7	20.9 ^a
BES3	1.47	317.3	1.21	105.5

^a Calculated over one day (day 3-4) because of declining cathode CH₄ during days 4-6.

The biocathode CH₄ production rate (mmol/d) during the CO₂-fed cycle was nearly linear in BES1, BES2 and BES3 (Figure 9.4C; Table 9.3), indicating that CO₂ was not limiting. The BES1 cathode had the lowest of the three rates. The CH₄ production rate in the BES3 cathode was 15% higher than the CH₄ production rate in the BES1 cathode. BES2 had the highest 3-d CH₄ production rate, which was 214% higher than the CH₄ production rate in the BES1 cathode. As previously mentioned, the presence of moderate amounts (up to 3% v/v H₂S) of H₂S in the CO₂ fed to a methanogenic biocathode can increase the BES current density and biocathode CH₄ production (see Section 7.3.1).

Table 9.3 - Mean Biocathode 3-Day CH₄ Production Rates and Final Gas Composition

BES	CO ₂ -fed Biocathode			Biogas-fed Biocathode		
	CH ₄ Rate (mmol/d)	Final Gas CO ₂ (% v/v)	Final Gas CH ₄ (% v/v)	CH ₄ Rate (mmol/d)	Final Gas CO ₂ (% v/v)	Final Gas CH ₄ (% v/v)
BES1	0.193±0.011 R ² = 0.971	10.5	89.1	0.061±0.030 R ² = 0.681	1.7	97.8
BES2	0.606±0.035 R ² = 0.972	5.0	94.2	0.223±0.031 ^a	ND ^b	99.5
BES3	0.222±0.018 R ² = 0.936	7.1	92.3	0.074±0.015 R ² = 0.921	0.5	98.5

^a Calculated over one day (day 3-4) because of declining cathode CH₄ during days 4-6.

^b Not detected.

Unlike in the previous CO₂-fed cycles, the mean CH₄ production rate in BES1 and BES2 was not linear (Figure 10.2C; Table 9.3) during the biogas-fed cycles. Additionally, the CH₄ production rate in BES3 was less linear than in the CO₂-fed cycle. This result is likely due to CO₂ substrate limitations in the biocathode, which is also illustrated by the lower quantities of CO₂ in the final gas (after 3-d incubation) of the biogas-fed cycles (Table 9.3). During the first day following biogas feeding (day 3-4), the CH₄ in the BES2 biocathode increased at nearly the same rate as it had at the end of the CO₂-fed cycle (day 2-3). However, between days 4-6, the CH₄ in the BES2 biocathode declined more significantly than would be expected by passive CH₄ transport to the anode alone (Figure 10.2C) (see Section 4.2.3). It is possible that anaerobic oxidation of CH₄ occurred in the anode, creating a larger CH₄ concentration gradient across the membrane and increasing CH₄ transport from cathode to anode. The anaerobic oxidation of CH₄ coupled with current production at an anode was recently described. In this previous study, the anode biofilm

was dominated by *Methanobacterium* (67% of Archaea) and *Geobacter* (38% of Bacteria) (Gao et al. 2017). Indeed, the anode biofilm in BES2 was enriched in both *Methanobacterium* and *Geobacter*. *Methanobacterium* represented 23% of total Archaea in the BES2 anode biofilm but only represented 5% and 1% of Archaea in the BES1 and BES3 anode biofilm. The OTU most closely related to *Geobacter sulfurreducens* was only observed in the BES2 anode biofilm, where it represented 2% of total Bacteria. Thus, it is possible that anaerobic oxidation of CH₄ occurred in the BES2 anode, leading to the reduction of CH₄ in the biocathode headspace. However, further study is necessary to determine if this process was responsible for the decrease in CH₄ observed in the BES2 cathode headspace.

Although the rate of CH₄ production was slower in the biogas-fed cycle, the final gas composition had a higher CH₄ content and lower CO₂ content than the final gas composition in the CO₂-fed cycles. Although a small amount of N₂ (transported from the anode) was present in the final gas, the CH₄ content ranged from 97.8-99.5%, which is well within the requirement for use as automobile fuel and in natural gas pipelines (Sun et al. 2015). Within one day of biogas feeding, the biogas in all three cathodes contained 96-98% CH₄ due to the rapid removal of CO₂ from the headspace. The results indicate that a shorter (≤ 1 d) incubation period is most beneficial for biogas upgrading. Furthermore, at longer incubation times, CH₄ transport to the anode might stimulate anaerobic methane oxidation and lead to a decrease in CH₄ output.

9.4 Summary

Anaerobic digester biogas contains a mixture of CO₂, CH₄ and trace gases (e.g., H₂S, N₂, H₂) and typically undergoes biogas upgrading prior to downstream use. Traditional methods of biogas upgrading often require expensive consumables, energy-intensive processes or produce a CO₂ waste stream. Instead, BESs may be used to upgrade biogas by converting CO₂ to CH₄ without these disadvantages. In order to scale up a BES for biogas upgrading, a continuous-flow system will be required and the system must be able to handle biogas from an anaerobic digester. Therefore, the objective of this study was to test BESs under more applied conditions by: i) testing a catholyte recycle system to approximate a continuous supply of CO₂; and ii) testing the performance of four developed BESs (control BES, BES with ZVI-amended biocathode, BES with H₂S-amended biocathode and BES with H₂S/ZVI-amended biocathode; see Chapter 8) when the biocathode was fed with biogas produced by a stock mesophilic anaerobic digester.

The recycling of catholyte increased the mean biocathode CH₄ production rate by 45%, indicating that recycling relieved mass transfer limitations at the interface of the cathode surface and the catholyte. A nearly linear rate of CH₄ production was observed throughout the course of 3, 7-d feeding cycles (21 d), indicating that a continuous-flow biocathode system is capable of maintaining a stable rate of CH₄ production over time.

When the biocathodes of three BESs (control, H₂S-amended biocathode and ZVI-amended biocathode) were fed with biogas from a stock anaerobic digester, the maximum current density in BES1 and BES2 increased by 13% and 35%, respectively. In contrast, the ZVI-amended biocathode in BES3 experienced an 18% decline in maximum current

density between the CO₂-fed cycle and the biogas-fed cycle. In the biogas-fed cycle, each biocathode removed CO₂ from the headspace to a lower fraction (i.e., greater CH₄ fraction) of total gas than in the CO₂-fed cycles. However, the CCE was lower in the biogas-fed cycles than the CO₂-fed cycles. Further research is needed to determine what mechanism(s) are responsible for the observed changes in BES performance.

CHAPTER 10. CONCLUSIONS AND RECOMMENDATIONS

10.1 Conclusions

BESs are a promising technology for biogas upgrading but more research is needed to scale the systems up to treat municipal- or industrial-sized biogas streams. However, the present research advances BES research in several areas, with the goal of progressing the technology towards field-scale applications.

First, this research showed that gas and carbon transport through the proton exchange membrane of a methanogenic BES may affect BES performance. Prior studies have not considered the transport of gases within the system and, in particular, the transport of CO₂ and CH₄, which may affect biocathode and bioanode microbial activity and communities, or affect product biogas quality. By understanding how gases and carbon are transported within the system, it is possible to design BESs that take advantage of natural gas flow to assist in the purification of biogas. Because CO₂ is produced in the liquid phase in the anode, if CO₂ migration through the membrane to the cathode could be promoted, biocathode CH₄ yields might be improved. Therefore, understanding the physicochemical processes was an important pillar of this research.

A second important conclusion of this work was the significant effect of Bacteria on the CH₄ production of a biocathode. Although Archaea produce CH₄ and have been the focus of most of the previous biocathode research, the present research found that biocathodes with similar archaeal communities, dominated by one phylotype related to *Methanobrevibacter arboriphilus*, produced CH₄ at significantly different rates due to

differences in the bacterial community. In the more productive biocathode, the bacterial community contained a larger relative abundance of exoelectrogens and putative producers of redox mediators. Furthermore, an analysis of the anode and cathode biofilm and suspended growth of four BESs under different conditions found the exoelectrogen *Ochrobactrum anthropi* at high abundance in both anode and cathode samples. The enrichment of heterotrophic bacteria and exoelectrogens in a CO₂-fed methanogenic biocathode necessitates a shift in thinking about methanogenic biocathodes. The Archaea present do not act independently but together with Bacteria as a complex interconnected microbial system.

This study also tested a novel ZVI-amended biocathode for CO₂ conversion to CH₄. The amendment of ZVI to a biocathode increased CH₄ production significantly, while affecting microbial communities in both the anode and cathode compartments. As ZVI undergoes anaerobic corrosion, it releases H₂, which is used by methanogens for CH₄ production. Simultaneously, ZVI releases Fe²⁺ ions, which may combine with other compounds in the media to form a precipitate. The precipitate that formed in the cathode under ZVI-amended conditions was found to be redox active and could have enabled more efficient electron transfer.

H₂S, a common biogas contaminant, has not previously been explored as a contaminant in the feed to a methanogenic biocathode. This research showed that H₂S is transported from the cathode to the anode compartment through the proton exchange membrane, where it becomes oxidized at the anode, donating electrons and increasing system current. At moderate initial concentrations ($\leq 3\%$ H₂S v/v), the increased current drives increased CH₄ production in the biocathode. Thus, although H₂S is inhibitory to

methanogenesis under typical bioreactor conditions, H₂S improves biocathode CH₄ production at relatively low concentrations. However, at concentrations that are >3% H₂S, the inhibition of methanogens in the biofilm leads to reduced CH₄ production. Regardless, most anaerobic digester biogas has a H₂S concentration of ≤1% and, therefore, would be in the range at which H₂S enhances current and CH₄ production.

With further research, BES technology may be scaled up to meet the needs of biogas upgrading. By expanding understanding of the biocathode physicochemical processes, microbial communities and response to ZVI and H₂S, this research may be used to guide the development of future designs of BES biogas upgrading systems.

10.2 Recommendations

10.2.1 Research Recommendations

Several research questions remain in the area of BES biogas upgrading. On the molecular scale, the mechanism(s) of electron transfer between a cathode surface and microorganism need to be explored in more depth. Although the present research indicated ZVI amendment to a biocathode resulted in a smaller fraction of H₂-mediated CH₄ production, it is not possible to attribute the remaining fraction entirely to direct electron transfer because other substances (e.g., phenazines) can also mediate electron transfer. Thus, future research into the precise mechanism(s) of electron transfer can help to elucidate the microbial relationships to the cathode surface. By developing biofilms that more directly utilize electrons, biocathode CCE may be improved.

Bacteria that are capable of transferring or accepting electrons externally have often been found associated with metals in the environment. Thus, the addition of ZVI in a biocathode may have an effect on not just the bacterial community but also on gene expression within that community. How genes are expressed can give insight into the biological processes occurring at or near the cathode surface. For example, hydrogenase genes may be upregulated in the case of H₂-mediated transfer and downregulated in the case of direct electron transfer. Hydrogenotrophic methanogens require hydrogenases to activate H₂ for use as a reductant with CO₂ and the identifying genes have been described for all five types of hydrogenase (Thauer et al. 2010). On the other hand, under H₂ limitation (e.g., direct electron transfer or non-H₂ mediated transfer), the expression of genes encoding F₄₂₀-reducing hydrogenase (*Frh*), formate dehydrogenase (*Fdh*) and formyl-MFR dehydrogenase (*Fwd*) is upregulated (Browne and Cadillo-Quiroz 2013). Thus, a transcriptomic analysis of biocathode systems under varied conditions (e.g., pH, temperature, ZVI-amended, H₂S-amended, etc.) may assist in engineering conditions to promote more efficient electron transfer within the system.

In addition to examining electron transfer mechanisms, research is needed to better understand the microbial relationships within the biocathode and the role that various types of Bacteria play. For example, a phylotype closely related to *Ochrobactrum anthropi* was among the most abundant phylotypes in both the anode and cathode samples in multiple BESs. This known exoelectrogen likely generated current in the anode but the role it served in the biocathode microbial community is not known. The roles of Bacteria may also be connected to other types of Bacteria. In the recent discovery of anaerobic CH₄ oxidation coupled with current at an anode, a consortium of *Methanobacterium* and *Geobacter* spp.

were required (Gao et al. 2017). Along this line, research is needed to understand how biocathode microorganisms work together in consortiums at the cathode surface.

Finally, further research should be conducted into the properties of the precipitates formed during ZVI-amended and ZVI/H₂S-amended biocathode operation. The molecular composition and redox properties of the ZVI precipitate were explored in the present research but more information could be gained by using additional techniques (e.g., inductively coupled plasma mass spectrometry; ICP-MS). The precipitate that formed in the ZVI/H₂S-amended biocathode should be further examined due to its magnetic properties that could be used as a way to remove H₂S from the gaseous headspace and recover it as a magnetic precipitate. Thus, further research into the unique biocathode biochemistry with ZVI and H₂S may lead to a technology desirable for other air pollution controls (e.g., H₂S removal) beyond biogas upgrading.

10.2.2 Development Recommendations

The development of BES biogas upgrading technology will also require progress in efficient reactor designs. One challenge is to design a reactor capable of handling a continuous-flow stream of CO₂ or biogas. The present study highlighted the positive results of a catholyte recycle (Figure 9.1), which could be adapted with a membrane system as shown in Figure 10.1 to deliver a continuous flow of CO₂ into the reactor, while purified biogas (i.e., CH₄) is continuously pumped out from the headspace. However, more research is needed to determine what the energetic costs of using a membrane system are and to address any fouling challenges.

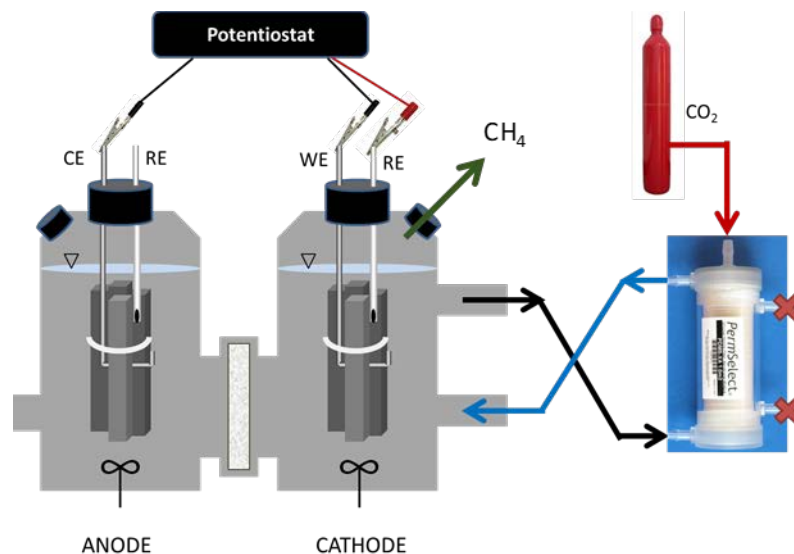


Figure 10.1 - Diagram of Membrane-Based Catholyte Recycle System

The architecture of the dual-chamber, H-style reactor is simple but not ideal. In the present study, high buffering of the media was required to maintain a near-neutral pH during batch operation, indicating that the proton exchange membrane did not allow proton transfer as rapidly as required to maintain the pH in both anode and cathode compartments. This problem may be addressed with two areas of research. First, better membrane materials need to be developed that are more selective for proton transfer and allow for more rapid exchange. Second, new reactor designs are needed that allow for more efficient proton transfer. An example of a process diagram and architecture of a proposed continuous-flow methanogenic BES is shown in Figure 10.2. By increasing the surface area of the membrane between the anode and cathode, a larger flux of protons may occur. Also, by delivering the CO_2 to the cathode centrally with a membrane system wrapped in

the carbon felt electrode, biofilm contact with CO₂ is enhanced. The product CH₄ would remain dissolved in the pressurized liquid until degassing in the effluent collection.

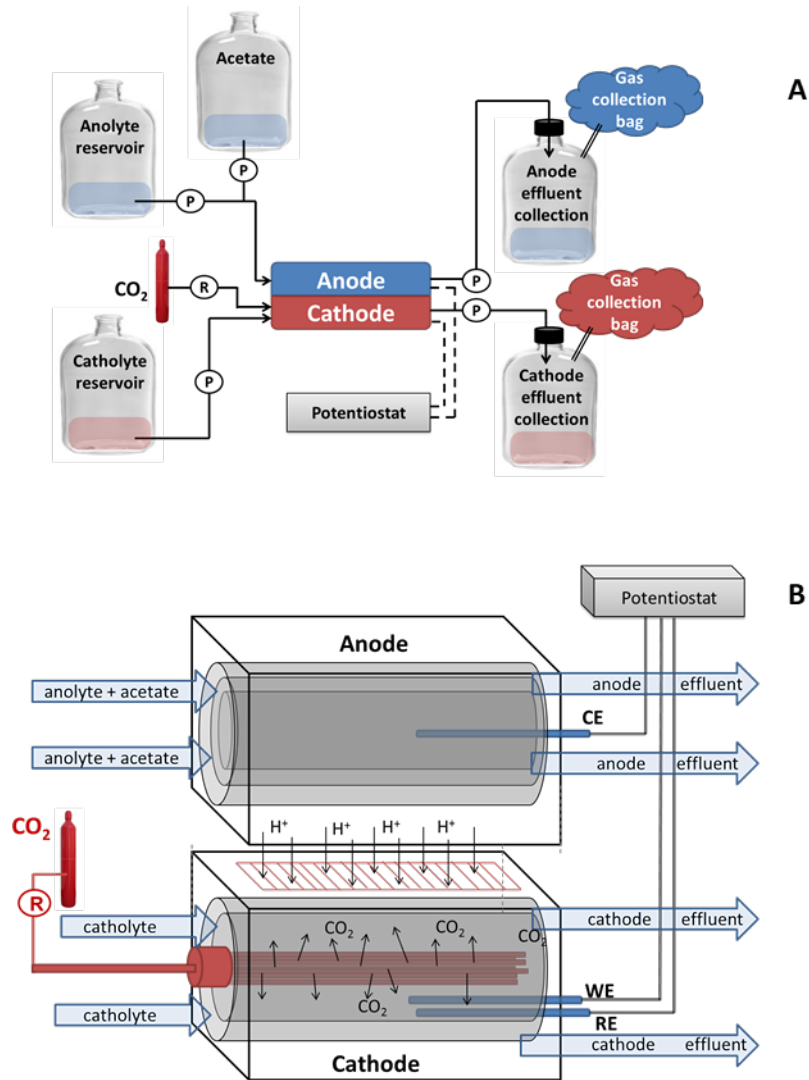


Figure 10.2 - Suggested Process Diagram (A) and Architecture (B) for a Continuous-Flow Methanogenic BES

BESs are a promising technology with many areas of research that can improve the processes and configurations in order to scale up the technology. By reusing CO₂ from

wastewater treatment for energy recovery, wastewater resource recovery facilities may be able to move closer to net-zero energy status and decrease reliance on fossil fuel energy.

REFERENCES

- Abatzoglou, N. and Boivin, S. (2009) A review of biogas purification processes. *Biofuels, Bioproducts and Biorefining* 3(1), 42-71.
- Abbasi, T., Tauseef, S.M. and Abbasi, S.A. (2012) *Biogas Energy*, pp. 11-23, Springer New York, New York, NY.
- Abdeen, F.R.H., Mel, M., Jami, M.S., Ihsan, S.I. and Ismail, A.F. (2016) A review of chemical absorption of carbon dioxide for biogas upgrading. *Chinese Journal of Chemical Engineering* 24(6), 693-702.
- Agrawal, A., Ferguson, W.J., Gardner, B.O., Christ, J.A., Bandstra, J.Z. and Tratnyek, P.G. (2002) Effects of carbonate species on the kinetics of dechlorination of 1,1,1-trichloroethane by zero-valent iron. *Environmental Science and Technology* 36(20), 4326-4333.
- Al-Hayes, R.A.M. and Winterton, R.H.S. (1981) Bubble diameter on detachment in flowing liquids. *International Journal of Heat and Mass Transfer* 24(2), 223-230.
- Al Kharafi, F.M., Saad, A.Y., Ateya, B.G. and Ghayad, I.M. (2010) Electrochemical oxidation of sulfide ions on platinum electrodes. *Modern Applied Science* 4(3), 2.
- Baïda, N., Yazourh, A., Singer, E. and Izard, D. (2002) *Pseudomonas grimontii* sp. nov. *International Journal of Systematic and Evolutionary Microbiology* 52(5), 1497-1503.
- Bajracharya, S., ter Heijne, A., Dominguez Benetton, X., Vanbroekhoven, K., Buisman, C.J.N., Strik, D.P.B.T.B. and Pant, D. (2015) Carbon dioxide reduction by mixed and pure cultures

- in microbial electrosynthesis using an assembly of graphite felt and stainless steel as a cathode. *Bioresource Technology* 195, 14-24.
- Banin, E., Vasil, M.L. and Greenberg, E.P. (2005) Iron and *Pseudomonas aeruginosa* biofilm formation. *Proceedings of the National Academy of Sciences of the United States of America* 102(31), 11076-11081.
- Bartoschek, S., Vorholt, J.A., Thauer, R.K., Geierstanger, B.H. and Griesinger, C. (2000) N-carboxymethanofuran (carbamate) formation from methanofuran and CO₂ in methanogenic archaea. *European Journal of Biochemistry* 267(11), 3130-3138.
- Bauer, F., Persson, T., Hulteberg, C. and Tamm, D. (2013) Biogas upgrading – technology overview, comparison and perspectives for the future. *Biofuels, Bioproducts and Biorefining* 7(5), 499-511.
- Belay, N. and Daniels, L. (1990) Elemental metals as electron sources for biological methane formation from CO₂. *Antonie van Leeuwenhoek* 57(1), 1-7.
- Bhandari, V. and Gupta, R. (2014) *The Prokaryotes*. Rosenberg, E., DeLong, E., Lory, S., Stackebrandt, E. and Thompson, F. (eds), pp. 989-1015, Springer, Berlin.
- Bollinger, N., Hassett, D.J., Iglewski, B.H., Costerton, J.W. and McDermott, T.R. (2001) Gene expression in *Pseudomonas aeruginosa*: Evidence of iron override effects on quorum sensing and biofilm-specific gene regulation. *Journal of Bacteriology* 183(6), 1990-1996.
- Bond, D.R., Holmes, D.E., Tender, L.M. and Lovley, D.R. (2002) Electrode-reducing microorganisms that harvest energy from marine sediments. *Science* 295(5554), 483-485.

- Bonin, P.M.L., Odziemkowski, M.S., Reardon, E.J. and Gillham, R.W. (2000) In situ identification of carbonate-containing green rust on iron electrodes in solutions simulating groundwater. *Journal of Solution Chemistry* 29(10), 1061-1074.
- Boone, D.R. and Garrity, G.M. (2001) *Bergey's Manual of Systematic Bacteriology: Volume One: The Archaea and the Deeply Branching and Phototrophic Bacteria*, Springer-Verlag, Berlin.
- Bouvet, O.M.M., Lenormand, P., Ageron, E. and Grimont, P.A.D. (1995) Taxonomic diversity of anaerobic glycerol dissimilation in the *Enterobacteriaceae*. *Research in Microbiology* 146(4), 279-290.
- Browne, P.D. and Cadillo-Quiroz, H. (2013) Contribution of transcriptomics to systems-level understanding of methanogenic Archaea. *Archaea* 2013, 1-11.
- Brune, A., Ludwig, W. and Schink, B. (2002) *Propionivibrio limicola* sp. nov., a fermentative bacterium specialized in the degradation of hydroaromatic compounds, reclassification of *Propionibacter pelophilus* as *Propionivibrio pelophilus* comb. nov. and amended description of the genus *Propionivibrio*. *International Journal of Systematic and Evolutionary Microbiology* 52(2), 441-444.
- Buan, N.R. and Metcalf, W.W. (2010) Methanogenesis by *Methanosarcina acetivorans* involves two structurally and functionally distinct classes of heterodisulfide reductase. *Molecular Microbiology* 75(4), 843-853.

- Caccavo, F., Lonergan, D.J., Lovley, D.R., Davis, M., Stolz, J.F. and McInerney, M.J. (1994) *Geobacter sulfurreducens* sp. nov., a hydrogen- and acetate-oxidizing dissimilatory metal-reducing microorganism. *Applied and Environmental Microbiology* 60(10), 3752-3759.
- Cappelletti, M., Zannoni, D., Postec, A. and Ollivier, B. (2014) *Microbial BioEnergy: Hydrogen Production*. Zannoni, D. and De Philippis, R. (eds), pp. 197-224, Springer Netherlands, Dordrecht.
- Cavenati, S., Grande, C.A., Rodrigues, A.E., Kiener, C. and Müller, U. (2008) Metal organic framework adsorbent for biogas upgrading. *Industrial and Engineering Chemistry Research* 47(16), 6333-6335.
- Chae, K.J., Choi, M., Ajayi, F.F., Park, W., Chang, I.S. and Kim, I.S. (2008) Mass transport through a proton exchange membrane (Nafion) in microbial fuel cells. *Energy and Fuels* 22(1), 169-176.
- Chaudhury, S., Agarwal, C. and Goswami, A. (2015) Transport properties of multivalent cations in Nafion-117 membrane with mixed ionic composition. *The Journal of Physical Chemistry B* 119(33), 10566-10572.
- Chen, S. and Dong, X. (2005) *Proteiniphilum acetatigenes* gen. nov., sp. nov., from a UASB reactor treating brewery wastewater. *International Journal of Systematic and Evolutionary Microbiology* 55(6), 2257-2261.
- Chen, Y., Cheng, J.J. and Creamer, K.S. (2008) Inhibition of anaerobic digestion process: A review. *Bioresource Technology* 99(10), 4044-4064.

- Cheng, S., Xing, D., Call, D.F. and Logan, B.E. (2009) Direct biological conversion of electrical current into methane by electromethanogenesis. *Environmental Science and Technology* 43(10), 3953-3958.
- Choi, E. and Rim, J.M. (1991) Competition and inhibition of sulfate reducers and methane producers in anaerobic treatment. *Water Science and Technology* 23(7-9), 1259.
- Costa, K.C., Lie, T.J., Jacobs, M.A. and Leigh, J.A. (2013) H₂-independent growth of the hydrogenotrophic methanogen *Methanococcus maripaludis*. *mBio* 4(2), 1-7.
- Daniels, L., Belay, N., Rajagopal, B.S. and Weimer, P.J. (1987) Bacterial methanogenesis and growth from CO₂ with elemental iron as the sole source of electrons. *Science* 237(4814), 509-511.
- Davey, M.E., Caiazza, N.C. and O'Toole, G.A. (2003) Rhamnolipid surfactant production affects biofilm architecture in *Pseudomonas aeruginosa* PAO1. *Journal of Bacteriology* 185(3), 1027-1036.
- Deepanraj, B., Sivasubramanian, V. and Jayaraj, S. (2014) Biogas generation through anaerobic digestion process-an overview. *Research Journal of Chemistry and Environment* 18(5), 80-93.
- Deutzmann, J.S., Sahin, M. and Spormann, A.M. (2015) Extracellular enzymes facilitate electron uptake in biocorrosion and bioelectrosynthesis. *mBio* 6(2).
- Dinh, H.T., Kuever, J., Muszmann, M., Hassel, A.W., Stratmann, M. and Widdel, F. (2004) Iron corrosion by novel anaerobic microorganisms. *Nature* 427(6977), 829-832.

- Dollhopf, S., Hashsham, S., Dazzo, F., Hickey, R., Criddle, C. and Tiedje, J. (2001) The impact of fermentative organisms on carbon flow in methanogenic systems under constant low-substrate conditions. *Applied Microbiology and Biotechnology* 56(3-4), 531-538.
- Feng, Y., Zhang, Y., Quan, X. and Chen, S. (2014) Enhanced anaerobic digestion of waste activated sludge digestion by the addition of zero valent iron. *Water Research* 52, 242-250.
- Ferry, J.G. (1993) *Methanogenesis: Ecology, physiology, biochemistry and genetics*, Springer US, Boston, MA.
- Freguia, S., Rabaey, K., Yuan, Z. and Keller, J. (2007) Electron and carbon balances in microbial fuel cells reveal temporary bacterial storage behavior during electricity generation. *Environmental Science and Technology* 41(8), 2915-2921.
- Fu, Q., Kuramochi, Y., Fukushima, N., Maeda, H., Sato, K. and Kobayashi, H. (2015) Bioelectrochemical analyses of the development of a thermophilic biocathode catalyzing electromethanogenesis. *Environmental Science and Technology* 49(2), 1225-1232.
- Gao, B. and Gupta, R. (2007) Phylogenomic analysis of proteins that are distinctive of Archaea and its main subgroups and the origin of methanogenesis. *BMC Genomics* 8(1), 1-23.
- Gao, Y., Lee, J., Neufeld, J.D., Park, J., Rittmann, B.E. and Lee, H.-S. (2017) Anaerobic oxidation of methane coupled with extracellular electron transfer to electrodes. *Scientific Reports* 7(1), 5099.
- Ge, X., Xu, F. and Li, Y. (2016) Solid-state anaerobic digestion of lignocellulosic biomass: Recent progress and perspectives. *Bioresource Technology* 205, 239-249.

- Geelhoed, J.S. and Stams, A.J.M. (2010) Electricity-assisted biological hydrogen production from acetate by *Geobacter sulfurreducens*. *Environmental Science and Technology* 45(2), 815-820.
- Geppert, F., Liu, D., van Eerten-Jansen, M., Weidner, E., Buisman, C. and ter Heijne, A. (2016) Bioelectrochemical power-to-gas: state of the art and future perspectives. *Trends in Biotechnology* 34(11), 879-894.
- Gölz, G., Sharbati, S., Backert, S. and Alter, T. (2012) Quorum sensing dependent phenotypes and their molecular mechanisms in *Campylobacteriales*. *European Journal of Microbiology and Immunology* 2(1), 50-60.
- Graber, J.R. and Breznak, J.A. (2004) Physiology and nutrition of *Treponema primitia*, an H₂/CO₂-acetogenic *Spirochete* from termite hindguts. *Applied and Environmental Microbiology* 70(3), 1307-1314.
- Graber, J.R., Leadbetter, J.R. and Breznak, J.A. (2004) Description of *Treponema azotonutricium* sp. nov. and *Treponema primitia* sp. nov., the first *Spirochetes* isolated from termite guts. *Applied and Environmental Microbiology* 70(3), 1315-1320.
- Grodzicki, M. and Amthauer, G. (2000) Electronic and magnetic structure of vivianite: cluster molecular orbital calculations. *Physics and Chemistry of Minerals* 27(10), 694-702.
- Gujer, W. and Zehnder, A.J.B. (1983) Conversion processes in anaerobic digestion. *Water Science and Technology* 15(8-9), 127.

- Hamelers, H.M., Ter Heijne, A., Sleutels, T.J.A., Jeremiasse, A., Strik, D.B.T.B. and Buisman, C.N. (2010) New applications and performance of bioelectrochemical systems. *Applied Microbiology and Biotechnology* 85(6), 1673-1685.
- Harimawan, A. and Ting, Y.-P. (2016) Investigation of extracellular polymeric substances (EPS) properties of *P. aeruginosa* and *B. subtilis* and their role in bacterial adhesion. *Colloids and Surfaces B: Biointerfaces* 146, 459-467.
- He, Z. and Angenent, L.T. (2006) Application of bacterial biocathodes in microbial fuel cells. *Electroanalysis* 18(19-20), 2009-2015.
- Heidrich, E.S., Curtis, T.P. and Dolfing, J. (2011) Determination of the internal chemical energy of wastewater. *Environmental Science and Technology* 45(2), 827-832.
- Henderson, A.D. and Demond, A.H. (2007) Long-term performance of zero-valent iron permeable reactive barriers: a critical review. *Environmental Engineering Science* 24(4), 401-423.
- Hilton, B.L. and Oleszkiewicz, J.A. (1988) Sulfide-induced inhibition of anaerobic digestion. *Journal of Environmental Engineering* 114(6), 1377-1391.
- Huang, J., Zhu, N., Cao, Y., Peng, Y., Wu, P. and Dong, W. (2015) Exoelectrogenic bacterium phylogenetically related to *Citrobacter freundii*, isolated from anodic biofilm of a microbial fuel cell. *Applied Biochemistry and Biotechnology* 175(4), 1879-1891.
- Huang, L., Regan, J.M. and Quan, X. (2011) Electron transfer mechanisms, new applications, and performance of biocathode microbial fuel cells. *Bioresource Technology* 102(1), 316-323.

- Huang, Y.-X., Guo, J., Zhang, C. and Hu, Z. Hydrogen production from the dissolution of nano zero valent iron and its effect on anaerobic digestion. *Water Research* 88, 475-480.
- IPCC (2014) *Climate Change 2014: Impacts, adaptation, and vulnerability. Part A: Global and sectoral aspects. Contribution of working group II to the fifth assessment report of the intergovernmental panel on climate change.* Field, C.B., Barros, V.R., Dokken, D.J., Mach, K.J., Mastrandrea, M.D., Bilir, T.E., Chatterjee, M., Ebi, K.L., Estrada, Y.O., Genova, R.C., Girma, B., Kissel, E.S., Levy, A.N., MacCracken, S., Mastrandrea, P.R. and White, L.L. (eds), pp. 1-32, Cambridge University Press, Cambridge, United Kingdom, and New York, NY, USA.
- Jayashree, C., Arulazhagan, P., Adish Kumar, S., Kaliappan, S., Yeom, I.T. and Rajesh Banu, J. (2014) Bioelectricity generation from coconut husk retting wastewater in fed batch operating microbial fuel cell by phenol degrading microorganism. *Biomass and Bioenergy* 69, 249-254.
- Jeon, B.Y., Jung, I.L. and Park, D.H. (2012) Enrichment and isolation of CO₂-fixing Bacteria with electrochemical reducing power as a sole energy source. *Journal of Environmental Protection* 3(1), 5.
- Jiang, R. and Chu, D. (2002) CO₂ crossover through a Nafion membrane in a direct methanol fuel cell. *Electrochemical and Solid-State Letters* 5(7), A156-A159.
- Jiang, Y., Su, M. and Li, D. (2014) Removal of sulfide and production of methane from carbon dioxide in microbial fuel cells–microbial electrolysis cell (MFCs–MEC) coupled system. *Applied Biochemistry and Biotechnology* 172(5), 2720-2731.

- Jitaru, M. (2007) Electrochemical carbon dioxide reduction - fundamental and applied topics. *Journal of the University of Chemical Technology and Metallurgy* 42(4), 333-344.
- Johnsen, A. and Karlson, U. (2004) Evaluation of bacterial strategies to promote the bioavailability of polycyclic aromatic hydrocarbons. *Applied Microbiology and Biotechnology* 63(4), 452-459.
- Johnson, J.L., Moore, L.V.H., Kaneko, B. and Moore, W.E.C. (1990) *Actinomyces georgiae* sp. nov., *Actinomyces gerencseriae* sp. nov., Designation of two genospecies of *Actinomyces naeslundii*, and inclusion of *A. naeslundii* serotypes II and III and *Actinomyces viscosus* serotype II in *A. naeslundii* genospecies 2. *International Journal of Systematic and Evolutionary Microbiology* 40(3), 273-286.
- Karhadkar, P.P., Audic, J.-M., Faup, G.M. and Khanna, P. (1987) Sulfide and sulfate inhibition of methanogenesis. *Water Research* 21(9), 1061-1066.
- Karri, S., Sierra-Alvarez, R. and Field, J.A. (2005) Zero valent iron as an electron-donor for methanogenesis and sulfate reduction in anaerobic sludge. *Biotechnology and Bioengineering* 92(7), 810-819.
- Kato, S. (2016) Microbial extracellular electron transfer and its relevance to iron corrosion. *Microbial Biotechnology* 9(2), 141-148.
- Kato, S., Hashimoto, K. and Watanabe, K. (2012) Methanogenesis facilitated by electric syntrophy via (semi)conductive iron-oxide minerals. *Environmental Microbiology* 14(7), 1646-1654.

- Kerstens, K., De Vos, P., Gillis, M., Swings, J., Vandamme, P. and Stackebrandt, E. (2006) The Prokaryotes. Dworkin, M., Falkow, S., Rosenberg, E., Schleifer, K.-H. and Stackebrandt, E. (eds), pp. 3-37, Springer New York.
- Ki, D., Park, J., Lee, J. and Yoo, K. (2008) Microbial diversity and population dynamics of activated sludge microbial communities participating in electricity generation in microbial fuel cells. *Water Science and Technology* 58(11), 2195-2201.
- Kim, H.-K., Jeong, J.-Y., Cho, H.-N. and Park, J.-Y. (2015) Kinetics of nitrate reduction with the packed bed iron bipolar electrode. *Separation and Purification Technology* 152, 140-147.
- Klindworth, A., Pruesse, E., Schweer, T., Peplies, J., Quast, C., Horn, M. and Glöckner, F.O. (2012) Evaluation of general 16S ribosomal RNA gene PCR primers for classical and next-generation sequencing-based diversity studies. *Nucleic Acids Research*, 1-11.
- Kokko, M.E., Mäkinen, A.E., Sulonen, M.L.K. and Puhakka, J.A. (2015) Effects of anode potentials on bioelectrogenic conversion of xylose and microbial community compositions. *Biochemical Engineering Journal* 101, 248-252.
- Krieg, N., Ludwig, W., Euzéby, J. and Whitman, W. (2010) *Bergey's Manual of Systematic Bacteriology*. Krieg, N., Staley, J., Brown, D., Hedlund, B., Paster, B., Ward, N., Ludwig, W. and Whitman, W. (eds), pp. 25-469, Springer New York.
- Kuchenreuther, J.M., Myers, W.K., Stich, T.A., George, S.J., NejatyJahromy, Y., Swartz, J.R. and Britt, R.D. (2013) A radical intermediate in tyrosine scission to the CO and CN- ligands of FeFe hydrogenase. *Science* 342(6157), 472-475.

- Kumar, R., Singh, L., Wahid, Z.A. and Din, M.F.M. (2015) Exoelectrogens in microbial fuel cells toward bioelectricity generation: a review. *International Journal of Energy Research* 39(8), 1048-1067.
- Kumru, M., Eren, H., Catal, T., Bermek, H. and Akarsubaşı, A.T. (2012) Study of azo dye decolorization and determination of cathode microorganism profile in air-cathode microbial fuel cells. *Environmental Technology* 33(18), 2167-2175.
- Küsel, K. and Drake, H.L. (2011) *Encyclopedia of Geobiology*. Reitner, J. and Thiel, V. (eds), pp. 1-5, Springer Netherlands, Dordrecht.
- Larsen, S.B., Karakashev, D., Angelidaki, I. and Schmidt, J.E. (2009) Ex-situ bioremediation of polycyclic aromatic hydrocarbons in sewage sludge. *Journal of Hazardous Materials* 164(2-3), 1568-1572.
- Lee, B., Park, J.-G., Shin, W.-B., Tian, D.-J. and Jun, H.-B. (2017) Microbial communities change in an anaerobic digestion after application of microbial electrolysis cells. *Bioresource Technology* 234, 273-280.
- Lenin, B.M., Venkata Subhash, G., Sarma, P.N. and Venkata Mohan, S. (2013) Bio-electrolytic conversion of acidogenic effluents to biohydrogen: An integration strategy for higher substrate conversion and product recovery. *Bioresource Technology* 133, 322-331.
- Leschine, S., Paster, B. and Canale-Parola, E. (2006) *The Prokaryotes*. Dworkin, M., Falkow, S., Rosenberg, E., Schleifer, K.-H. and Stackebrandt, E. (eds), pp. 195-210, Springer New York.

- Li, T., Wang, G., Xu, X., Nie, R., Khue, V.A., Zhan, Q. and Zhao, J. (2016a) Importance of external electric field in development of electrocatalysis promotion internal micro-electrolysis for copper (II) removal. *Oxidation Communications* 39(1), 291-304.
- Li, Y., Zhang, Y., Liu, Y., Zhao, Z., Zhao, Z., Liu, S., Zhao, H. and Quan, X. (2016b) Enhancement of anaerobic methanogenesis at a short hydraulic retention time via bioelectrochemical enrichment of hydrogenotrophic methanogens. *Bioresource Technology* 218, 505-511.
- Liu, Y., Balkwill, D.L., Aldrich, H.C., Drake, G.R. and Boone, D.R. (1999) Characterization of the anaerobic propionate-degrading syntrophs *Smithella propionica* gen. nov., sp. nov. and *Syntrophobacter wolinii*. *International Journal of Systematic and Evolutionary Microbiology* 49(2), 545-556.
- Logan, B.E. (2009) Exoelectrogenic bacteria that power microbial fuel cells. *Nature Reviews Microbiology* 7(5), 375-381.
- Lohner, S.T., Deutzmann, J.S., Logan, B.E., Leigh, J. and Spormann, A.M. (2014) Hydrogenase-independent uptake and metabolism of electrons by the archaeon *Methanococcus maripaludis*. *ISME J* 8(8), 1673-1681.
- Lorowitz, W.H., Nagle, D.P. and Tanner, R.S. (1992) Anaerobic oxidation of elemental metals coupled to methanogenesis by *Methanobacterium thermoautotrophicum*. *Environmental Science and Technology* 26(8), 1606-1610.
- Lovley, D.R. and Phillips, E.J. (1988) Novel mode of microbial energy metabolism: organic carbon oxidation coupled to dissimilatory reduction of iron or manganese. *Applied and Environmental Microbiology* 54(6), 1472-1480.

- Lu, M., Chan, S., Babanova, S. and Bretschger, O. (2016) Effect of oxygen on the per-cell extracellular electron transfer rate of *Shewanella oneidensis* MR-1 explored in bioelectrochemical systems. *Biotechnology and Bioengineering*, 114(1), 96-105.
- Ma, H., Cheng, X., Li, G., Chen, S., Quan, Z., Zhao, S. and Niu, L. (2000) The influence of hydrogen sulfide on corrosion of iron under different conditions. *Corrosion Science* 42(10), 1669-1683.
- Ma, S., Odgaard, M. and Skou, E. (2005) Carbon dioxide permeability of proton exchange membranes for fuel cells. *Solid State Ionics* 176(39–40), 2923-2927.
- Matias, P.M., Pereira, I.A.C., Soares, C.M. and Carrondo, M.A. (2005) Sulphate respiration from hydrogen in *Desulfovibrio* bacteria: a structural biology overview. *Progress in Biophysics and Molecular Biology* 89(3), 292-329.
- Mayhew, L.E., Lau, G.E. and Templeton, A.S. (2016) Distinct geochemistries of water–basalt–Fe⁰ reactions in the presence versus absence of CO₂-driven microbial methanogenesis. *Chemical Geology* 428, 92-105.
- McCartney, D.M. and Oleszkiewicz, J.A. (1991) Sulfide inhibition of anaerobic degradation of lactate and acetate. *Water Research* 25(2), 203-209.
- McLennan, M.K., Ringoir, D.D., Frirdich, E., Svensson, S.L., Wells, D.H., Jarrell, H., Szymanski, C.M. and Gaynor, E.C. (2008) *Campylobacter jejuni* biofilms up-regulated in the absence of the stringent response utilize a calcofluor white-reactive polysaccharide. *Journal of Bacteriology* 190(3), 1097-1107.

- Medina-Ramos, J., DiMeglio, J.L. and Rosenthal, J. (2014) Efficient reduction of CO₂ to CO with high current density using in situ or ex situ prepared bi-based materials. *Journal of the American Chemical Society* 136(23), 8361-8367.
- Michel, C., Garrido, F., Roche, E., Belval, S.C. and Dictor, M.-C. (2011) Role of exopolymeric substances (EPS) in the stability of the biofilm of *Thiomonas arsenivorans* grown on a porous mineral support. *Journal of Microbiology Biotechnology* 21(2), 183-186.
- Mikucki, J.A., Liu, Y., Delwiche, M., Colwell, F.S. and Boone, D.R. (2003) Isolation of a methanogen from deep marine sediments that contain methane hydrates, and description of *Methanoculleus submarinus* sp. nov. *Applied and Environmental Microbiology* 69(6), 3311-3316.
- Misiti, T., Tandukar, M., Tezel, U. and Pavlostathis, S.G. (2013) Inhibition and biotransformation potential of naphthenic acids under different electron accepting conditions. *Water Research* 47(1), 406-418.
- Müller, F., Maack, G.-C. and Buescher, W. (2017) Effects of biogas substrate recirculation on methane yield and efficiency of a liquid-manure-based biogas plant. *Energies* 10(3), 325-335.
- Muñoz, R., Meier, L., Diaz, I. and Jeison, D. (2015) A review on the state-of-the-art of physical/chemical and biological technologies for biogas upgrading. *Reviews in Environmental Science and Bio/Technology* 14(4), 727-759.
- Nam, J.-Y., Kim, H.-W. and Shin, H.-S. (2010) Ammonia inhibition of electricity generation in single-chambered microbial fuel cells. *Journal of Power Sources* 195(19), 6428-6433.

- Nanzyo, M., Onodera, H., Hasegawa, E., Ito, K. and Kanno, H. (2013) Formation and dissolution of vivianite in paddy field soil. *Soil Science Society of America Journal* 77(4), 1452-1459.
- Nesbø, C., Bradnan, D., Adebuseyi, A., Dlutek, M., Petrus, A., Foght, J., Doolittle, W.F. and Noll, K. (2012) *Mesotoga prima* gen. nov., sp. nov., the first described mesophilic species of the *Thermotogales*. *Extremophiles* 16(3), 387-393.
- Nevin, K.P., Hensley, S.A., Franks, A.E., Summers, Z.M., Ou, J., Woodard, T.L., Snoeyenbos-West, O.L. and Lovley, D.R. (2011) Electrosynthesis of organic compounds from carbon dioxide is catalyzed by a diversity of acetogenic microorganisms. *Applied and Environmental Microbiology* 77(9), 2882-2886.
- Nopharatana, A., Pullammanappallil, P.C. and Clarke, W.P. (2007) Kinetics and dynamic modelling of batch anaerobic digestion of municipal solid waste in a stirred reactor. *Waste Management* 27(5), 595-603.
- Oksanen, J., Blanchet, G., Friendly, M., Kindt, R., Legendre, P., McGlenn, D., Minchin, P.R., O'Hara, R.B., Simpson, G.L., Solymos, P., Stevens, M.H.H., Szoecs, E. and Wagner, H. (2016) *vegan: Community Ecology Package*.
- Okutman Tas, D. and Pavlostathis, S.G. (2005) Microbial reductive transformation of pentachloronitrobenzene under methanogenic conditions. *Environmental Science and Technology* 39(21), 8264-8272.
- Paddick, J.S., Brailsford, S.R., Kidd, E.A.M., Gilbert, S.C., Clark, D.T., Alam, S., Killick, Z.J. and Beighton, D. (2003) Effect of the environment on genotypic diversity of *Actinomyces*

- naeshundii* and *Streptococcus oralis* in the oral biofilm. Applied and Environmental Microbiology 69(11), 6475-6480.
- Park, H.S., Kim, B.H., Kim, H.S., Kim, H.J., Kim, G.T., Kim, M., Chang, I.S., Park, Y.K. and Chang, H.I. (2001) A novel electrochemically active and Fe (III)-reducing bacterium phylogenetically related to *Clostridium butyricum* isolated from a microbial fuel cell. Anaerobe 7(6), 297-306.
- Petersson, A. and Wellinger, A. (2009) Biogas upgrading technologies - developments and innovations. IEA Bioenergy, 1-20.
- Peu, P., Picard, S., Diara, A., Girault, R., Béline, F., Bridoux, G. and Dabert, P. (2012) Prediction of hydrogen sulphide production during anaerobic digestion of organic substrates. Bioresource Technology 121, 419-424.
- Pham, T., Boon, N., Aelterman, P., Clauwaert, P., De Schamphelaire, L., Vanhaecke, L., De Maeyer, K., Höfte, M., Verstraete, W. and Rabaey, K. (2008) Metabolites produced by *Pseudomonas* sp. enable a gram-positive bacterium to achieve extracellular electron transfer. Applied Microbiology and Biotechnology 77(5), 1119-1129.
- Phillips, D.H., Nooten, T.V., Bastiaens, L., Russell, M.I., Dickson, K., Plant, S., Ahad, J.M.E., Newton, T., Elliot, T. and Kalin, R.M. (2010) Ten year performance evaluation of a field-scale zero-valent iron permeable reactive barrier installed to remediate trichloroethene contaminated groundwater. Environmental Science and Technology 44(10), 3861-3869.

- Price-Whelan, A., Dietrich, L.E.P. and Newman, D.K. (2007) Pyocyanin alters redox homeostasis and carbon flux through central metabolic pathways in *Pseudomonas aeruginosa* PA14. *Journal of Bacteriology* 189(17), 6372-6381.
- Puig, S., Serra, M., Vilar-Sanz, A., Cabré, M., Bañeras, L., Colprim, J. and Balaguer, M.D. (2011) Autotrophic nitrite removal in the cathode of microbial fuel cells. *Bioresource Technology* 102(6), 4462-4467.
- Qadri, F., Haque, M.A., Hossain, A. and Albert, M.J. (1994) Production of slime polysaccharides by *Shigella dysenteriae* Type 1. *Microbiology and Immunology* 38(1), 11-18.
- Rabaey, K., Boon, N., Höfte, M. and Verstraete, W. (2005) Microbial phenazine production enhances electron transfer in biofuel cells. *Environmental Science and Technology* 39(9), 3401-3408.
- Rabaey, K., Boon, N., Siciliano, S.D., Verhaege, M. and Verstraete, W. (2004) Biofuel cells select for microbial consortia that self-mediate electron transfer. *Applied and Environmental Microbiology* 70(9), 5373-5382.
- Rabaey, K. and Rozendal, R.A. (2010) Microbial electrosynthesis — revisiting the electrical route for microbial production. *Nature Reviews Microbiology* 8(10), 706-716.
- Reardon, E.J. (1995) Anaerobic corrosion of granular iron: measurement and interpretation of hydrogen evolution rates. *Environmental Science and Technology* 29(12), 2936-2945.

- Refaey, S.A.M., Taha, F. and El-Malak, A.M.A. (2005) Corrosion and inhibition of stainless steel pitting corrosion in alkaline medium and the effect of Cl⁻ and Br⁻ anions. *Applied Surface Science* 242(1-2), 114-120.
- Reissmann, S., Hochleitner, E., Wang, H., Paschos, A., Lottspeich, F., Glass, R.S. and Böck, A. (2003) Taming of a poison: biosynthesis of the NiFe-hydrogenase cyanide ligands. *Science* 299(5609), 1067.
- Rice, E. W.; Eaton, A. D.; Baird, R. B. *Standard Methods for the Examination of Water and Wastewater*, 22nd ed.; WEF: Washington, DC, 2012.
- Rismani-Yazdi, H., Carver, S.M., Christy, A.D. and Tuovinen, O.H. (2008) Cathodic limitations in microbial fuel cells: An overview. *Journal of Power Sources* 180(2), 683-694.
- Rittmann, B.E. and McCarty, P.L. (2001) *Environmental biotechnology: principles and applications*, McGraw-Hill.
- Rosenbaum, M., Aulenta, F., Villano, M. and Angenent, L.T. (2011) Cathodes as electron donors for microbial metabolism: Which extracellular electron transfer mechanisms are involved? *Bioresource Technology* 102(1), 324-333.
- Rosenbaum, M., Cotta, M.A. and Angenent, L.T. (2010) Aerated *Shewanella oneidensis* in continuously fed bioelectrochemical systems for power and hydrogen production. *Biotechnology and Bioengineering* 105(5), 880-888.

- Rozzi, A. and Remigi, E. (2004) Methods of assessing microbial activity and inhibition under anaerobic conditions: a literature review. *Reviews in Environmental Science and Bio/Technology* 3(2), 93-115.
- Sakai, S., Ehara, M., Tseng, I.-C., Yamaguchi, T., Bräuer, S.L., Cadillo-Quiroz, H., Zinder, S.H. and Imachi, H. (2012) *Methanolinea mesophila* sp. nov., a hydrogenotrophic methanogen isolated from rice field soil, and proposal of the archaeal family *Methanoregulaceae* fam. nov. within the order *Methanomicrobiales*. *International Journal of Systematic and Evolutionary Microbiology* 62(6), 1389-1395.
- Salonen, A., Nikkilä, J., Jalanka-Tuovinen, J., Immonen, O., Rajilić-Stojanović, M., Kekkonen, R.A., Palva, A. and de Vos, W.M. (2010) Comparative analysis of fecal DNA extraction methods with phylogenetic microarray: Effective recovery of bacterial and archaeal DNA using mechanical cell lysis. *Journal of Microbiological Methods* 81(2), 127-134.
- Sander, R. (2015) Compilation of Henry's law constants (version 4.0) for water as solvent. *Atmospheric Chemistry and Physics* 15(8), 4399-4981.
- Sauer, K., Camper, A.K., Ehrlich, G.D., Costerton, J.W. and Davies, D.G. (2002) *Pseudomonas aeruginosa* displays multiple phenotypes during development as a biofilm. *Journal of Bacteriology* 184(4), 1140-1154.
- Savelieva, O., Kotova, I., Roelofsen, W., Stams, A.M. and Netrusov, A. (2004) Utilization of aminoaromatic acids by a methanogenic enrichment culture and by a novel *Citrobacter freundii* strain. *Archives of Microbiology* 181(2), 163-170.

- Scholz, M., Melin, T. and Wessling, M. (2013) Transforming biogas into biomethane using membrane technology. *Renewable and Sustainable Energy Reviews* 17(0), 199-212.
- Sethuraman, V.A., Khan, S., Jur, J.S., Haug, A.T. and Weidner, J.W. (2009) Measuring oxygen, carbon monoxide and hydrogen sulfide diffusion coefficient and solubility in Nafion membranes. *Electrochimica Acta* 54(27), 6850-6860.
- Seviour, T., Doyle, L.E., Lauw, S.J.L., Hinks, J., Rice, S.A., Nesatyy, V.J., Webster, R.D., Kjelleberg, S. and Marsili, E. (2015) Voltammetric profiling of redox-active metabolites expressed by *Pseudomonas aeruginosa* for diagnostic purposes. *Chemical Communications* 51(18), 3789-3792.
- Shi, L., Dong, H., Reguera, G., Beyenal, H., Lu, A., Liu, J., Yu, H.-Q. and Fredrickson, J.K. (2016) Extracellular electron transfer mechanisms between microorganisms and minerals. *Nature Reviews Microbiology* 14(10), 651-662.
- Shi, L., Müller, S., Loffhagen, N., Harms, H. and Wick, L.Y. (2008) Activity and viability of polycyclic aromatic hydrocarbon-degrading *Sphingomonas* sp. LB126 in a DC-electrical field typical for electrobioremediation measures. *Microbial Biotechnology* 1(1), 53-61.
- Siegert, M., Li, X.-F., Yates, M.D. and Logan, B.E. (2014) The presence of hydrogenotrophic methanogens in the inoculum improves methane gas production in microbial electrolysis cells. *Frontiers in Microbiology* 5, 778.
- Siegert, M., Yates, M.D., Spormann, A.M. and Logan, B.E. (2015) *Methanobacterium* dominates biocathodic archaeal communities in methanogenic microbial electrolysis cells. *ACS Sustainable Chemistry and Engineering*.

- Simon, M. and Azam, F. (1989) Protein content and protein synthesis rates of planktonic marine bacteria. *Marine ecology progress series*. Oldendorf 51(3), 201-213.
- Singer, P.C. (1972) Anaerobic control of phosphate by ferrous iron. *Journal (Water Pollution Control Federation)* 44(4), 663-669.
- Singhal, S., Agarwal, S., Arora, S., Sharma, P. and Singhal, N. (2017) Upgrading techniques for transformation of biogas to bio-CNG: a review. *International Journal of Energy Research*, 1-13.
- Stouthamer, A.H. (1973) A theoretical study on the amount of ATP required for synthesis of microbial cell material. *Antonie van Leeuwenhoek* 39(1), 545-565.
- Sun, M., Mu, Z.-X., Chen, Y.-P., Sheng, G.-P., Liu, X.-W., Chen, Y.-Z., Zhao, Y., Wang, H.-L., Yu, H.-Q., Wei, L. and Ma, F. (2009) Microbe-assisted sulfide oxidation in the anode of a microbial fuel cell. *Environmental Science and Technology* 43(9), 3372-3377.
- Sun, Q., Li, H., Yan, J., Liu, L., Yu, Z. and Yu, X. (2015) Selection of appropriate biogas upgrading technology-a review of biogas cleaning, upgrading and utilisation. *Renewable and Sustainable Energy Reviews* 51, 521-532.
- Tandukar, M., Huber, S.J., Onodera, T. and Pavlostathis, S.G. (2009) Biological chromium(VI) reduction in the cathode of a microbial fuel cell. *Environmental Science and Technology* 43(21), 8159-8165.
- Team, R.C. (2014) *R: A Language and Environment for Statistical Computing*, R Foundation for Statistical Computing.

- Thauer, R.K., Kaster, A.-K., Goenrich, M., Schick, M., Hiromoto, T. and Shima, S. (2010) Hydrogenases from methanogenic Archaea, nickel, a novel cofactor, and H₂ storage. *Annual Review of Biochemistry* 79(1), 507-536.
- Tran, H.-T., Kim, D.-H., Oh, S.-J., Rasool, K., Park, D.-H., Zhang, R.-H. and Ahn, D.-H. (2009) Nitrifying biocathode enables effective electricity generation and sustainable wastewater treatment with microbial fuel cell. *Water Science and Technology* 59(9), 1803-1808.
- Tugtas, A.E. (2007) Effect of nitrate reduction on the methanogenic fermentation: process interactions and modeling.
- Uchiyama, T., Ito, K., Mori, K., Tsurumaru, H. and Harayama, S. (2010) Iron-corroding methanogen isolated from a crude-oil storage tank. *Applied and Environmental Microbiology* 76(6), 1783-1788.
- van der Wielen, P.W.J.J., Lipman, L.J.A., van Knapen, F. and Biesterveld, S. (2002) Competitive exclusion of *Salmonella enterica* serovar enteritidis by *Lactobacillus crispatus* and *Clostridium lactatifermentans* in a sequencing fed-batch culture. *Applied and Environmental Microbiology* 68(2), 555-559.
- Vega, C.A. and Fernández, I. (1987) Mediating effect of ferric chelate compounds in microbial fuel cells with *Lactobacillus plantarum*, *Streptococcus lactis*, and *Erwinia dissolvens*. *Bioelectrochemistry and Bioenergetics* 17(2), 217-222.
- Veldkamp, H. (1960) Isolation and characteristics of *Treponema zuelzeriae* nov. spec., an anaerobic, free-living spirochete. *Antonie van Leeuwenhoek* 26(1), 103-125.

- Villano, M., Aulenta, F., Ciucci, C., Ferri, T., Giuliano, A. and Majone, M. (2010) Bioelectrochemical reduction of CO₂ to CH₄ via direct and indirect extracellular electron transfer by a hydrogenophilic methanogenic culture. *Bioresource Technology* 101(9), 3085-3090.
- Villano, M., Monaco, G., Aulenta, F. and Majone, M. (2011) Electrochemically assisted methane production in a biofilm reactor. *Journal of Power Sources* 196(22), 9467-9472.
- Wang, A., Liu, L., Sun, D., Ren, N. and Lee, D.-J. (2010) Isolation of Fe(III)-reducing fermentative bacterium *Bacteroides* sp. W7 in the anode suspension of a microbial electrolysis cell (MEC). *International Journal of Hydrogen Energy* 35(7), 3178-3182.
- Weiland, P. (2010) Biogas production: current state and perspectives. *Applied Microbiology and Biotechnology* 85(4), 849-860.
- Weisenberger, S. and Schumpe, A. (1996) Estimation of gas solubilities in salt solutions at temperatures from 273 K to 363 K. *AIChE Journal* 42(1), 298-300.
- Wentzien, S. and Sand, W. (2004) Tetrathionate Disproportionation by *Thiomonas intermedia* K12. *Engineering in Life Sciences* 4(1), 25-30.
- Wick, L., de Munain, A., Springael, D. and Harms, H. (2002) Responses of *Mycobacterium* sp. LB501T to the low bioavailability of solid anthracene. *Applied Microbiology and Biotechnology* 58(3), 378-385.

- Wick, L.Y., Mattle, P.A., Wattiau, P. and Harms, H. (2004) Electrokinetic transport of PAH-degrading Bacteria in model aquifers and soil. *Environmental Science and Technology* 38(17), 4596-4602.
- Wick, L.Y., Shi, L. and Harms, H. (2007) Electro-bioremediation of hydrophobic organic soil-contaminants: A review of fundamental interactions. *Electrochimica Acta* 52(10), 3441-3448.
- Willumsen, P., Karlson, U., Stackebrandt, E. and Kroppenstedt, R.M. (2001) *Mycobacterium frederiksbergense* sp. nov., a novel polycyclic aromatic hydrocarbon-degrading *Mycobacterium* species. *International Journal of Systematic and Evolutionary Microbiology* 51(5), 1715-1722.
- Wilson, E.L. and Kim, Y. (2016) The yield and decay coefficients of exoelectrogenic bacteria in bioelectrochemical systems. *Water Research* 94, 233-239.
- Wu, D., Shen, Y., Ding, A., Qiu, M., Yang, Q. and Zheng, S. (2013) Phosphate removal from aqueous solutions by nanoscale zero-valent iron. *Environmental Technology* 34(18), 2663-2669.
- Xing, D., Zuo, Y., Cheng, S., Regan, J.M. and Logan, B.E. (2008) Electricity generation by *Rhodopseudomonas palustris* DX-1. *Environmental Science and Technology* 42(11), 4146-4151.
- Xu, S. and Liu, H. (2011) New exoelectrogen *Citrobacter* sp. SX-1 isolated from a microbial fuel cell. *Journal of Applied Microbiology* 111(5), 1108-1115.

- Xue, A., Shen, Z.-Z., Zhao, B. and Zhao, H.-Z. (2013) Arsenite removal from aqueous solution by a microbial fuel cell–zerovalent iron hybrid process. *Journal of Hazardous Materials* 261(0), 621-627.
- Yamaguchi, T., Koval, C.A., Noble, R.D. and Bowman, C.N. (1996) Transport mechanism of carbon dioxide through perfluorosulfonate ionomer membranes containing an amine carrier. *Chemical Engineering Science* 51(21), 4781-4789.
- Yates, M.D., Siegert, M. and Logan, B.E. (2014) Hydrogen evolution catalyzed by viable and non-viable cells on biocathodes. *International Journal of Hydrogen Energy* 39(30), 16841-16851.
- Yenigün, O. and Demirel, B. (2013) Ammonia inhibition in anaerobic digestion: A review. *Process Biochemistry* 48(5–6), 901-911.
- Yong, Y.-C., Yu, Y.-Y., Li, C.-M., Zhong, J.-J. and Song, H. (2011) Bioelectricity enhancement via overexpression of quorum sensing system in *Pseudomonas aeruginosa*-inoculated microbial fuel cells. *Biosensors and Bioelectronics* 30(1), 87-92.
- Yousaf, S., Anam, M. and Ali, N. (2017) Evaluating the production and bio-stimulating effect of 5-methyl 1, hydroxy phenazine on microbial fuel cell performance. *International Journal of Environmental Science and Technology* 14(7), 1439-1450.
- Yu, J., Cho, S., Kim, S., Cho, H. and Lee, T. (2012) Comparison of exoelectrogenic Bacteria detected using two different methods: U-tube microbial fuel cell and plating method. *Microbes and Environments* 27(1), 49-53.

- Yu, S., Wei, Q., Zhao, T., Guo, Y. and Ma, L.Z. (2016) A novel survival strategy of *Pseudomonas aeruginosa*: using exopolysaccharides to sequester and store iron to stimulate Psl-dependent biofilm formation. *Applied and Environmental Microbiology*, AEM. 01307-01316.
- Zeppilli, M., Villano, M., Aulenta, F., Lampis, S., Vallini, G. and Majone, M. (2015) Effect of the anode feeding composition on the performance of a continuous-flow methane-producing microbial electrolysis cell. *Environmental Science and Pollution Research* 22(10), 7349-7360.
- Zhang, G.-d., Zhao, Q.-l., Jiao, Y., Zhang, J.-n., Jiang, J.-q., Ren, N. and Kim, B.H. (2011) Improved performance of microbial fuel cell using combination biocathode of graphite fiber brush and graphite granules. *Journal of Power Sources* 196(15), 6036-6041.
- Zhang, H., Tian, Y., Wang, L., Mi, X. and Chai, Y. (2016) Effect of ferrous chloride on biogas production and enzymatic activities during anaerobic fermentation of cow dung and phragmites straw. *Biodegradation* 27(2), 69-82.
- Zhang, L., Zhou, S., Zhuang, L., Li, W., Zhang, J., Lu, N. and Deng, L. (2008) Microbial fuel cell based on *Klebsiella pneumoniae* biofilm. *Electrochemistry Communications* 10(10), 1641-1643.
- Zhang, R., El-Mashad, H.M., Hartman, K., Wang, F., Liu, G., Choate, C. and Gamble, P. (2007) Characterization of food waste as feedstock for anaerobic digestion. *Bioresource Technology* 98(4), 929-935.

- Zhao, Z., Zhang, Y., Wang, L. and Quan, X. (2015) Potential for direct interspecies electron transfer in an electric-anaerobic system to increase methane production from sludge digestion. *Scientific Reports* 5, 11094.
- Zhaxybayeva, O., Swithers, K.S., Foght, J., Green, A.G., Bruce, D., Detter, C., Han, S., Teshima, H., Han, J., Woyke, T., Pitluck, S., Nolan, M., Ivanova, N., Pati, A., Land, M.L., Dlutek, M., Doolittle, W.F., Noll, K.M. and Nesbø, C.L. (2012) Genome sequence of the mesophilic *Thermotogales* bacterium *Mesotoga prima* MesG1.Ag.4.2 reveals the largest *Thermotogales* genome To date. *Genome Biology and Evolution* 4(8), 812-820.
- Zhen, G., Kobayashi, T., Lu, X. and Xu, K. (2015) Understanding methane bioelectrosynthesis from carbon dioxide in a two-chamber microbial electrolysis cells (MECs) containing a carbon biocathode. *Bioresource Technology* 186, 141-148.
- Zuo, Y., Xing, D., Regan, J.M. and Logan, B.E. (2008) Isolation of the exoelectrogenic bacterium *Ochrobactrum anthropi* YZ-1 by using a U-Tube microbial fuel cell. *Applied and Environmental Microbiology* 74(10), 3130-3137.